Università del Piemonte orientale
"Amedeo Avogadro"

Department of Translational Medicine
Ph.D. Course in:

# "Food, Health and Longevity"
**Curricula Physiopathology of Aging**

XXXV cycle (2019-2022)

# *In vitro* and *In vivo* Studies on Nutraceutical Treatment Strategies to Promote Healthy Ageing in Some of the Major Age-related Diseases

SSD: BIO09

Candidate: Sara Ruga

Coordinator: Prof.ssa Antonia Follenzi

Tutor: Prof Claudio Molinari e Prof.ssa Nicoletta Filigheddu

# SUMMARY

One of the global problems of humanity is preserving the quality of life as the average age of the population rises. At the same time, a significant increase in the proportion of the elderly in developed countries populations has resulted in an increase in mortality caused by major old age diseases, which has the causative factor on human age-related processes, such as osteoarticular disease, metabolic disorders, sarcopenia, neuropathy, and cognitive impairment. As a result, it is not a coincidence that the concept of healthy Ageing is one of the top priorities of the World Health Organization (WHO), in line with the *Global strategy and action plan on ageing and health 2016–2020* and the related *UN Decade of Healthy Ageing (2021–2030)*, following a multisectoral action for a life course approach to healthy ageing. This strategy for achieving healthy ageing addresses global priorities to improve the majority of health problems of older age, which are related to chronic conditions; luckily, many of these can be slowed down or even kept in check by healthy behaviors. In addition, its necessary take into account that although total life expectancy increases, the 'healthy' life span is always the same, lengthening the 'sick' life span without ameliorating the characteristics of human longevity. Therefore, even at a very advanced age, physical activity and good nutrition can help maintain health and well-being, bringing powerful benefits. Thus, health problems and declines in the body's functional capacities can be managed effectively, especially if detected early enough. Since ageing is a complex and inevitable biological process associated with numerous chronically debilitating health effects, developing effective and early intervention strategies for healthy ageing is an active and challenging research area. Indeed, these strategies can ensure an acceptable level of health during the ageing process, especially for people with deteriorating cognitive, motor, and metabolic abilities. In this context, an appropriate dietary regimen and the use of nutraceuticals based on natural extracts can have significant beneficial responses to counteract stress and diseases during ageing. Based on recent findings, nutraceuticals are value-added dietary supplement products having immense potential in modulating key mechanisms and functions related to ageing, acting mainly to restore the impaired physiological mechanisms and metabolic processes. In this context, this PhD thesis aims to clarify from an experimental scientific point of view the mechanism of action of some "food supplements" useful in the field of health improvement during Ageing. Notably, it reported new advanced strategies based on dietary supplements and natural products (chosen by their biological properties on the target site), analyzing their beneficial effects related to the down-regulation of the biological processes in the specific field, including 1) neurodegenerative disorders and cognitive impairment; 2) peripheral nervous system dysfunction; 3) metabolic syndrome and cardiovascular disease; 4) sarcopenia and osteoporosis; 5) osteoarticular disorders and osteoarthritis.

As a concerning the field 1) neurodegenerative disorders and cognitive impairment, is important to remind that ageing exerts a progressive general decline in health and well-being, showing a link between brain ageing and the inhibition of growth/survival factors production. In this context, recent studies have found abnormal brain-derived neurotrophic factor (BDNF) levels involved in the pathogenesis of various diseases of the central nervous system (e.g., stroke, depression, anxiety, Alzheimer's disease, and Parkinson's disease). Regulation of BDNF signaling may represent a potential treatment for several nervous diseases. The decay that occurs during Ageing can have central or

peripheral aspects. This thesis contains the results of experiments aimed at investigating the possibility of attenuating both of these manifestations. To investigate the central damages related to Ageing, both *in vitro* and *in vivo*, the possibility of orally administering a BDNF-based supplement and its efficacy in promoting endogenous protection on the main mechanisms leading to neurodegeneration were explored. In particular, the main important findings include for the first time that BDNF SKA can cross both intestinal and blood brain barrier (BBB) and can stimulate BDNF endogenous production leading to improved neuroplasticity. In addition, the new SKA method (sequentially kinetic activated, a particular type of preparation which allows the administration of doses of active ingredient in physiological amounts) revealed a possible important application to modulate the dose of the drug, maintaining the safety of the use and the beneficial properties of the molecule prepared by SKA method. Furthermore, BDNF SKA exerted beneficial effects on the metabolism of the proteins apolipoprotein E, β-amyloid and Sirtuin 1, thus contributing to maintain the health of both neurons and astrocytes. Thus, the BDNF prepared in this way confirms its ability to slow down the mechanism related to ageing and counteract the cognitive decline also related to neurodegenerative diseases. At the same time, neurotrophins, such as BDNF, are considered new biomarkers valuable to explore another key aspect of ageing involving other pathological conditions, included in the area of field 2, peripheral nervous system dysfunction. In particular, the second experimental phase took into consideration neuropathic pain such as that caused by a lesion or disease of the somatosensory system, which often affects elderly people. Moreover, elderly patients are often poly-medicated with a growing risk of drug interaction and recurrent hospitalization. Since some standard pharmaceutical therapies can cause dependence or intolerance, non-pharmacological treatments, such as food supplements, have gained great interest in recent years. In this context, the beneficial effects on peripheral nerves of palmitoylethanolamide (PEA) and *Equisetum Arvense* were evaluated with the hypothesis of using them as a new food supplement. Since the main route of administration in humans is oral, it is essential to first analyze the bioavailability of the combination of the two active ingredients in an *in vitro* 3D intestinal barrier to mimic the human oral intake and, secondly, in an *in vitro* 3D nerve tissue model to modulate the intracellular mechanisms involved in peripheral neuropathy. The results obtained demonstrate, for the first time, the efficacy of PEA and *Equisetum Arvense* in modulating the nerve recovery mechanism after Schwann cell injury and offering the initial response in relieving pain after first-pass metabolism. The therapeutic potential of natural remedies may apply to other ageing diseases, such as metabolic disorders and musculoskeletal diseases, which are also related to neuropathic pain. In fact, as part 3 of this thesis, the possibility of controlling the changes in cholesterol metabolism, which are at the basis of metabolic syndrome and cardiovascular diseases, was investigated using plant-extracted active ingredients. Indeed, it is widely accepted that abnormal cholesterol levels in the blood are risk factors for cardiovascular diseases, such as hypercholesterolemia which often cause severe cardiovascular events. There are well-established treatment options available to prevent the occurrence of atherosclerosis due to LDL-hypercholesteremia, including statins. However, more information about the safety of this treatment needs to be obtained as statins can induce myopathy and other serious diseases in chronic use. To overcome this problem, some nutraceuticals with the same activity as statins may be promising options for preventing and treating hypercholesterolemia. Therefore, in this field 3, the effectiveness of a new food supplement, called Esterol10®, based on a combination of natural extracts, was evaluated by analyzing the biological

mechanisms and processes involved in cholesterol metabolism comparing data with Atorvastatin in an *in vitro* model. From the results obtained, it is possible to affirm for the first time that Esterol10® acts on the intracellular mechanisms that lead to a reduction in total cholesterol and an improvement in the biosynthesis of free cholesterol and bile acids. Furthermore, Esterol10® can modulate the LDL receptor preventing lipids accumulation and the main intracellular pathways involved in cholesterol metabolism. All these findings confirmed the important anti-cholesterolemic role of Esterol10® compared to a common therapy available on the market. Although the positive effects on cardiovascular events mediated by statin therapy have several side effects, adverse effects that include statin associated muscle symptoms (SAMS) are commonly reported. This frequent condition in humans revealed a range from mild-to-moderate muscle pain, weakness, or fatigue to potentially life-threatening rhabdomyolysis, which is reported by 10% to 25% of patients receiving statin therapy. To reduce the lousy quality of life of the patients in statins chronic treatment, in part 4 of the experimental activity sarcopenia and osteoporosis were considered. In this phase, the ability of a new formulation composed of magnesium, potassium, vitamin D and curcumin to prevent damage from hypercontraction in an *in vitro* exercise model was explored. In these experiments, for the first time, significant results about a positive effect on mitochondrial activity, ATP production, oxygen consumption, and myoblast differentiation were obtained. Consequently, additional experiments were performed mimicking strenuous exercise and, as expected, the new food supplement revealed beneficial effects on skeletal muscle cells controlling hypercontraction, restoring ion fluxes, reducing inflammation signaling, and supporting the main mechanism involved in aerobic activity. Furthermore, in the context of phase 4, it is also important to consider the role of osteoporosis as a risk factor for fractures, which occur in elderly patients. In fact, the changes in bone Ageing that lead to osteoporosis depend on several causes, including hormonal alterations, skeletal unloading and accumulation of senescent cells. Typically, the maintenance of bone homeostasis requires a balance of activity from osteoblasts and osteoclasts. Moreover, osteoporosis results from decreased bone formation and increased bone resorption due to osteoblasts and osteoclasts. Currently, several treatments for bone mass loss are approved by the FDA, but most of them are associated with serious adverse effects. For that, alternative options are most required, and recent studies have proposed improving osteoblast differentiation for osteoporosis prevention and treatment. On the other hand, several natural extracts that are safe and inexpensive have demonstrated some positive effects on bone-related diseases. In this context, a new food supplement based on *Artemisa annua, Boswellia serrata and Equisetum arvense* has been investigated to improve osteoblast activities by modulating alkaline phosphatase (ALP) and mineralized nodules in an *in vitro* co-culture of osteoblast/osteoclast. The main results revealed for the first time that the protein levels of osteoclastic markers were significantly decreased. At the same time, the balance between osteoprotegerin (OPG)/RANKL was maintained by osteoblast OPG production, which inhibits osteoclast formation by inducing osteoblast functions. Moreover, since these extracts will be used as human food supplements, an *in vitro* 3D intestinal model analysis was carried out that mimicked the oral human intake. Additionally, *in vivo* experiments demonstrated that the combination of *Artemisa annua, Boswellia serrata and Equisetum arvense* significantly promoted bone formation in aged-induced osteoporotic mouse model. Particularly significant was the increase in the osteoblast-related parameters and bone histomorphometry parameters. Collectively, these results demonstrated for the first time that this new

formulation can promote osteoblastic differentiation via the activation of the conventional pathways and promote bone formation. Finally, another decline condition related to the ageing process that greatly impacts older people's quality of life is osteoarthritis (OA). This common and debilitating joint disorder contributes to joint pain and functional impairment. For this reason, the application of nutraceuticals in the area of field 5, osteoarticular disorders and osteoarthritis, has also been investigated. The pathogenesis of OA remains unknown mainly, although inflammation has been reported to exert an important role in its progression. In recent years, hyaluronic acid (HA) has attracted great attention as a new treatment option for OA, due to its anti-inflammatory properties, stopping cartilage degeneration, and aiding tissue repair. Nowadays, viscosupplementation is based upon the hypothesis that HA administration could improve joints' rheological properties, promoting the endogenous synthesis of HA and possibly more functional HA, thereby improving mobility and articular function and decreasing pain. Therefore, in this field, the ability of a new plant-derived high molecular weight (called GreenIuronic®) was investigated to maintain joint homeostasis and prevent the harmful processes of OA. The results showed for the first time that the chemical–biological profile of GreenIuronic® permits it to cross the intestinal barrier without side effects and explains several beneficial effects on chondrocyte functions. Furthermore, in the OA model, this new plant-derived HA can modulate the molecular mechanism underlying the prevention of cartilage degradation by restoring and improving the endogenous repair mechanism.

In conclusion, considering the data obtained from all fields, it is possible to define a new interdisciplinary field that aims to understand the relationship between ageing and nutraceutical supplementation. Indeed, it is essential to understand the main biological mechanisms of ageing process to optimize and modulate it by using natural active principles. Further, these data pave the way for developing new anti-ageing or healthy ageing therapies that may promote the identification and development of 'geroprotectors'. Overall, the results also define the concept of food supplements as a potent factor that can mitigate some of the deleterious aspects of ageing, including predisposition to diseases, and support the correct use of natural extracts. These innovative approaches could be inserted in the context of the global strategy and plan of action on ageing and health also established by WHO, in which "*ensure healthy lives and promote well-being for all at all ages through universal health coverage*" is a primary goal.

# INDEX

# 1) INTRODUCTION

Human longevity has significantly expanded over the past century due to better living conditions and the ongoing advancement of medical technology. Aging is the permanently gradual loss of physiological function that ultimately results in age-related illnesses, including cancer, cardiovascular diseases, musculoskeletal problems, and arthritis. These age-related illnesses place a significant financial and emotional strain on patients, their families, and society at large [1]. In the European Union (EU), for instance, it is predicted that the proportion of people 65 will rise significantly over the coming decades: from about 25% in 2010, it increased to 29.6% in 2016 and is expected to reach 51.2% in 2070; these data are of particular relevance when one considers that the World Health Organization (WHO) classifies a society as "aging-society" if at least 7% of the population is 65 years or older if this number rises to 14% or higher, the society is classified as "aged-society", and when the old-age dependency rate reaches 20% or higher, the society is classified as "super-aged-society" [2]. In this context, forecasts of Italy's demographic future return a potential crisis picture: the resident population is decreasing from 59.6 million in 2020 to 58 million in 2030, 54.1 million in 2050, and 47.6 million in 2070. Moreover, the ratio of young to old will be 1 to 3 in 2050, while the working-age population will decline in 30 years from 63.8 percent to 53.3 percent of the total [3]. Aging is directly proportional to numerous chronic illnesses, including osteoarthritis, cancer, cardiovascular disease, and dementia. Moreover, the National Healthcare System's finances are heavily impacted by the diagnosis and treatment of these chronic illnesses [4]. Most illnesses and ailments that shorten life expectancy are caused by aging. Therefore, aging-related diseases must be seen as multiple trajectories of the same process with a varied pace based on various genetic backgrounds and lifestyle choices [5]. The regulatory systems of the body work intricately and cooperatively maintain functional homeostasis in cells and tissues by sensing and regulating nutrient availability and response, cell division and regeneration, fending off foreign and infectious agents, as well as maintaining memory and quickness of the neurological responses. Human health results from dynamic interactions and controls by several genetic, non-genetic, and environmental elements. Any preventative or therapeutic strategy aims to restore this "healthy" state of homeostasis since these systems are inevitably disrupted throughout aging and diseases [5]. Aging is not thought to be a controlled process, unlike growth and development, and mounting evidence indicates that the apparent macro phenotype of aging is largely the accumulation of microscopic cellular damage over time [6]. Consequently, a cellular senescence-centric perspective of aging is quickly gaining popularity, and cellular senescence is emerging as an all-encompassing phenomenon that relates cellular aging to organismal aging. Therefore, gerontologists are studying age-related diseases using innovative and integrative methods. Indeed, cellular senescence is involved in the pathogenesis of various age-related human disorders, such as but not limited to arthritis, diabetes, neurodegenerative disorders, sarcopenia, cancer, and cardiovascular diseases [7]. Instead, the only known non-genetic elements that can positively affect aging and health are exercise, lifestyle, and nutrition. Additionally, it is believed that nutrition is the most effective way to prevent or delay some of the negative effects of aging, such as a person's propensity for certain diseases [8].

Different factors can affect cell senescence and the progression of age-related diseases. Among these are oxidative stress, telomere shortening, DNA damage, protein fibrillization/aggregation, inflame-aging process, immunosenescence, and low levels of IGF-1. The primary hallmarks, which are

unequivocally deleterious to the cell, include genomic instability, telomere attrition, epigenetic alterations, and loss of proteostasis. The antagonistic hallmarks, which are beneficial at low levels but at high levels, become deleterious, are deregulated nutrient sensing, cellular senescence, and mitochondrial dysfunction. Finally, the integrative hallmarks affecting tissue homeostasis and function are stem cell exhaustion and altered intercellular communication. In particular, oxidative stress (OS) is one of the main epigenetic variables associated with aging and can also result in high-grade inflammation. OS is a key factor in cell damage or injury since endogenous or exogenous agents could induce tissue or organ damage via OS [9]. his pro-inflammatory condition can increase inflammatory cytokines and markers, including interleukin-6 and tumor necrosis factor-alpha (TNF-$\alpha$). This can activate the NF-KB pathway and induce mitochondrial superoxide and reactive oxygen species (ROS) production. Inflamm-aging is a significant contributor to human frailty, the aging process, and cell senescence, particularly in age-related disorders; on the other side, inflammation can cause oxidative stress, which might slow down the aging process and the spread of disease [10]. Moreover, it is possible to identify nine pillars that represent common denominators of aging in different organisms: the primary hallmarks, which are unequivocally deleterious to the cell, including genomic instability, telomere attrition, epigenetic alterations, and loss of proteostasis; at the same time the antagonistic hallmarks, which are beneficial at low levels but at high levels become deleterious, are deregulated nutrient sensing, cellular senescence, and mitochondrial dysfunction, and, finally, the integrative hallmarks, affecting tissue homeostasis and function, are stem cell exhaustion and altered intercellular communication [11].
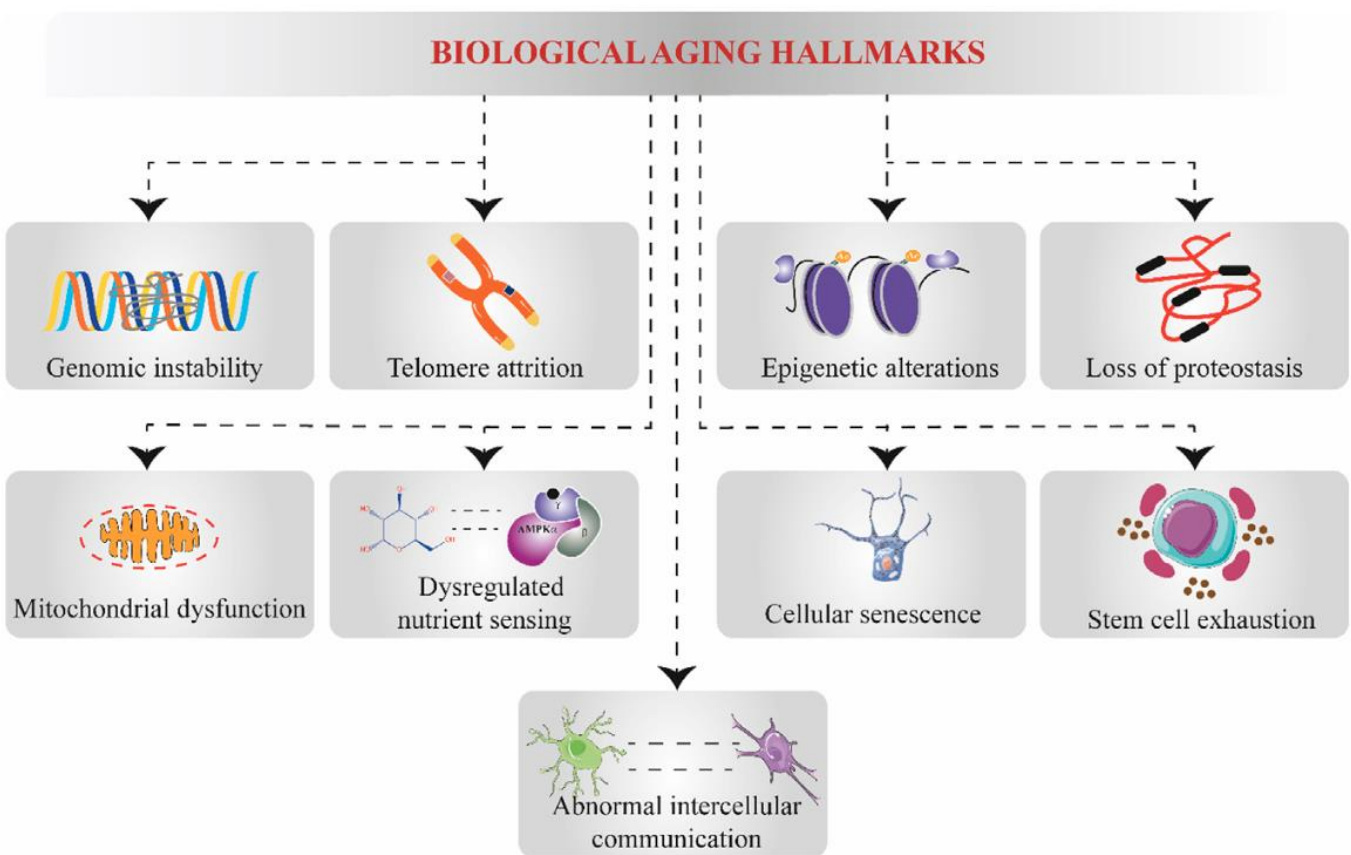


Figure 1. Systematic representation of causal hallmarks underlying biological aging.

Based on this, the shortening of telomeres is the key aspect of the "hallmarks of aging" previously described: telomeres are repetitive DNA sequences capping chromosomes, which shortens every time cells divide [12]. The primary function of telomeres is to protect the chromosomes from degradation rearrangements, end-to-end fusions, and chromosome loss by recruiting shelterin. They are, in turn, protected by the action of the enzyme telomerase. In addition to DNA replication during mitosis, telomere length shortens progressively with oxidative stress or with senescence and aging [13]. Interactions between telomeric DNA and shelterin complexes safeguard chromosome ends from DNA damage response (DDR) and maintain genome stability. When telomeres lose their protective structure, there is a condition of genomic instability, and the replicative senescence is triggered through DDR pathways. Specifically, short telomeres are detected as DNA double-strand breaks when critical telomere shortening is reached [14] inducing DDR, a signaling cascade that converges on ATM kinase, which activates p53, resulting in cellular senescence through the repression of RB. Cellular senescence leads to exhaustion and function decline of stem cells and chronic inflammation in tissue which ultimately drive aging [15]. In addition, emerging evidence suggests that telomere attrition and metabolic compromise share a strong relationship. Recent studies have shown that telomere shortening can also affect mitochondria activity via multiple ways to initiate the aging process: when DNA damage occurs due to telomere dysfunction, p53 and DDR pathways are activated, which in turn suppress PGC-1 and PGC-1, subsequently leading to mitochondrial dysfunction [15]. In addition, short telomeres are perceived as double-strand breaks by PARP1-dependent nicotinamide adenine dinucleotide (NAD+), which can initiate DNA repair signaling, a process that requires NAD+ consumption. Overactivation of PARP1 results in NAD+ consumption, thereby limiting the activity of the NAD+-dependent deacetylase sirtuin 1 (SIRT1) [16], which enhances mitochondrial function and biogenesis through the transcription factor PGC-1$\alpha$, and thus loss of SIRT1 activity could contribute to mitochondria dysfunction, particularly in muscle [16]. Along with the aforementioned role in mitochondrial biogenetics, PGC-1 also controls cellular metabolism in mammals, and the availability of nutrients affects its physiological level [17]. Instead, nutrient sensing pathways are currently the most involved pathways in aging biology research due to their broad scope and link to cellular metabolism. These nutrient-sensing pathways detect and respond to nutrient levels and initiate cascading responses downstream, such as growth, energy, and reproduction. By interacting with one another, the IGF1, mTORC1, AMPK, SIRT1, and AMPK signaling pathways regulate aging, and dietary availability has several interrelated effects on these processes. For instance, decreasing intracellular glucose increases AMPK and raises NAD+ levels, which results in mTORC1 activity being inhibited and SIRT1 activity being increased. Because inhibition shifts the balance toward mTORC2, boosting essential age-dependent proteins required for metabolic regulation, suppressing of mTORC1 activity is projected to be advantageous for extending life. Additionally, it is well known that IGF1 signaling activity shortens lifespan via mTORC1; nevertheless, under caloric restriction, AMPK inhibits mTORC1 but increases lifetime.

On the other hand, in nutrient-restricted situations, SIRT1 activation by AMPK or NAD+ indirectly enhances metabolism and mitochondrial balance through PGC1. Lifespan can be extended by stabilizing mitochondrial metabolism and homeostasis. Contrarily, DNA instability caused by replication errors and DNA damage in cells can disrupt the transcription of genes essential to metabolism and long life and start cellular senescence, shortening lifespan. Rapamycin suppresses

mTORC1 activity in the therapeutic pharmacology of natural products, whereas berberine and resveratrol promote AMPK and SIRT1 activity, respectively [17].
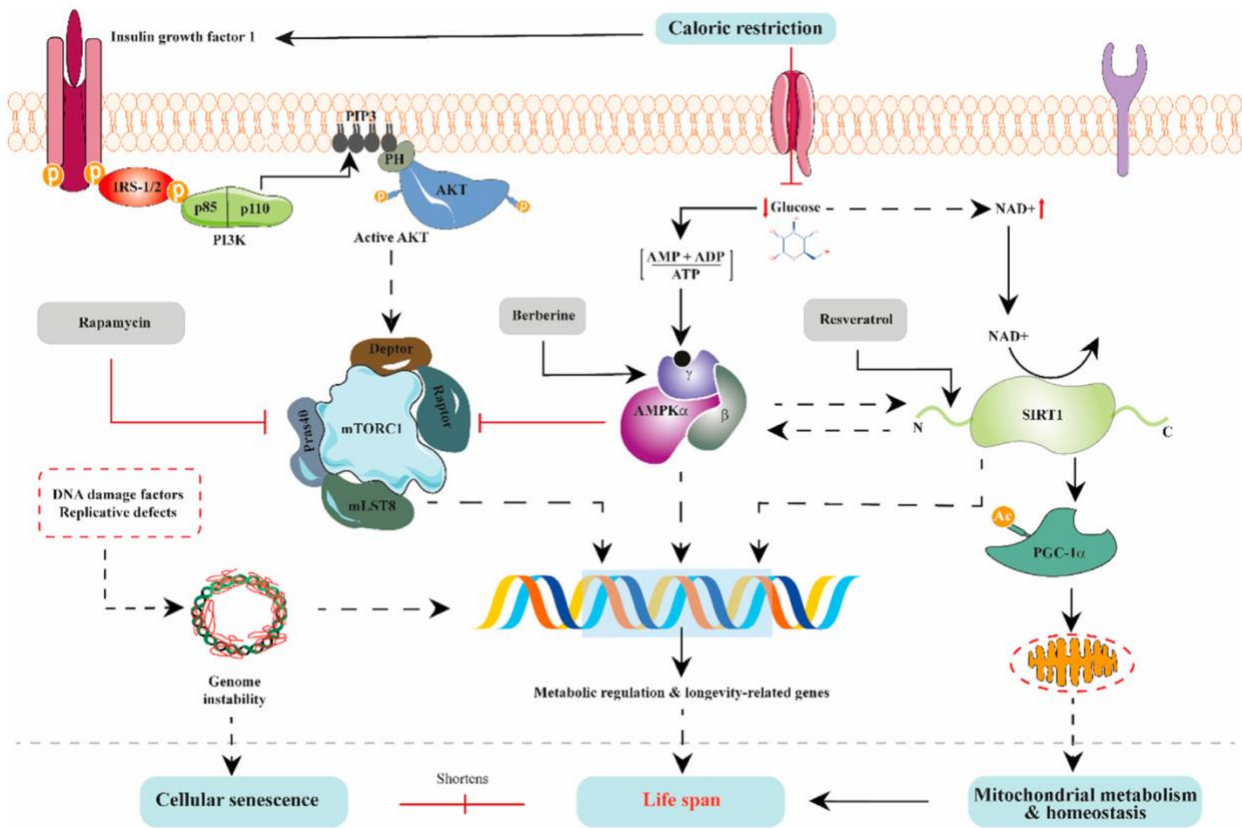


Figure 2. The interlinked regulation of nutrient-sensing pathways

Another hallmark of aging is epigenetic alterations: with aging, there are distinct epigenetic changes, including reduced global heterochromatin, formation of distinct heterochromatin foci, remodeling and loss of nucleosomes, changes in the abundance of histone variants, altered histone marks, global hypomethylation of DNA with distinct areas of hypermethylation, changes in ncRNA abundance, and relocalization of chromatin-modifying factors [18]. Numerous signs of aging, such as mitochondrial failure, genetic instability, and cellular senescence, may be caused by epigenetic alterations. Global and loci-specific alterations to chromatin structure occur as people age. There are some differences in the chromatin of young and old people: young chromatin is primarily tightly packaged heterochromatin with HP1 protein binding and repressive histone marks, DNA cytosine methylation is widely distributed, and classical histone proteins make up nucleosomes. In contrast, globally diminished heterochromatin and localized heterochromatin regions known as senescence-associated heterochromatin foci are characteristics of the chromatin of old people's cells. Moreover, repressive histone marks are reduced whereas active histone marks are elevated, there is a general nucleosome loss and non-canonical histone variations are present in nucleosomes. Additionally, except for CpG islands, where there is hypermethylation, there is universal DNA hypomethylation [18]. Metabolic alterations also influence the proteostasis system that, via feed-forward connectivity, drives the aging program. During cell age, they lose their ability to properly fold proteins, maintain protein folding,

and eliminate misfolded proteins. This leads to the accumulation of abnormal protein aggregates and loss of protein homeostasis. Loss of proteostasis can accelerate aging and the onset of neurodegenerative diseases such as Alzheimer's disease and Parkinson's disease [19]. The fast decrease of the proteostasis system throughout aging may be explained by the nature of the system, which is constantly flooded with newly translated proteins that must go through organellar targeting and folding to prevent off-pathway misfolding [20]. By hindering the folding of newly synthesized proteins, misfolded and aggregated proteins will stifle essential folding and quality control components and hasten the degeneration of proteostasis systems. Cellular function and the wiring of the metabolic and proteostatic pathways are expected to be harmed by widespread loss of protein function and the accumulation of various species of misfolded and aggregated proteins; therefore, the interconnectedness and feedback control of the organellar sub-system proteostasis may help to explain why it fails to function properly as we age [21]. Additionally, mitochondrial function and the proteostasis system in the cytoplasm and nucleus are intimately linked. The downstream import of freshly produced proteins into mitochondria is adversely affected by disruption of the cytosolic proteostasis mechanism; on the contrary, the cytosolic proteostasis system may become overburdened with mistargeted precursor proteins as a result of mitochondrial malfunction, which inhibits the import of proteins from the cytosol. Due to this interconnectedness, sophisticated regulatory systems are required to coordinate not just the proteostasis system but also basic metabolism in order to maintain mitochondrial function [22].

The above-mentioned mechanisms, such as DNA damage, epigenetic alterations, telomere shortening, cellular senescence, and mitochondrial dysfunction, can trigger cellular senescence, which is the transition to quiescence where cells cease dividing and is characterized by the secretion of inflammatory signaling factors [23]. Senescent cells accumulate during aging in all tissues, and this accumulation influences cellular homeostasis since it leads to increased inflammation, decreased tissue function and causes stem cell exhaustion, which all contribute to aging [24]. The shortening of telomeres and mutations also occur in stem cells leading them to senescence, and this stem cell exhaustion can, for instance, lead to neurodegenerative diseases or a decline in hematopoiesis which in turn leads to less production of adaptive immune responses [25].

Finally, aging is associated with changes in communications between cells, mainly driven by the development of chronic inflammation in aged people named inflammaging. This inflammation is seen as a consequence of several hallmarks of aging described above, including cellular senescence and loss of proteostasis because misfolded proteins constitute a danger signal that triggers the innate immune response, and it is also linked to age-associated diseases, functional decline, and frailty [26]. Again, an important role is played by mitochondria, as they can secrete damage-associated molecular patterns (DAMPs) such as ATP, mtDNA, and ROS [27], danger signals released by cells during stress, apoptosis, or necrosis to trigger an immune response. For example, high levels of mtDNA have been found in the plasma of people over the age of 50 years with concomitant high levels of inflammatory cytokines [28]. In addition to increased inflammation, there is a decrease in the adaptive immune response during aging: T cells are important for the adaptive immune response to prevent infection [27], but in the elderly, their activity is reduced, making them more susceptible to disease [29]. Furthermore, interestingly, mice with T cells specifically deficient in a mitochondrial DNA stabilizing protein exhibited multiple features associated with aging, including neurological, metabolic, muscular, and

cardiovascular disorders [30]. Furthermore, defective T cells initiated an early inflammatory program that induced premature senescence [30].

Summarizing, all of the signs and symptoms of aging are connected, and mitochondrial dysfunction, in particular, is connected to all of them. High levels of ROS can cause telomere attrition, genomic instability, epigenetic changes, stem cell exhaustion, and cellular senescence, but they can also improve proteostasis. Low levels of NAD+ can cause genomic instability, while damage to mitochondrial DNA (mtDNA) can cause genomic instability, cellular senescence, and altered intercellular communication. Lower mitochondrial dynamics can be caused by aging traits such as genomic instability and dysregulated nutrition sensing and reduced mitochondrial dynamics can also cause cellular senescence. Proteostasis is compromised by diminished mitophagy, which is brought on by epigenetic changes and improper nutrition sensing. Oxidative phosphorylation, which is influenced by unregulated nutrient sensing, epigenetic changes, and defective proteostasis, influences the hallmarks of stem cell exhaustion, cellular senescence, impaired proteostasis, and altered intercellular communication. Finally, reduced levels of mitochondrial proteins can result from epigenetic changes. The dashed line represents the effect of aging-related symptoms on mitochondrial dysfunction.
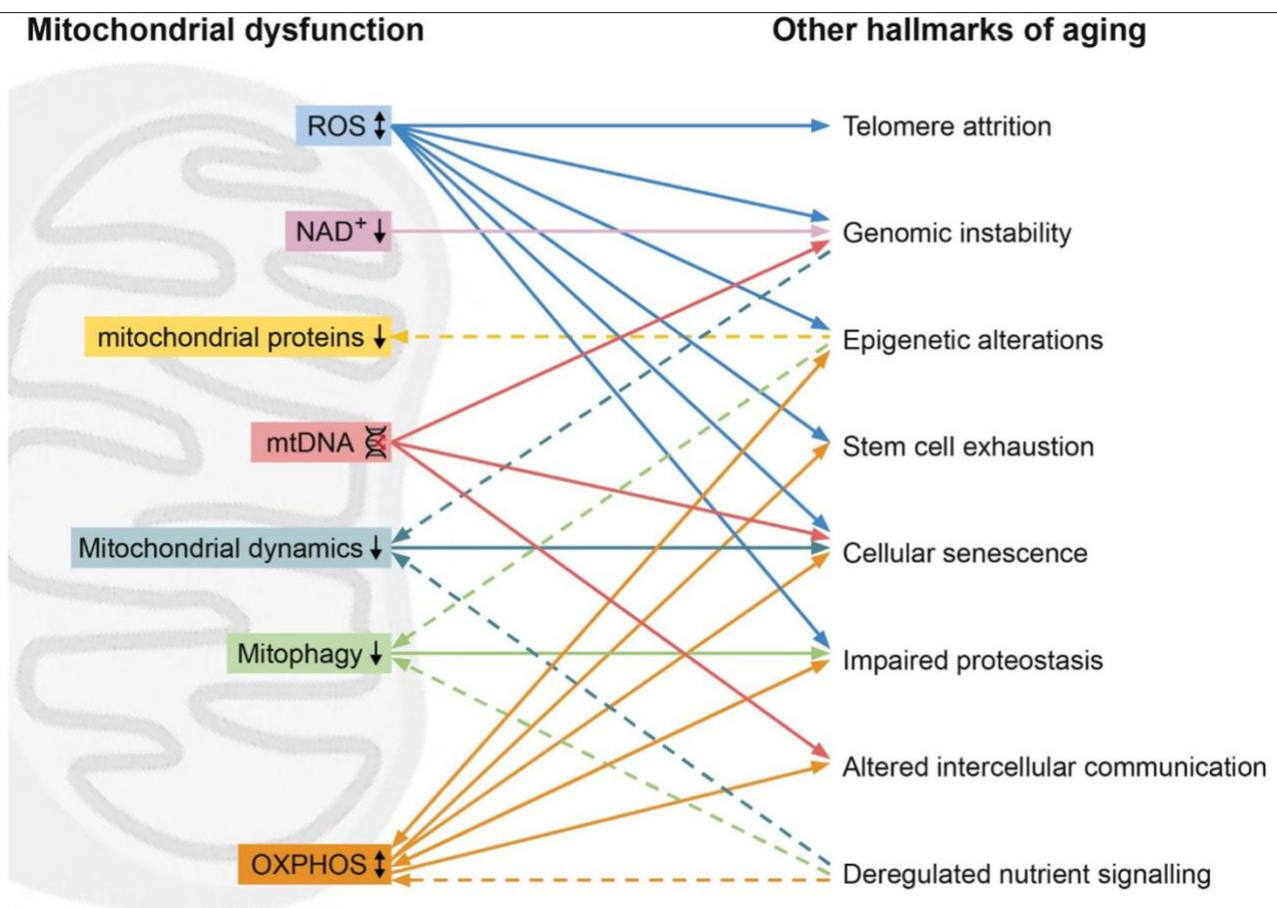


Figure 3. Mitochondrial dysfunction (left) and its relationship with other hallmarks (right)

As a consequence, many chronic diseases and pathological conditions are at least in part determined by the mechanisms described above. This is consistent with the idea that the distinction between aging and illness would rely on the rate and severity of cellular and molecular aging processes, the genetic susceptibility of specific organs and systems, and lifestyle and habitual patterns. Therefore, with time, all functional domains experience a physiological deterioration that may ultimately result in overt

clinical illnesses that are favored by organ/system-specific genetic and environmental variables; thus, a continuum between the healthy juvenile stage and the impaired and unhealthy senior state is produced by this progressive process [31].

Since aging is thought to be associated with the emergence of major diseases and a general decline in physical and cognitive function, several related problems include the ineffectiveness of medicinal treatment therapies, their toxicity, their inability to provide radical solutions in some diseases, and the necessity of multiple drug therapy in certain chronic diseases. It is, therefore, necessary for alternative treatment methods to be sought [32]. In this context, healthy food, lifestyle, and dietary antioxidants are required to increase the quality of life and slow aging. Now, the world of nutraceuticals has begun to be added to these concepts; instead, the relationship between diet and aging is quite interesting. Nutraceuticals are a class of products on the border between nutrients and drugs that provide supplementation of specific nutrients with beneficial effects on health [33]. The term nutraceuticals is a chimerical word, resulting from the fusion of "nutrition" and "pharmaceutical"; Stephen Defelice first formulated it in 1989 and according to his definition, "nutraceuticals are food or part of a food that provides medical or health benefits including the prevention and/or treatment of a disease" [34]. According to the Food and Drugs Administration (FDA) a "dietary supplement" is a product intended to supplement one or more nutrients with the intent of increasing their total daily intake [35]. A "functional food" is instead defined as a food product to be taken as a part of the usual diet to have beneficial effects beyond basic nutritional functions. Functional foods can be enriched with ingredients that usually are not present in that particular food or contain an amount of a specific nutrient larger than usual. FDA regulates dietary supplements to ensure their safety, wholesomeness and their labeling to be truthful and not misleading [36]. Similarly, the European Commission regulates the nutraceutical market through the European Food Safety Authority (EFSA), which authorizes the labeling of food products with health claims. Basically, a health claim must be based on accepted scientific evidence demonstrating a significant effect on humans and a cause-and-effect relationship between food consumption and claimed effects on humans. Producers must declare the target population for the intended health claim and the recommended quantity of nutrient necessary to obtain the claimed beneficial effect; they must declare if there are categories of persons who should avoid using the nutrient [37].

A variety of nutraceuticals were reported to promote longevity. Therefore, this thesis aims to highlight the importance of antiaging nutraceuticals (natural and/or synthetic) in the field of some of the main aging-related diseases. It is intended to summarize the main findings of supplementation therapy, which is thought to slow aging by delaying or even preventing the development of a range of chronic conditions. Furthermore, the role of some antiaging nutraceuticals and their mechanisms for extending life are taken into account, mimicking both *in vitro* and *in vivo* models, evaluating some of the main aging-related diseases like central and peripheral nerve system impairment, metabolic disorders, and muscle-skeletal disease.

## 1.1. Aging and neurodegenerative disorders

Over the last few decades, an increase in population aging has been observed, and according to a recent UN report, the global share of older adults from the age of 60 is expected to double from 2013 to 2050. [38]. These data show, on the one hand, that the average life expectancy is long, but on the other hand,

they do not frame the health status of the elderly. Individuals over the age of sixty become more and more prone to developing neurodegenerative disorders, such as Alzheimer's disease (AD) or Parkinson's disease (PD) [39]. Alzheimer's (AD) dementia is a particular onset and course of cognitive and functional decline associated with age and particular neuropathology. Alzheimer's described primary neuropathology, and in the mid-1980s, subsequently evolved into a more specific neuropathological definition that recognizes the comorbid neuropathologies that frequently contribute to clinical dementia. Deficits in the ability to encode and store new memories characterize the initial stages of the disease. Subsequent progressive changes in cognition and behavior accompany the later stages. Changes in amyloid precursor protein (APP) cleavage and production of the APP fragment beta-amyloid (Aβ), along with hyperphosphorylated tau protein aggregation, cause a reduction in synaptic strength, synaptic loss, and neurodegeneration. Metabolic, vascular, and inflammatory changes and comorbid pathologies are key components of the disease process [40]. Typically, AD onset is likely driven by a complex interplay between genetic and environmental factors. It is now thought that about 70% of AD risk is attributable to genetic factors. For example, the APOE gene, which has three variants, ε2, ε3, and ε4, is the single biggest risk for sporadic AD: compared to non-ε4 carriers, ε4 heterozygotes have an odds ratio (OR) for AD of approximately 3, rising around 12 in homozygotes. Genome-wide association studies using thousands of samples have identified more than 20 genetic risk factors, implicating inflammatory, cholesterol metabolism, and endosomal-vesicle recycling pathways. These relatively common risk genes each confer only a minimal increased risk, but combined in a polygenic risk score can almost double case prediction from chance. In particular, microglial activation in response to amyloid deposition is now recognized to play a crucial role in AD pathogenesis [41]. Instead, PD is the most common neurodegenerative motor disorder, in which dysfunction of movements results from the progressive death of dopaminergic neurons in the *substantia nigra pars compacta* [42]. Parkinson's disease is manifested by motor and non-motor symptoms. The classic findings of Parkinson's disease are motor symptoms. They include resting tremors, bradykinesia, postural instability, and rigidity. The pathological hallmark of Parkinson's disease is depigmentation of the substantia nigra and locus coeruleus with neuronal loss in the *pars compacta* of the *substantia nigra*. Both apoptosis and autophagy are involved in the process. Neuronal loss is also seen in the basal nucleus of Meynert and the dorsal motor nucleus of the vagus nerve. Lewy bodies, eosinophilic cytoplasmic inclusion bodies containing alpha-synuclein, are noted in affected areas. The primary cause of Parkinson's disease remains unclear. How Lewy bodies are specifically related to the disease's progression is unknown. Current theories of how neuronal loss occurs in Parkinson's disease include mitochondrial dysfunction, inflammation, abnormalities in protein handling, and oxidative stress. [43]. However, Parkinson's disease involves neurotransmitters other than dopamine and regions of the nervous system outside the basal ganglia. Previously, Parkinson's disease was thought to be caused primarily by environmental factors, but research reveals that the disease develops from a complicated interplay of genetics and environment. Thus, Parkinson's disease is now viewed as a slowly progressive neurodegenerative disorder that begins years before the diagnosis can be made, implicates multiple neuroanatomical areas, results from a combination of genetic and environmental factors, and manifests with a broad range of symptoms [44].

The main feature that unites these conditions is the neurotoxic aggregation of specific proteins in the brain. A link was also found between oxidative stress and the development of neuronal plaques, as well as a link between the formation of the beta-amyloid peptide and ROS 45]. Specifically, oxidative

stress leads to the aggregation of $\alpha$-sinuclein in dopaminergic neurons, which in turn induces the formation of intracellular ROS [46]. Finally, the activity of antioxidant enzymes is greatly decreased, and the production of ROS induces lipid peroxidation, causing a reduced membrane permeability and triggering cytotoxicity mechanisms through an increased calcium inflow. High levels of ROS are, therefore, related to the impaired mitochondrial activity; indeed, mitochondria exert crucial functions in most neurodegenerative diseases. When mitochondrial activities are impaired, low production of ATP, high levels of ROS, and apoptosis occur [47]. Inevitably, therefore, neurons expressing the APP show reduced motility and density in axons [48]. Similarly, the tau protein alters mitochondrial traffic in the neuronal cell, resulting in impaired mitochondrial transport [49]. All these events contribute to the loss of neuronal cells that cannot be replaced, leading to cognitive decay.

As with other organs and systems, the brain's functional abilities decrease progressively during aging: as age progresses cognitive performance undergoes a general decline that is manifested by decreases in learning, in memory, attention, decision-making speed, sensory perception and motor coordination [50]. Age-related cognitive impairment is associated with changes in the central nervous system, especially in the prefrontal cortex and hippocampus. These changes can lead to the development of neurodegenerative diseases [51]. More specifically, brain physiological aging is associated with alterations in brain architecture; for example, brain weight decreases by 2-3% every decade after fifty years, characterized by an increase in a state of low-grade inflammation [52]. Some studies have shown that physiological brain aging has been associated with the increase of proinflammatory cytokines, but present in much higher concentrations in the case of neurodegenerative diseases. The formation of a proinflammatory environment speeds up neuronal aging contributing to the onset of cognitive disorders and the promotion of neurodegenerative processes [53]. So with aging it is possible notice a change in the phenotype of microglia cells: in older individuals microglial cells present larger cellular bodies, index of an activated and set phenotype to respond to proinflammatory stimuli with the release of cytokines. Astrocytes also change with age, in fact in older individuals they produce greater amounts of fibrillar acid proteins (GFAP) and pro-inflammatory factors. With advancing age, therefore, microglia and astrocytes provide less support to neurons and promote the formation of a highly proinflammatory microenvironment in the brain [53]. In particular, neuronal aging has also been associated with ROS-induced inflammation, as it modulates the production of pro-inflammatory factors such as cytokines, causing cognitive dysfunction and memory loss [54]. To overcome this condition, recent studies have identified the use of neurotropophins as a possible therapeutic targe to slow down cognitive decline. In this context brain-derived neurotrophic factor (BDNF) is one of the most distributed and extensively studied neurotrophins in the mammalian brain. Many studies shown how BDNF could act as a potent protective factor that is able to confer protection against neurodegeneration. It regulates many different cellular processes involved in the development and maintenance of normal brain function by binding and activating the TrkB, a member of the larger family of Trk receptors. In the brain, BDNF is expressed by glutamatergic neurons, glial cells, such as astrocytes isolated from the cortex and hippocampus, but not from the striatum, and microglia. Several lines of evidence also suggest that the BDNF/TrkB signaling is involved in adult neurogenesis in the hippocampus with differing effects in the dentate gyrus (DG) and subventricular zone (SVZ). Adult neurogenesis in the dentate gyrus is enhanced by voluntary exercise, exposure to an enriched environment, and chronic antidepressant administration. In addition, studies also show that BDNF is

an important regulator of synaptic transmission and long-term potentiation (LTP) in the hippocampus and in other brain regions. The effects of BDNF on LTP are mediated by the TrkB receptor. Especially in the hippocampus, this neurotrophin is thought to act on both the pre- and post-synaptic compartments, modulating synaptic efficacy, either by changing the pre-synaptic transmitter release, or by increasing post-synaptic transmitter sensitivity to induce a long-lasting increase in synaptic plasticity. Additionally, converging data now suggest a role for BDNF in the pathophysiology of brain-associated illnesses. Deficits in BDNF signalling are reported to contribute to the pathogenesis of several major diseases, such as Huntington's disease, AD, depression, schizophrenia, bipolar, and anxiety disorders [55]. Neurotrophic factors have been extensively investigated in the context of neurodegenerative diseases. The alterations in the regulation of specific neurotrophic factors and their receptors seem to be involved in neurodegeneration. Neurotrophins prevent cell death and support neuronal proliferation and maturation, enhancing the growth and function of affected neurons in AD and PD. In current therapies for AD and PD which focus on prevention of neurodegeneration, application of neurotrophic factors has emerged as one of the therapeutic approaches in early, middle and even late stages of these disorders. By activating the PI3K/Akt kinase pathway, neurotrophins inhibit processes that elicit cell death. It was found that the decrease in expression of NTs, especially BDNF observed in the aging process and in neurodegenerative diseases, may contribute to degeneration and death of neurons. A decrease in BDNF levels in the blood and brain was observed in patients with depression or suffering from PD and AD. Decreased BDNF concentration in serum and brain is accompanied by an increase in degeneration of dopaminergic neurons in PD, which leads to movement disorders, cognitive deficit, and mental disorders and also correlates with memory impairment in AD. There are data indicating that a decrease in BDNF levels in PD may contribute to overexpression of alpha-synuclein (ASN) and inhibition of dopamine (DA) synthesis. Moreover, it was reported that ASN overexpression downregulated BDNF transcription and impaired BDNF trafficking in neurons. BDNF participates in the regulation of tyrosine hydroxylase (TH), which is also reduced in PD, consequently leading to motor disorders. The neuroprotective effect of BDNF is the result of activation of the TrkB/MAPK/ERK1/2/PI3K/Akt pathway, which leads to attenuation of apoptosis, glutamate, and nitric oxide (NO) neurotoxicity and cell damage caused by oxidative stress. An increase in oxidative stress, glutamate neurotoxicity, NO production, and the process of apoptosis are observed in PD and other neurological disorders [56]. A deficient BDNF/TrkB underlies neurodegeneration. It was demonstrated that deprivation of BDNF/TrkB increases inflammatory cytokines and activates the JAK2/STAT3 pathway, resulting in the upregulation of transcription factor C/EBPβ. This, in turn, results in increased expression of δ-secretase, leading to both APP and Tau fragmentation by δ-secretase and neuronal loss, which can be blocked by expression of STAT3 Y705F, knockdown of C/EBPβ, or the δ-secretase enzymatic-dead C189S mutant. Inhibition of this pathological cascade can also rescue impaired synaptic plasticity and cognitive dysfunctions [57].

## 1.2. Peripheral nervous system dysfunction

Peripheral nervous system (PNS) aging is poorly understood. While sensorimotor peripheral nerve impairment has been related to falls and mobility disability, the association of sensorimotor impairments to other peripheral (e.g., autonomic function) and central (e.g., cognition) nervous system declines are less clear [58]. Aging profoundly influences several morphologic and functional features

of the PNS. Morphologic studies have reported a loss of myelinated and unmyelinated nerve fibers in elderly subjects and several abnormalities involving myelinated fibers, such as demyelination, remyelination, and myelin balloon figures. The deterioration of myelin sheaths during aging may be due to a decrease in the expression of the major myelin proteins (P0, PMP22, MBP). Axonal atrophy, frequently seen in aged nerves, may be explained by a reduction in the peripheral nerve's expression and axonal transport of cytoskeletal proteins. Aging also affects functional and electrophysiologic properties of the PNS, including a decline in nerve conduction velocity, muscle strength, sensory discrimination, autonomic responses, and endoneurial blood flow. The age-related decline in nerve regeneration after injury may be attributed to changes in neuronal, axonal, Schwann cell, and macrophage responses [59]. Changes in the structure of peripheral nerves during aging include the loss of axons and demyelination, which may impair electrical conductance along the nerve. Indeed, studies in rodent models of aging and premature aging (progeria) have reported age as a risk factor for the decline in the function of peripheral sensorimotor nerves. The myelin sheath produced by Schwann cells that surrounds the large, myelinated nerve fibers is enriched in both lipids and proteins, which could leave the peripheral nerve environment highly vulnerable to oxidative damage [60]. The PNS is comprised of three types of cells: neuronal cells, glial cells, and stromal cells. Key roles are played by cells other than neurons in the maintenance and function of the peripheral nerves. Schwann cells heath nerves in a layer of myelin and provide trophic support by releasing important neurotrophins such as the Nerve Growth Factor (NGF). Myelin improves conduction velocity by limiting the sites of ionic transfer along the axon to the nodes of Ranvier, resulting in a faster, "jumping" action potential propagation that is termed saltatory conduction. The most heavily myelinated fibers are the large motor neurons (Type A$\alpha$), followed by afferent muscle spindles (Type A$\beta$). Nerve conduction velocities in these neurons are approximately 30-120m/s. Unmyelinated neurons (Type C), such as the sensory neurons involved in transmitting pain and temperature and postganglionic sympathetic, are the slowest, conducting at approximately 1-2 m/s. The non-neuronal cells and connective tissues surrounding neuronal axons provide a complex stromal connective tissue scaffold for the nerve and are important in understanding and classifying nerve injuries. Encasing the individual axons is the deepest structural layer, the endoneurium. The perineurium circumferentially bundles axons together to form fascicles. The outermost connective tissue layer of the nerve, the epineurium, consists of two parts. Dispersed between fascicles is the epifascicular epineurium while surrounding the nerve trunk proper is the epineural epineurium. Microvessels progressively branch through the nerve according to the structural layers providing blood to the axons. Due to their more peripheral location, epineural vessels are more susceptible to trauma than the deeper vessels of the nerve [61].

There are three essential pathologic reactions of peripheral nerves induced by toxic agents: neuronopathy, in which the injury is concentrated on the neuronal cell body; axonopathy, in which the axon is the primary site of injury; and myelinopathy (demyelination), in which the myelin sheath or Schwann cell are involved. Primary damage to the axon (axonopathy) leads to loss of the distal axon and secondary disintegration of its myelin sheath, sometimes with swelling and chromatolysis of the neuronal cell body (i.e., the "axonal reaction") to support axon regrowth. Primary injury to the cell body (neuronopathy) can destroy the neuron cell body and cause irreparable secondary loss of its axon and associated degeneration of the entire myelin sheath. Direct damage to the myelin sheath or Schwann

cell leads to early segmental demyelination associated with retained axons (as shown). However, in a later stage, the axon also may undergo secondary degeneration due to the loss of trophic factors produced by Schwann cells. Rectangular structures at the end of axons are representative of portions of innervated skeletal muscle fibers [62].

Peripheral demyelinating diseases (PDD) refer to a spectrum of disorders that involves substantial damage to axons and glial cells, particularly Schwann cells in the PNS. The incidence of these diseases is variable. Disease states are manifestations of damage against the myelin sheath caused by various inciting factors, such as infectious agents, auto-immune processes, or genetic mutations. Oxidative stress, the primary risk factor in many diseases, has also been implicated in demyelination disorders [63]. Myelination is a process whereby Schwann cells develop a multi-layered membrane called the myelin sheath around the axonal membrane. More giant axons (>1 um) are explicitly selected by Schwann cells to form multiple internodes of the myelin sheath. Myelination begins with the establishment of a 1:1 relationship with the axon. At this level, the production of myelin structural proteins such as myelin protein zero (P0), peripheral myelin protein (PMP22), and myelin basic protein (MBP) are increased along with lipid biosynthesis [64]. The myelin sheath is made of multiple sleeves of whitish lipoprotein plasma membranes of Schwann cells wrapped around the axon of a neuron in a spiral fashion. It is constituted of water, lipid, and proteins that exist as the segmented internodal structure around the axons. These internodes create insulation that facilitates the propagation of action potentials through saltatory conduction (jumping) at the node of Ranvier. Myelin sheath not only facilitates the conduction velocity of nerve impulses but also confers protection and nutritional support to axons. However, exposure to various factors such as autoimmunological insult, trauma, and injury to the nerve could trigger demyelination and, eventually neurodegeneration [65]. Demyelination describes the loss of the myelin sheath, where Schwann cells are being destroyed or unwrapped from axons. Demyelination causes neurological disability due to conduction block and axonal degeneration. [63]. Nowadays, treatments for chronic NP consist of different lines of therapies that are chosen according to the patient's condition [66]. Therefore, strategies to improve axonal regeneration, neuronal survival, myelination, and reinnervation of target organs after nerve injury, include surgical and non-surgical therapeutic approaches are available [67]. Despite the progress in understanding the pathophysiology of peripheral nerve injuries, the advancement in reconstructive microsurgery, and the innovations in the fields of tissue engineering and regenerative medicine, there are no repair techniques or therapeutic approaches that can ensure full recovery of normal sensorimotor functions of adult patients following severe nerve injuries [68]. In this context, many supplements have been shown to be useful in counteracting the degeneration of the peripheral nervous system. Recent research has emphasized the anti-inflammatory and immune-modulating role of palmitoylethanolamide (PEA) as it has a neuroprotective effect, acting on several molecular targets in the central and peripheral nervous system [69]. In addition, PEA is an endogenous agonist of endocannabinoid system, acting on CB1 and CB2 receptors, having been described as a valuable option to successfully modulate chronic NP in animal models, bringing an alternative of treatment for patients that do not respond well to other pharmacological therapies [70]. At the same time, numerous studies have described distinct biological effects of *Equisetum arvense* L. extracts, for instance antioxidant and neuroprotective properties [71], since it plays an important role in the oxidative stress response mechanism and in the activation of SIRT1 mediating chronic pain associated with peripheral nerve injury [72].

## 1.3. Metabolic syndrome and cardiovascular disease

As is well known, a high blood cholesterol level is the 6th highest risk factor for death worldwide and several factors can raise cholesterol levels in humans. Cholesterol increases the risks of heart disease, stroke, and other vascular diseases. Globally, one-third of ischemic heart disease is attributable to high blood cholesterol. Hypercholesterolemia is the root cause for atherosclerosis and other cardiac complications [33]. Individuals with elevated low-density lipoprotein cholesterol (LDL-C) and high levels of total cholesterol [73] are prone to the development of coronary heart disease through numerous pathogenetic mechanisms. The recent American Heart Association 2016 update on Heart Disease and Stroke Statistics once again verified that only 75.7% of US children and 46.6% of US adults present targeted TC levels (< 170 mg/dL for untreated children and < 200 mg/dL for untreated adults), a trend that is comparable to other Western countries [74]. Current treatment involves lifestyle changes such as diet and exercise and may include lipid-lowering therapy, depending on the severity of dyslipidemia and CV risk [75]. Specific lifestyle interventions for hypercholesterolemia include a diet low in saturated fat (< 7% of total energy), such as the Mediterranean diet and DASH (Dietary Approaches to Stop Hypertension). These and other diets high in fruits, vegetables, whole grains, nuts, low-fat dairy products, poultry, and fish, with limited portions of lean red meat and sugary foods and beverages, are the most recommended [76]. Other lifestyle changes include moderate- to high-intensity physical activity (≥ 150 min/week), weight loss of 5% to 10% for overweight or obese patients, and smoking cessation, including avoidance of passive tobacco smoke [76,77]. If maintained over the long-term, these lifestyle modifications can reduce LDL-C and non–high-density lipoprotein cholesterol (HDL-C) levels by 5% to 15% and may even significantly reduce the risk of CVD [78]. Patients unable to reach their target cholesterol goals through lifestyle interventions should consider using lipid-lowering nutraceuticals. These can be taken alone or in conjunction with pharmacological therapy, which is indicated for those with out-of-target lipid values or who are intolerant to statins [79]. Current guidelines highlight the key role of lifestyle intervention in the treatment of patients with increased cholesterol levels [80]. This is particularly true in patients whose therapeutic targets are reachable with non-pharmacological measures. Reduction in the amount of nutrients which negatively affect lipid profile is the cornerstone of diet modification: total fat intake should not exceed 35% of total caloric intake [81]; intake of saturated fatty acids (SFAs) should be reduced below 6% of total caloric intake and trans-saturated fatty acids below 1%; dietary cholesterol intake < 200 mg/day is still far to be accepted as a strong recommendation [80]. Also, consuming foods that favorably affect lipid metabolism should be encouraged. Several dietary components are supposed to improve cholesterol metabolism. These nutrients may be naturally taken with the diet by increasing the consumption of foods such as fish, nuts, vegetables, and fruits. To achieve a "therapeutic" intake of healthy nutrients, it could be helpful to supplement our diet with either artificially enriched foods or nutraceuticals. Indeed, a standard diet contains only a modest amount of these nutrients [82]. The lipid-lowering nutraceuticals currently available are varied in terms of the mechanism of action and effectiveness in reducing the cholesterol level [83]. Among these, those derived from plants are considered the best for improving the plasma lipid profile because they mainly act in reducing the levels of LDL-C which is the main approach for managing coronary heart disease (CHD) and cardiovascular (CVD) risks [82]. The literature counted over 40 nutraceuticals with a supposed beneficial effect on lipid metabolism [84]. Some of these substances have proven efficacy in reducing both serum lipids and CV risk; in

addition, some of them have been demonstrated to affect beneficially surrogate markers of vascular damage, such as arterial intima-media thickness (IMT), endothelial dysfunction and arterial stiffness [85]. However, many trials investigating the effect of nutraceuticals on lipid metabolism have important methodological drawbacks in terms of study design, population characterization and outcome selection. Several statins are commercially available, and their use can be selected based on the patient's individual needs, therapeutic goals, and tolerability [86]. Indeed, statins are recommended for dyslipidemia to reduce the risk of primary and secondary cardiovascular disease as they play an essential role in lowering LDL-C cholesterol levels, as well as having other non-lipid properties, such as inflammatory, antithrombotic, antioxidant, or antiapoptotic activity [87]. Furthermore, statin-based therapy may not be sufficient to reduce cardiovascular risk in high and very high-risk patients [86]. For this reason, research has been dedicated to the study of different natural compounds. The herbal remedies are increasingly used in an attempt to improve the lipid profile of individuals with early atherosclerosis and those with other risk factors, such as hypertension or diabetes mellitus [88]. As a result, innovative nutritional strategies have been developed to reduce major cardiovascular risk factors, including dietary changes or consumption of functional foods and dietary supplements specifically targeted for the treatment of dyslipidemia. Nowadays, there is a great need to determine a recommendation for the possible role of nutraceuticals in patients with statin-associated adverse effects. However, at the same time, it is fundamental to underline that the nutraceuticals, both in patients with good adherence to statin therapy and with statin intolerance, cannot replace drug therapy, but could help achieve therapeutic goals [87]. In this context, it is important to consider the available clinical evidence on the efficacy and safety of fermented red rice extract (RYR), a very popular natural extract with some lipid-lowering effects. It contains monacolins which are now widely accepted as lipid-lowering molecules since they inhibit 3-hydroxy-3-methyl-glutaryl-CoA (HMGCoA) reductase, the enzyme that controls the speed of the cholesterol synthesis pathway. Although monacolin K and lovastatin have the same structure, their pharmacokinetic profiles and bioavailability differ. Monacolin K is only one of several RYR components that can modify the pharmacokinetic profile of lovastatin [73]. However, several adverse effects associated with the intake of RYR products have been reported during clinical trials in a similar way to that seen from treatment with lovastatin [86]. In contrast, the scientist documented the possible synergistic effects of RYR with other antioxidants such as green tea dry extract, Coenzyme Q10 (CoQ10), and resveratrol [73]. In particular, the interaction between RYR and natural extracts with different mechanisms of action can have a synergistic effect and the study highlighted that the intake of RYR can be combined with other botanicals or other drugs, which can prevent possible side effects [86]. Several studies have shown that natural extracts containing antioxidants, or in any case able to counteract oxidative stress, can represent a promising adjuvant therapy in hypercholesterolemia. Indeed, these molecules are able to reduce the risk of cardiovascular diseases by increasing the resistance to oxidation of LDL-C [89]. Furthermore, AMP-activated protein kinase (AMPK) has recently been evaluated as a key regulator of a naturally extracted active ingredient capable of preventing CVD. For example, it is suggested that polyphenolic compounds can be used to activate AMPK to reduce oxidative damage and inflammation, which play a critical role in the development of chronic disease [90]. In nature, several nutraceutical combinations have shown significant lipid-lowering effects and a potential positive impact on cardiovascular risk by modulating the proprotein convertase subtilisin/kexin type 9 (PCSK9)

factor which plays a particular role in regulating LDL-C levels by degrading the LDL receptor (LDLr) [91].

## 1.4. Sarcopenia and osteoporosis

With the accelerated population aging and the tendency of involution of the bone and muscle tissues among older adults, the consequences of these muscular and bone changes are approaching epidemic status. One of the most pervasive and macroscopic phenomena occurring with aging is the progressive decline of skeletal muscle mass, strength, and function, leading to a condition indicated as sarcopenia. Indeed, primary sarcopenia is also called sarcopenia of aging [92]. Not only aging but also physical inactivity, neuromuscular compromise, resistance to postprandial anabolism, insulin resistance, lipotoxicity, endocrine variables, oxidative stress, mitochondrial dysfunction, and inflammation are some of the pathophysiological pathways that lead to sarcopenia [93]. The prevalence of sarcopenia ranges from 3% to 24% depending on the diagnostic criteria used and increases with age, indeed it is also found in concurrence with rheumatoid arthritis [93]. Sarcopenia is generally thought to be a major risk factor for poor health outcomes linked to disability, frailty, loss of independence, morbidity, and death in older persons, it is also related with a lower quality of life and, even if several factors are involved in its pathophysiology, its etiology is still unclear [94]. The health care system will soon face the challenge of a dramatic increase in the prevalence of sarcopenia because the number of elderly individuals is increasing [95]. According to more recent research, several mechanisms that change the physiology of skeletal muscle are usually responsible for sarcopenia's beginning and progression. Some of these mechanisms are also considered significant contributors to the aging process. Endocrine alterations, loss of regenerative ability, denervation of muscle fibers, increased deposition of intermuscular and intramuscular fat, mitochondrial dysfunction, oxidative stress, and inflammation are a few of the factors involved in the pathophysiology of sarcopenia [96]. These two latter mechanisms, in particular, are also involved in the aging process and the loss of regenerative capacity of satellite cells, the muscle's stem cells. Emerging epidemiological and molecular studies indicate that immunosenescence and inflammaging strongly contribute to the pathophysiology of sarcopenia [97]. Furthermore, the age-related changes in the cells of the innate immune system indirectly contribute to sarcopenia by increasing systemic inflammation. In physiological conditions, in response to damage, neutrophils migrate in skeletal muscle, followed by M1 macrophages that lead to muscle inflammation; this early phase is followed by infiltration of M2 macrophages that produce soluble factors that repair the muscle injury and promote regeneration [98]. With aging, the activity of neutrophils decreases, especially in terms of migration capacity. It has been hypothesized that once in the muscle, neutrophils with impaired migration capacity can contribute to increased inflammation [97]. In addition, an increase in pro-inflammatory cytokines and a protracted inflammatory response to muscle injury are linked to inadequate muscular healing, which results in muscle atrophy and weakening [99].

As already mentioned, it has been suggested that sarcopenia may be related to systemic inflammation, but this depends on how severe the inflammation is. Using data from four species (mice, rats, rhesus monkeys, and humans), a comparative analysis of skeletal muscle changes at various ages revealed not only a human-specific age-related rise in phosphorylated NF-kB but also a conserved decrease in mitochondrial content and reduction in oxidative phosphorylation complexes in both monkeys and humans [100]. Moderate inflammation is beneficial and fundamental to activate a stress response, but

when the inflammation becomes chronic and more elevated, the response to muscle injury turns detrimental. Specifically, only the metabolic quality of skeletal muscle may be impacted by a mild level of systemic inflammation present in physiological aging; in contrast, a more severe systemic inflammation (often accompanied by a local inflammation) present in a condition of accelerated aging contributes to the loss of muscle mass and strength and the development of sarcopenia [97]. Moreover, studies revealed that inflammaging contributes to the genesis of sarcopenia by affecting the balance between anabolic and catabolic muscle processes [101]. Increased levels of TNF-$\alpha$, IL-6, IL-10, and CRP in particular, promote the breakdown of muscle protein and prevent protein synthesis by activating the NF-B and ubiquitin-proteasome pathway; this transition toward catabolism is followed by myofiber proteolysis, atrophy, and loss of regeneration capacity, which results in a reduction in skeletal muscle function [97]. Specifically, short-term increases in TNF-$\alpha$ promote the repair of muscle, while persistent TNF-$\alpha$, which will further damage the muscle [102], low or transient increases in IL-6 benefit muscle, and fiber growth, while persistently high levels of IL-6 causing muscle damage [103], IL-10 might positively regulate muscle by alleviating inflammation [104], and CRP exerts detrimental effects on muscle [105]. Recent research suggests that a self-sustaining cycle between immunosenescence, inflammaging, and oxidative stress accelerates the advancement of sarcopenia [106]. In actuality, there is a tight relationship and overlap between the molecular pathways of oxidative stress and inflammation in ROS production. These species have pathological effects on human health that are not only linked to the onset of sarcopenia but also a variety of other age-related illnesses, such as common endocrine dysfunctions associated with old age, such as decreased pancreatic beta-cell function and thyroid autoimmunity, among others [106]. Unrestrained oxidative stress and inflammation accumulation may serve as a transitional stage between slow aging and accelerated aging. Muscle deterioration is frequently accompanied by additional pathophysiological signs of accelerated aging, such as increased fat mass and reduced bone density, which can result in osteoporosis and obesity [107]. Furthermore, the literature has documented a few mechanisms on how sarcopenia and bone interact, through genetic, molecular, mechanical, and functional alterations [108]. The complications of these conditions have a great socioeconomic impact on the population since the decline of muscle and bone strength presents manifestations in the reduction of mobility and functionality, greater predisposition to falls, fractures, functional dependence, and increased morbidity and mortality risk and so older adults who present sarcopenia and osteoporosis generally require more health care and specialized long-term care, which represents high costs and considerable social impact [108]. Even osteoporosis, like sarcopenia, is linked and commonly associated with aging. During human growth, bone tissue continues to adjust to variations in mechanical loads and its growth is controlled by osteocytes, which serve as "sensors" for stimuli and translate mechanical stress into biological signals, as well as by the ongoing activity of osteoblasts, involved in bone deposition, and osteoclasts, involved in bone resorption [109]. Bone mass decreases with changes to its structure and mechanical qualities as a result of age. These musculoskeletal degenerations have the following causes: the age-related decrease in the levels of sex hormones [110], the loss of muscle strength and increased body fat and the alteration in the expression of genes involved in proliferation/senescence and cellular metabolism [111]. Moreover, with aging, loss of osteocyte lacunar density in human cortical bone triggers the accumulation of microcracks, a sign of bone deterioration contributing to osteoporosis [112]. On a molecular level, reduction of osteoprogenitors and osteoblasts with age reduces the OPG levels which

in turn allows the activation of osteoclast-based resorption, thus tilting the balance of bone homeostasis, causing osteopenia and osteoporosis [113]. Inheritable changes in several genes have been implicated in the pathogenesis of idiopathic osteoporosis and skeletal aging [114]. Several osteoblastic genes such as *WNT10B, RUNX2, RANKL, Osterix, Osteocalcin, OPG,* and *SOST,* were found to be differentially expressed in patients with male idiopathic osteoporosis, characterized with low bone volume and decrease in trabecular number. These changes were attributed to dysfunctional osteoblasts, and reduction in *WNT10B, RUNX2, RANKL,* and *SOST* gene expression [113]. Moreover, certain *WNT1* mutations were linked to early onset osteoporosis, high fracture rate and low bone turnover [115]. The clinical signs of osteoporosis include shortening of the body, increased risk of fracture, and diminished respiratory function brought on by the curvature of the spine following vertebral fracture [116], indeed the pharmacological treatment is usually focused on the bone remodeling but also the use of natural compound is gaining popularity thanks to the presence of fewer side effects and the suitability in long-term treatment [117]. For example, clinical and experimental studies have shown that resveratrol prevented bone loss by attenuating the damage caused by oxidative stress; more specifically, resveratrol, due to its antioxidant effect, effectively decreased RANKL production and inhibited osteoclastogenesis. Moreover, resveratrol promotes the formation of osteoblasts by induction of BMP2 through Src kinase-dependent estrogen receptor activation and treatment with resveratrol also activates the osteogenic factors Runx2 and Sirtuin 1 (SIRT1) [117]. Moreover, also the extract *Artemisia* has been demonstrated to be effective in the treatment of osteoporosis since it promotes the differentiation of osteoblasts through the increase of the amount of alkaline phosphatase (ALP) [118]. Also, *Equisetum Arversum* is used in the treatment of osteoporosis since it enhances bone regeneration and inhibits osteoclastogenesis [119].

### 1.5. Osteoarticular disorders and osteoarthritis

The most common chronic diseases affecting the elderly are rheumatic and osteoarticular diseases, which include osteoarthritis (OA) and rheumatoid arthritis (RA). These illnesses impact a person's autonomy, employment capacity, and life expectancy. Similar pathophysiological processes are present in these chronic inflammatory illnesses, which include enhanced bone remodeling/resorption, a phenotype associated with aging, and a buildup of activated immune cells and soluble substances in the joints and skeletal tissue [120]. The most common chronic joint disease, OA, affects most people over 65 and is a primary musculoskeletal cause of decreased mobility in the elderly. Its prevalence rises with age. Because there are currently no effective interventions to slow the progression of OA or prevent the irreversible degradation of cartilage other than total joint replacement surgery, the precise molecular mechanisms underlying the breakdown of cartilage matrix and the development of OA are poorly understood [121]. The mechanisms responsible appear to be multifactorial and may include an age-related pro-inflammatory state that has been termed "inflamm-aging." Age-related inflammation can be both systemic and local. Systemic inflammation can be promoted by aging changes in adipose tissue that result in increased production of cytokines such as interleukin (IL)-6 and TNF$\alpha$. Numerous studies have shown an age-related increase in blood levels of IL-6 that has been associated with decreased physical function and frailty. Importantly, higher levels of IL-6 have been associated with an increased risk of knee OA progression [122]. One of the mechanisms by which aging promotes chronic inflammation that could be important in OA is through cell senescence. Cell senescence was

originally used to describe the state of growth arrest that occurred after extensive proliferation of fibroblasts induced by multiple passages in culture [123]. This form of replicative senescence has been thought to serve as a mechanism to prevent unlimited proliferation of cells that would lead to cancer. Various markers have been used to identify senescent cells, including senescence-associated β-galactosidase (SA-β-gal), increased expression of the cyclin-dependent kinase inhibitor p16INK4a, and formation of senescence-associated heterochromatin. Cell senescence is not just a phenomenon observed with cultured cells, but rather senescent cells have been shown to accumulate in various tissues with aging [124].

Ageing-associated changes that affect articular tissues promote the development of OA [125]. Various processes contribute to the development of OA by promoting a proinflammatory, catabolic state accompanied by increased susceptibility to cell death that together led to increased joint tissue destruction and defective repair of damaged matrix [126]. During the early stages of OA, the cartilage surface is still intact: the molecular composition and organization of the extracellular matrix is altered first [127]. The articular chondrocytes, which possess little regenerative capacity and have a low metabolic activity in normal joints, exhibit a transient proliferative response and increased matrix synthesis attempting to initiate repair caused by pathological stimulation. This response is characterized by chondrocyte cloning to form clusters and hypertrophic differentiation, including expression of hypertrophic markers such as Runx2, ColX, and Mmp13 [128]. Changes in the structure and composition of the articular cartilage encourage chondrocytes to create more catabolic substances that contribute to cartilage breakdown. The collagen network then breaks down, which disturbs the integrity of the cartilage. The articular chondrocytes will thereafter experience apoptosis, leading to the eventual loss of all articular cartilage. Because of the reduced joint space brought on by the complete loss of cartilage, there will be pain and restricted joint movement. Other symptoms of OA include loosening and weakening of muscles and tendons, subchondral sclerosis, bone eburnation, osteophyte growth, and more [129]. In addition to growth arrest, senescent cells exhibit a number of other features that include secretion of pro-inflammatory cytokines, chemokines, growth factors, and matrix metalloproteinases (MMPs) which has been referred to as the senescence-associated secretory phenotype (SASP) [130]. The SASP could promote age-related pathologies, such as osteoarthritis, by increasing local levels of pro-inflammatory mediators and matrix degrading enzymes. Freund et al [131] composed a list of 83 SASP factors that had been reported in the literature in studies examining various inducers of cell senescence. The factors were divided by the level of increase from high (>4 fold) to intermediate (2-4 fold) to small (<2 fold). Interestingly, all of the SASP factors produced at high levels by senescent cells have been found in OA tissues and/or synovial fluid. These include GM-CSF, GROα,β,γ, IGFBP-7, IL-1α, IL-6, IL-7, IL-8, MCP-1, MCP-2, MIP1α, MMP-1, MMP-10, and MMP-332-38. Many of the SASP factors present at intermediate levels, such as ICAM-1, IL-1β, MCP-4, MIF, MMP-13, oncostatin M, RANTES, and TIMP-2 have also been recognized as potential mediators in OA [132-134]. The mechanisms responsible for cell senescence and in particular for the SASP are still being elucidated but appear to include DNA damage and activation of the p38 MAP kinase [135]. Another consistent finding has been expression of p16INK4a that activates the pRB tumor suppressor and promotes formation of senescence-associated heterochromatin foci which function to silence genes regulating cell proliferation [136]. Deletion of cells expressing p16INK4a in mice was found to prevent the development of age-related changes in tissues that included muscle, adipose tissue, and the eye

[137]. As detailed above, chondrocytes in OA have been found to have evidence of DNA damage that could promote the development of a senescent phenotype [138] and have been shown to have increased expression of p16INK4a. Knockdown of p16INK4a in cultured OA chondrocytes restored matrix gene expression [139]. Studies of the role of p16INK4a in promoting the SASP in chondrocytes are warranted and would increase the understanding of the mechanisms by which chondrocyte senescence contributes to a pro-inflammatory state in cartilage. There is biologic evidence to suggest a link between age-related inflammation and the development of OA. The sources of age-related pro-inflammatory mediators that might contribute to OA include both peripheral sources, such as adipose tissue that increases with age, as well as local production within joint tissues. Although cell senescence and the development of the SASP serves as an attractive mechanism linking aging, inflammation, and OA, there is insufficient evidence that this occurs with normal aging in joint tissues. Excessive mechanical loading of the joint that is severe enough to lead to OA may result in stress-induced senescence and increased production of pro-inflammatory mediators [122]. Given that OA is a chronic disease that becomes more prevalent with age, it is difficult to separate effects of age from disease, particularly in studies of human tissues. It seems unlikely that any single pro-inflammatory mediator plays a key role in linking aging and OA. At least in male mice, deletion of IL-6, the cytokine that has been perhaps most closely related to aging, resulted in more severe rather than less severe OA [140]. Future studies will need to examine the balance of multiple pro-inflammatory and anti-inflammatory factors in order to better understand mechanisms by which this balance is disrupted in aging. Targeting these mechanisms and restoring a proper balance may help to slow or stop the progression of age-related chronic conditions including OA.

Given these premises, nutraceuticals are value-added dietary supplement products having immense potential in modulating key mechanisms and functions related to ageing, acting mainly to restore the impaired physiological mechanisms and metabolic processes. Therefore, this PhD thesis aims to clarify from an experimental scientific point of view the mechanism of action of some novel longevity-related natural products useful in the field of health improvement during ageing. Notably, it reported new strategies based on dietary supplements (chosen by their biological properties on the target site), analyzing their beneficial effects related to the down-regulation of the biological processes in the specific field, including neurodegenerative disorders and cognitive impairment, peripheral nervous system dysfunction, metabolic syndrome and cardiovascular disease, sarcopenia and osteoporosis, osteoarticular disorders and osteoarthritis, which are described in detail in the following chapters.

# 2) THE ROLE OF BDNF ON AGING-MODULATION MARKERS

Research on neuronal ageing is taken from the article entitled "*The Role of BDNF on Aging-Modulation Markers*" [141]. Research on brain aging and on neurodegenerative diseases is one of the most important challenges that the scientific community has been facing in recent years. The mechanisms underlying brain aging recently described an important role exerted by a class of cell growth and survival factors called neurotrophins. Neurotrophins belong to a family of small proteins playing a fundamental role in both the central and the peripheral nervous systems. The main functions of these proteins are the regulation of axonal growth and neuronal differentiation. The neurotrophins family includes nerve growth factor, neurotrophin-3, neurotrophin-4/5 and even more important, brain-derived neurotrophic factor (BDNF). Therefore, the aim of this study was to analyze the effect of low doses of BDNF on ROS production in both cultured astrocytes and cortical neurons by observing the behavior of endogenous antioxidant mechanisms. Furthermore, experiments were carried out to improve the tolerability of the substance by studying its ability to exert beneficial effects on the molecular pathways linked to viability in the nervous tissue. Finally, experiments were conducted both *in vitro* and *in vivo* to evaluate the characteristics of intestinal absorption after oral intake of BDNF and to evaluate the ability of BDNF to cross the BBB.

## 2.1. MATHERIALS AND METHODS

### 2.1.1. Preparation of BDNF Solutions
All dilutions were prepared starting from a stock solution (0.001 ng/mL) of BDNF 4CH in 0.9% NaCl. Based on previous knowledge on activated blends [142], BDNF solutions were prepared at two different concentrations: 1 pg/mL for *in vitro* studies and 1.20 pg/mL for *in vivo* studies. Each concentration was prepared using the sequential kinetic activation (SKA) method [142]. These solutions are kinetically energized by a mechanically applied force via a standardized shaking process (sequential kinetic activation named SKA), characterized by vertical shaking corresponding to 100 oscillations in 10 s. All solutions were prepared by GUNA Laboratories (GUNA S.p.a, Milan, Italy). For each treatment, the volume of each solution was calculated by comparing the volume added to the sample treated with 50 ng/mL BDNF for *in vitro* study [143] and with 25ng/mL BDNF [144] for *in vivo* experiments. The BDNF used to compare the results obtained with BDNF 1 pg/mL SKA was not subjected to SKA treatment in order to replicate the same experimental conditions as in other studies.

### 2.1.2. Astrocytes Isolation
Primary mouse astrocyte cultures were extracted from C57BL/6 mouse pups, following a classical technique [145] according to the National Guideline for the Use and Care of Laboratory Animals. Briefly, within 24 h of birth pups were euthanized, and cortices were dissected, minced, mechanically digested and left to settle for 30 min at room temperature. The cell suspension was centrifuged at 800 rpm for 5 min and pelleted cells were resuspended in Neuronal Basal Medium (Sigma-Aldrich, Milan, Italy) supplemented with 5% fetal bovine serum (FBS, Sigma-Aldrich, Milan, Italy), 1% penicillin/streptomycin (Sigma-Aldrich, Milan, Italy) and 2 mM L-glutamine (Sigma-Aldrich, Milan,

Italy), plated in multi-wells and maintained in culture for 6 days before treatment. The cells were plated $4 \times 10^4$ astrocytes/cm$^2$ on a 24-well Transwell support to prepare the model BBB; $1 \times 10^4$ on 96-well plates for MTT and crystal violet staining; $4 \times 10^4$ cells were plated in black 96-well plates to study oxygen consumption and mitochondrial membrane potential; $5 \times 10^4$ cells were plated on 24-well plates to analyze reactive oxygen species (ROS) production; $2 \times 10^5$ cells were plated on 24-well plates to quantify BDNF; and $1 \times 10^6$ in 6-well plates to analyze the intracellular pathways by Western blot and ERK activity by ELISA test.

### 2.1.3. Primary Cortical Neuronal Cells

Primary mouse cortical neuronal cultures were obtained from the brains of P0 C57BL/6 mouse pups, as reported in literature [146]. All procedures used in these studies follow the guidelines in accordance with the National Institutes of Health Guidelines. Cortices were dissected from embryonic brains and the tissue was mechanically dissociated and left to settle for 30 min at room temperature. After centrifuging only, the supernatant was re-suspended in Neuronal Basal medium (Sigma-Aldrich, Milan, Italy) supplemented with 2% B27 (Sigma-Aldrich, Milan, Italy), 1% penicillin/streptomycin (Sigma-Aldrich, Milan, Italy) and 2 mM L-glutamine (Sigma-Aldrich, Milan, Italy). Cells were plated on pre-coated plates with 10 μg/mL poly-L-lysine at a density of $1 \times 10^6$ cells/mL and were maintained in incubator at 37 °C with 5% CO$^2$ and 95% humidity. At three days from plating, the medium was changed. All experiments were performed on primary cortical neuronal cells grown for 9–10 days *in vitro*. The cells were plated $1 \times 10^4$ on 96-well plates for MTT; $5 \times 10^4$ cells were plated on 24-well plates to analyze reactive oxygen species (ROS) production; $2 \times 10^5$ cells were plated on 24-well plates to quantify BDNF; and $4 \times 10^4$ cells were plated in black 96-well plates to study oxygen consumption and mitochondrial membrane potential.

### 2.1.4. *In vitro* Experimental Protocol

Before treatment, both primary cortical neuronal cells and astrocytes were maintained in Dulbecco's modified Eagle's medium (DMEM, Sigma-Aldrich, Milan, Italy) without red phenol and FBS, supplemented with 1% penicillin/streptomycin (Sigma-Aldrich, Milan, Italy) 2 mM L-glutamine (Sigma-Aldrich, Milan, Italy) and 1 mM sodium pyruvate (Sigma-Aldrich, Milan, Italy) at 37 °C, 5% CO$_2$ and 95% humidity for 1h. Cells were treated with 1 pg/mL BDNF SKA and 50 ng/mL BDNF at T0, checked every 24 h, and maintained for 6 days (named 6 days protocol). The vehicle, a saline solution, was also analyzed. Moreover, the involvement of TrkB using a specific antagonist, 1 μg/mL ANA-12 (Sigma-Aldrich, Milan, Italy) [147] treating cells 30 min before stimulation was investigated. Additional experiments were carried out to analyze the ability of BDNF solutions to restore the damage caused by oxidative stress, a major cause of aging and neurodegeneration. Both cortical neuronal cells and astrocytes were pre-treated with 200 μM H$_2$O$_2$ (Sigma-Aldrich, Milan, Italy) [148] for 30 min and then treated with 1 pg/mL BDNF SKA and 50 ng/mL BDNF. Finally, astrocytes were used in time-course study within 24 h to mimic the human posology.

### 2.1.5. Intestinal Barrier *In vitro* Model

CaCo-2 cells (human epithelial colorectal adenocarcinoma cells), purchased from American Type Culture Collection (ATCC, Manassas, VA, USA), were used as an experimental model [149] to predict

the features of intestinal absorption following oral intake [150]. These cells were grown in a complete medium composed of Dulbecco's Modified Eagle's Medium/Nutrient F-12 Ham (DMEM-F12, Sigma-Aldrich, Milan, Italy) supplemented with 10% fetal bovine serum (FBS, Sigma-Aldrich, Milan, Italy), 2 mM L-glutamine (Sigma-Aldrich, Milan, Italy), 1% penicillin-streptomycin (Sigma-Aldrich, Milan, Italy) and maintained in an incubator at 37 °C with 5% $CO_2$ and 95% humidity. Cells were used from passages 46 to 49 and seeded in 24-well polyester Corning® Costar® transwell plates (Sigma-Aldrich, Milan, Italy) in complete medium. The cells were cultured for up to 21 days in a humidified incubator maintained at 37 °C in an atmosphere of 5% $CO_2$, changing medium every 3 days first basolaterally and then apically. The monolayer integrity was checked every 3 days (at the time of the medium change) [151]. After 21 days, 1pg/mL BDNF SKA and 50 ng/mL BDNF were added to culture medium under different pH conditions, as reported in literature [151]; pH 6.5 preparations were added to the apical side, whereas pH 7.4 was added to the basolateral side. The slightly acidic pH (pH 6.5) in the apical side represents the average pH in the lumen of the small intestine, whereas the neutral pH (pH 7.4) in the basolateral side mimics the pH of the blood. During treatments, the cells were maintained in an incubator at 5% $CO_2$, and at the end of stimulations the BDNF quantity was measured by ELISA kit after 30 min and 1, 3, 4, 5and 6h from stimulation. This model is suitable to predict the absorption of substances after oral intake by evaluating the apparent permeability coefficient (Papp) [151]. Briefly, the Papp (cm/s) was calculated as [149]:

$$Papp = dQ/dt \times 1/m0 \times 1/A \times VDonor$$

dQ: amount of substance transported (nmol or μg)

dt: incubation time (sec)

m0: amount of substrate applied to donor compartment (nmol or μg)

A: surface area of transwell membrane ($cm^2$)

VDonor: volume of the donor compartment ($cm^3$)

Negative controls without cells were tested to exclude transwell membranes influence.

### 2.1.6. Blood–Brain Barrier (BBB) Experimental Model

Astrocytes were co-cultured with human umbilical vein endothelial cells (HUVEC) cells according to methods reported in literature [152]. HUVEC were purchased from ATCC®. Cells were cultured in EGM Media (Lonza, Basel, Switzerland) supplemented with 10% FBS (Sigma-Aldrich, Milan, Italy), 1% penicillin/streptomycin (Sigma-Aldrich, Milan, Italy) and 2 mM Glutamine (Sigma-Aldrich, Milan, Italy) at 37 °C in a humidified atmosphere of 95% air, 5% $CO_2$. In brief to create the BBB barrier, $4 \times 10^4$ astrocytes/$cm^2$ were plated on the basolateral side of the flipped 6.5 mm Transwells® with polyester membrane with 0.4 μm pore size (Corning Costar, Sigma-Aldrich, Milan, Italy) and left to attach for 4 h. Transwells® were then placed into the normal orientation and the cells left to grow for 48 h. After this time, $1 \times 10^5$ HUVEC cells/$cm^2$ were plated in the apical compartment. The inserts were then placed in a 24-well plate. After 7 days of culture, the Transwells® were treated and permeability studies were performed [153]. To understand the ability of tested substances to cross the blood–brain barrier the medium at the bottom side of the Transwells® was quantified over time by measuring the volume and the concentration of BDNF.

### 2.1.7. Brain-Derived Neurotrophic Factor (BDNF) Quantification

Brain-derived neurotrophic factor (BDNF) quantification was measured by Rat BDNF Elisa Kit (Thermo ScientificTM, Waltham, MA, United States) in cellular supernatants obtained from basolateral environment of BBB, primary cortical neuronal cells, astrocytes, serum and brain tissue to quantify BDNF, following the manufacturer's instructions. Tissues were washed in saline solution, weighed, cut in small pieces and homogenized 100 mg tissue/300 μL with cold lysis buffer (0.1 M Tris, 0.01 M NaCl, 0.025 M EDTA, 1% NP40, 1% Triton X-100; Sigma-Aldrich, Milan, Italy) supplemented with 2 mM sodium orthovanadate, 0.1 M sodium fluoride (Sigma-Aldrich, Milan, Italy), 1:100 mix of protease inhibitors (Sigma-Aldrich, Milan, Italy), and 1:1000 phenylmethylsulfonyl fluoride (PMSF; Sigma-Aldrich, Milan, Italy), using an electric potter at 1600 rpm for 2 min. The tissue extracts were centrifuged at 13000 rpm for 20 min at 4 °C.

The cellular and tissue supernatants were collected, and each sample was tested by ELISA kit. Briefly, biotinylated detection antibody was added into each well and the plate was incubated for 1 h at room temperature. Then, after 45 min of incubation with HRP-conjugated streptavidin, TMB substrate solution was added for 30 min and subsequently the reaction was stopped by adding Stop Solution. BDNF concentration was determined by measuring the absorbance through a spectrometer (VICTOR X4, multilabel plate reader) at 450 nm and calculated by comparing results to BDNF standard curve.

### 2.1.8. MTT Assay

MTT-based In vitro Toxicology Assay Kit (Sigma-Aldrich, Milan, Italy) was performed on both cell types to determine cell viability, as previously described [154]. Briefly, at the end of each stimulation, the cells were incubated with 1% MTT dye for 2 –3 h at 37 °C in incubator, until the purple crystals were dissolved in equal volume of MTT Solubilization Solution. The relative viability (%) was based on absorbance measuring through a spectrometer (VICTOR X4, Multilabel Plate Reader) at 570 nm with correction at 690 nm. Finally, viability was calculated comparing results to control cells (defined as 100% viable).

### 2.1.9. Crystal Violet Staining

After each treatment astrocytes were fixed with 1% glutaraldehyde (Sigma-Aldrich, Milan, Italy) for 15 min at room temperature, washed, and stained with 100 μL 0.1% aqueous crystal violet (Sigma-Aldrich, Milan, Italy) for 20 min at room temperature. To multi-well plates, 100 μL of 10% acetic acid was added and mixed before reading the absorbance at 595 nm using a spectrometer (VICTOR X4, multilabel plate reader). The estimated number was calculated by comparing the results to the control cells counted at T0.

### 2.1.10 ROS Production

The rate of reactive species of oxygen (ROS) was measured using a standard protocol based on the addition of cytochrome C (Sigma-Aldrich, Milan, Italy) to the samples and to another sample of 100 μL superoxide dismutase (Sigma-Aldrich, Milan, Italy). They were added for 30 min in an incubator at 37 °C, 5% $CO_2$, and 95% humidity to determine the antioxidant capability of BDNF solutions on the BBB model, primary cortical neuronal cells and astrocytes. At the end of stimulations, 100 μL of

supernatant were measured at 550 nm using a spectrometer (VICTOR X4, multilabel plate reader) and O2 was expressed as the mean ± SD (%) of nanomoles per reduced cytochrome C per micrograms of protein compared to control [155].

### 2.1.11 NO Production

Nitric Oxide (NO) production was measured by Griess Assay (Promega Corporation, Madison, Wisconsin, United States). After 6 days of treatment, supernatants of basolateral BBB were mixed with equal volumes of Griess reagent and incubated in the dark at room temperature for 10 min; absorbance was measured by a spectrometer at 570 nm. NO production corresponded to the NO (µmol) produced after each stimulation by samples, each containing 1.5 µg of protein [156].

### 2.1.12 Mitochondrial Membrane Potential

The mitochondrial membrane potential was analyzed following manufacturer's instructions of Oxygen Consumption/Mito membrane Potential Dual Assay Kit (Cayman Chemical Company, Ann Arbor, MI, United States) [142]. The mitochondrial membrane potential was measured using JC-1 aggregates at an excitation/emission of 560/590 nm and monomers at an excitation/emission of 485/535 nm in a fluorescence spectrometer (VICTOR X4, multilabel plate reader). The results are expressed as means ± SD (%) compared to control cells in both cell types.

### 2.1.13 ERK Activation Assay

ERK/MAPK activity was measured by the InstantOne™ ELISA (Thermo Fisher, Milan, Italy) on astrocytes lysates following the manufacturer's instructions [155]. Briefly, 50 µL/well of astrocytes lysed with cell lysis buffer were tested in InstantOne ELISA microplate strips after 1 h at room temperature on a microplate shaker with the antibody cocktail. At the end, the detection reagent was added for 20 min and then stopped by adding stop solution. The strips were measured by a spectrometer (VICTOR X4 multilabel plate reader) at 450 nm. The results were expressed as mean absorbance (%) compared to control.

### 2.1.14 Western Blot

To perform Western blot analysis, $1 \times 10^6$ astrocytes plated in 6-well were lysed in ice with Ripa Buffer (50 mM Hepes, 150 mM NaCl, 0,1% SDS, 1% Triton X-100, 1% deoxycholate acid, 10% glycerol, 1.5 mM MgCl2, 1 mM EGTA, 1 mM NaF; Sigma-Aldrich, Milan, Italy) supplemented with 2 mM sodium orthovanadate and 1:100 mix Protease Inhibitor Cocktail (Sigma-Aldrich, Milan, Italy). 30 µg proteins were resolved on 8% and 15% SDS-PAGE gels. Brain tissue was also analyzed by Western blot to verify the mechanisms observed in cell culture. At the end of treatments brain tissue was excised out, washed in ice saline solution, weighed, cut in small pieces, and homogenized 100 mg tissue/300 µL with cold lysis buffer (0.1 M Tris, 0.01 M NaCl, 0.025 M EDTA, 1% NP40, 1% Triton X-100; Sigma-Aldrich, Milan, Italy) supplemented with 2 mM sodium orthovanadate, 0.1 M sodium fluoride (Sigma-Aldrich, Milan, Italy), 1:100 mix of protease inhibitors (Sigma-Aldrich, Milan, Italy), and 1:1000 phenylmethylsulfonyl fluoride (PMSF; Sigma-Aldrich, Milan, Italy), using an electric potter at 1,600 rpm for 2 min. The tissue extracts were centrifuged at 13,000 rpm for 20 min at 4 °C and 40µg of each lysate were resolved on 8% and 15% SDS- PAGE gel. Polyvinylidene difluoride (PVDF) membranes (GE Healthcare Europe

GmbH, Milan, Italy) obtained from cell and brain tissue lysates were incubated overnight at 4 °C with specific primary antibody: anti-phospho-tyrosine receptor kinase B (p-TrkB, Tyr515; 1:250, Santa Cruz, CA, United States), anti-tyrosine receptor kinase B (trkB; 1:250, Santa Cruz, CA, United States), anti-Apolipoprotein E (apoE, E4; 1:250, Santa Cruz, CA, United States), anti-phospho-Sirtuin1 (pSIRT1, Ser47; 1:1000, Sigma-Aldrich, Milan, Italy), anti-Phospho-p44/p42 Mitogen-activated protein kinase (pERK/MAPK, Thr202/Tyr204; 1:1000, Euroclone, Milan, Italy), anti-p44/p42 Mitogen-activated protein kinase (ERK/MAPK; 1:1000, Euroclone, Milan, Italy) and anti-Phospho-Tau (pTau, Ser262; 1:250, Thermo Fisher Scientific, Waltham, MA, United States). In addition, in brain anti-BDNF (1:500, Sigma-Aldrich, Milan, Italy) and anti-β-Amyloid (APP, B-4, 1:500, Santa Cruz, CA, United States) were also investigated. All protein expressions were normalized to the specific total protein (if possible), verified through β-actin detection (1:5000, Sigma-Aldrich, Milan, Italy) and expressed as mean ± SD (%).

**2.1.15 Animal Model**

12-month-old mice wild type C57BL/6jOlaHsd of comparable age to an elderly human (about 80 years old) [157] purchased from Envigo++++ (Bresso, Italy), were used to confirm the effects of BDNF solutions in a complex model (n = 52). Starting from a new protocol to induce a spontaneous intake [158], we created a new rissole without bromophenol blue containing 1.2 pg/mL BDNF SKA or 25 ng/mL BDNF which is voluntary eaten by old mice. The quantity of rissoles was calculated considering the quantity of food and daily water normally taken by the animals [159]. The animals had access to food and water ad libitum and the experimental subjects were transferred to a single cage and kept in a single holding room and housed in a constant temperature of 21–22 °C, humidity of 5–55%, for 3 h [158]. Due to the short time taken to administer the rissole, mice showed no signs of social deprivation, such as increased aggressiveness. These signs have in fact been observed for periods of social deprivation of 6 h [160]. After this time, the rissole was added in the lower part of the cage, but the mouse had free access to food and water in the upper part. Time of stimulation started from the addition of the rissole. During the whole period of treatment, the mice were monitored to assess their health status. Serum was obtained from blood of intracardiac withdrawal after inducing anesthesia, and brain tissue was obtained after animal death. All experimental procedures on animals were reviewed and approved by the University Committee OPBA (Organismo preposto al benessere degli animali) in accordance with local ethical standards and protocols approved by national guidelines (Approval No. 41/2019-PR). Animals were randomized into four different times of treatment: untreated (12 animals, 4 for each time of treatment), 24 h (20 animals), 24 h plus 24 h (10 animals) and 6-day protocol (only one administration for 6 days, 10 animals). In particular, 24 animals were sacrificed after 24 h and 14 animals were sacrificed after 48 h (24 h with rissole plus 24 h without rissole administration but the animals had access to food and water ad libitum in the upper part of cage). Finally, to demonstrate the efficacy of treatment, 14 animals were sacrificed 6 days after the only administration of BDNF solution (6-day protocol). All groups were sacrificed at specific time points (24 h, 24 h plus 24 h and 6 days) by $CO_2$ asphyxiation and blood drawn at the same time. The blood was centrifuged at 3500 rpm for 15 min at room temperature and the serum was conserved at −80 °C for subsequent experiments. In addition, the brain was removed, frozen and conserved at −80 °C for successive analysis by ELISA and Western blot on whole brain tissue lysates.

### 2.1.16 Statistical Analysis

Each part of the study is supported by at least 4 independent experiments both *in vitro* and *in vivo*. All results were analyzed by one-way analysis of variance (ANOVA) followed by Bonferroni post hoc test; data are expressed as mean ± SD of at least four independent experiments for each experimental protocol produced in triplicates. The percentage values were compared through Mann–Whitney U test. Comparisons between the two groups were performed using a two-tailed Student's t-test. Multiple comparisons between groups were analyzed by two-way ANOVA followed by a two-sided Dunnett post hoc testing. p-Value < 0.05 was considered statistically significant.

### 2.2. RESULTS

The effectiveness of BDNF SKA was investigated by both *in vitro* and *in vivo* experiments, comparing 1 pg/mL and 1.2 pg/mL to BDNF 50 ng/mL and 25 ng/mL, respectively.

### 2.2.1. The Potential Intestinal Absorption as Evaluated *In vitro*

Since BDNF SKA can be used by oral administration in human, the *in vitro* intestinal absorption was investigated. An *in vitro* intestinal barrier model was carried out to understand the ability of 1 pg/mLe and comparable to that of 5 BDNF SKA compared to 50 ng/mL BDNF to cross the intestinal barrier and to become available to the body. Analyzing the volume in the basolateral compartment 1 pg/mL BDNF SKA showed a significant increase in absorption capacity compared to saline and comparable to that of 50 ng/ml of BDNF at each stimulation time (Table 1). In particular, the maximum Papp, the permeability constant value, was observed at 1 h of treatment with 1 pg/mL BDNF SKA (about 4.18 ± 0.1), supporting the hypothesis that BDNF SKA can cross the intestinal barrier. Following a standard conversion to predict the human absorption after oral intake starting from the Papp values obtained from Caco-2 cells, the BDNF bioavailability in human (Table 1) showed an increase caused by 1 pg/mL BDNF SKA compared to saline solution and 50 ng/mL BDNF at each time of treatments and confirmed a higher level at 1 h of stimulation (about 4% compared to 50 ng/mL BDNF). These data confirm that 1 pg/mL BDNF SKA is able to cross the intestinal barrier and to has a good bioavailability compared to 50 ng/mL BDNF.

Since safety is the main problem affecting human use, additional experiments on ROS production were performed on the intestinal barrier to exclude any adverse effects. Both 50 ng/mL BDNF and 1 pg/mL BDNF were able to maintain ROS at physiological levels (p > 0.05 vs. saline solution and control), supporting the safe use of this substance. Besides, the higher effect of 1 pg/mL BDNF compared to 50 ng/mL was observed after 3 and 4 h of treatment (p < 0.05; compared to saline solution, 50 ng/mL BDNF and control) demonstrating the best antioxidant action of BDNF SKA.

These data support the hypothesis that BDNF SKA is able to cross the intestinal barrier and reach the blood in the first 3–4 h after oral intake.

| Stimulations | 30 min | 1 h | 3 h | 4 h | 5 h | 6 h |
|---|---|---|---|---|---|---|
| 1 pg/mL BDNF SKA | 2.91 ± 0.3 | 4.18 ± 0.1 | 3.36 ± 0.2 | 3.27 ± 0.3 | 2.02 ± 0.2 | 1.97 ± 0.3 |
| Saline | 0.11 ± 0.1 | 0.29 ± 0.1 | 0.36 ± 0.1 | 0.5 ± 0.1 | 0.57 ± 0.1 | 0.6 ± 0.1 |
| 50 ng/mL BDNF | 3 ± 0.3 | 3.98 ± 0.3 | 4 ± 0.3 | 3.2 ± 0.2 | 1.98 ± 0.2 | 1.02 ± 0.1 |
| 1 pg/mL BDNF SKA | 32.75 | 39.8 | 36.5 | 34.85 | 26.6 | 26 |
| Saline | <20 | <20 | <20 | <20 | <20 | <20 |
| 50 ng/mL BDNF | 33.2 | 38.15 | 39.8 | 33.2 | 25.8 | 20 |

Table 1. The Papp values obtained on intestinal barrier model and plasmatic human absorption derived from Papp value. Saline= saline solution Data are expressed as means +- SD (%) of four independent experiments reproduced in triplicates.

### 2.2.2 Permeability of BDNF SKA Through Blood–Brain Barrier (BBB)

Since the most important parameter after oral intake is the ability of BDNF to reach the brain tissue, more experiments were performed using the BBB *in vitro* model. The analysis on the basolateral volume of 1 pg/mL BDNF SKA and 50 ng/mL BDNF showed no significant difference between 1 pg/mL BDNF SKA and 50 ng/mL BDNF (Figure 4A), but the quantification showed a significant increase ($p < 0.05$) of both 1 pg/mL BDNF SKA and 50 ng/mL BDNF compared to control and to saline solution (about 41% and about 44%, respectively). These data suggest that only one treatment for six days appears to be more important to obtain a greater effect. Furthermore, ROS production was analyzed in order to exclude any adverse effect caused by BDNF solutions. As shown in Figure 4B, there was no difference evident between 1 pg/mL BDNF SKA and 50 pg/mL BDNF and the effects of both solutions were not significant ($p > 0.05$) compared to control, indicating a physiological ROS production. These data confirmed the hypothesis of the higher effectiveness of administration protocol.

Since maintaining the balance of oxidative condition is an important parameter to preserve the integrity of brain cells, some additional experiments were carried out to analyze NO production within the BBB (Figure 4C). At basolateral level, the NO production induced by protocol A was significantly reduced compared to control ($p < 0.05$). In particular, there was no significant difference between 1 pg/mL BDNF SKA and 50 ng/mL BDNF treatment, suggesting that BDNF solutions were not cytotoxic. These results suggest that 1 pg/mL BDNF SKA had a similar effect to 50 ng/mL SKA despite the different concentrations and that only one treatment is able to induce a beneficial effect. Finally, BDNF SKA is confirmed to act without any adverse effect at the neuronal level.
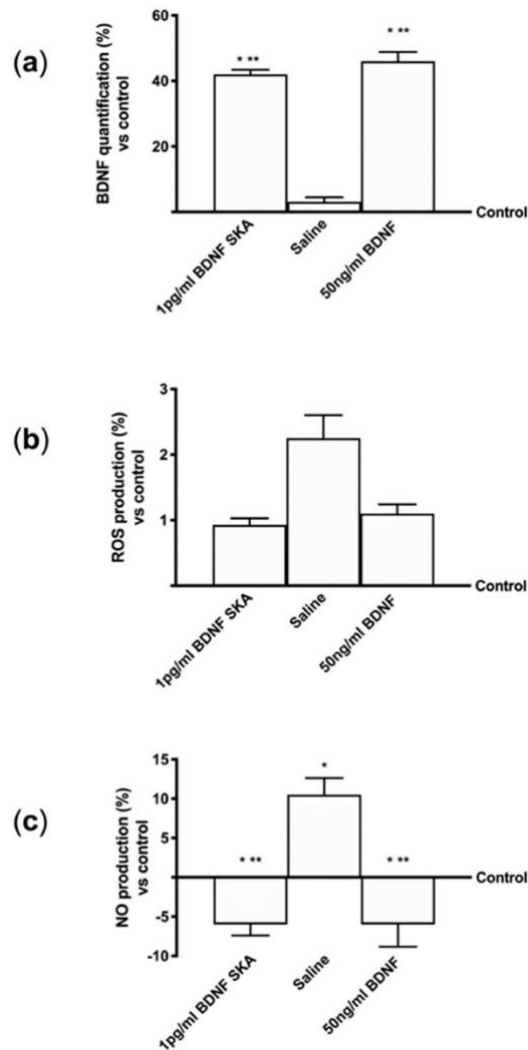
Figure 4. Analysis of the effects at blood–brain barrier (BBB) level. (a) Brain-derived neurotrophic factor (BDNF) quantification, (b) reactive oxygen species (ROS) production and (c) NO measurements are reported. Data are expressed as means ± SD (%) of four independent experiments performed in triplicates normalized to control (0 line as control). * $p < 0.05$ vs. control; ** $p < 0.05$ vs. saline solution.

## 2.2.3 Topic Action of BDNF SKA on Monolayer Culture

BDNF has been demonstrated to be able to act on both cortical neuronal cells and astrocytes, additional experiments were performed in order to investigate cell viability and ROS production in these monolayer cultured cells. In particular, 1 pg/mL of BDNF SKA induced a significantly greater cell viability (Figure 5A) both in primary cortical neuronal cells and in astrocytes compared to control ($p < 0.05$) and 50 ng/mL of BDNF (in neuronal cells approximately 124% and 75%, respectively, in the astrocytes approximately 58.6% and 171%, respectively). These findings suggest that though BDNF SKA was used at lesser concentrations it was able to determine a greater effect on cell viability compared to the higher concentration; furthermore, these results support the hypothesis of the effectiveness of the single administration compared to multiple administrations. Since an important contributing factor to brain aging is the exaggerated ROS production, additional experiments on ROS production were performed on both cell types following both protocols of treatments (Figure 5B). Results obtained from these experiments show that 1 pg/mL BDNF SKA was able to maintain ROS production within physiological range in both cortical neuronal cells and astrocytes ($p > 0.05$ vs. control). These data suggest that BDNF SKA is able to maintain the redox balance even in monolayer

cultured cells. Although 50 ng/mL BDNF also shows similar properties, the effect was significantly lower compared to 1 pg/mL BDNF SKA.

Basing on previous observation of viability and ROS production in astrocytes, the involvement of BDNF solutions in cell proliferation was also investigated by crystal violet staining. As reported in Figure 5C, 1 pg/mL BDNF SKA treatment was able to increase the proliferation of astrocytes ($p < 0.05$) compared to control (about 43.9% and 13.4%, respectively) and to saline solution (about 43.5% and 29.6%, respectively). In addition, the importance of the concentration used was confirmed as well. Indeed, 1 pg/mL BDNF SKA is more effective than 50 ng/mL BDNF (about 3.1%).
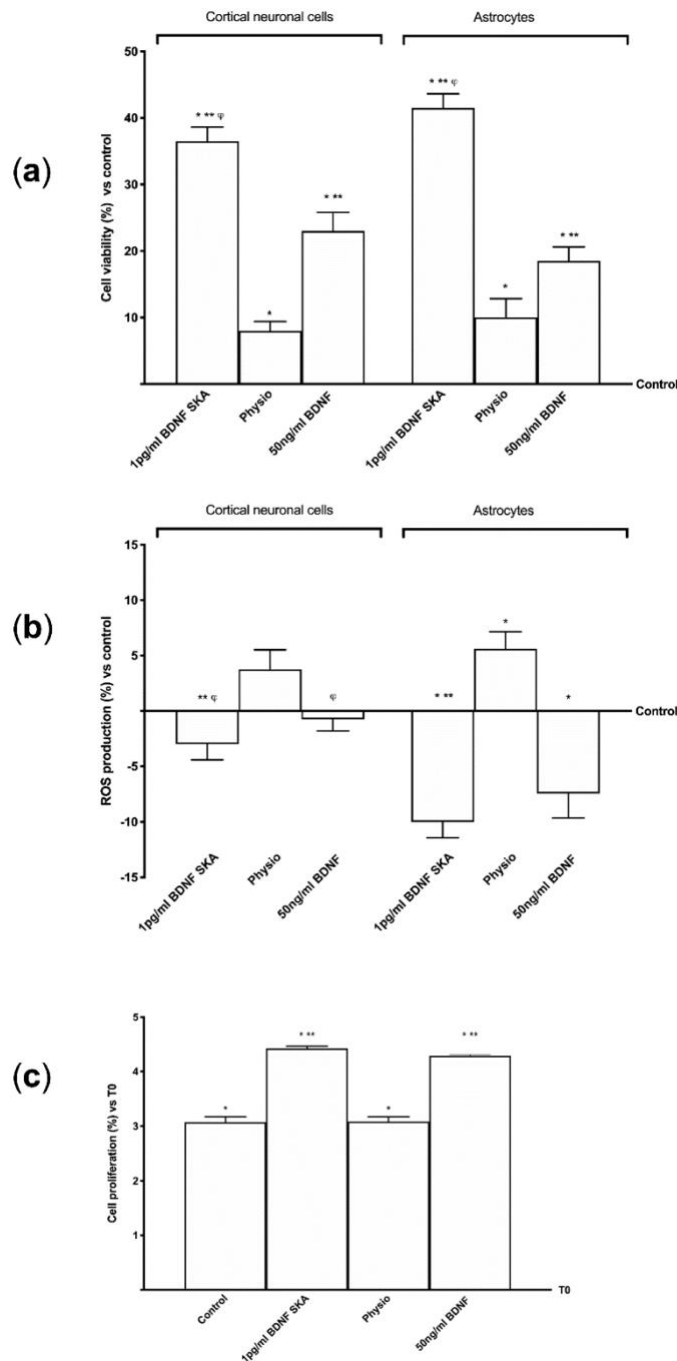


Figure 5. Effects of BDNF solutions on primary cortical neuronal cells and astrocytes. (a) Cell viability and (b) ROS production measured on both cell types. (c) The effects on astrocytes proliferation are shown. Data are expressed as means ± SD (%) of four independent experiments performed in triplicates normalized to control (0 line as control). * $p < 0.05$ vs. control; ** $p < 0.05$ vs. saline solution; φ $p < 0.05$ vs. the same treatments between primary cortical neuronal cells and astrocytes in the same protocol.

## 2.2.4 Intracellular Pathways Activated by BDNF SKA on Monolayer Culture

Since all results reported above show a better influence in astrocytes compared to the same protocol on neurons, the intracellular pathways involved were investigated only on astrocytes.

In this phase of the study, the intracellular pathways involved in the previously observed effects were studied. The effects induced by 1 pg/mL BDNF SKA on ApoE expression, SIRT1 phosphorylation, ERK/MAPK pathway and the levels of activation of the BDNF receptor, TrkB, were studied.

As reported in Figure 6A, BDNF solutions seemed to act by the TrkB receptor. No significant differences were observed between 50 ng/mL BDNF and 1pg/mL BDNF SKA, indicating the ability of 1 pg/mL BDNF SKA to lead TrkB receptor to exert its effects despite the low dose used. As far as the ApoE expression is concerned, was significantly increased by 1 pg/mL BDNF SKA ($p < 0.05$) compared to 50 ng/mL BDNF (about 80%) (Figure 6B). As illustrated in Figure 6C, phosphorylation of SIRT1 induced by 1 pg/mL BDNF SKA ($p < 0.05$) was increased compared to 50ng/mL BDNF (about 30%), supporting the efficacy of the dosage to increase the presence of this molecule. Finally, as shown in Figure 6D, BDNF has been observed to increase the ERK1/2 expression and the greater effect was obtained with 1 pg/mL BDNF SKA ($p < 0.05$) compared to 50 ng/mL BDNF (about 37%).
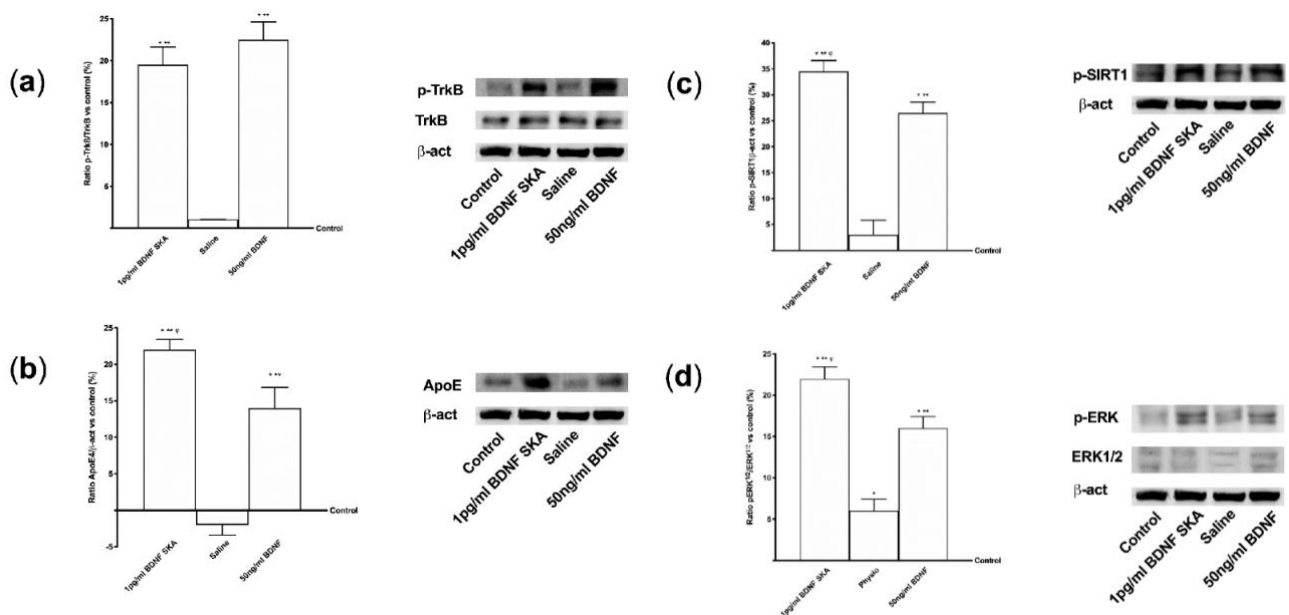


Figure 6. Analysis of intracellular pathways activated by BDNF solutions in astrocytes. In the left column densitometric analysis and in the right the examples of Western blot are reported. (a) TrkB receptor, (b) ApoE(4), (c) SIRT1 and (d) ERK/MAPK expressions are shown. Data are expressed as means ± SD (%) of five independent experiments normalized on specific total protein if possible and verified by β-actin detection. * $p < 0.05$ vs. control; ** $p < 0.05$ vs. saline solution; φ $p < 0.05$ vs. 50 ng/mL BDNF.

Additional experiments were performed to confirm the involvement of the TrkB receptor in previously observed effects, using a pre-treatment with the selective TrkB antagonist ANA-12 (1 μg/mL) on astrocytes. As reported in Figure 7, in the presence of both BDNF solutions, TrkB expression was abolished by the pre-treatment with 1 μg/mL ANA-12, confirming that both BDNF solutions acted through the TrkB receptor to explain their effects on astrocytes. These data confirm the importance of

the dosage and the protocol of treatment to obtain a beneficial effect on astrocytes under physiological conditions.
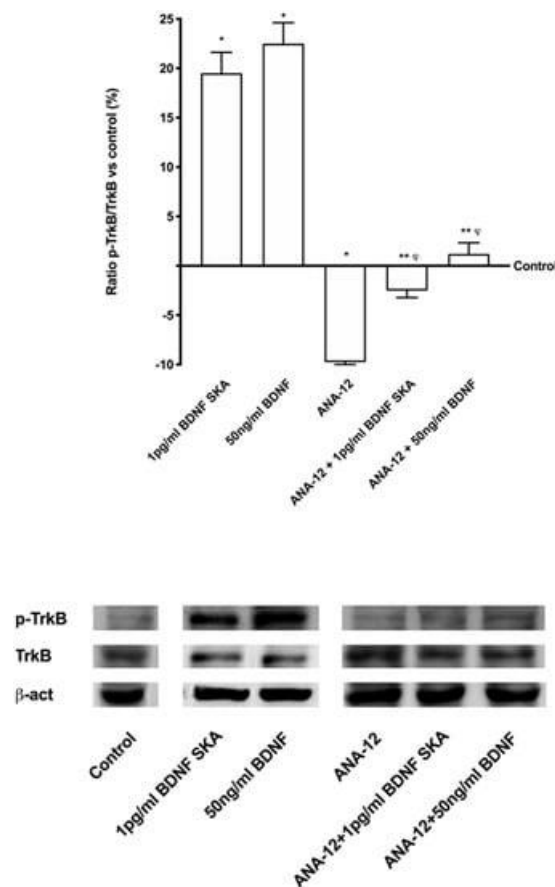


Figure 7. Analysis of TrkB receptor under blocking condition on astrocytes. In the upper panel densitometric analysis and in the lower panel an example of Western blot is reported. Data are expressed as means ± SD (%) of five independent experiments normalized on specific total protein and verified by β-actin detection. ANA-12 = 1 μg/mL ANA-12. * $p < 0.05$ vs. control; ** $p < 0.05$ ANA-12; φ $p < 0.05$ vs. the same treatments without ANA-12.

### 2.2.5 Effects of BDNF Solutions Under Oxidative Conditions

Cell viability and ROS production were evaluated in cortical neuronal cells and astrocytes in order to understand the potential aging-prevention mechanism of 1 pg/mL BDNF SKA and 50 ng/mL BDNF 50 ng/mL under oxidative conditions. Exposure to 200 μM $H_2O_2$, in both cell types significantly reduced ($p < 0.05$) cell viability compared to control (Figure 8A), indicating cell loss caused by oxidative injury. Conversely, following post-treatment with 1 pg/mL BDNF SKA and 50 ng/mL BDNF, cell viability increased in a different manner between cell types. Indeed, only in astrocytes did both BDNF solutions significantly increase cell viability ($p < 0.05$), but the main effect was observed with 1 pg/mL BDNF SKA in both cell types ($p < 0.05$ vs. $H_2O_2$ alone), confirming the importance of doses and posology also under pathological conditions. Additional experiments on ROS production were performed. Exposure of cortical neuronal cells and astrocytes to 200 μM $H_2O_2$ significantly increased the intracellular ROS production compared to control ($p < 0.05$), as illustrated in Figure 8B, confirming the presence of oxidative damage. Post-treatment with 1 pg/mL BDNF SKA and 50 ng/mL BDNF in both cell types caused a significant reduction of ROS production ($p < 0.05$) compared to $H_2O_2$ alone, supporting the hypothesis of the importance of BDNF during degeneration to prevent cell loss. These data suggest

that 1 pg/mL BDNF SKA is able to counteract the damage induced by oxidative stress with greater effectiveness compared to 50 ng/mL BDNF.
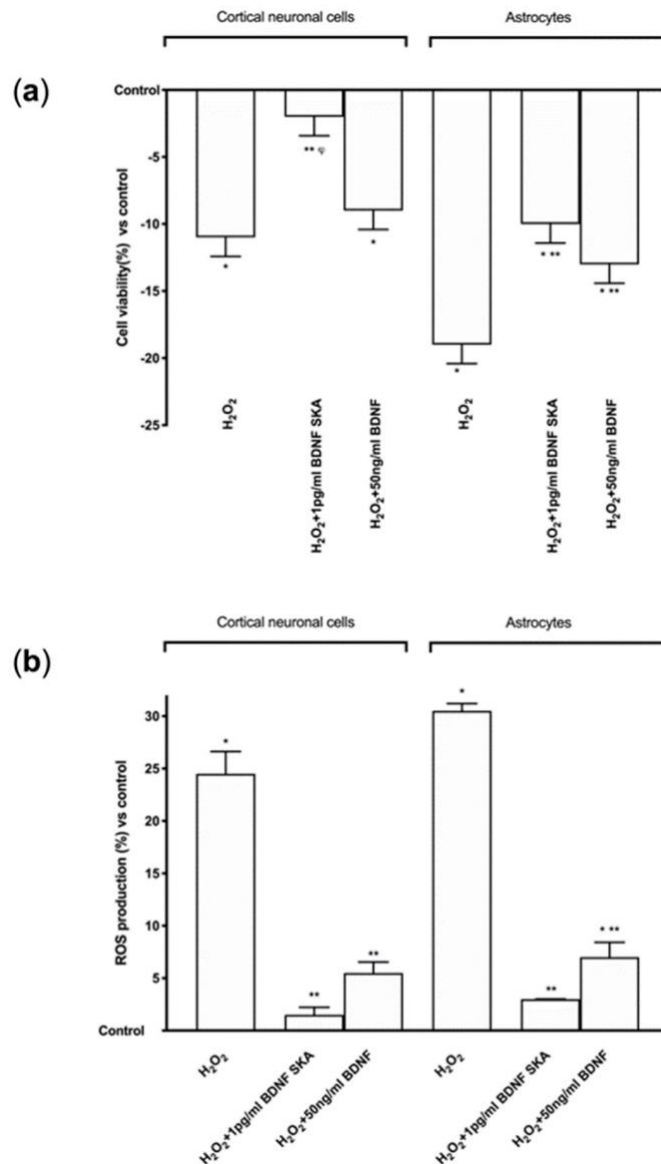


Figure 8. Cell viability and ROS production on both protocols in primary cortical neuronal cells and astrocytes under oxidative condition. (a) Cell viability and (b) ROS production measured in primary cortical neuronal cells (on the left) and astrocytes (on the right) after treatments. $H_2O_2$ = 200μM $H_2O_2$ added 30 min before stimulations. Data are expressed as means ± SD (%) of five independent experiments performed in triplicates normalized to control (0 line as control). * $p < 0.05$ vs. control; ** $p < 0.05$ vs. $H_2O_2$; φ $p < 0.05$ vs. $H_2O_2$+50 ng/mL BDNF in the same cells.

Since the data obtained from the two cell types were comparable, the analysis of intracellular pathways under oxidative conditions was conducted only on astrocytes. BDNF solutions exerted their biological actions by improving TrkB receptor expression even in the presence of $H_2O_2$, as shown in Figure 9A, ($p < 0.05$ versus control). No significant changes were observed between the two BDNF solutions. Moreover, the expressions of ApoE and of Tau, an important protein that modulates the stability of axonal microtubules, were analyzed. As reported in Figure 9B, the stimulation with H2O2 alone caused a significant decrease of ApoE expression compared to control ($p < 0.05$), indicating a loss of neuroplasticity. Conversely, the treatments with 1pg/mL BDNF SKA and 50 ng/mL BDNF repaired the

damage and the expression of ApoE was increased. In particular the main effect was observed by 1 pg/mL BDNF SKA compared to 50 ng/mL BDNF ($p < 0.05$, about ten fold larger). The presence of the damage was confirmed by Tau phosphorylation, as reported in Figure 9C, where the level was even higher than control ($p < 0.05$). After treatment with 1 pg/mL BDNF SKA compared to 50 ng/mL BDNF the phosphorylation was significantly reduced ($p < 0.05$, about 56%), indicating the efficacy of 1 pg/mL BDNF SKA to restore damage. In addition, the analysis of SIRT1 confirms the protection exerted by 1 pg/mL BDNF SKA and 50 ng/mL BDNF against $H_2O_2$ damage (Figure 9D); 1 pg/mL BDNF SKA and 50 ng/mL BDNF were able to induce a significant increase in SIRT1 phosphorylation compared to $H_2O_2$ alone ($p < 0.05$) and to control ($p < 0.05$). However, the main effect was shown by 1 pg/mL BDNF SKA compared to 50ng/mL BDNF (about 85%). All these findings support the hypothesis that treatment with BDNF SKA can protect neuronal cells from the damage induced by the aging process better than high dose BDNF. Finally, as reported in Figure 9E, the activation of TrkB induced cells' survival by the involvement of ERKs/MAPK; indeed, 1 pg/mL BDNF SKA and 50 ng/mL BDNF added after the injury were able to induce a significant increase on ERK activity compared to $H_2O_2$ alone ($p < 0.05$) and to control ($p < 0.05$). However, the main effect was observed in presence of 1 pg/mL BDNF SKA compared to 50 ng/mL BDNF (about 90%).
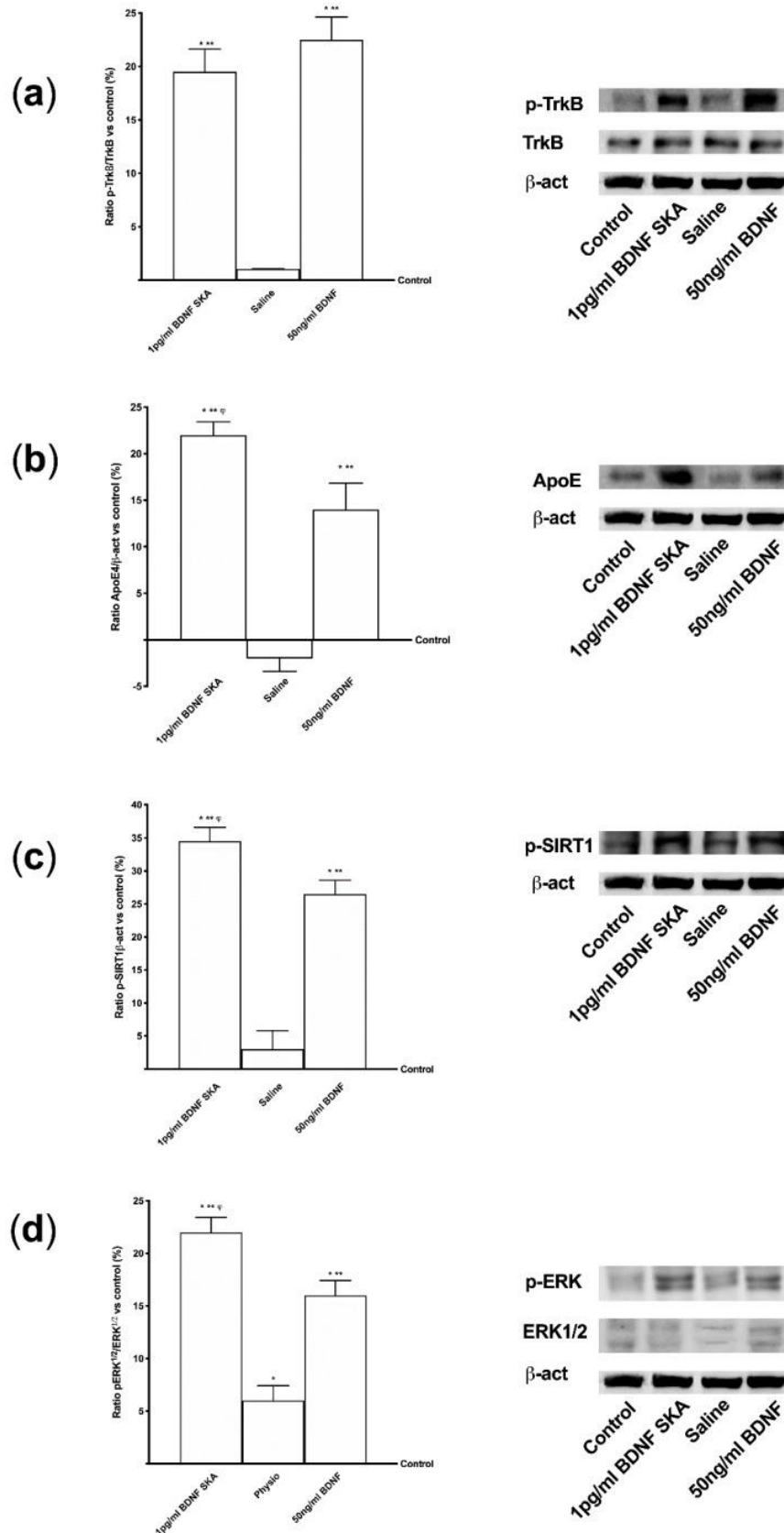
Figure 9. Analysis of intracellular pathways activated by BDNF solutions in astrocytes under oxidative condition. Kinase activity, densitometric analysis and Western blot are reported. (a) TrkB receptor, (b) ApoE(4), (c) Tau, and (d) SIRT1 expressions and (e) ERK/MAPK activity. Data are expressed as means ± SD (%) of five independent experiments and the densitometric analyses are normalized on specific total protein if possible and verified by β-actin detection. * $p < 0.05$ vs. control; ** $p < 0.05$ vs. $H_2O_2$; φ $p < 0.05$ vs. $H_2O_2$+50 ng/mL BDNF.

42

### 2.2.6 Daily Duration of the Effects of BDNF Solutions on Neurons and Astrocytes

Since BDNF can be used as a dietary supplement in humans, some experiments were carried out to better clarify the optimal dosing schedule. The effects of 1 pg/mL BDNF SKA and 50 ng/mL BDNF during 24 h on both cell types were studied analyzing BDNF concentration, cell viability and mitochondrial potential.

As reported in Figure 10A, treatments with 1 pg/mL BDNF SKA and 50 ng/mL BDNF on both cell types caused a similar time-dependent increase in BDNF concentration. This effect showed significance from 1 h, compared to control ($p < 0.05$), and the maximum effect was observed at 24 h (23% and 22% compared to control, respectively, in neurons; about 26% and 25% compared to control, respectively, in astrocytes). No significant changes between the two BDNF solutions were observed, indicating the comparable effectiveness of low dose SKA to high-concentration BDNF. However, 1 pg/mL BDNF had better tolerability, demonstrated by better cell viability ($p < 0.05$) compared to 50 ng/mL BDNF. This effect was significant starting from 6 h in neurons and 3 h in astrocytes, with a maximum effect on both types of cells at 24 h (about 80% and about 60% vs. 50 ng/mL, respectively), as shown in Figure 10B.

Since cell viability depends on mitochondrial activity, the analysis of mitochondrial potential variation was performed (Figure 10C). Both BDNF solutions modulated mitochondrial potential in a time-dependent manner with a significant increase from 3 h in neurons and from 30 min in astrocytes compared to control ($p < 0.05$). However, no significant changes were observed between the two BDNF solutions.

These results therefore allow us to state that low dose BDNF SKA administration has more beneficial effects on neurons and astrocytes than high dose BDNF, prolonged over time to cover 24 h.
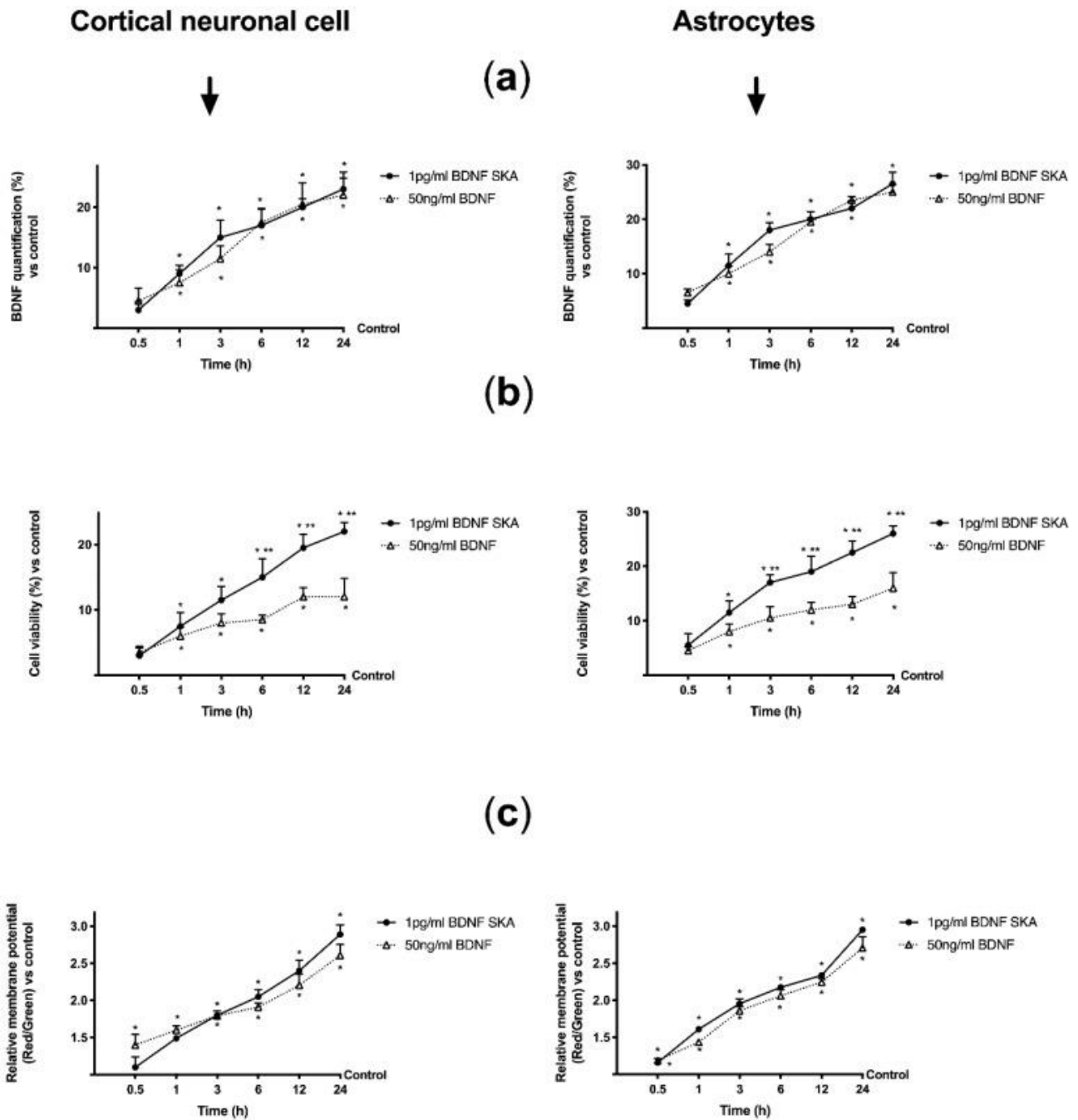
Figure 10. Effects of BDNF solutions within 24h on primary cortical neuronal cells and astrocytes. In the left column primary cortical neuronal cells and in the right column astrocytes are shown. (a) BDNF quantification and (b) cell viability measured after BDNF treatments. Data are expressed as means ± SD (%) of five independent experiments performed in triplicates normalized to control (0 line as control). (c) The mitochondrial membrane potential is investigated in the same condition. Data are expressed as means ± SD of five independent experiments performed in triplicates normalized to control (1 line as control). * $p < 0.05$ vs. control; ** $p < 0.05$ between 1 pg/mL BDNF SKA and 50 ng/mL BDNF.

### 2.2.7. Analysis of Bioavailability of BDNF Solutions and Their Effects in Mouse Brain

To confirm the ability of BDNF solutions to cross enterohepatic circle and the blood–brain barrier and act in brain tissue, some experiments were performed *in vivo* using wild type C57BL mice. Since in humans the administration would be daily, in some experiments 1.2 pg/mL BDNF SKA and 25 ng/mL BDNF were administered to animals by rissoles and BDNF concentration in both serum and brain tissues were analyzed after 24 h. In addition, to verify the stability of the effects, additional experiments

44

were carried out adding 24h without stimulations. As reported in Figure 11A, 1.2 pg/mL BDNF SKA had a greater ability to get through the enterohepatic circle compared to 25 ng/mL BDNF (about 43%) and to control ($p < 0.05$) at 24 h. Moreover, 1.2 pg/mL BDNF SKA tended to remain in blood circulation longer (at least 24 h longer), compared to 25 ng/mL BDNF (about 68%). Since BDNF is present in blood, it is important to verify its presence also in brain tissue (Figure 11B). In administration of both 1.2 pg/mL BDNF SKA and 25 ng/mL BDNF, it was able to enter the brain, as illustrated by BDNF quantification analysis ($p < 0.05$ vs. control). In addition, 1.2 pg/mL BDNF SKA was able to remain for a longer time (24 h plus 24 h) in brain tissue compared to 25 ng/mL BDNF (about 55%, $p < 0.05$) and 1.2 pg/mL BDNF SKA at 24 h (about 20%, $p < 0.05$). These findings demonstrate the importance of doses and posology of administration of BDNF SKA to induce a better influence on brain tissue.
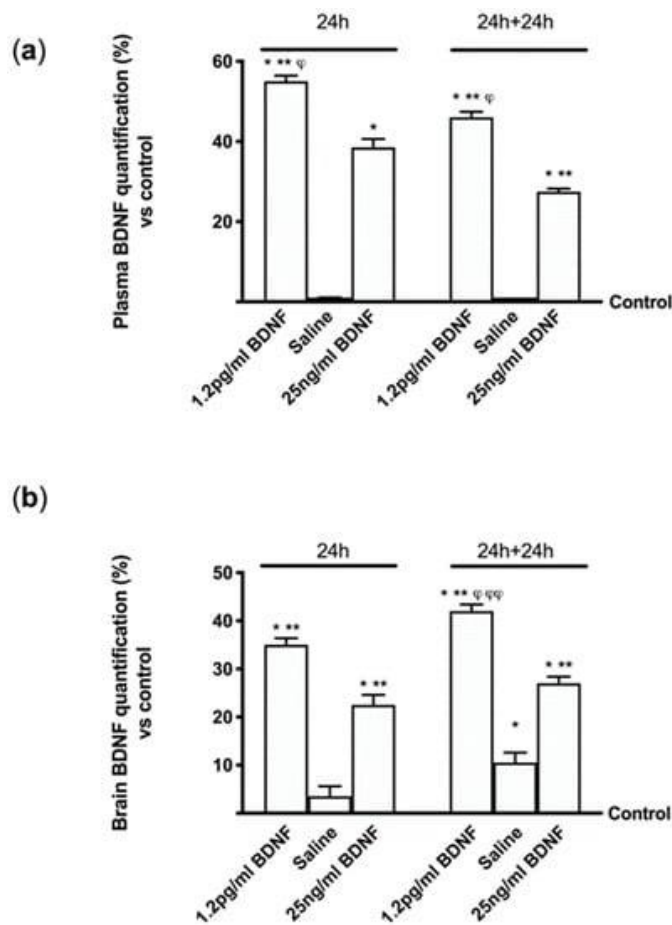


Figure 11. BDNF quantification in mice in serum and brain tissue. (a) Serum quantification and (b) BDNF quantification in brain tissue are reported. Each graph contains on the left the results obtained at 24h (12 animals) and on the right (12 animals) at 24 h plus 24 h (24 h+24 h). Data are expressed as means ± SD (%) normalized to control (0 line as control). * $p < 0.05$ vs. control; ** $p < 0.05$ vs. saline solution; $\varphi$ $p < 0.05$ vs. the same treatments at the same time of administration; $\varphi\varphi$ $p < 0.05$ vs. the same treatments at 24 h and 24 h plus 24 h.

To verify whether the mechanism activated by BDNF solutions is the same as the one observed in cells during *in vitro* experiments, the effects of 1.2 pg/mL BDNF SKA and 25 ng/mL BDNF on some main markers were investigated by Western blot. Since BDNF is necessary for survival of neurons in the brain, after encoding by this gene its expression was investigated, as reported in Figure 12A. 1.2 pg/mL BDNF SKA and 25 ng/mL BDNF both at 24 h and 24 h plus 24 h were able to induce the expression of BDNF compared to control ($p < 0.05$), indicating a better influence of stimulations. Moreover, 1.2 pg/mL

BDNF SKA at 24 h and 24 h plus 24 h caused a significant increase compared to and 25 ng/mL BDNF (about 50% and about 62%, respectively), indicating the induction of endogenous production of BDNF by physiological mechanism, as shown by the significant increase induced by 1.2 pg/mL BDNF SKA at 24 h plus 24 h with respect to at 24 h ($p < 0.05$, about 24%).

These effects were mediated by the TrkB receptor, which was expressed in a similar manner in both times of treatment between 1.2 pg/mL BDNF SKA and 25 ng/mL BDNF ($p < 0.05$ vs. control, Figure 12B). Since β-Amyloid precursor protein (APP) plays a central role, the beneficial effects exerted by both BDNF solutions were also assessed by the quantification of APP, as shown in Figure 12C. 1.2 pg/mL BDNF SKA and 25 ng/mL BDNF increased APP compared to control ($p < 0.05$) at 24h and 1.2 pg/mL BDNF SKA seemed to have a greater effect compared to 25 ng/mL BDNF (about 2.5 times). In addition, the APP activity at 24 h plus 24 h demonstrated the physiological action of 1.2 pg/mL BDNF SKA compared to 25 ng/mL BDNF ($p < 0.05$), indicating a better regulation exerted by 1.2 pg/mL BDNF SKA on central nervous tissue.
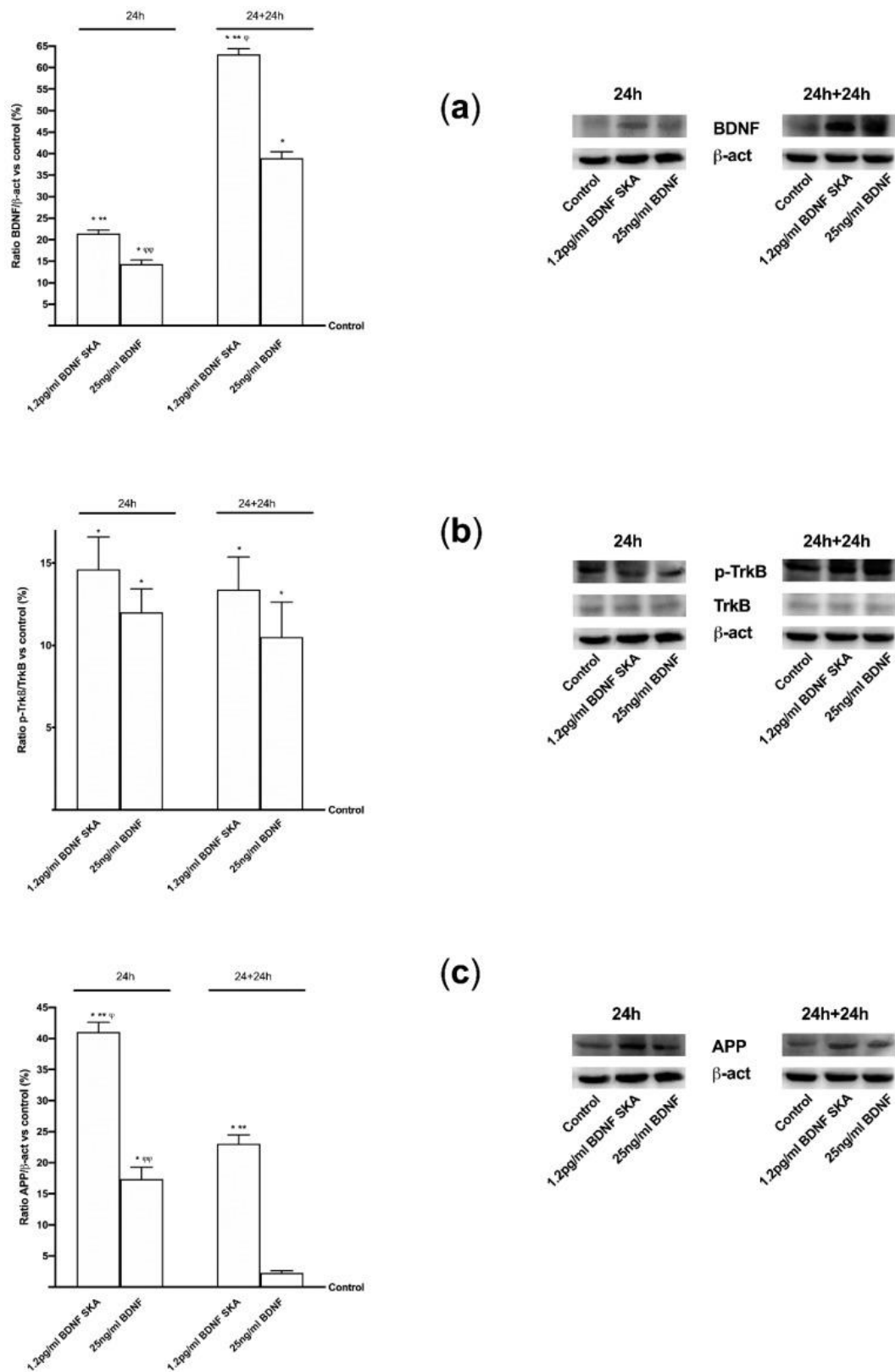
Figure 12. Western blot and densitometric analysis of BDNF protein (a), TrkB (b) receptor and (c) APP protein expressions in brain tissue. In the left column densitometric analysis and in the right the examples of Western blot are reported. Each graph contains on the left the results obtained at 24 h (12 animals) and on the right (12 animals) at 24 h plus 24 h (24 h+24 h). Data are expressed as means ± SD (%) of independent experiments normalized on specific total protein if possible and verified by β-actin detection. * $p < 0.05$ vs. control; ** $p < 0.05$ vs. 25 ng/mL BDNF at the same time of administration; φ $p < 0.05$ vs. 1.2 pg/mL BDNF SKA between 24 h and 24 h plus 24 h; φφ $p < 0.05$ vs. 25 ng/mL BDNF between 24 h and 24 h plus 24 h.

47

Moreover, since *in vivo* and *in vitro* studies suggested that ApoE may drive neurodegeneration through an Aβ-dependent mechanism, ApoE expression was assessed as well. As reported in Figure 13A, a significant increase of ApoE expression compared to control ($p < 0.05$) was observed in the presence of both 1.2 pg/mL BDNF SKA and 25 ng/mL BDNF in both time points, indicating a positive effect of BDNF on central nervous tissue. Moreover, the activation of TrkB by 1.2 pg/mL BDNF SKA and 25 ng/mL BDNF was able to induce a significant increase in ERKs expression compared to control ($p < 0.05$) in both time points. Therefore, a potential role of BDNF in tissue recovery through the involvement of ERKs/MAPK (Figure 13B) can be hypothesized. These findings support what was observed in astrocytes. However, the main effect was observed at 24 h in the presence of 1.2 pg/mL BDNF SKA compared to 25 ng/mL BDNF ($p < 0.05$, about three fold) and to 1.2 pg/mL BDNF SKA at 24 h plus 24 h ($p < 0.05$, about 30%). The last test of this series of experiments concerned the study of the expression of SIRT1. The analysis of SIRT1 confirms the beneficial effects exerted by 1.2 pg/mL BDNF SKA and 25 ng/mL BDNF (Figure 13C). In both 24 h and 24 plus 24 h, 1.2 pg/mL BDNF SKA and 25 ng/mL BDNF were able to induce a significant increase on SIRT1 phosphorylation compared to control ($p < 0.05$). However, the main effect was shown by 1.2 pg/mL BDNF SKA on both time points compared to 25 ng/mL BDNF (about 70% and 73%, respectively, $p < 0.05$). All these findings support the hypothesis that treatment with BDNF SKA can induce physiological mechanisms potentially able to slow down degeneration and protect brain during time.
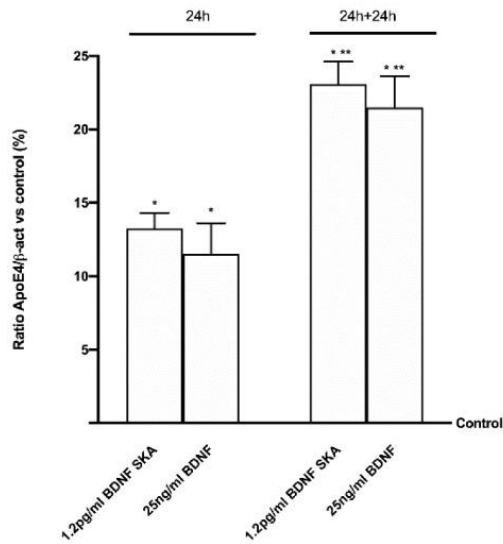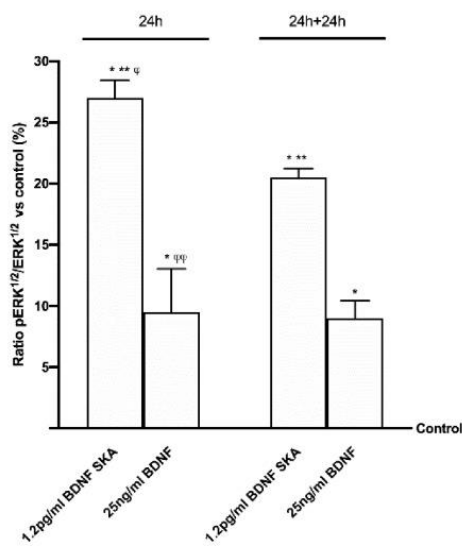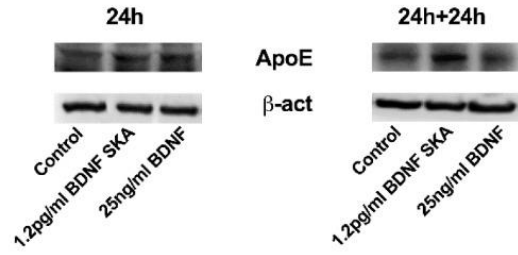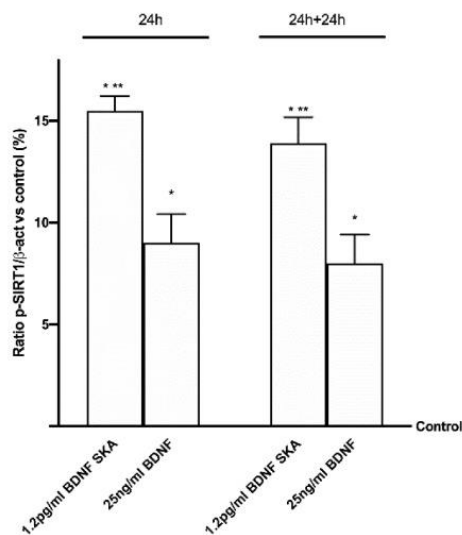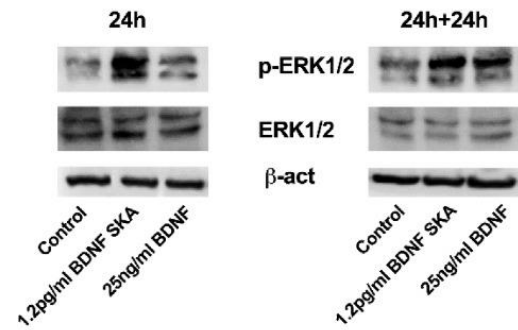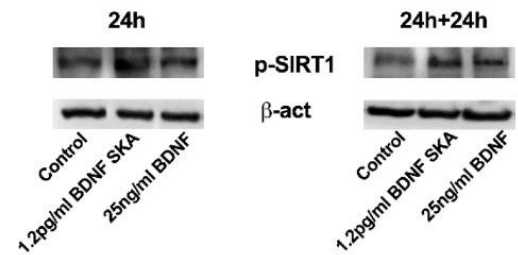
Figure 13. Western blot and densitometric analysis of ApoE (a), ERK/MAPK (b,c) SIRT1 expressions in brain tissue. In the left column densitometric analysis and in the right the examples of Western blot are reported. Each graph contains on the left the results obtained at 24 h (12 animals) and on the right (12 animals) at 24 h plus 24 h (24 h + 24 h). Data are expressed as means ± SD (%) of independent experiments normalized on specific total protein if possible and verified by $\beta$-actin detection. * p < 0.05 vs. control; ** p < 0.05 vs. 25 ng/mL BDNF at the same time of administration; $\varphi$ p < 0.05 vs. 1.2 pg/mL BDNF SKA between 24 h and 24 h plus 24 h; $\varphi\varphi$ p < 0.05 vs. 25 ng/mL BDNF between 24 h and 24 h plus 24 h.

49

## 2.2.8. Effects of BDNF Solutions in Mouse Brain During Time

To verify whether the efficacy of BDNF SKA was maintained for a long time, the mice were treated following the 6-day protocol previously used in cells experiments. As reported in Figure 14A, the administration of 1.2 pg/mL BDNF SKA and 25 ng/mL BDNF maintained the serum BDNF levels up to six days compared to control ($p < 0.05$). Besides, 1.2 pg/mL BDNF SKA was able to maintain high BDNF level compared to 25 ng/mL BDNF (about two fold higher). Similarly, the administration of 1.2 pg/mL BDNF SKA demonstrated better effectiveness ($p < 0.05$) compared to 25 ng/mL BDNF (about 80%) at brain tissue level (Figure 14B). These data suggest that BDNF SKA tends to remain present for a long time in brain tissue even in the absence of treatment, by triggering its physiological production better than BDNF at a high dose.

To confirm this, some additional experiments were performed to analyze BDNF protein (Figure 14C) and TrkB receptor by Western blot (Figure 14D). Both proteins show a significant increase at six days after both BDNF solutions, but 1.2 pg/mL BDNF SKA exerted a significant increase compared to 25 ng/mL BDNF (about two fold higher for each one, respectively, $p < 0.05$). These findings support the hypothesis of a fine endogenous regulation exerted by BDNF SKA on brain maintenance and function.
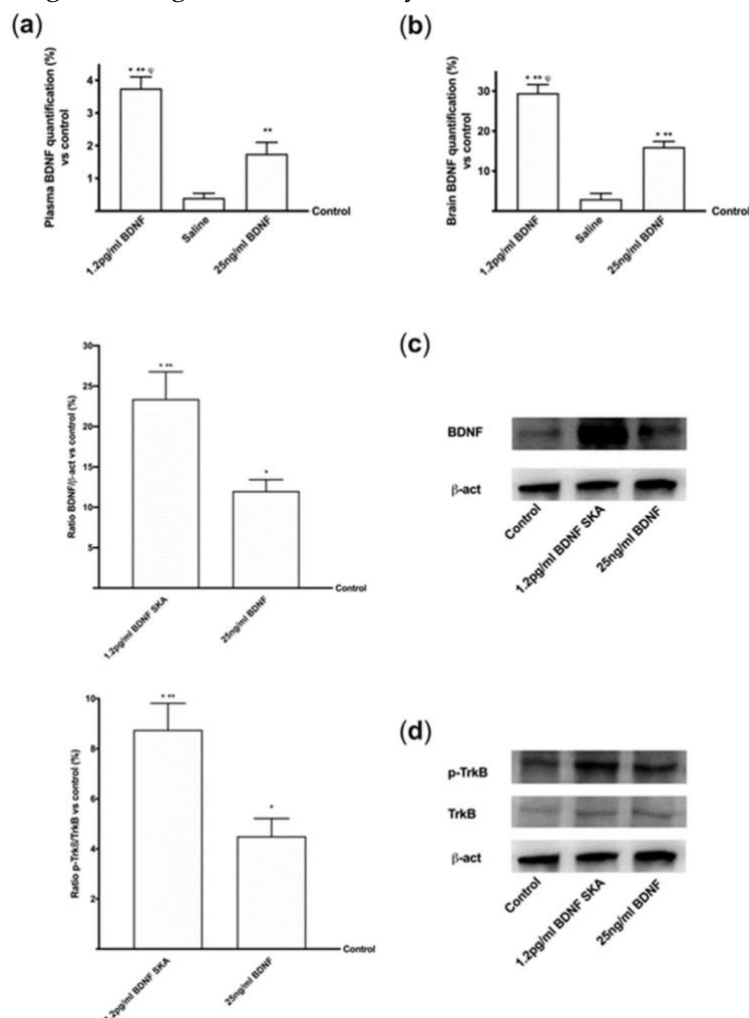


Figure 14. BDNF quantification and intracellular pathways in brain measured in the 6-dayprotocol. (a) Serum and (b) brain tissue BDNF quantification in mice. Data are expressed as means ± SD (%) of n = 7 independent experiments normalized to control value (0 line). * $p < 0.05$ vs. control; ** $p < 0.05$ vs. saline solution; φ $p < 0.05$ vs. 25ng/mL BDNF. (c) BDNF and (d) TrkB receptor expressions in mice brain reported as densitometric analysis (on the left) and examples of Western blot (on the right). Data are expressed as means ± SD (%) of n = 7 independent experiments normalized on specific total protein if possible and verified by β-actin detection. * $p < 0.05$ vs. control; ** $p < 0.05$ vs. 25 ng/mL BDNF.

# 3) NEW APPROACH TO THE TREATMENT OF NEUROPATHIC PAIN. IN VITRO STUDY ON THE CELLULAR EFFECTS OF A COMBINATION WITH PALMITOYLETHANOLAMIDE

Research on neuropathic pain is taken from the article entitled "*New approach to the treatment of neuropathic pain: in vitro study on the cellular effects of a combination with palmitoylethanolamide*" [161]. Neuropathic pain is a typical patient disorder resulting from damage and dysfunction of the peripheral neuraxis. Injury to peripheral nerves in the upper extremities can result in a lifelong reduction in quality of life and devastating loss of sensory and motor function. Since some standard pharmaceutical therapies can cause dependence or intolerance, nonpharmacological treatments have gained great interest in recent years. In this context, the beneficial effects of a new combination of palmitoylethanolamide and *Equisetum arvense* are evaluated in the present study. The bioavailability of the combination was initially analyzed in a 3D intestinal barrier simulating oral intake to analyze its absorption/biodistribution and exclude cytotoxicity. In a further step, a 3D nerve tissue model was performed to study the biological effects of the combination during the key mechanisms leading to peripheral neuropathy. The results demonstrate that the combination successfully crossed the intestinal barrier and reached the target site, modulating the nerve recovery mechanism after Schwann cell injury and offering the initial response in relieving pain. In conclusion, this work supported the efficacy of palmitoylethanolamide and *Equisetum arvense* in reducing neuropathy and modifying the major pain mechanisms, outlining a possible alternative nutraceutical approach.

## 3.1 MATHERIALS AND METHODS

### 3.1.1 Agents Preparation
0.2µM PEA 80mesh and 50µg/ml *Equisetum A*. (titled 10% silica) alone and combined (named EQUIPEA®) (Patent N° 102022000008066 and 102022000016404 from Futura srl) were used to verify their effectiveness to cross the intestinal barrier and reach the peripheral nervous system. In addition, to analyze the effects of this new combination, the results were compared with other PEA forms present on the market. In particular, micronized PEA and ultra-micronized PEA were used maintaining the same PEA concentrations. Both the concentrations of PEA and Equisetum A. derived from the literature [162,163] and confirmed by dose-response studies that used ranging from 0.1µM to 0.4µM and 25µg/ml to 100µg/ml, respectively. All substances tested were prepared directly in Dulbecco's Modified Eagle's Medium (DMEM, Merck Life Science, Rome, Italy) without phenol red and supplemented with 0.5% fetal bovine se-rum (FBS, Merck Life Science, Rome, Italy), 2 mM L-glutamine (Merck Life Science, Rome, Italy), and 1% penicillin–streptomycin (Merck Life Science, Rome, Italy) for all analysis.

### 3.1.2. Cell Culture
The human epithelial intestinal CaCo-2 cell line, purchased from the American Type Culture Collection (ATCC), was used as an experimental model to predict the features of intestinal absorption following oral intake [164]. This cell line was cultured in Dulbecco's Modified Eagle's Medium/Nutrient F-12

Ham (DMEM-F12, Merck Life Science, Rome, Italy) containing 10% FBS (Merck Life Science, Rome, Italy), 2 mM L-glutamine and 1% penicillin–streptomycin (Merck Life Science, Rome, Italy) and maintained in an incubator at 37 °C and 5% $CO_2$ [165]. Experiments were carried out using cells at passage numbers between 26 to 32 to maintain the correct paracellular permeability and transport properties [59]. Cells were plated in a variety of ways, including 1×10^4 cells on 96 well plates to study cell viability and ROS production synchronizing cells for 8h with DMEM without red phenol and supplemented with 0.5% FBS, 2 mM L-glutamine, and 1% penicillin–streptomycin at 37 °C; 2×10^4 cells on 6.5 mm Transwell® (Corning® Costar®, Merck Life Science, Rome, Italy) with a 0.4 μm pore polycarbonate membrane insert (Corning® Costar®, Merck Life Science, Rome, Italy) in a 24 well plate to perform the absorption analyses [166].

Rat-derived Schwann, RSC-96 cell line, was obtained from ATCC and was cultured in Dulbecco's Modified Eagle's Medium (Merck Life Science, Rome, Italy) supplemented with 10% FBS, 2 mM L-glutamine and 1% penicillin–streptomycin [167] maintaining the cultures at 37 °C with 5% $CO_2$. RSC96 cells were subcultured 2–3 times a week, and passages between 10 and 15 were used for the experiments [168].

The rat neuronal PC12 cell line purchased from ATCC, was cultured in Roswell Park Memorial Institute-1640 (RPMI, Merck Life Science, Rome, Italy) supplemented with 2mM Glutamine, 10% Horse Serum (HS, Merck Life Science, Rome, Italy) and 5% FBS. The cultures were maintained at sub-confluency at 37°C with 5% $CO_2$ and cells used for experiments were between passages 3 and 13 [169]. PC12 cells are one of the most frequently employed neuronal cell lines for *in vitro* screening for neuroprotective compounds [64]. 4x10^6 RSC96 cells and 1×10^5 PC12 cells were seeded in a co-culture system to reproduce 3D EngNT *in vitro* in the peripheral nerve environment [167].

### 3.1.3. Experimental protocol

The experiments were divided into two steps: the first one investigated the effects of all PEA forms and *Equisetum A*. on CaCo-2 cells analyzing cell viability and ROS production in a dose-response study and the better concentration of all substances alone and combined were used in *in vitro* intestinal permeability assay to verify the ability to cross the intestinal barrier maintain a correct tight junction (TJ) activity [170]. In particular, cells were plated in the Transwell® system to verify intestinal integrity by TEER measurement following the treatments. In addition, this *in vitro* intestinal model was also used to analyze TJ activity by ELISA test and the permeability rate by Papp assay. All these experiments were time-dependent from 2h to 6h [170]. Moreover, at the end of each stimulation, the basolateral environment was collected to be used to stimulate the 3D EngNT co-culture. In the second step, the 3D EngNT co-culture was used to investigate the effects of the stimulations on the nerve tissue model *in vitro* after 14 days of culture, maturation time and 24h of treatments. In this model, mitochondrial metabolism and ROS production were investigated. Finally, additional experiments were also carried out pretreating for 14 days the 3D EngNT co-culture with 200ng/ml glial growth factor 2 (GGF), which is a well-established model to mimic peripheral nerve injuries since it can reproduce robust demyelination [66]. Under demyelination conditions, the 3D EngNT co-culture was stimulated with PEA alone and combined with Equisetum A. and with the ultra-micronized PEA in a commercial form (named PEA from the market), in order to evaluate if this new combination can restore neurite damages. Therefore, mitochondrial metabolism, ROS production, and inflammatory

factors were measured; in addition, the re-myelination mechanisms and peripheral nerve recovery were investigated in these conditions. Finally, 10μM AM251 (Cayman Chemical, XX) and 10μM AM630 (Cayman Chemical, XX) (CB1 and Cb2 blockers, respectively) [67] were also tested to verify the mechanism of analgesic effect due to the involvement of GABA signalling.

### 3.1.4. *In vitro* Intestinal Barrier Model

In order to evaluate whether all PEA forms and Equisetum A. samples could be able to cross the intestinal barrier, an *in vitro* intestinal barrier model was created using Transwell® system, following a standard protocol reported in literature [149,171] and approved by European Medicines Agency (EMA) and Food and Drug Administration (FDA) to predict absorption, metabolism, and bioavailability of several substances after oral intake in humans [172,173]. Briefly, CaCo-2 cells, plated as previously described, were maintained in a complete medium changing it every other day on the basolateral and apical sides for 21 days before the simulations [149]. During all maturation time, the transepithelial electrical resistance (TEER) values were evaluated by EVOM3, coupled with STX2 chopstick electrodes (World Precision Instruments, Sarasota, FL, USA) to evaluate mature intestinal epithelial formation and a correct paracellular mechanism. On the 21st day, when TEER values were $\geq$ 400 $\Omega cm^2$ [174], absorption analysis had started. Before the stimulation, on the apical side, the medium was brought to pH 6.5 as the pH in the lumen of the small intestine, while the pH 7.4 on the basolateral side represented blood [175]. The cells were stimulated with all substances from 2h to 6h before the successive analysis, including the permeability assay measured by Papp (cm/s) analysis [165], following formula:

$$Papp = dQ/dt \twoheadrightarrow 1/m0 \twoheadrightarrow 1/A \twoheadrightarrow V \, Donor$$

dQ: amount of substance transported (nmol or μg);

dt: incubation time (sec);

m0: amount of substrate applied to donor compartment (nmol or μg);

A: surface area of Transwell® membrane ($cm^2$);

VDonor: volume of the donor compartment ($cm^3$).

Negative controls without cells were tested to exclude the Transwell® membrane's in-fluence. The analysis was performed in triplicates and reproduced five times.

### 3.1.5 3D EngNT Co-cultures setup

The 3D nerve tissue model was prepared according to the literature [167]. The interaction between RSC96 and PC12 cell lines is a key feature to mimic *in vitro* the peripheral nerve environment, regenerating neurites and supporting Schwann cells [167, 176]. Briefly, 1 mL of a solution, containing 80% v/v Type I rat tail collagen (2 mg/mL in 0.6% acetic acid, Thermo Fischer, Milan, Italy), 10% v/v Minimum Essential Medium (MEM, Merck Life Science, Milano, Italy), 5.8% v/v neutralizing solution (Biosystems, Monza, Italy) and 4.2% Schwann cell suspension (4 × 106 RSC96 cells per 1 mL gel), was added in a rectangular scaffold with dimensions of 16.4 mm × 6.5 mm × 5 mm. When the gel had set, it was immersed in 10 mL DMEM and incubated at 37°C with 5% $CO_2$ for 24h to permit cellular self-alignment; at the end of the time, the gel was stabilized using plastic compression (120g weight for 1 min). Once the gel has been aligned and stabilized, it was cut into equal segments according to the samples to be treated. Each gel segment was transferred in a 24-well plate and 1x10^5 PC12 was seeded

on top of each segment for establishing the co-cultures; this passage is crucial to permit neurites extension across the horizontal plane following the aligned Schwann gels. The 24-well plate containing gels was incubated for 1h at 37°C to allow attachment of neuronal cells to the collagen gel and then 1mL of culture medium (containing DMEM supplemented with 10% FBS, 100 U/mL of Penicillin and 100 µg/mL of Streptomycin, all purchased from Merck Life Science, Milano, Italy) was added to each well.

### 3.1.6. Cell Viability

The cell viability based on *In vitro* Toxicology Assay Kit (Merck Life Science, Rome, Italy) was verified at the end of each stimulation, following a classical protocol reported in the literature [149]. The absorbance of all solubilized samples (treated and untreated) at 570 nm with correction at 690 nm measured by a spectrometer (Infinite 200 Pro MPlex, Tecan, Männedorf, Switzerland) was expressed comparing data to the control sample (untreated samples defined as 0% line) and reported as means of five independent experiments performed in triplicate.

### 3.1.7. ROS production

The ROS production was quantified by analyzing the reduction of cytochrome C using a standard protocol [165], measuring the absorbance at 550 nm through the spectrometer (Infinite 200 Pro MPlex, Tecan, Männedorf, Switzerland). $O_2$ ratio was ex-pressed as the mean ± SD (%) of nanomoles per reduced cytochrome C per microgram of protein compared to the control (untreated samples) of five independent experiments performed in triplicate.

### 3.1.8. Occludin Quantification Assay

The Human Occludin (OCLN) ELISA kit (MyBiosource, San Diego, CA, USA) was used according to the manufacturer's instruction [165]. CaCo-2 cells were lysed with cold Phosphate-Buffered Saline (PBS, Merck Life Science, Rome, Italy) 1×, centrifuged at 1500× g for 10 min at 4 °C, and 100 µL of each sample were analyzed. The enzymatic reaction was measured by a spectrometer (Infinite 200 Pro MPlex, Tecan, Männe-dorf, Switzerland) at 450 nm. The results were obtained by comparing data to the standard curve (range from 0 to 1500 pg/ml) and were expressed as a percentage (%) versus control (0 line) of five independent experiments performed in triplicate.

### 3.1.9. Claudin 1 ELISA kit

The Human Claudin1 was measured in CaCo-2 lysates by ELISA kit (Cusabio Technology LLC, Huston Houston, USA), following the manufacturer's instructions [165]. CaCo-2 cells were lysed with cold Phosphate-Buffered Saline (PBS, Merck Life Science, Rome, Italy) 1×, centrifuged at 1500× g for 10 min at 4 °C, and 100 µL of each sample were analyzed and read at 450 nm by a spectrometer (Infinite 200 Pro MPlex, Tecan, Männedorf, Switzerland). The results were obtained by comparing data to the standard curve (range from 0 to 1000 pg/ml) and were expressed as a mean ± SD (%) versus control (0 line) of five independent experiments performed in triplicate.

### 3.1.10 Human Tight Junction Protein 1 (ZO-1) analysis

The Human Tight Junction Protein 1 (TJP1) ELISA kit (MyBiosource, San Diego, CA, USA) was used following the manufacturer's instructions [165]. CaCo-2 cells were lysed with cold Phosphate-Buffered Saline (PBS, Merck Life Science, Rome, Italy) 1×, centrifuged at 5000× g for 5 min at 4 °C, and 100 μL of each sample were analyzed. The plates were read by a spectrometer (Infinite 200 Pro MPlex, Tecan, Männedorf, Switzerland) at 450 nm. The data were obtained compared to the standard curve (range from 0 to 1000 pg/ml) and the results were expressed as a mean ± SD (%) versus control (0 line) of five independent experiments performed in triplicate.

### 3.1.11. TNF$\alpha$ assay

TNF$\alpha$ quantification was obtained using the TNF-$\alpha$ ELISA kit (Merck Life Science, Milano, Italy) according to the manufacturer's instructions [177]. The absorbance of the samples was measured at 450 nm using a plate reader (Infinite 200 Pro MPlex, Tecan, Männedorf, Switzerland) and the results were expressed as a mean ± SD (%) versus control (0 line) of five independent experiments performed in triplicate.

### 3.1.12. Interleukin 2 assay

Interleukin 2 quantification was determined using the Rat IL-2 (Interleukin 2) ELISA Kit (FineTest, Wuhan) according to the manufacturer's instructions on cell lysates [178]. Briefly, 100μL of each sample was added into each well and the plate was incubated at 37°C for 90 minutes. At the end of incubation time, the material in each well was removed and wells were washed twice with Wash Buffer. 100μL of Biotin-labelled antibody working solution was added into the above wells and the plate was incubated at 37°C for 60 minutes. At the end of incubation, the solution in each well was removed and the wells were washed three times with Wash Buffer. Then, 100μL of SABC Working Solution was added into each well and plate was incubated at 37°C for 30 minutes. At the end, the wells were washed five times and 90μL of TMB substrate were put in each well. After 10-20 minutes, 50μL of Stop Solution was put in each well and the plate was read immediately at 450nm using a plate reader (Infinite 200 Pro MPlex, Tecan, Männedorf, Switzerland). A standard curve was plotted relating the intensity of the color (O.D.) to the concentration of standards (range from 31.25 to 2000pg/mL) and the results were expressed as mean ± SD (%) versus control (0 line) of five independent experiments performed in triplicate.

### 3.1.13 NRG1 assay

The NRG1 Rat ELISA Kit (FineTest, Wuhan) according to the manufacturer's instructions, was used in cell culture supernatants. Briefly, 100μL of each sample was added into each well and the plate was incubated at 37°C for 90 minutes. At the end of incubation time, the material in each well was removed and wells were washed twice with Wash Buffer. 100μL of Biotin-labelled antibody working solution was added into the above wells and the plate was incubated at 37°C for 60 minutes. At the end of incubation, the solution in each well was removed and wells were washed three times with Wash Buffer. Then, 100μL of SABC Working Solution was added into each well and plate was incubated at 37°C for 30 minutes. At the end, the wells were washed five times and 90μL of TMB substrate was put in each well. After 10-20 minutes, 50μL of Stop Solution was put in each well and the plate was read immediately at 450nm using a plate reader (Infinite 200 Pro MPlex, Tecan, Männedorf, Switzerland).

The data were obtained compared to the standard curve (range from 0.156 to 10ng/mL) and the results were expressed as mean ± SD (%) versus control (0 line) of five independent experiments performed in triplicate.

### 3.1.14. Myelin protein zero assay
Myelin protein zero (MPZ) production was determined using Rat ELISA kit (MyBiosource, San Diego, CA, USA) in cell lysates, according to the manufacturer's in-struction. Briefly, 100μL of each sample was added into each well and the plate was incubated at 37°C for 2 hours. At the end of incubation time, 100μL of Biotin antibody was added into the wells and the plate was incubated at 37°C for 60 minutes. At the end of incubation, the solution in each well was removed and wells were washed three times with Wash Buffer. Then, 100μL of HRP-avidin Solution was added into each well and plate was incubated at 37°C for 1 hour. At the end, the wells were washed five times and 90μL of TMB substrate was put in each well. After 30 minutes at 37°C, 50μL of Stop Solution was put in each well and the plate was read immediately at 450nm using a spectrometer (Infinite 200 Pro MPlex, Tecan, Männedorf, Switzerland). The concentration was expressed as ng/mL compared to a standard curve (range from 0.06 to 18 ng/ml) and the results were reported as mean ± SD (%) versus control (0 line) of five independent experiments performed in triplicate.

### 3.1.15. NGFR assay
The Rat NGFR ELISA kit (Thermo Fischer, Milan, Italy) (MyBiosource, San Diego, CA, USA) according to the manufacturer's, was used on cell lysates. Briefly, 100μL of each sample was added into each well and the plate was incubated at 37°C for 2 hours. At the end of incubation time, 100μL of Biotin antibody was added into the wells and the plate was incubated at 37°C for 60 minutes. At the end of incubation, the solution in each well was removed and wells were washed three times with Wash Buffer. Then, 100μL of HRP-avidin Solution was added into each well and plate was incubated at 37°C for 1 hour. At the end, the wells were washed five times and 90μL of TMB substrate was put in each well. After 30 minutes at 37°C, 50μL of Stop Solution was put in each well and the plate was read immediately at 450nm using a spectrometer (Infinite 200 Pro MPlex, Tecan). The data were obtained compared to the standard curve (range from 0.312 to 20 ng/ml) and the results were expressed as a mean ± SD (%) versus control (0 line) of five independent experiments performed in triplicate.

### 3.1.16. Human beta-NGF assay
The Rat beta-NGF ELISA kit (Abcam, Cambridge, UK) was used in cell lysates following the manufacturer's instructions [179]. Briefly, 100μL of diluted samples were incubated overnight at 4 °C, washed 4 times with 1× Wash Buffer, and then 100μL of detection antibody was added to each well and incubated for 1 h at room temperature with gentle shaking. Then the wells were washed 4 times and 100μL of streptavidin-HRP and the plate was incubated for 45 minutes; after the incubation, the wells were washed again and 100μL of TMB Substrate were added. Finally, the plate was incubated for 30 min at room temperature in the dark with gentle shaking and the re-action stopped with 50μL of Stop Solution. The absorbance was measured by the spectrometer at 450nm (Infinite 200 Pro MPlex, Tecan, Männedorf, Switzerland), and ex-pressed as pg/mL compared to a standard curve (range from

15 to 15000 pg/ml) and the results were reported as mean ± SD (%) versus control of five independent experiments performed in triplicate.

### 3.1.17. Estrogen Receptor beta assay

The Rat Estrogen Receptor beta (ERb) ELISA Kit (Cloud-Clone, Houston, USA) was used on cell lysates, according to the manufacturer's instruction [180]. Briefly, 100μL of each sample was added into each well and the plate was incubated at 37°C for 1 hour. At the end of all reactions, 50μL of Stop Solution was put in each well and the plate was read immediately at 450nm using a spectrometer (Infinite 200 Pro MPlex, Tecan). The concentration was obtained compared to a standard curve (range from 0.312 to 20 ng/ml) and the results were expressed as mean ± SD (%) versus con-trol of five independent experiments performed in triplicate.

### 3.1.18. Gamma-aminobutyric acid assay

M, Wuhan, China) on cell lysates was performed following the manufacturer's instructions [181]. Briefly, 50μL of the sample was added with 50μL of Biotin-labeled antibody in each well and incubated for 45 minutes at 37°C; then the plate wash washed 3 times and 100μL of SABC Working solution was added in each well and the plate was incubated for 30 minutes at 37°C. At the end of incubation, each well was washed 5 times and then 90μL of TMB Substrate Solution was added in the wells be-fore incubating the plate at 37°C for 15 minutes; then 50μL of stop solution was added in each well and the absorbance was measured by the spectrometer at 450 nm (Infinite 200 Pro MPlex, Tecan, Männedorf, Switzerland). The concentration was analyzed compared to a standard curve (range from 6 to 400 pg/ml) and the results generated were expressed as mean ± SD (%) versus control of five independent experiments per-formed in triplicate.

### 3.1.19. Western Blot

3D EngNT co-culture was lysed in ice with Complete Tablet Buffer (Roche, Ba-silea, Svizzera) supplemented with 2mM sodium orthovanadate (Na3VO4), 1 mM phenylmethanesulfonyl fluoride (PMSF) (Merck Life Science, Rome, Italy), 1:50 mix Phosphatase Inhibitor Cocktail (Merck Life Science, Rome, Italy), and 1:200 mix Protease Inhibitor Cocktail (Merck Life Science, Rome, Italy). According to the standard protocol, 30μg of protein of each sample was resolved on 8% or 10% SDS-PAGE gels, and polyvinylidene difluoride membranes (PVDF, GE, Healthcare Europe GmbH) were incubated overnight at 4 °C with the following specific primary antibodies: anti-CB1 (1:500; Santa Cruz, California, USA), anti-CB2 (1:500; Santa Cruz, California, USA). Protein expression was normalized and verified through anti-β-actin detection (Merck Life Science, Rome, Italy). The results were expressed as means ± SD (% vs. control).

### 3.1.20. Statistical Analysis

Data collected were processed using Prism GraphPad statistical software 9.4.1 using one-way analysis of variance (ANOVA), followed by Bonferroni post hoc tests. Comparisons between the two groups were performed using a two-tailed Student's t-test. Multiple comparisons among groups were analyzed by two-way ANOVA followed by a two-sided Dunnett post hoc test. All results were

expressed as mean ± SD of at least 5 independent experiments produced in triplicates. Differences with a $p<0.05$ were considered statistically significant.

## 3.2. RESULTS

### 3.2.1. Safety analysis of different concentration of PEA and Equisetum on CaCo-2 Cells

Several experiments were performed on the CaCo-2 cell line to exclude any cyto-toxic effect. In particular, cell viability and ROS production were investigated at 3h and at 6h, maximum and minimum times of PEA absorption [162]. For this reason, the analysis was carried out testing PEA 80mesh and *Equisetum Arvense* (in a range of 0.1μM to 0.4μM and from 25μg/ml to 100μg/ml, respectively) and comparing them with another PEA form present in the market, named ultra-micronized PEA (PEA-um). As demonstrated in Table 2, both PEA 80mesh and PEA-um improved cell viability in all tested concentrations, excluding any cytotoxic effect ($p<0.05$). It should be emphasized that cell treated with PEA 80mesh demonstrated a highly beneficial effect, im-proving cell viability better than the other PEA form ($p<0.05$). Considering only PEA 80mesh, as shown in Table 2, the concentration of 0.2μM showed a more significant improvement in cell viability compared to the other concentration tested (about 8% compared to 0.1μM and about 24% compared to 0.4μM, $p<0.05$) suggesting that this treatment dosage may support improved bowel activity. At the same time, the same test was performed by also analyzing the beneficial effect of *Equisetum Arvense* and, as shown in Table 2, all the concentrations tested were able to improve cell viability ($p<0.05$) confirming, also in this case the absence of a toxic effect. More in detail, at 3h of stimulation, the three concentrations tested revealed a similar trend, suggesting that there was no biological difference between them. However, at 6h *Equisetum Arvense* 50μg/ml was able to maintain higher cell viability than the other concentrations test-ed (about 32% compared to 25μg / ml and about 9% compared to 100μg / ml, $p<0.05$), suggesting a possible long effect on mitochondrial metabolism at the intestinal level. Consequently, the ROS production was analyzed on CaCo-2 cells to confirm the safety of PEA 80mesh and *Equisetum Arvense*, analyzing the effect at the same time previously explored. As shown in Table 3, none of the concentrations tested increased ROS production. In particular, PEA 80mesh 0.2μM was able to maintain low ROS levels throughout the stimulation period better than PEAum, and *Equisetum Arvense* 50μg / ml demonstrated antioxidant capacity by reducing the quantity of ROS produced compared to the control ($p<0.05$).

For this reason, the concentrations chosen for the final formulation were PEA 80mesh 0.2μM and *Equisetum Arvense* 50μg/ml (named EQUIPEA®). Indeed, when these agents were added together, the beneficial effects on cell viability and ROS pro-duction were amplified compared to single agents ($p<0.05$), confirming the absence of toxic events and the safety of the combination.

| Dose Time | PEA-um | | | PEA 80mesh | | | Equisetum A. | | | PEA 80mesh + Equisetum A. |
|---|---|---|---|---|---|---|---|---|---|---|
| | 0.1μM | 0.2μM | 0.4μM | 0.1μM | 0.2μM | 0.4μM | 25μg/mL | 50μg/mL | 100μg/mL | 50μg/mL + 0.2μM |
| 3h | 80 ± 1.71 | 90 ± 1.21 | 72 ± 1.46 | 85 ± 0.83 | 92 ± 1.23 | 70 ± 1.48 | 45 ± 0.85 | 49 ± 1.48 | 46 ± 1.57 | 94 ± 1.33 |
| 6h | 76 ± 1.48 | 87 ± 1.67 | 70 ± 1.11 | 78 ± 1.74 | 90 ± 1.26 | 68 ± 1.27 | 30 ± 1.27 | 44 ± 1.22 | 40 ± 1.57 | 91 ± 1.07 |

Table 2. Analysis of cell viability measured by MTT test on CaCo-2 cells. The effects of PEA80mesh and *Equisetum Arvense*, alone and combined, compared to PEA-um at 3h and 6h were reported. PEA-um = PEA ultra-micronized. Data are mean ± SD (%) of five independent experiments per-formed in triplicates normalized to control values (0%).

| Dose Time | PEA-um | | | PEA 80mesh | | | Equisetum A. | | | PEA 80mesh + Equisetum A. |
|---|---|---|---|---|---|---|---|---|---|---|
| | 0.1μM | 0.2μM | 0.4μM | 0.1μM | 0.2μM | 0.4μM | 25μg/mL | 50μg/mL | 100μg/mL | 50μg/mL + 0.2μM |
| 3h | 4 ± 1.14 | 5 ± 1.67 | 7 ± 1.48 | 3 ± 1.78 | 2 ± 1.74 | 1 ± 1.19 | -8 ± 1.74 | -9 ± 1.46 | -9 ± 1.71 | -15 ± 0.89 |
| 6h | 8 ± 1.15 | 7 ± 1.56 | 10 ± 1.22 | 7 ± 1.41 | 6 ± 1.38 | 5 ± 1.47 | -9 ± 1.38 | -9 ± 1.17 | -9 ± 1.48 | -12 ± 1.23 |

Table 3. Analysis of ROS production measured by Cytochrome C reduction on CaCo-2 cells. The effects of PEA80mesh and *Equisetum Arvense*, alone and combined, compared to PEA-um at 3h and 6h were analyzed. PEA-um = PEA ultra-micronized. Data are mean ± SD (%) of five independent experiments performed in triplicates normalized to control values (0%).

### 3.2.2. Permeability and absorption mechanism analyzed *In vitro* Intestinal Barrier Model

Further experiments were conducted to obtain important about the intestinal absorption and the transport mechanism of PEA 80mesh combined with *Equisetum Arvense* compared to PEA-um, using an *in vitro* intestinal barrier able to mimic the in human physiology of the small intestine. In particular, the transepithelial electrical resistance (TEER), the values of the apparent permeability coefficient (Papp) and Tigh Junction activity (TJ) were evaluated. The TEER analysis showed that all PEA forms (Figure 15A) are able to maintain epithelial integrity and the ionic conductance of the paracellular pathway, also confirming the peak in permeability at 3h. Similarly, *Equisetum Arvense* maintains epithelial integrity but suggests poor bioavailability ($p<0.05$). The combination was able to improve the absorption rate with a more physiological behavior than the single components and to PEA-um ($p<0.05$) while maintaining the epithelial integrity and by increasing the ion flow of paracellular exchanges through the intestinal epithelium ($p<0.05$). In order to confirm the correct functioning of the intestinal epithelium, the TJ activity (Figure 15 B-D) and the permeability rate (Figure 15E-F) were explored. The data obtained from TJ analysis demonstrated that the combination with PEA 80mesh 0.2μM and *Equisetum Arvense* 50μg / ml has a better effect compared to the single agents, confirming the result previously obtained about the chosen concentration. Indeed, Claudin-1, Occluding and ZO-1 activities were improved by the combination of PEA 80mesh 0.2μM and *Equisetum Arvense* 50μg / ml compared to PEA-um (about 47.5%, 31% and 37% respectively). Finally, the analysis of the basolateral environment confirmed our previous findings, indicating that the permeability rate of PEA 80mesh 0.2μM combined with *Equisetum Arvense* 50μg / ml was higher than PEA-um ($p< 0.05$) and the main effect was evident at 3h of stimulation (about 29%, $p< 0.05$).

All these results revealed that the combination with PEA 80mesh 0.2μM and *Equisetum Arvense* 50μg / ml has a better absorption profile compared to PEA-um, confirming an improvement in the bioavailability, and suggesting a synergistic effect of the combination of PEA 80mesh 0.2μM and *Equisetum Arvense* 50μg / ml to improve the intestinal absorption.
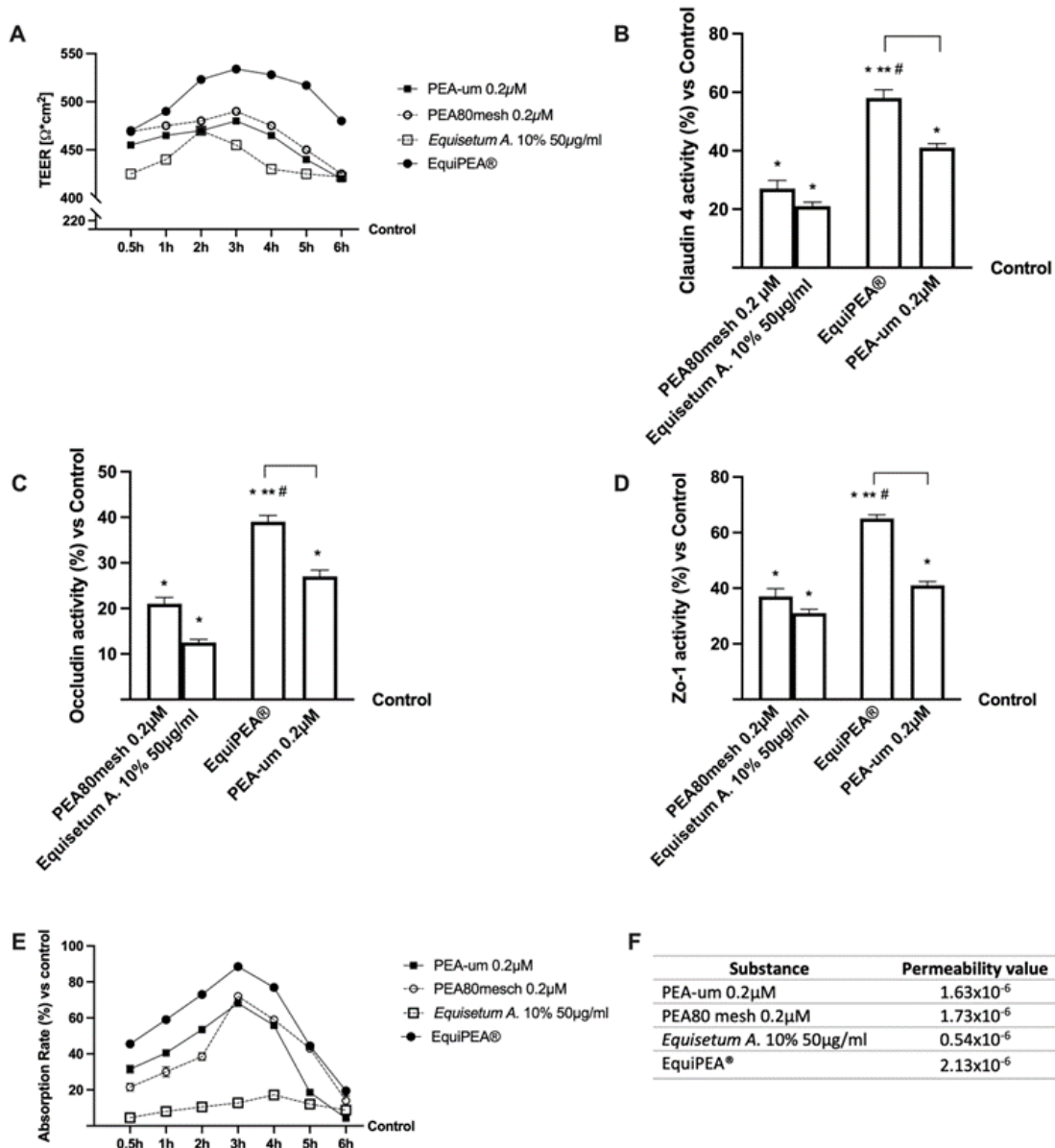


Figure 15. Permeability study on CaCo-2 cells. In (A) TEER Value using EVOM3; from (B-D) the analysis of TJ measured by ELISA test (Claudin1, Occludin and Zo-1, respectively); in (E) evaluation of passage through the intestinal barrier by fluorescent tracer; in (F): the Papp values in which data $< 0.2 \times 10^{-6}$ cm/s means very poor absorption with a bioavailability $< 1\%$, data between $0.2 \times 10^{-6}$ and $2 \times 10^{-6}$ cm/s with bioavailability between 1 and 90 %, and data $> 2 \times 10^{-6}$ cm/s means very good absorption with a bioavailability over 90 %. PEA-um= PEA ultra-micronized. From (B-E) data are means ± SD (%) of five independent experiments performed in triplicates normalized to control values (0% line) and $* p < 0.05$ vs. control; $** p < 0.05$ vs. PEA 80mesh 0.2μM; $\# < 0.05$ vs. *Equisetum Arvense* 50μg/ml; the bar $p<0.05$ vs PEA-um. On the contrary, in (A) the control samples are specifically reported and all agents are $p<0.05$ vs control and $* p<0.05$ vs PEA-um; in (F) all agents are $p<0.05$ vs control

### 3.2.3. Effect of the combination of PEA 80mesh and Equisetum Arvense on 3D EngNT Co-cultures

Since the treatments with PEA, in all its forms, are considered an effective remedy for treating peripheral nerve damages, further analyses were conducted on a 3D EngNT to investigate the ability of PEA 80mesh combined with *Equisetum Arvense* to reach and act into the peripheral nerve after intestinal passage. As shown in Figure 16, all PEA forms tested can reach the target, after intestinal passage, without any negative effect on mitochondrial metabolism and oxidative stress ($p<0.05$). In particular, the combination of PEA 80mesh 0.2µM and *Equisetum Arvense* 50µg/ml was able to amplify the cell viability ($p<0.05$, Figure 16A) compared to PEA-um, demonstrating an ability to maintain the mitochondrial well-being and at the same time, demonstrating an ability to reduce the amount of ROS production (approximately 26% and 83%, respectively, $p<0.05$, Figure 16B). These data were further confirmed by analysing of MPZ, a structural protein required for normal peripheral nerve myelination (Figure 16C). As expected, both PEA forms improve MPZ activity ($p<0.05$) compared to the control. However, the presence of *Equisetum Arvense* with PEA 80mesh significantly improved this marker (approximately 27%, $p<0.05$) compared to PEA-um, confirming the synergistic effect of the substances. Therefore, these data, obtained under physiological condition, demonstrate that the combination PEA 80mesh and *Equisetum Arvense* acts at the SNP level and greatly influences myelin sheath protection.
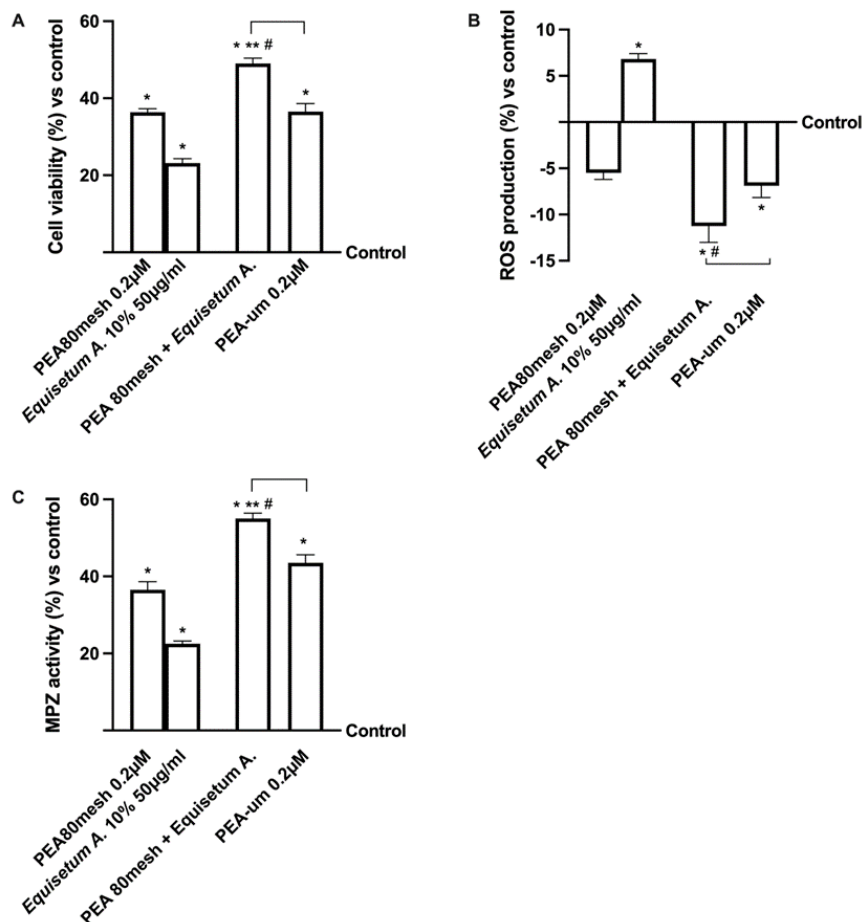


Figure 16. Analysis of EquiPEA® on 3D EngNT in physiological condition. A: mitochondrial metabolism by MTT tes; B: ROS production by Cytochrome C reduction; C: MPZ by ELISA test. PEA-um= PEA ultra-micronized. Data are mean ± SD of five independent experiments performed in triplicates vs. control values (0% line) and * $p < 0.05$ vs. control; ** $p < 0.05$ vs. PEA 80mesh 0.2µM; # < 0.05 vs. *Equisetum Arvense* 50µg/ml; the bar $p<0.05$ vs PEA-um.

### 3.2.4. Biological effects of the combination PEA 80mesh plus Equisetum Arvense on *in vitro* model of PNI

Since the study must mimic the peripheral nerve tissue damage *in vitro*, the 3D EngNT was pre-treated starting from 14 days of maturation with 200 ng/ml GGF to reproduce robust demyelination before stimulation with the same agents used before. In this context, further experiments were conducted by analyzing the effects on mitochondrial metabolism and ROS production (Figure 17A, B). In particular, nerve tissue treated with only 200ng/ml GGF significantly reduced biological activity of the nerve and improved ROS production compared to control ($p < 0.05$). On the contrary, both these negative conditions were significantly counteracted by the presence of all forms of PEA. In particular, the stimulation with PEA 80mesch combined with *Equisetum Arvense* was able to improve cell viability compared to PEA 80mesh alone (about 90%, $p < 0.05$) and to PEA-um (about 73%, $p < 0.05$). At the same time, it is also able to reduce the oxidative stress produced during the damage better the PEA 80mesh alone (about 80%, $p < 0.05$) and PEA-um (about 71%, $p < 0.05$), supporting the important findings previously observed about the synergic effect of the substances.

In addition, this recovery mechanism was also confirmed by the analyses of the inflammatory markers mainly involved during neuropathy, such as TNF$\alpha$ and IL-2 (Figure 17 C-D). Effectively, the beneficial properties of all agents tested could counteract the inflammation process activated by 200ng/ml GGF ($p < 0.05$) on both markers. Specifically, GGF pre-treatment improved the inflammation response compared to the control (about 30% for TNF$\alpha$ and 20% for IL-2, $p < 0.05$). However, the successive treatment with the combination of PEA 80mesh plus *Equisetum Arvense* was able to reduce the damage better than PEA 80mesh alone ($p < 0.05$) and PEA-um (approximately 57% for TNF$\alpha$ and 78% for IL-2, $p < 0.05$).
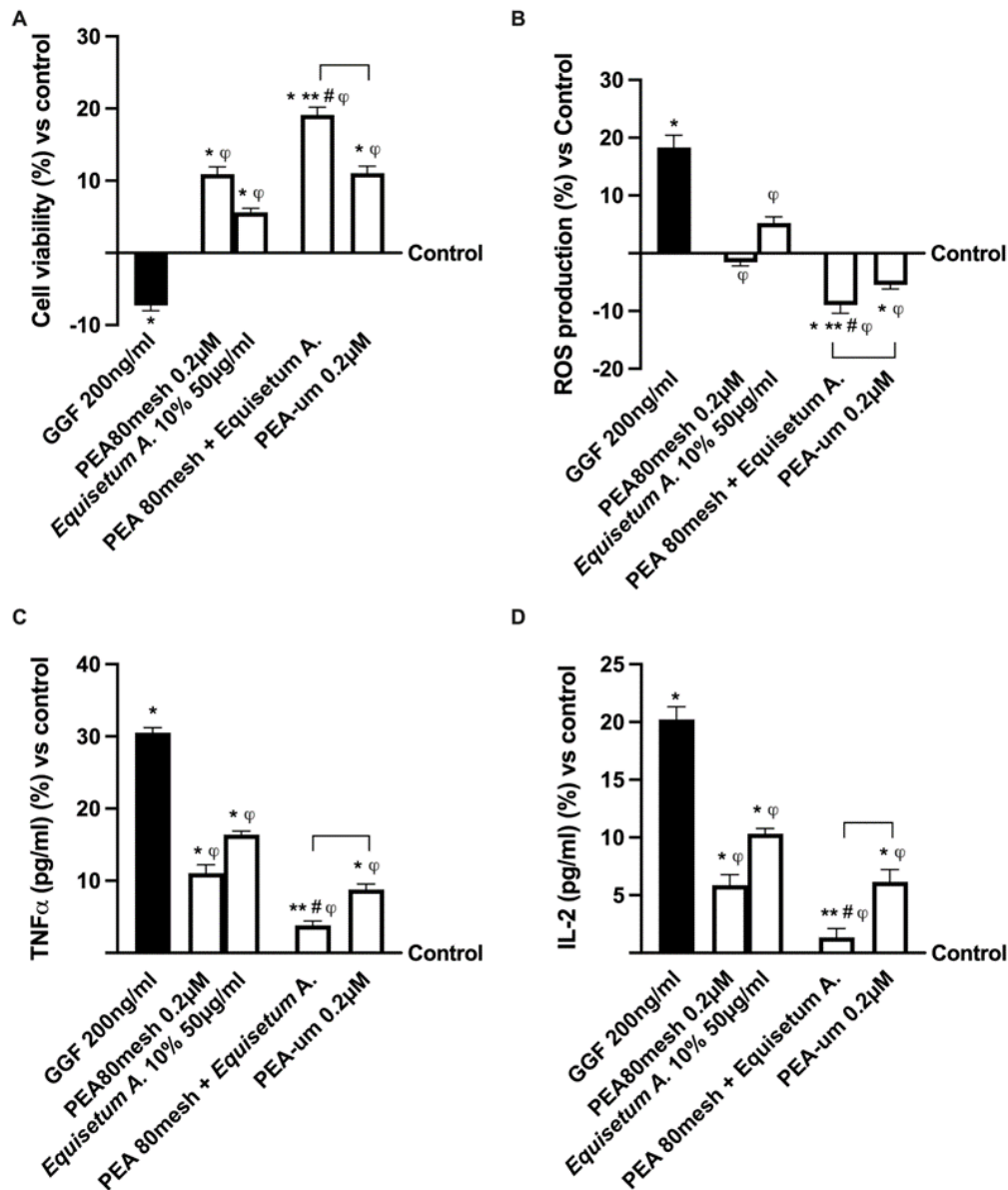
Figure 17. Analysis of PEA 80mesh plus *Equisetum Arvense* effects under PNI condition. In (A) mitochondrial metabolism by MTT; in (B) NGF determination by ELISA test; in (C) TNFa quantification by ELISA test; in (D) IL-1b analysis by ELISA test. PEA-um= PEA ultra-micronized. Data are means ± SD (%) of five independent experiments performed in triplicates normalized to control values (0% line). * p < 0.05 vs. control; ** p < 0.05 vs. PEA 80mesh 0.2µM; # < 0.05 vs. *Equisetum Arvense* 50µg/ml; the bar p<0.05 vs PEA-um; φ p < 0.05 vs. GGF 200ng/ml

In addition, since the main target of PEA is the endocannabinoid system, it was evaluated the biological mechanisms of both CB1 and CB2 receptors and their role to induce GABAergic signalling under PNI condition. Unsurprisingly, as shown in Figure 18 (from A to C), all the considered PEA forms activated both CB1 and CB2 receptors (p<0.05), confirming the crucial role of this bioactive lipid in modulating the endocannabinoid system and changing the behaviour due to pain. Also in this case, the use of *Equisetum Arvense* 50µg/ml in the formulation amplifies the beneficial effect induced by PEA 80mesh (approximately 2 times more for CB1 and one time more for CB2) and especially compared to PEA-um (about 2 times more for CB1 and one time more for CB2), suggesting that this formulation acts modulating the endocannabinoid system to reduce the damage. Furthermore, the beneficial effect exerted by PEA was confirmed by the analysis of GABA activity (Figure 18D) in which the functionality

63

was statistically increased by all PEA forms compared to control (p<0.05) and thanks to *Equisetum Arvense* 50μg/ml, PEA 80mesh amplified it effects by 1.5 times and this effect was also better than PEA-um (p<0.05). Since the base of analgesic effect of PEA depend on the relationship between endocannabinoid system and GABA activation, additional experiments investigate the role of GAB in presence of CB1 and CB2 blockers (10μM AM251 and AM60) added 30 min before the addiction of PEA forms and *Equisetum Arvense* (Figure 18E). In particular, its cloud be observed that the block of CB1 receptor mediated by antagonist AM 251 inhibited the GABA activity meanwhile the use of AM630 antagonist of CB2 receptor does not influence the GABA activity which was maintained at the basal level. The presence of all PEA forms confirmed the GABA activity; indeed, in presence of CB1 antagonist the GABAergic system was prevented, and this condition was maintained also during the presence of *Equisetum Arvense* (p<0.05 vs control), supporting the active role exerted by PEA on CB1 to induce analgesic effect.

Therefore, it is possible to confirm the beneficial role exerted by the combination to modulate the main molecular mechanisms involved in PNI condition *in vitro*.
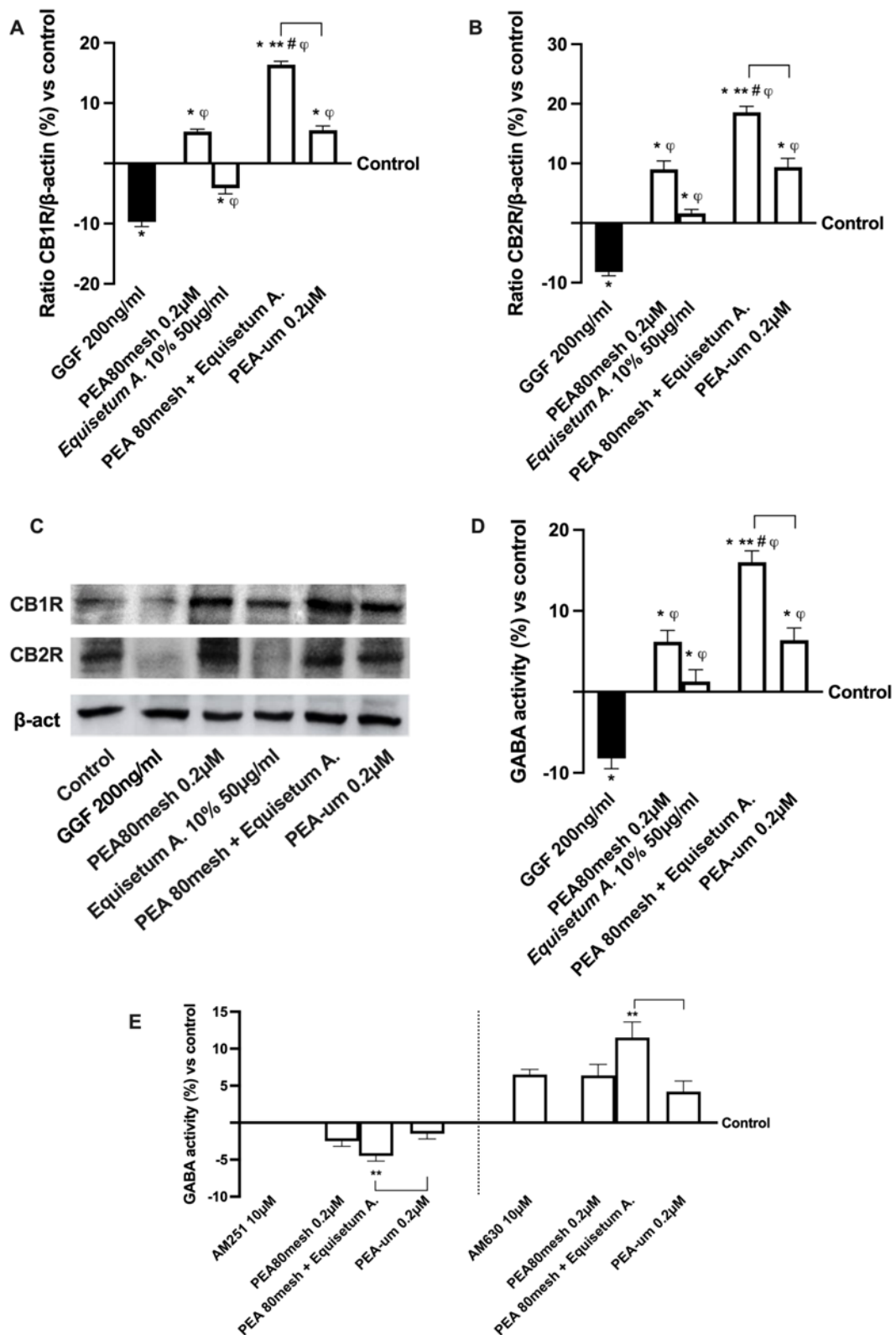
Figure 18. Analysis of EQUIPEA® on CB1/2 receptors and GABA activity under PNI condition. In (A) CB1R and in (B) CB2R densitometric analysis of the specific Western blot, which is reported as an example in (C); in (D, E) GABA activity by ELISA test in absence or presence of CB1/2 blockers. PEA-um= PEA ultra-micronized. Data are mean ± SD (%) of five independent experiments performed in triplicates normalized to control values (0% line). * $p < 0.05$ vs. control; ** $p < 0.05$ vs. PEA 80mesh 0.2µM; # $p < 0.05$ vs. *Equisetum Arvense* 50µg/ml; the bar $p<0.05$ vs PEA-um; $\phi$ $p < 0.05$ vs. GGF 200ng/ml.

Finally, the role of Schwann cells was also investigated by analyzing the modulation of neuropathic pain *in vitro*. As reported in Figure 19, after nerve injury induced by 200ng/ml GGF, myelinating cells were subjected to degradation as demonstrated by p75 analysis and, consequently, to the inhibition of MPZ activity (about 18% and -10% respectively, $p<0.05$). At the same time, the PNI condition influenced the expression of NRG1 and the ERb activity ($p<0.05$ compared to control). Conversely, all PEA forms reduced the damage confirming their positive role in counteracting the demyelination process (all markers $p<0.05$ compared to the damage). In particular, the combination of PEA 80mesh and *Equisetum Arvense* induced the greatest effects compared to PEA80mesh alone and PEA-um ($p<0.05$). Indeed, PEA 80mesh combined with *Equisetum Arvense* was able to revert the damage modulating the markers involved in maintaining the myelin sheath to normal activity. In particular, it improved the activity of p75 (Figure 5A) about 64% compared to PEA 80mesh alone and PEA-um (143%, $p<0.05$) and MPZ (Figure 19B) about 50% compared to PEA 80mesh alone and this effect was more evident compared to PEA-um ($p<0.05$). At the same time, NRG1 (Figure 19C) and Erb3 (Figure 19D) activities were increased by the presence of the combination with PEA 80mesh plus *Equisetum Arvense* compared to PEA 80mesh alone (about 70% and about 63%, respectively) supporting the hypothesis of the improvement of both these markers to ameliorate the nerve injury and restore the myelinization process. In this context, the increase on NGF (Figure 19E) due to PEA 80mesh plus *Equisetum Arvense* compared to PEA 80mesh alone (about 23%) and PEA-um (about 100%) confirmed this important mechanism of action.

All these findings suggest that the new combination correctly modulates the biological activity of Schwann cells, also during PNI. Indeed, all these results demonstrated the considerable effect of PEA 80mesh combined with *Equisetum Arvense* in modulating Schwann cells during the development and the relief of nerve injury, suggesting an increased beneficial effect compared to treatments already on the market.
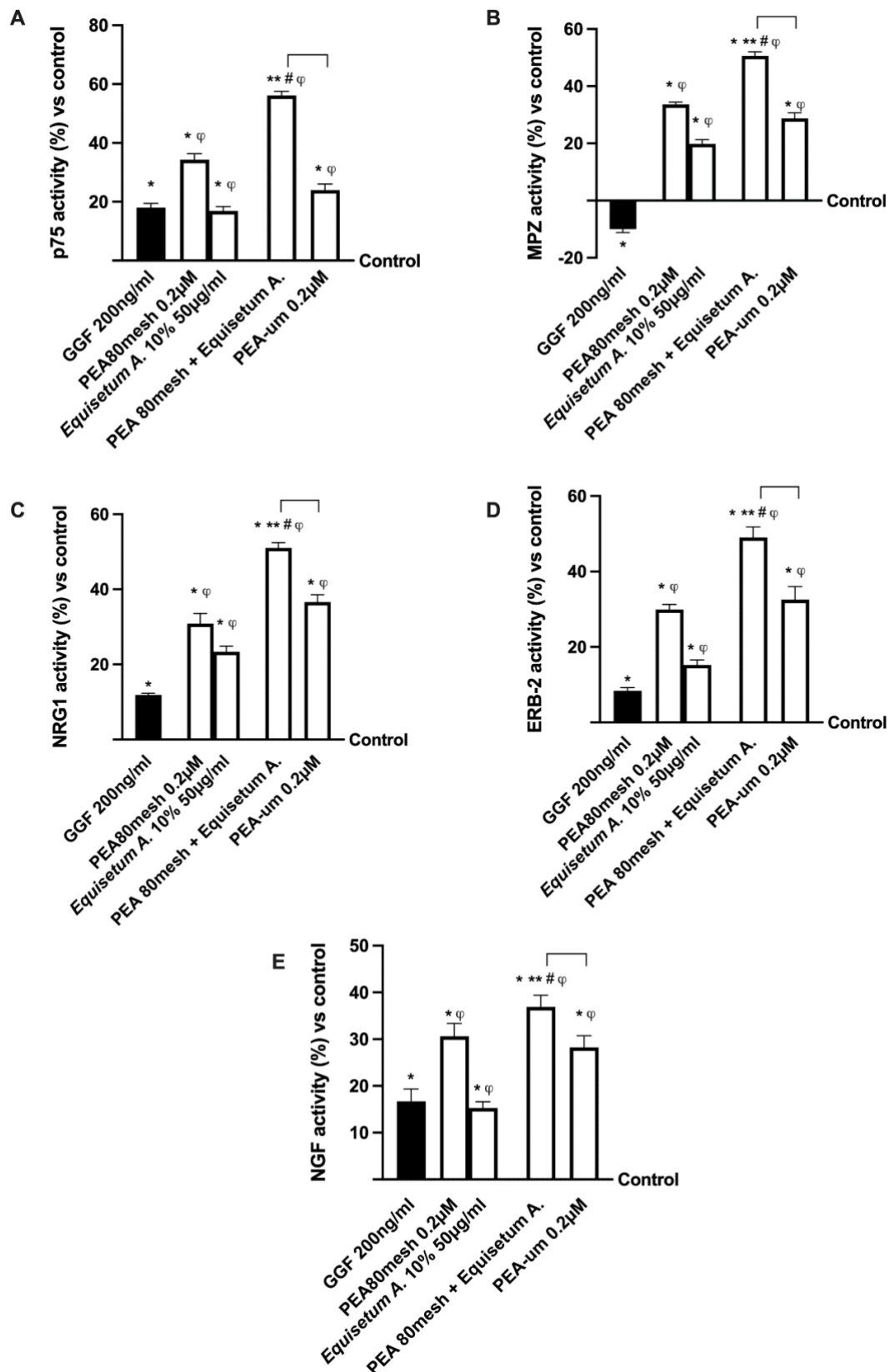
Figure 19. Analysis of Schwann cell activity under PNI condition. In (A) p75 activity by ELISA test; in (B) MPZ by ELISA test; in (C) NRG1 by ELISA test; in (D) ERB-3 by ELISA test. PEA-um= PEA ultra-micronized. Data are mean ± SD (%) of five independent experiments performed in triplicates normalized to control values (0% line). * $p < 0.05$ vs. control; ** $p < 0.05$ vs. PEA 80mesh 0.2μM; # $< 0.05$ vs. *Equisetum Arvense* 50μg/ml; the bar $p<0.05$ vs PEA-um; φ $p < 0.05$ vs. GGF 200ng/ml.

# 4) THE ACTIVITY OF TEN NATURAL EXTRACTS COMBINED IN A UNIQUE BLEND TO MAINTAIN CHOLESTEROL HOMEOSTASIS—*IN VITRO MODEL*

Research on cholesterol homeostasis is taken from the article entitled "*The Activity of Ten Natural Extracts Combined in a Unique Blend to Maintain Cholesterol Homeostasis-In vitro Model*" [182]. Hypercholesterolemia is a major cause of cardiovascular disease and statins, the HMGCoA inhibitors, are the most prescribed drugs. Statins reduce the production of hepatic cholesterol, leading to greater expression of the LDL receptor and greater absorption of circulating LDL, reducing peripheral LDL levels. Unfortunately, statins are believed to induce myopathy and other severe diseases. To overcome this problem, safe nutraceuticals with the same activity as statins could hold great promise in the prevention and treatment of hypercholesterolemia. In this study, the anti-cholesterol efficacy of a new nutraceutical based on 10 natural extracts combined (Esterol10®) was evaluated. In this context, HepG2 cells were used to study the biological mechanisms exerted by the new formulation analyzing different processes involved in cholesterol metabolism, also comparing data with Atorvastatin. The results indicate that these 10 extracts lead to a reduction in total hepatocyte cholesterol and an improvement in the biosynthesis of free cholesterol and bile acids. Furthermore, the anti-cholesterol activity was also confirmed by the modulation of the LDL receptor and by the accumulation of lipids, as well as by the main intracellular pathways involved in the metabolism of cholesterol. In conclusions, Esterol10® is safe and effective with anti-cholesterol activity, potentially providing an alternative therapy to those based on statins for hypercholesterolemia disease.

## 4.1 MATERIALS AND METHODS

### 4.1.1. Cell Culture
The human epithelial hepatocellular carcinoma HepG2 cells were purchased from the American Type Culture Collection (ATCC, Manassas, VA, USA) and were grown in Dulbecco's modified Eagle's medium (DMEM, Merck Life Science, Milano, Italy), supplemented with 10% fetal bovine serum (FBS, Merck Life Science, Milano, Italy), 2 mM L-glutamine (Merck Life Science, Milano, Italy) and 1% penicillin-streptomycin (Merck Life Science, Milano, Italy) at 37 °C and 5% $CO_2$ [183]. The cells used in these experiments had a passage range of 90–95% [184]. After reaching 80–90% confluence, the cells were cultured in different ways based on different experimental protocols: $1 \times 10^4$ cells in 96 well plates to study cell viability by MTT test and LDL uptake; $1 \times 10^6$ cells were cultured in 6-well plates to measure the total cholesterol, and ALT quantification, HMGCoA reductase and related metabolic pathways using ELISA assay and Western blot analysis.

### 4.1.2. Experimental Protocol
HepG2 cells were used to verify the mechanism of action of several natural extracts, alone and combined, compared to RYR, in order to evaluate a possible new strategy to reduce cholesterol accumulation. Before stimulations, the cells were synchronized overnight with DMEM without red phenol and FBS, supplemented with 1% penicillin/streptomycin, 2 mM l-glutamine, and 1 mM sodium

pyruvate in an incubator at 37 °C, 5% $CO_2$, 95% humidity. During all the experiments, the medium was changed with a fresh medium with a high concentration of glucose (30 mM, Merck Life Science, Milano, Italy), and the untreated cells were grown in the presence of normal or 30 mM glucose as the controls [183]. Firstly, to evaluate the effects on HepG2 cells leading to finding the non-toxic concentration, a dose–response study was performed, testing the extracts in a range reported in the literature. Indeed, the cells were treated with increasing concentrations of sage extract (from 0.029 to 0.3 µM) [12], Red Yeast Rice (RYR, from 1 to 50 µM) [10], Vitamin D3 (from 1 to 100 nM) [185], Resveratrol (from 1 to 40 µM) [186], Quercetin (from 5 to 10 µM) [40], Astaxanthin (from 1.7 to 17 nM) [187], CoQ10 (from 1 to 100 µM) [42], Vitamin K2 (from 0.01 to 1 µM) [188], Sodium Selenite (from 1 to 10 µM) [189], Folic Acid (from 25 to 75 µg/mL) [190]. The best concentration of each extract was maintained for all successive experiments.

Secondly, the cells were stimulated with sage extract, Red Yeast Rice, Vitamin D3, Resveratrol, Quercetin, Astaxanthin, CoQ10, Vitamin K2, Sodium Selenite and Folic Acid, alone and combined (named Esterol10®) comparing data to 1 µM RYR alone [91] for 24 h, to exclude any cytotoxic effects by MTT test.

All substances, donated by Uriach Italy srl, were prepared directly in the simulation's medium. In addition, total cholesterol, LDL concentration, and ALT activity were also analyzed using a colorimetric assay in order to evaluate cholesterol metabolism and the possible liver injury. Finally, additional experiments were carried out to verify the effectiveness of the combination (Esterol10®) compared to RYR alone analyzing HMGCoA reductase and the main intracellular pathways involved in cholesterol metabolism. The stimulation time was 24 h [90; 191], corresponding to the duration of anticholesterolemic activity experiments as described above. Atorvastatin (1.25 µM), a concentration comparable with that available in the literature, was applied as a positive control because it is a well-known anticholesterolemic substance [184]. All reported data were obtained by comparing results with those obtained on untreated cells under physiological or high glucose medium.

### 4.1.3. MTT Viability

A3-(4,5-Dimethylthiazol-2-yl)-2,5-Diphenyltetrazolium Bromide (MTT) test was performed following a standard protocol [192] to exclude cytotoxic effects. Briefly, after stimulations, both cell types were incubated with 1% of MTT dye (Merck Life Science, Milano, Italy) in DMEM white for 2 h at 37 °C in an incubator, and then purple formazan crystals were dissolved in an equal volume of MTT solubilization solution. Cell viability was determined by measuring the absorbance at 570 nm with correction at 690 nm, through a spectrometer (VICTOR × 4 Multilabel Plate Reader, PerkinElmer, Waltham, MA, USA), and calculated by comparing results to control cells without any stimulus (baseline 0%).

### 4.1.4 Measurement of Total and Free Cholesterol

The anticholesterolemic activity was determined by a Cholesterol Quantitation Kit (Merck Life Science, Milan, Italy) following the manufacturer's instructions. The fractions of the total, free, and esterified cholesterol were analyzed [184]. Briefly, after stimulation, the medium was removed and the cells were extracted with 200 µL of chloroform:isopropanol:IGEPAL CA-630 (7:11:0.1). The samples were centrifuged at 13,000× g for 10 min and the supernatants were transferred to a new tube which was

aired dry at 50 °C for 30 min to remove chloroform. Dried lipids were dissolved with 200 μL of the Cholesterol Assay Buffer with 50 μL of the Reaction Mix and the samples were incubated for 60 min at 37 °C protected from light. The absorbance was measured at 570 nm by a spectrometer (VICTORX4, multilabel plate reader) and the results were normalized to a sample protein concentration and expressed as μg/μL.

### 4.1.5 LDL Uptake Quantification

The LDL assay was performed using LDLC colorimetric assay kits (cholesterol oxidase/phenol aminophenazone method, Elabscience, Wuhan, China) according to the user manual [193]. Briefly, 2.5 μL of each sample was added to 180 μL of Reagent 1 and then incubated for 5 min at 37 °C. The absorbance was measured by a spectrometer at 546 nm (VICTOR × 4, multilabel plate reader) and the results were calculated by comparing data to control cells (baseline 0%).

### 4.1.6. The Bile Acids Production

The evaluation of the production of bile acids by the HepG2 cells, after stimulations were verified using the fluorometric assay (total bile acid assay) as reported in the literature [194]. Briefly, after stimulations, the cells were washed with cold phosphate-buffered saline (PBS), lysed by sonication in cold PBS 1X (Merck Life Science, Milan, Italy), and centrifuged at 10,000× g for 10 min at 4 °C. Bile acid determination is based on the fluorescence of resorufin measured by a spectrofluorometer at an excitation wavelength of 560 nm and an emission wavelength of 590 nm. The obtained results were normalized on the protein concentration and expressed as a percentage (%) compared to the control (0% line).

### 4.1.7. HMGCoA Reductase ELISA Kit

The HMGCoA Reductase ELISA Kit is suitable for the quantitative detection of HMGCoA Reductase/HMGCR (LSBio, Seattle, DC, USA) following the manufacturer's instructions [195]. Briefly, cells after stimulations were collected, lysed by freezing and thawing 3 times, and centrifuged at 1500× g for 10 min at 2–8 °C. A volume of 100 μL of each sample was incubated with 100 μL of 1× Biotinylated Detection Antibody working solution for 60 min at 37 °C and then with 100 μL 1× HRP-Streptavidin Conjugate for 30 min at 37 °C. After that, 90 μL of TMB Substrate for 15 min at 37 °C in the dark and then 50 μL of Stop Solution were added to each well. The absorbance was measured at 450 nm using a plate reader (VICTORX4 multilabel plate reader) and the results were generated to a standard curve (0.625–40 ng/mL) and expressed as ng/μL.

### 4.1.8. Transaminase Analysis

The ALT assay (Merck Life Science, Milan, Italy) was performed using a colorimetric method to evaluate the levels and activity of metabolic enzymes which are elevated in damaged tissues especially in liver tissue, according to the manufacturer's recommendations [196]. Briefly, the cells were homogenized with 200 μL of ALT Assay Buffer and then centrifuged at 15,000× g for 10 min. A volume of 100 μL of the Master Reaction Mix was added to each sample and after 2–3 min, the measurement was started at 570 nm using a plate reader (VICTORX4 multilabel plate reader). The plate protected from light was incubated at 37 °C taking measurements every 5 min. The final measurement was the

penultimate reading before the most active sample was near the end of the linear range of the standard curve. The results were generated comparing data to the standard curve (0–10 nmol/mL) and expressed as milliunit/mL.

### 4.1.9. Lipid Accumulation Assay

Total lipid accumulation was evaluated by Hepatic Lipid Accumulation Assay Kit (Abcam, Cambridge, UK) following the recommendations of the instructions [183]. Briefly, after stimulation, the cells were fixed in 75 µL of Fixative for 15 min, washed with 100 µL of Wash Solution, stained with 75 µL of Oil Red O Working Solution for 20 min at room temperature, and observed under a microscope (Leica DM1000). In order to quantify the lipid accumulation, 100 µL of Dye Extraction Solution were added to each well, gently mixed for 25 min, and the absorbance was measured at 490–520 nm using a plate reader (VICTORX4 multilabel plate reader). The results were obtained comparing samples OD to control cells (baseline 0%).

### 4.1.10 SREBP-2 Detection Assay

At the end of stimulations, cells were lysed to evaluate the levels of SREPBP-2 following the ELISA kit manufacturer's instruction (LSBio, Seattle, DC, USA) [195]. A volume of 100 µL of samples was added to 96 well ELISA plates and incubated for 2 h at 37 °C. After that, 100 µL of Detection Reagent A was added to each well for 60 min at 37°C in agitation. Then, the plate was incubated with 100 µL of Detection Reagent B for 60 min at 37 °C. At the end, 90 µL of TMB Substrate solution was added for 15 min at 37 °C in the dark. Finally, 50 µL of Stop Solution was added to the plate and the absorbance was measured at 450 nm using a plate reader (VICTORX4 multilabel plate reader). The results were obtained comparing data to standard curves (0.312–20 ng/mL) and expressed as ng/µL.

### 4.1.11. ERK/MAPK Detection Assay

ERK/MAPK activities were measured by the InstantOne™ ELISA (Thermo Fisher) on cell lysates following the manufacturer's instructions [196]. Briefly, cells at the end of treatments were lysed with 100 µL Cell Lysis Buffer Mix, 50 µL/well of each sample was tested in InstantOne ELISA microplate strips, and in each well, the Antibody Cocktail was added and incubated for 1 h at room temperature on a microplate shaker. At the end, the Detection Reagent was added to each well, and after 20 min, the reaction was stopped by adding a stop solution to each. The strips were measured by a spectrometer (VICTOR X4, multilabel plate reader) at 450 nm. The results were expressed as mean absorbance (%) compared to the control.

### 4.1.12. PCSK9 Detection Assay

PCSK9 activity was measured by analyzing PCSK9 level in culture supernatants of HepG2 cells, measured using an ELISA kit according to the manufacturer's instructions (BioVision, CA, USA; Elabscience Biotechnology, Wuhan, China) [197]. Briefly, 100 µL of biotinylated anti-human PCSK9 antibody working solution was added into each well and the plate was incubated at 37 °C for 60 min; the wells were washed with PBS 1× and then incubated for an additional 30 min at 37 °C with 100 µL of ABC working solution. At the end of the time, 90 µL of TMB was added into each well and the plate was incubated at 37 °C in the dark for 20–25 min. Color development at 450 nm was measured using a

microplate reader (VICTOR X4 Multilabel Plate). The results were calculated by generating a standard curve (0–10 pg/mL) and expressed as pg/mL.

### 4.1.13. Cell Lysates and Western Blot

HepG2 cells were lysed in ice with Complete Tablet Buffer (Roche, Basel, Switzerland) supplemented with 2 mM sodium orthovanadate (Na3VO4), 1 mM phenylmethanesulfonyl fluoride (PMSF) (Sigma-Aldrich, St. Louis, MO, USA), 1:50 mix Phosphatase Inhibitor Cocktail (Sigma-Aldrich, St. Louis, MO, USA), and 1:200 mix Protease Inhibitor Cocktail (Sigma-Aldrich, St. Louis, MO, USA). According to the standard protocol, 35 μg of protein of each sample was resolved on 10% SDS-PAGE gels, and polyvinylidene difluoride membranes (PVDF, GE, Healthcare Europe GmbH) was incubated overnight at 4 °C with the following specific primary antibodies: anti-LDL receptor (1:500; Santa Cruz, CA, USA), anti-pSRC (1:500; Santa Cruz, CA, USA), anti-SRC (1:500; Santa Cruz, CA, USA), anti-pAMPK (1:500; Santa Cruz, CA, USA), anti-AMPK (1:500; Santa Cruz, CA, USA) and anti-HMGCr (1:500; Santa Cruz, CA, USA). Protein expression was normalized and verified through anti-β-actin (Sigma-Aldrich, St. Louis, MO, USA). The results were expressed as means ± SD (% vs. control).

### 4.1.14. Statistical Analysis

Data reported were obtained from at least five independent experiments performed in triplicate for each experimental protocol and analyzed using Prism GraphPad statistical software. Results reported are expressed as means ± SD using a one-way ANOVA followed by Bonferroni post hoc test for statistical analysis. $p$ values $< 0.05$ were considered statistically significant.

## 4.2. RESULTS

### 4.2.1. Effects of Several Natural Extracts, RYR, and Atorvastatin on HepG2 Cell Viability

Before exploring the potential anti-cholesterol activity of the new formulation, the effects of the single agents and the RYR alone were evaluated on the viability of HepG2 cells by means of a dose-response study to verify the toxicological analysis, considering 24 h as the relevant exposure time. As reported in Figure 20A–E, all substances were able to induce a reduction in HepG2 cell viability as well as reported in the literature, compared to control. These molecular mechanisms may underlie the agent-induced apoptosis or self-protective response of HepG2 cells. For this reason, the concentration able to maintain or produce little increase in cell viability ($p < 0.05$ vs. control) was chosen for each agent to be used in the final formulation (Figure 20F). In particular, Sage extract 10 μM, Quercetin 10 μM, Vitamin D3 1 nM, Vitamin K2 1 μM, CoQ10 1 μM, Resveratrol 1 μM, Astaxanthin 9 nM, Sodium Selenite 1 μM, Folic Acid 1 μM, and RYR 1 μM were chosen. In addition, when all the agents were added together, no significant changes were observed indicating maintenance of a self-protection response even by the complete formulation (named Esterol10®). Finally, no adverse effect on HepG2 cell viability was observed for atorvastatin.
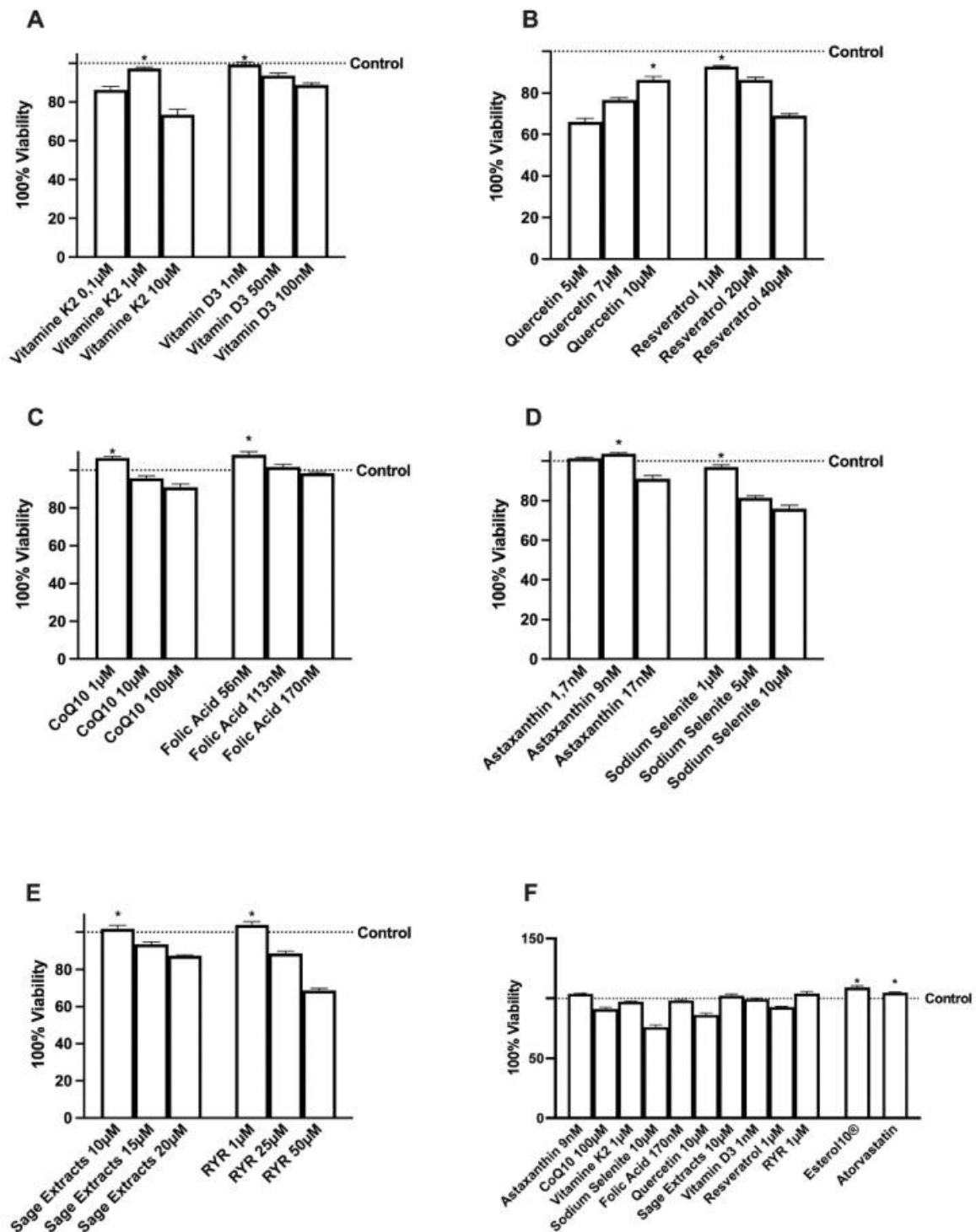
Figure 20. Cell viability of HepG2 cells incubated with the agents alone and combined, for 24 h. RYR = Red Yeast Rice. From A to E the dose-response study on cell viability was measured by MTT test of each single extract such as vitamin K2 and vitamin D3 (A), quercetin and resveratrol (B), CoQ10 and folic acid (C), astaxanthin and sodium selenite (D), sage extract and RYR (E). In (F) the effects of the better concentration of single agents alone and combined (Esterlo10®) were compared to RYR and atorvastatin alone. Viability was calculated as the reduction percentage of cells in the culture medium without the addition of test substances. Data are mean ± SD of five independent experiments performed in triplicates. * $p < 0.05$ vs. control.

## 4.2.2. Effects of Esterol10, RYR, and Atorvastatin on Hepatic Cholesterol Biosynthesis

In light of the results obtained, the evaluation of anti-cholesterol activity was investigated by testing Sage extract 10 μM, Quercetin 10 μM, Vitamin D3 1 nM, Vitamin K2 1 μM, CoQ10 1 μM, Resveratrol 1 μM, Astaxanthin 9 nM, Sodium Selenite 1 μM, Folic Acid 1 μM, and RYR 1 μM in a unique blend

73

(named as Esterol10®) and comparing the data with RYR 1 μM alone and to Atorvastatin 1.25 μM. The biosynthesis of cholesterol was evaluated by analyzing HMGCoA reductase, absorption through LDLr and quantification of lipoproteins, accumulation by total and free cholesterol, and conversion into bile acids following the physiological homeostasis. As reported in Figure 21, HMGCoA reductase that catalyzes the production of mevalonate from HMGCoA which is the rate-limiting step for cholesterol synthesis was analyzed by ELISA (Figure 21A) and Western blot and the relative densitometric analysis (Figure 21B) on HepG2 cells treated with Esterol10® was compared to data from RYR and Atorvastatin. Esterol10® was able to statistically reduce the activity of the enzyme and the receptor expression compared to RYR (about 35% and about 30%, respectively) and Atorvastatin (about 72% and about 50%, respectively), supporting the ability of the combination to prevent the negative consequences of the chronic use of statins leading to the diabetogenic effects. Furthermore, the RYR revealed fewer adverse effects similar to atorvastatin (approximately 27% and approximately 28%, respectively), supporting the hypothesis on the concentration of RYR-dependent side effects.
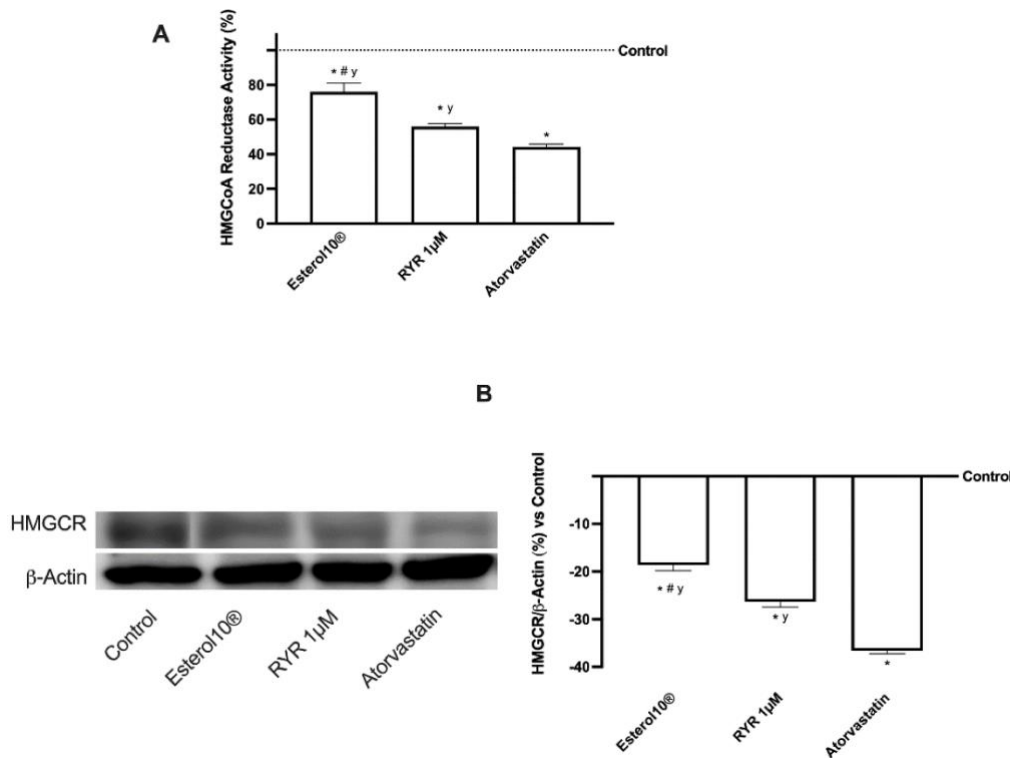


Figure 21. HMGCoA reductase activity (A) and HMGCR expression (B) on HepG2 cells. The abbreviations are the same reported in Figure 20. Data are mean ± SD of five independent experiments performed in triplicates. In panel B, the images reported are an example of a Western blot obtained with technical replicates. * $p < 0.05$ vs. control; # $p < 0.05$ vs. RYR; y $p < 0.05$ vs. Atorvastatin.

### 4.2.3. Effects of Esterol®, RYR, and Atorvastatin on Cholesterol Metabolism

Since the hepatic cholesterol after the enzymatic esterification and incorporation into lipoproteins is transported to the peripheral tissues by LDL or excreted as free cholesterol or eliminated by cholesterol-derived bile acids, additional experiments were carried out to analyze this mechanism. Consequently, it is important to define if Esterol10® is an effective treatment for hypercholesterolemia compared to 1 μM RYR and 1.25 μM Atorvastatin by reducing cholesterol through lowering total

cholesterol and/or by increasing free cholesterol hepatic content. As shown in Figure 22A, all formulations tested are able to significantly reduce the total cholesterol content in HepG2 cells ($p < 0.05$ vs. control by all substances); in particular Esterol10® exerted the main effect compared to RYR (about 56%) and Atorvastatin (about 74%) supporting the better influence of the single agents combined in the formulation. In addition, only Esterol10® is effective in increasing free cholesterol production (Figure 22B); in particular, this effect was more evident compared to RYR ($p < 0.05$, about 22%) which induced a little increase compared to control ($p < 0.05$). As expected, atorvastatin showed no effect on free cholesterol, while total cholesterol was significantly reduced by approximately 20%.

To confirm the anti-cholesterol activity, the involvement of the LDLr and the consequences of LDL uptake on HepG2 cells were also investigated by Western blot and ELISA. In fact, by increasing the expression of the LDLr gene, the LDLr protein on the plasma membrane of the hepatocytes and the absorption of LDL were improved by Esterol10® ($p < 0.05$) compared to RYR (about 1.5 times more on the LDL receptor and about 90% LDL uptake) and atorvastatin (about 1 time over LDL receptor and about 80% LDL uptake) as shown in Figure 22 C,D.
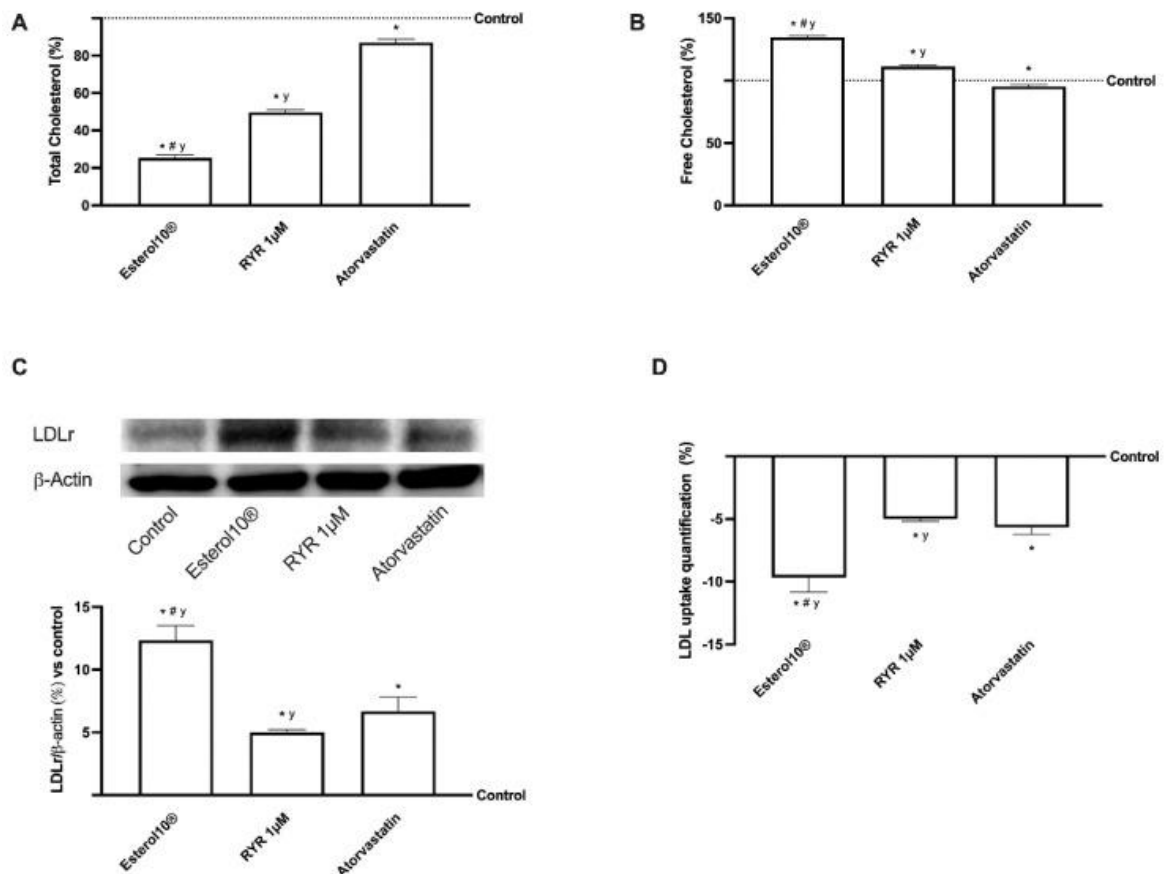


Figure 22. Total Cholesterol (A), Free Cholesterol (B), LDLr (C), and LDL uptake quantification (D) on HepG2 cells. The abbreviations are the same reported in Figure 20. Data are mean ± SD of five independent experiments performed in triplicate. In (C), the images reported are an example of a Western blot obtained with technical replicates. * $p < 0.05$ vs. control; # $p < 0.05$ vs. RYR; y $p < 0.05$ vs. Atorvastatin.

### 4.2.4. Effects of Esterol10®, RYR, and Atorvastatin on Choleresis Process

Increased hepatic free cholesterol content is the major form of cholesterol released through bile, and is a key step in general cholesterol homeostasis (route of excretion). As the control of this production is considered an important target for the treatment of hypercholesterolemia, the potential ability of 1 μM of Esterol10, 1 μM RYR, and 1.25 μM Atorvastatin to increase the conversion of cholesterol to bile acid was therefore investigated (Figure 23). In particular, Esterol10® has been shown to significantly increase bile acid production in the *in vitro* hepatic model by approximately 1.5-fold more than RYR (p < 0.05) and one-fold more than Atorvastatin (p < 0.05), indicating that it is the best formulation with choleretic action. Furthermore, the RYR increased bile acid production by approximately 9% compared to the control, while atorvastatin was able to increase bile acid production by approximately 6%, less than the RYR, confirming their ability to stimulate the synthesis of bile acids.
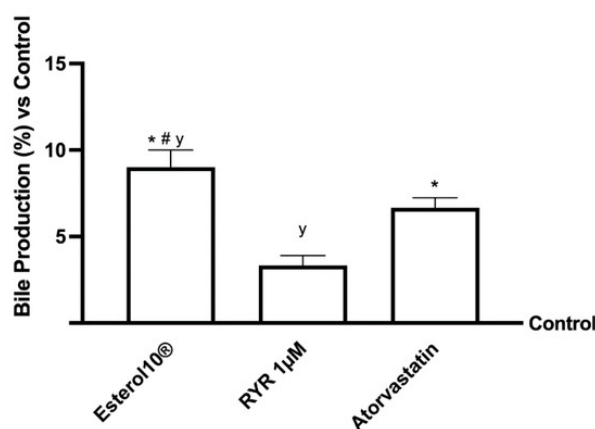


Figure 23. Bile acid production following treatment of hepatic *in vitro* model. The abbreviations are the same as reported in Figure 20. Data are mean ± SD of five independent experiments performed in triplicate. * p < 0.05 vs. control; # p <0.05 vs. RYR and y p < 0.05 vs. Atorvastatin.

### 4.2.5. Effects of Esterol10®, RYR, and Atorvastatin on the Intracellular Pathways Leading to Cholesterol Homeostasis

Many nutraceuticals and statins have also been shown to induce the expression of the PCSK9 gene which binds directly to LDLr to lower plasma cholesterol. This mechanism may be involved in the activation of the transcriptional activity of the sterol responsive element binding protein (SREBP). In particular, SREBP-2 preferentially transcribes the genes involved in the biosynthetic pathway of cholesterol. This mechanism is also important for activating the AMPK/SREBP pathway to reduce lipid accumulation in the liver. AMPK is an important protein involved in energy metabolism and the regulation of fatty acid metabolism [90]. In this context, as reported in Figure 24, these proteins and their mechanisms have also been studied in HepG2 cells after stimulation with 1 μM Esterol10®, 1 μM RYR, and 1.25 μM Atorvastatin. As shown in panel A and B, Esterol10® is able to improve the activity of PCSK9 (about 20% more than 1 μM RYR and about 2 times more than Atorvastatin, p < 0.05); on the contrary, treatment with Esterol10® inhibits the activity of SREBP-2, about 42% less than 1 μM RYR and about once more than Atorvastatin (p < 0.05), showing that SREBP phosphorylation can regulate protein expression, and confirming the involvement of AMPK/SREBP signaling in treatment with Esterol10®. Since PCSK9 is also directly associated with CD36, which is often associated with inflammation and steatosis, it regulates LDLr levels and complex the AMPK signaling cascade which includes the SRC kinase [198]. Therefore, the same trend observed by PCSK9/SREBP, was also observed

by the expressions AMPK (panel C) and SRC (panel D). Indeed, Esterol10® is able to activate the AMPK pathway (about 18% more than 1 μM RYR and about 90% compared to Atorvastatin, $p < 0.05$) and to inhibit SRC (about 73% less than 1 μM RYR and about 91% compared to Atorvastatin, $p < 0.05$) indicating that Esterol10® plays a fundamental role on the AMPK/SRC pathway supporting our hypothesis of an active role of Esterol10® in the modulation of cholesterol metabolism. Furthermore, numerous evidence indicates that the extracellular signal-regulated kinases (ERK) signaling pathway is involved in the regulation of PCSK9 and LDLr [199]; thus, to further confirm the activity of Esterol10® in regulating the cholesterol level, we also studied the activity of ERKs/MAPK by means of ELISA tests. As shown in panel E, Esterol10® could increase the ERK1/2 signal pathway (approximately 25% compared to 1 μM RYR and approximately 1.5 times more than Atorvastatin, $p < 0.05$) indicating, once again, which could regulate cholesterol metabolism even at the beginning of the cascade signaling. Collectively, these results suggest that Esterol10® enhanced PCSK9 expression and reduced SREBP-2 activity in HepG2 cells, also regulating the AMPK/SRC pathway through activation of the ERK1/2 signaling pathway.
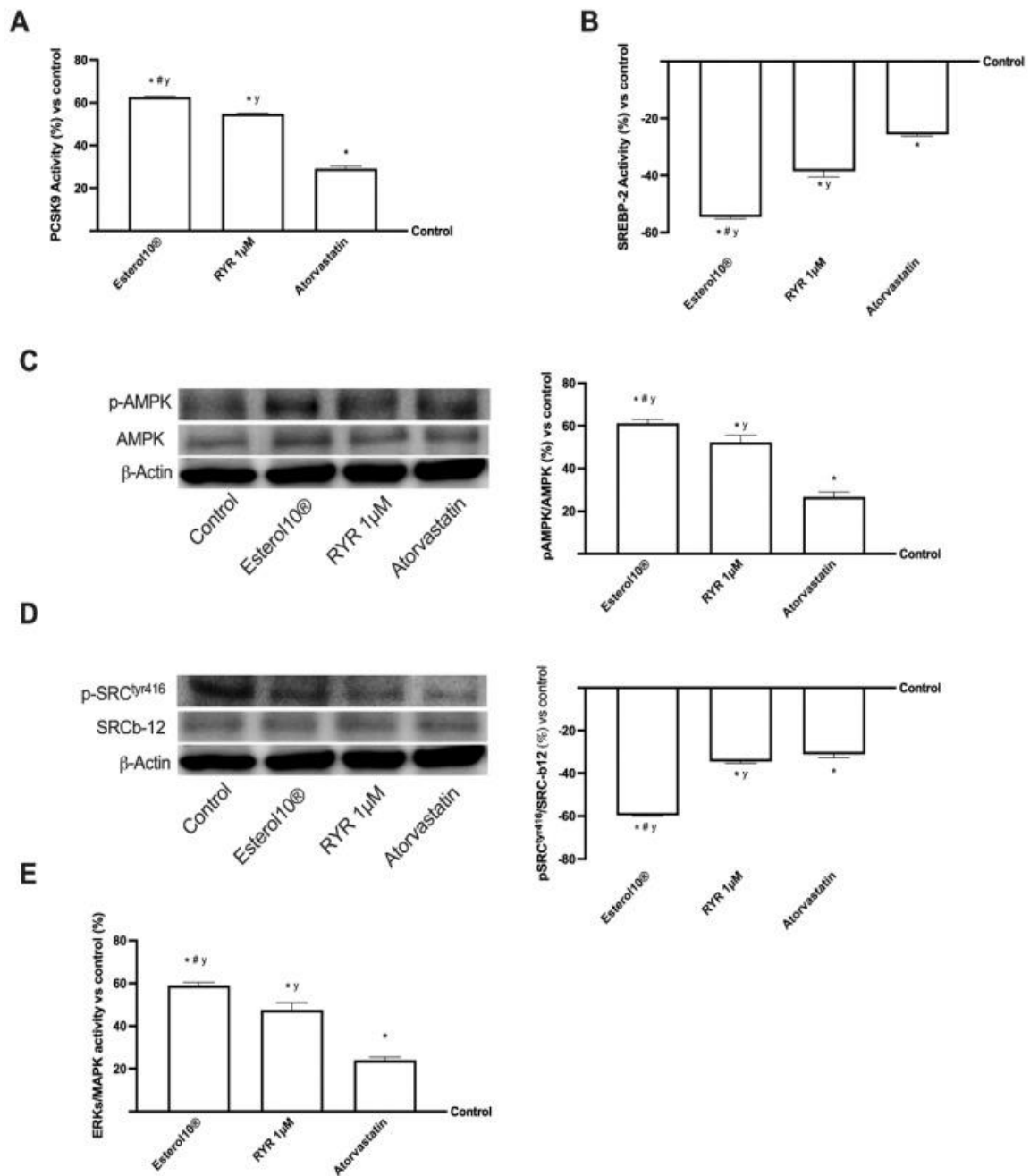
Figure 24. Intracellular pathways activated in HepG2 cells. In (A,B,E) the protein activity of PCSK9, SRC, and ERK was measured by an ELISA test; in (C,D) the analysis of AMPK and SRC performed by Western Blot and densitometric analysis. The abbreviations are the same reported in Figure 20. Data are mean ± SD of five independent experiments performed in triplicates. The images reported are an example of a Western blot obtained with technical replicates. * $p < 0.05$ vs. control; # $p < 0.05$ vs. RYR; y $p < 0.05$ vs. Atorvastatin.

78

### 4.2.6. Effects of Esterol10®, RYR, and Atorvastatin on Liver Injury Markers

Some researchers have suggested that statin and monacolin K treatment is closely related to biochemical parameters responsible for liver injury. To explore this aspect, the tissue damage associated with our treatment was assessed by measuring alanine aminotransferase (ALT). According to the results shown in Figure 25 (panel A), ALT activity decreased significantly after treatment with Esterol10® compared to the control ($p < 0.05$) and compared to 1 $\mu$M RYR (about 7 times more) and to Atorvastatin (about 2 times more) confirming the positive role of Esterol10® in reducing liver damage; this is normally found after chronic treatment with statins, which is known leads to other risk factors, such as hypertension or diabetes mellitus. Furthermore, the effects of Esterol10® on the accumulation of HepG2 lipids were confirmed by determining the TG total content, both quantitatively and qualitatively, using the Oil Red stain and the lipid accumulation test, respectively, after 1 $\mu$M of Esterol10®, 1 $\mu$M RYR, and 1.25 $\mu$M of Atorvastatin for 24 h. As shown in Figure 25B, the total lipid accumulation determined by Oil Red staining was significantly higher ($p < 0.05$) in control cells than in other treatments; in particular, the attenuation of lipid accumulation was further contrasted by Esterol10® compared to Atorvastatin and, even more evidently, by 1 $\mu$M RYR. Furthermore, Esterol10® significantly reduced ($p < 0.05$) lipid levels compared to the control at 1 $\mu$M RYR and Atorvastatin (approximately 75%, 40%, and 88%, respectively). These results also demonstrate for the first time that Esterol10® regulates lipid metabolism without side effects.
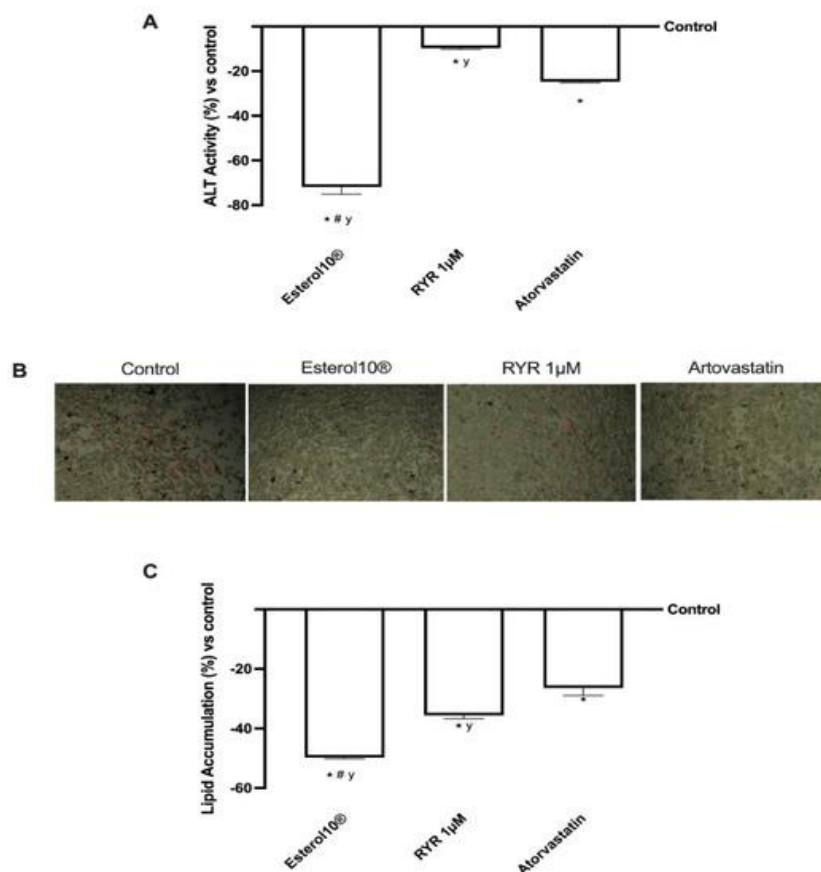


Figure 25. Tissue integrity analysis. In (A), ALT activity was measured by an ELISA test. Images captured under the microscope at an original magnification of ×20 and reported in (B) showed the intercellular oil droplets stained by the Oil Red stain. These oil droplets are solubilized for quantification by spectrophotometric analysis reported in (C). The abbreviations are the same as shown in Figure 20. Data are mean ± SD of five independent experiments performed in triplicate. * $p < 0.05$ compared to the control; # $p < 0.05$ vs. RYR; y $p < 0.05$ vs. Atorvastatin.

# 5) PREVENTING C2C12 MUSCULAR CELLS DAMAGE COMBINING MAGNESIUM AND POTASSIUM WITH VITAMIN D3 AND CURCUMIN

Research on prevention of hypercontraction damage is taken from the article entitled "*Preventing c2c12 muscular cells damage combining magnesium and potassium with vitamin D3 and curcumin*" [192]. Physical activity is defined as any bodily movement produced by skeletal muscles which causes energy consumption; moderate and constant physical activity is known to be beneficial and to slow the muscle loss process associated with aging. The aim of the present study was to test, in an *in vitro* exercise model, the biological effects of a new formulation composed of magnesium and potassium combined with vitamin D and curcumin created to support muscle activity and to prevent hypercontraction damage. In this context, C2C12 cells were treated with vitamin D, buffered magnesium bisglycinate, curcumin, and potassium citrate. Cell viability, morpho-functional changes, calcium and magnesium movements, and the main kinases involved in glucose uptake were analyzed. The glycogen level and lactate were also evaluated. Important results about a positive effect on mitochondrial activity, ATP production, oxygen consumption and in the physiological differentiation of C2C12 cells were obtained. Further experiments were performed under conditions that mimic the biological aspects of strenuous exercise. The combination of magnesium, vitamin D3, curcumin, and potassium citrate revealed beneficial effects on skeletal muscle cells under physiological conditions as well as while mimicking intense activity. In particular, in an *in vitro* model, they were able to control the hypercontraction, restoring ion fluxes, reducing inflammation signaling and supporting the main mechanism involved on aerobic activity. In conclusion, the results have indicated for the first time that this new combination could be considered as a new nutraceutical formulation to improve physical performance and muscle recovery.

## 5.1. MATERIALS AND METHODS

### 5.1.1. 2C12 cell culture

C2C12 murine myoblasts were purchased from American Type Culture Collection (Manassas, VA, USA). Cells were grown in Dulbecco's Modified Eagle Medium (DMEM; Sigma-Aldrich, Milan, Italy) supplemented with 10% FBS (Sigma-Aldrich, Milan, Italy), 100U/ml penicillin/streptomycin and maintained in an incubator at 37 °C, 5% $CO_2$ and maintained at 40–70% density to obtain cell growth (proliferation) without cell differentiation. Depending on the various experimental protocols used, $1 \times 10^4$ cells were plated on 96-well plates to study the mitochondrial activity by MTT test and ATP level; $4 \times 10^4$ cells were plated in black 96-well plates to study oxygen consumption and mitochondrial membrane potential; $10 \times 10^4$ cells/well were seeded in six-well plates to investigate with Western blot the intracellular pathways activated, to analyze the activities by ELISA and the Glucose/Glycogen and lactate productions. To synchronize the cell cycle, C2C12 cells were incubated with DMEM without red phenol for 24 h before stimulation. The growth medium was changed with 2%FBS, containing various several agents alone and combined for a time ranging from 1 h to 8 h and 24 h–72 h to verify the early phase of differentiation and the main mechanism activated. This condition was maintained during all experimental protocols used. The effects of vitamin D3, magnesium bisglycinate, potassium

citrate, and curcumin were tested in the presence or absence of a high concentration of caffeine (2.5 mM) an agent that causes calcium release from the SR, to mimic the effects of muscle contraction [200].

### 5.1.2. Experimental protocol

C2C12 cell line was used to evaluate the effects of vitamin D3, magnesium bisglycinate, potassium citrate, and curcumin alone or in combination to support the cellular mechanisms underlying exercise. In addition, the role of severe contraction caused by caffeine as a side effect was investigated in presence of the more effective combination of the substances tested alone to prevent or restore the muscle damage. This study was divided into three phases. In the first phase, a dose-dependent study of the single agents (ranging from 1 h to 24 h) on cell viability was investigated to exclude negative effects. In particular, the concentrations of the substances were obtained from the literature: vitamin D3 (V) 0.001μM–1μM; 15% magnesium bisglycinate chelate buffered (M) 0.1μM-5mM; potassium citrate (K) 0.1mM–5mM; curcumin (C) 1μM–100 μM were tested [182, 201]. The main effects observed were obtained by M and K 1 mM, VD 100 nM and C 100 μM, and these concentrations were used together to verify the properties of a new combination, named MKVC, in the second and third phases of the study. In the second phase, the main intracellular mechanisms underlying exercise were investigated and in the third phase, the same analyses were carried out in presence of caffeine 2.5 mM to mimic a hypercontractility condition [202]. All substances were prepared directly into medium in a 10X concentration without adding other agents and directly used to obtain the reported final concentration.

### 5.1.3. Cell viability

Cell viability was analyzed at the end of each stimulation using MTT-based *in vitro* Toxicology Assay Kit (Sigma-Aldrich, Milan, Italy), as previously described [175] Details of the method are given in Supplementary 1.

### 5.1.4. Oxygen consumption and mitochondrial membrane potential

The oxygen consumption and mitochondrial membrane potential were immediately and simultaneously quantified by Oxygen Consumption/Mitomembrane Potential Dual Assay Kit (Cayman Chemical Company; Ann Arbor, MI, USA) following the manufacturer's instructions as reported in literature (details are given in Supplementary 2) [203].

### 5.1.5. ATP assay

At the end of each stimulation, the cells were immediately treated with the components of the ATP assay kit (Calbiochem, San Diego, USA), following the manufacturer's instructions (details are given in Supplementary 3) [204].

### 5.1.6. [Mg2+]i movements

Intracellular Magnesium concentration ([Mg2+]i) was measured using Mg2+-sensitive fluorescent dye Mag-fura-2AM (Furaptra, Biotium) as previously described [175]. Briefly, the cells were incubated in a Hanks salt solution (Thermo Fisher Scientific, Waltham, USA) without Mg2+ containing 10 mM glucose and supplemented with 20 mM HEPES/Tris (pH 7.4), 1.3 mM CaCl2, and 5 μM Mag-fura-2AM

at 37 °C for 30 min. The cells loaded fluorescent with Mag-fura-2AM was monitored at regular intervals starting from 3min to 300min (15, 30, 60, 120, 150, 180, 210, 240, 270) with excitation at 340 nm and 380 nm. The acquisitions were obtained using a Fluorescence Spectrometer VICTORX4 multilabel plate reader at an emission wavelength of 510 nm with an exposure time of 100 ms. The fluorescence ratios (340/380 nm) were calculated and compared to control; Rmax and Rmin were analyzed by the addition of 50 mM MgCl2 and 100 mM EDTA, respectively [205].

### 5.1.7. [Ca2+] movements

Calcium movements analysis was performed following a classical technique [175] Cells have been washed twice with sterile PBS 1 × and incubated with 5 μM Fura-2AM (Sigma-Aldrich, Milan, Italy) for 30 min in the dark in PSS buffer without Ca2+ (1.5 mM KCl, 10 mM HEPES, 10 mM d-Glucose, 2 mM l-Glutamine, pH 7.4), under shaking at 37 °C. After the stimulations, the fluorescence was measured by a fluorescence spectrometer (VICTORX4 multilabel plate reader) at excitation wavelengths of 340 nm and 510 nm for emission. The results were reported as means ± SD% compared to control cells.

### 5.1.8. TNF$\alpha$ assay

TNF-$\alpha$ concentration in C2C12 cells was determined using TNF$\alpha$ ELISA kit (Sigma, Milan, Italy) according to the manufacturer's instructions [206].

### 5.1.9. Glucose uptake

Cells were lysed in the extraction buffer as reported on the manufacturer's instruction of Glucose Uptake Colorimetric Assay Kit (Sigma-Aldrich) [207].

### 5.1.10. Glycogen measurement

The glycogen synthesis assay was performed following the manufacturer's instructions (BioVision, Life Research, Scoresby Victoria, Australia)[208].

### 5.1.11. Lactate measurement

As reported in literature [209] the quantification of lactate level on C2C12 cells was measured after lyses on supernatants using a lactate assay kit (BioVision) according to the manufacturer's instructions. The contents of pyruvate and lactate were normalized to the total protein amount.

### 5.1.12. Akt activation assay

PI3K/Akt activities were measured by the InstantOneTM ELISA (Thermo Fisher, Milan, Italy) following the manufacturer's instructions [155].

### 5.1.13. Phospho-p38/MAPK ELISA test

The phosphorylation levels of p38/MAPK were analyzed on cells lysates following the manufacturer's instructions as reported on Supplementary 8 (ELISA Kit, Abcam) [210].

### 5.1.14. Cell lysates and Western blot

At the end of each treatment, C2C12 cells were washed twice with ice-PBS 1X and lysed in ice using Ripa Buffer (50 mM Hepes, 150 mM NaCl, 0,1% SDS, 1%TRITON 100x, 1% deoxycholate acid, 10% glycerol, 1,5 mM MgCl2, 1 mM EGTA, 1 mM NaF; all purchased from Sigma-Aldrich) supplemented with 2 mM sodium orthovanadate (Sigma-Aldrich), 1 mM phenylmethanesulfonyl fluoride (PMSF; Sigma-Aldrich) and 1:100 mix Protease Inhibitor Cocktail (Sigma-Aldrich). 40 μg of protein of each sample was resolved into 8% and 15% SDS-PAGE gels, and polyvinylidene difluoride (PVDF) membranes (GE Healthcare) were incubated overnight at 4 °C with specific primary antibody: anti-rabbit Cyclin D1 (1:1000, Cell Signalling), anti-mouse Desmin (1:1000, Santa-Cruz), anti-rabbit Phospho-AMPK (1:1000, Millipore), anti-mouse AMPK (1:500, Santa-Cruz), anti-mouse Phospho-JNK (1:500, Santa-Cruz), anti-mouse JNK (1:500, Santa-Cruz) and anti-mouse SMA (1:1000, Santa-Cruz). Protein expression was normalized and verified through anti-mouse β-actin detection (1:5000; Sigma-Aldrich) and reported as mean ± SD (% vs control).

### 5.1.15. *In vitro* experimental model for examining the skeletal muscle cell biology of exercise

Due to its powerful ergogenic and metabolic stimulating effects in skeletal muscle, caffeine has been used in a series of experiments to mimic exercise-like conditions to test the MKVC combination in a hypercontractility scenario. Caffeine was used at 2.5 mM, as suggested by studies in the literature [200].

### 5.1.16. Statistical analysis

Data reported were obtained from at least five independent experiments performed in triplicates for each experimental protocol and analyzed using Prism GraphPad statistical software. Results are reported as means ± SD using One-way ANOVA followed by Bonferroni post hoc test for statistical analysis. $p$ values < 0.05 were considered statistically significant.

## 5.2. RESULTS

### 5.2.1. Dose-response and time-dependent study of cell viability on C2C12 cells

To verify the effects and to exclude any cytotoxic effects, C2C12 cells were stimulated with magnesium (M), potassium citrate (K), vitamin D3 (V) and curcumin (C) alone in dose-response and time-dependent experiments (24–72 h) by analyzing cell viability using MTT assay. As shown in Fig. 26A–D, in the first set of experiments all substances were able to induce an increase in cell viability during the time without cytotoxic effects. In particular, M and K (Fig. 26A and B, respectively) showed an inversely proportional effect where the 1 mM concentration was able to induce a greater effect than the other concentrations throughout the analyzed period ($p < 0.05$). V and C (Fig. 26C and D, respectively) showed a directly proportional effect to the dose used and V 100 nM and C 100 μM were able to induce greater effects than other concentrations tested throughout the period analyzed. All these data confirmed that none of the substances had cytotoxic effect overtime on muscle cells and 1 mM for M, 1 mM for K, 100 nM for V and 100 μM for C were the concentrations tested in combination and maintained in all subsequent experiments. As reported in Fig. 26E, the effect of the combination of tested substances, named MKVC, was also investigated on cell viability to verify its effectiveness and to exclude any negative effects. Data confirmed a time-dependent effect with a maximum effect at 24 h compared to control ($p < 0.05$, about 92%) and to all other time points ($p < 0.05$, about 52% at 8 h, 48% at 8 h and 17% at 72 h), indicating the effectiveness of the combination in stabilizing the effects of individual agents on mitochondrial health over time.
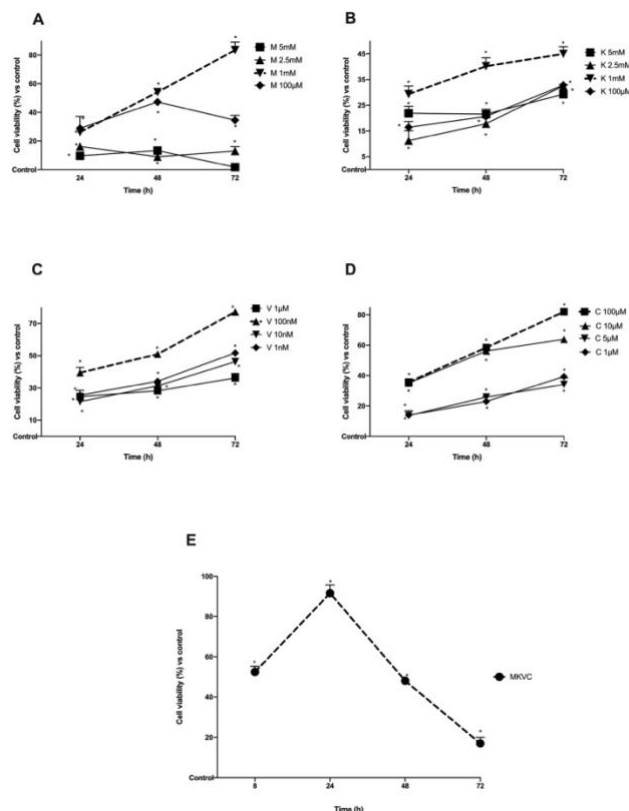


Figure 26. Cell viability measured by MTT. From panel A to D single agents were tested alone in a dose-response and time-dependent study. M = magnesium in panel a; K = potassium citrate in panel b; V = vitamin D3 in panel c; C = curcumin in panel d. The best dose chosen from the tested range of individual agents is indicated in red. Data reported are expressed as means ± SD of five independent experiments. *$p < 0.05$ vs control. In E the cell viability of the combined product named MKVC. MKVC = magnesium, potassium citrate, vitamin D and curcumin added together. *$p < 0.05$ vs control.

### 5.2.2. Morpho-functional changes in C2C12 cells treated with MKVC

To understand if this new combination was also able to induce a physiological differentiation on myotubes of C2C12 cells, further experiments were carried out by stimulating the cells for 24 h and 72 h analyzing the differentiation phases, using cyclin D1 and desmin by Western blot analysis (Fig. 27A and B, respectively). The MKVC combination was able to induce a greater effect than the control ($p < 0.05$) confirming that cyclin D1 expression is abundant in proliferating myoblasts and similar data were derived from desmin analysis. Furthermore, this combination induced a greater effect at 72 h than at 24 h ($p < 0.05$ vs control) indicating that differentiation began at 24 h (about 27.7% and 35% on both proteins, respectively) confirming the hypothesis of better effect in conditions of intense activity.
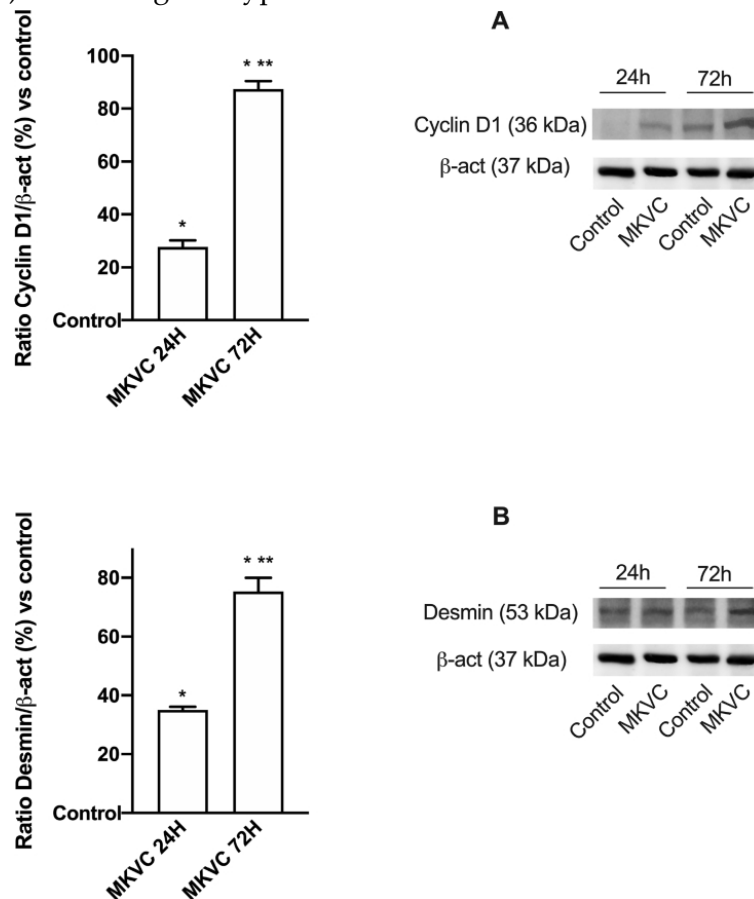


Figure 27. Western blot and densitometric analysis. In A cyclin D1 and in B desmin expressions caused by MKVC during time (at 24 h and 72 h). An example of Western blot normalized through β-act is reported. Data are reported as means ± SD of six independent experiments. The abbreviations are the same as reported in Fig. 1. ∗$p < 0.05$ vs control; ∗∗$p < 0.05$ vs 24 h of stimulation.

Mitochondrial activity is crucial for myoblast proliferation, and it is always accompanied by increased ATP production and oxygen consumption. The analysis of mitochondria by JC1 suggested that MKVC has a significant impact on mitochondrial activity, particularly on mitochondrial membrane potential. It was able to induce a greater increase compared to control ($p < 0.05$) at 24 h versus 72 h (about 9% and about 7%, respectively), as shown in Fig. 28A, confirming a physiological increase in the chemical energy of the cells. In order to obtain more information on mitochondrial metabolism during exercise, oxygen consumption and ATP production were also studied. As shown in Fig. 28B and C, the rate of oxygen consumption and ATP production played an important role in myoblast proliferation. Indeed, MKVC induced an increase in oxygen and ATP consumption compared to the control ($p < 0.05$) and

between the two times at 24 h, no significant changes were observed that could indicate the physiological activity of the mitochondria.
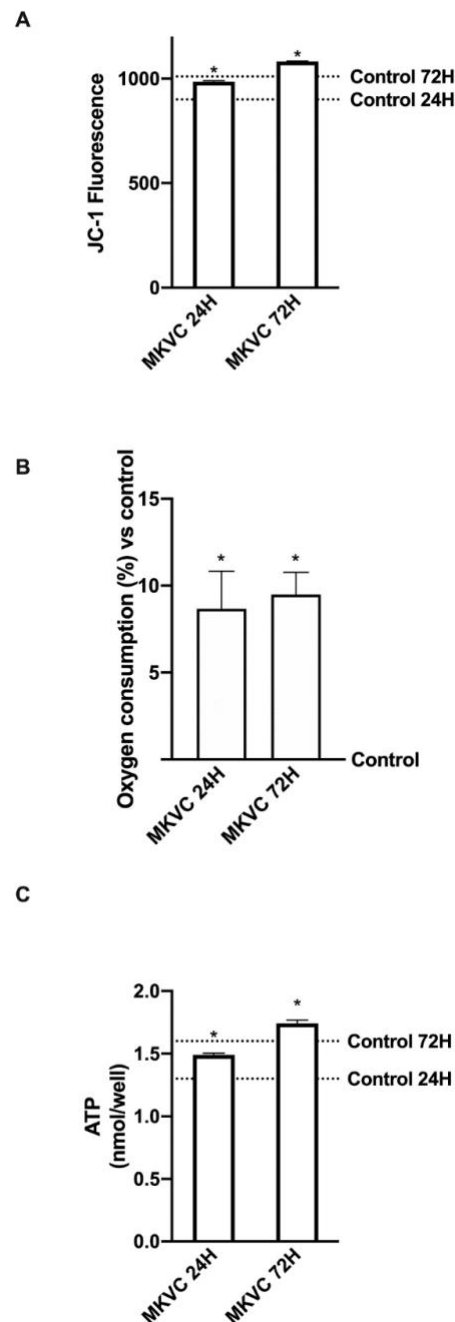


Figure 28. Analysis of cellular energy. In A mitochondrial potential membrane, in B oxygen consumption and in C ATP levels caused by MKVC during time (at 24 h and 72 h). Data are reported as means ± SD of six independent experiments. The abbreviations are the same as reported in Fig. 1. $*p < 0.05$ vs control.

### 5.2.3. Calcium-magnesium flux analysis to determine the effects on biology of contraction-relaxation cycle

As it is known, muscle contraction during exercise depends on variations in the intracellular concentrations of calcium ions (Ca2 +). Since the behavior of calcium in C2C12 cells is like that observed in *in vivo* experiments, changes in calcium and magnesium levels by Fura-2AM and Furaptra were analyzed *in vitro*, respectively. These experiments were carried out to clarify the importance of Mg2+

and Ca2+ movements after treatments with MKVC under free-Mg2+ and Ca2+ medium conditions. The balance between calcium and magnesium movements is a reference of the cycles of contraction and relaxation and, as reported in Fig. 29, it showed an alternating pattern from 3 min to 180 min with respect to the control ($p > 0.05$). The presence of magnesium in the formulation produces a physiological movement of calcium ions. This up and down flow was supposed to be related to the contraction-relaxation cycle. MKVC showed a significant effect over time that was significant at 5 min and 60 min (45% and 47% respectively), supporting MKVC effects on the contraction-relaxation cycle. In addition, these effects regulate a physiological balance between Mg2+ and Ca2+ flux. Data suggest that MKVC is able to reduce electrolyte flux peaks also at a physiological level, indicating lower energy consumption during muscle activity over time.
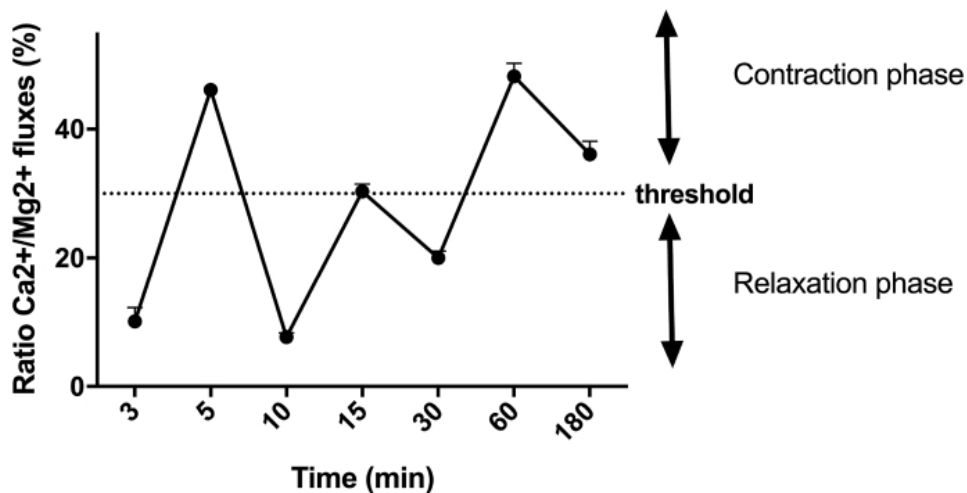


Figure 29. Effect on contraction of MKVC. The graph shows a ratio from calcium movements and magnesium flux normalized to control values ranging from 3min to 180min. After the administration of MKVC (time 0), a series of oscillations of the Ca2+/Mg2+ ratio was observed, which correspond to cycles of contraction and relaxation of the cells. Data are reported as means ± SD (%) of five independent experiments. All time points are ∗$p < 0.05$ vs control.

### 5.2.4. Assessment of muscle activity and inflammation in C2C12 cells

Following the treatment, an immune response could be triggered to assist myoblast proliferation. Since TNFα expression can increase myoblast proliferation, to understand if pro-inflammatory cytokines play a role in this context, TNFα quantification was performed on C1C12 myoblast at the two-time point chosen on the effects on cell viability at 8 h (the beginning of effect) and 24 h (maximum effect). As shown in Fig. 30A, MKVC induced TNF-α released at 8 h hours and 24 h (about 8.7% respect with control and 16% respect with 8 h) in a physiological way; indeed at 8 h the production was near the control values ($p > 0.05$) and at 24 h the production was less than control ($p < 0.05$) indicating that no inflammation response was taking place. Furthermore, since MKVC administration results in normal cytokine production under physiological conditions over time, the data suggest that this formulation may be more effective in hypercontractility conditions. Since muscle is the most important user of glucose, the accumulation and degradation of glycogen in skeletal muscle plays a central role in systemic glucose homeostasis. To evaluate glucose/lactate concentration and glycogen accumulation, C2C12 cells were treated with MKVC and their respective analysis were performed. As shown in Fig. 30B and C, glycogen and glucose concentrations were more present in the myoblast at 8 h than 24 h compared to control ($p < 0.05$) (about 10.5% and 79% respectively). The glucose concentration showed the same trend as the glycogen variation suggesting that these two main reserves of muscle fuels were

consumed under physiological conditions after MKVC stimulation. At the base of this mechanism there is also the lactate role, which is a metabolic intermediate mainly produced in muscles under anaerobic conditions, especially during exercise. Lactate was previously regarded as "a metabolic waste product" but is now known to be an important fuel source, either used within cells or exported to adjacent organs. Lactate analysis was performed by intra- and extra-cellular analysis and as shown in Fig. 30D, the extra-cellular level was more abundant at 8 h than 24 h with respect to control ($p <$ 0.05); at 8 h lactate level was about 2% respect 24 h. These data suggest that under physiological conditions, MKVC induces a lower intracellular accumulation of lactate with consequent greater consumption of glucose supporting the aerobic activity.
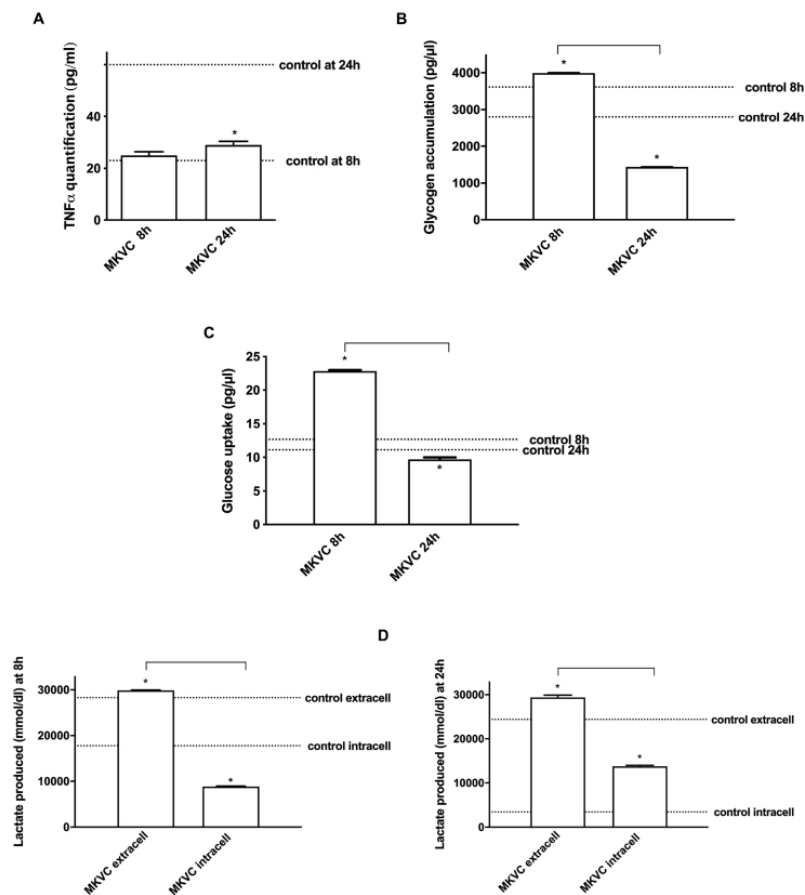


Figure 30. Analysis of several contraction parameters. In A TNF-$\alpha$ ELISA assay, in B glycogen accumulation, in C glucose uptake, and in D lactate analysis with intracellular and extracellular quantification. All these parameters were investigated at two time points. The abbreviations are the same as used in Fig. 1. Data are reported as means ± SD of five independent experiments. ∗p < 0.05 vs control; the bars p < 0.05 between the different time points.

### 5.2.5. Analysis of the intracellular pathways activated by MKVC on C2C12 cells

To explore whether MKVC can support different phases and moments in the intracellular mechanisms involved in an exercise, further experiments were performed by analyzing some important kinases in muscle cells. As reported in Fig. 31A, the activity assay of p38/MAPK was analyzed as a marker of contractile response at 8 h and 24 h of stimulations. Data confirmed MKVC's role in aiding the activation of this intracellular pathway at 8 h. Moreover, the effect at 24 h is reduced leading to the energy conservation state. In contrast, the effect at 8 h supported previous findings on the proliferation phase induced by MKVC compared to control (p < 0.05). A second major pathway supporting protein synthesis and glucose uptake, PI3K/Akt (Fig. 31B), confirmed its ability to support a late phase of cell

activation since MKVC can induce its activation ($p < 0.05$) compared to control. Furthermore, at 24 h its activation was reduced compared to 8 h ($p < 0.05$, about 46%) but it was increased compared to control ($p < 0.05$, about 12%) indicating that the effects on myoblasts were maintained over time.

Another key regulator of cellular metabolism, which plays a predominant role in catabolic mechanisms is the glucose transporter AMPK, which has also been studied. As reported in Fig. 31C MKVC appears to improve muscle metabolism at 8 h in which a greater expression of AMPK is observed (about 36% than 24 h, $p < 0.05$) compared to control ($p < 0.05$, about 18%). The effectiveness of MKVC is maintained over time and demonstrated for the first time that MKVC can induce glucose uptake according to the classic activation mechanisms with mitochondrial modulation. Furthermore, to support the effectiveness of the contraction and to rule out the inflammatory response, the evaluation of JNK ½ was carried out. As reported in Fig. 31D, MKVC improved the biology linked to contractile response, offering a physiological picture of the muscular cell activity at 8 h, it maintained an effect equal to the control which was drastically reduced at 24 h supporting a lower level of hypercontraction with a reduction of 5.5 times in the presence of high glucose. These data support the effectiveness of MKVC in addition to improving metabolism also in reducing any associated inflammatory processes.

Finally, other experiments were conducted evaluating SMA as a marker of muscle regeneration, including post-trauma and anti-muscle damages. As demonstrated in Fig. 31E, after MKVC stimulation, myoblasts appear better at maintaining physiological contractile activities at 8 h as they had a greater effect compared to control ($p < 0.05$ about 17.7%), and this effect was amplified at 24 h compared to control ($p < 0.05$) and to 8 h ($p < 0.05$ about 50.8%), indicating that this effect is consolidated over time. These data support the *in vitro* efficacy of MKVC in maintaining muscle survival systems, even after hypercontraction-related damage.
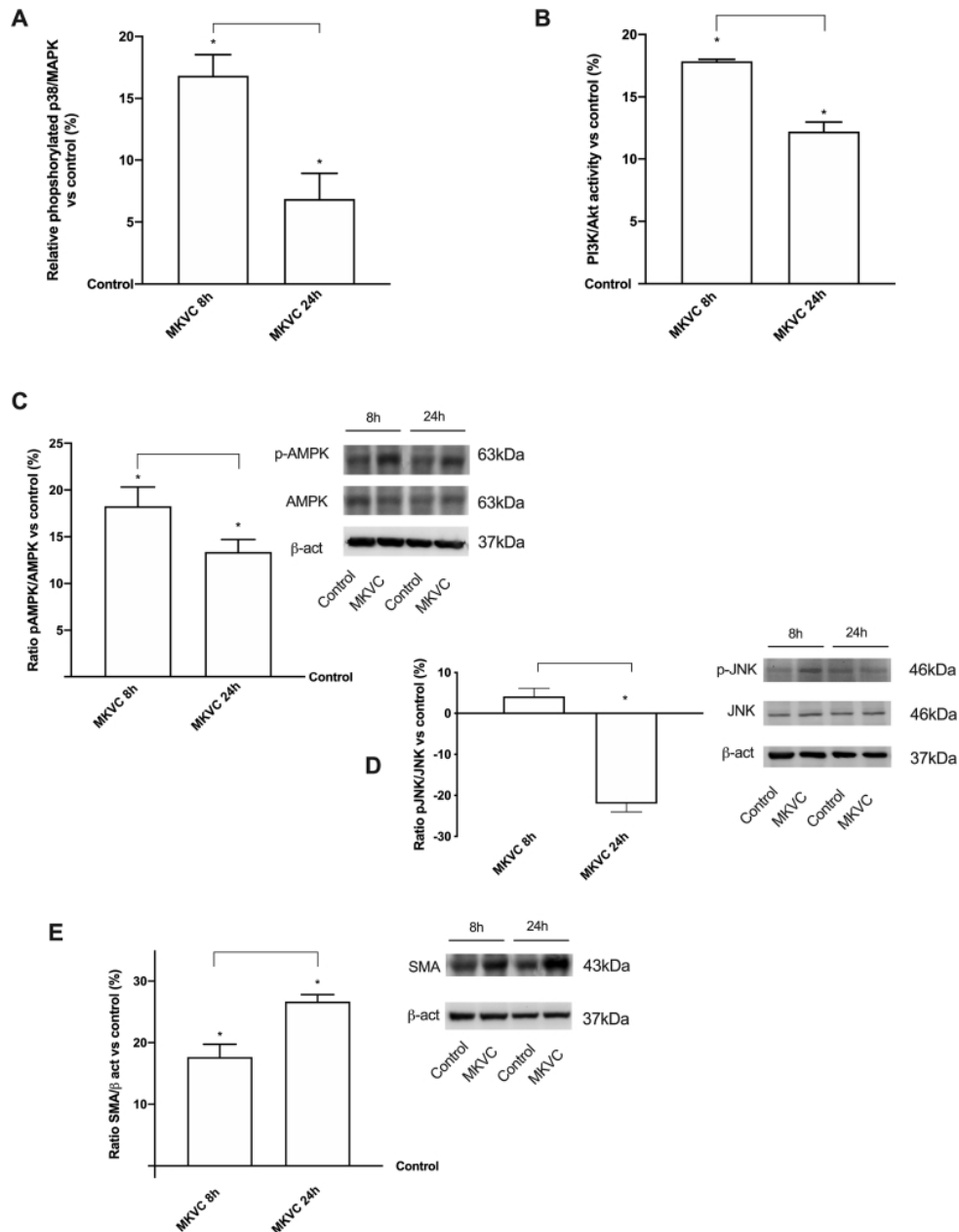
Figure 31. Protein activity, Western blot and densitometric analysis on C2C12 cells. In A p38 phosphorylation and in B PI3K/Akt activity measured both by ELISA test. Data are reported as means ± SD of four independent experiments reported as % vs control (0 line). The abbreviations are the same as reported in Fig. 1. ∗$p < 0.05$ vs control; the bar between 8 h and 24 h of MKVC stimulation. In C AMPK phosphorylation, in D JNK phosphorylation and in E SMA expression was analyzed by Western blot and densitometric analysis. The images reported are an example of each protein from five independent experiments normalized on specific total protein when possible and verified by β-actin detection. Data are reported as means ± SD (%) vs control (0 line).

## 5.2.6. Simulated hypercontraction induced by caffeine

It is well established from *in vitro* studies that caffeine has a direct effect on muscle contraction. It plays a key role in the functioning of the sarcoplasmic reticulum, increasing calcium permeability and making it readily available for the contraction mechanism [211,200] Caffeine was administered to the C2C12 cells to provide a 'strenuous exercise-like treatment', thus studying the biological aspects of exercise to examine exercise-regulated changes in signal transduction and metabolism. Cells were pre-treated with 2.5 mM caffeine and then treated with MKVC at 8 and 24 h. To understand the effects on

contraction-related molecular mechanisms, calcium and magnesium levels were analyzed. As reported in Fig. 32A, caffeine does not allow an adequate relaxation phase. On the other hand, MKVC has a better contraction modulation effect (about 15% less than caffeine), supporting the effects of MKVC in facilitating relaxation after hypercontraction, compared to control ($p < 0.05$) and compared to caffeine treatment, which instead delays relaxation ($p < 0.05$). Ultimately, these data state that MKVC better modulates calcium movements, bringing them back to more physiological values and remodeling the contractile phase with less cellular fatigue.

Since *in vivo* exercise induces a cascade of intracellular mechanism (e.g., activation of AMPK), proteomic (e.g., GLUT4), and metabolic changes (e.g., increased glucose uptake), additional experiments *in vitro* were carried out to confirm the effects of MKVC. Consequently, additional parameters such as glucose uptake, glycogen consumption, and lactate accumulation were studied following pre-treatment with caffeine. As shown in Fig. 32B–D, caffeine alone induced a biological response compatible with a state of severe contraction accompanied by high glucose uptake, high glycogen concentration, and a significant increase in extracellular lactate ($p < 0.05$). This indicates a negative condition of the cells compared to a state of hypercontractility. The stimulation with MKVC was able to reduce this negative condition, leading the extracellular lactate to the control value ($p < 0.05$ vs caffeine alone). Since the strong contraction can cause muscle hypertrophy accompanied by cell death in which the stress condition is maintaining for a long time, additional experiments were performed analyzing some intracellular pathways leading to glucose transport (e.g., AMPK) and muscle regeneration (e.g., SMA). As reported in Fig. 32E, following stimulation with caffeine, MKVC allows the restoration of normal glucose uptake with greater effectiveness at 8 h, compared to control ($p < 0.05$). MKVC was able to modulate the AMPK pathway after caffeine stimulation suggesting its ability to restore and recover muscle cell metabolism after hypercontractility. Finally, the analysis of regeneration and myogenesis markers such as smooth muscle actin (SMA) showed similar results (Fig. 32F). Indeed, MKVC was able to counteract the negative effect of caffeine and the main effects were observed at 8 h compared to control ($p < 0.05$) and compared to caffeine about twice. In addition, this effect is maintained over time suggesting a long-term effect on the restoration of functionality and on complete post-trauma regeneration.

All these results support the hypothesis that MKVC may play different roles during different phases of muscle activity and reveals beneficial effects during a strong contraction in an *in vitro* model.
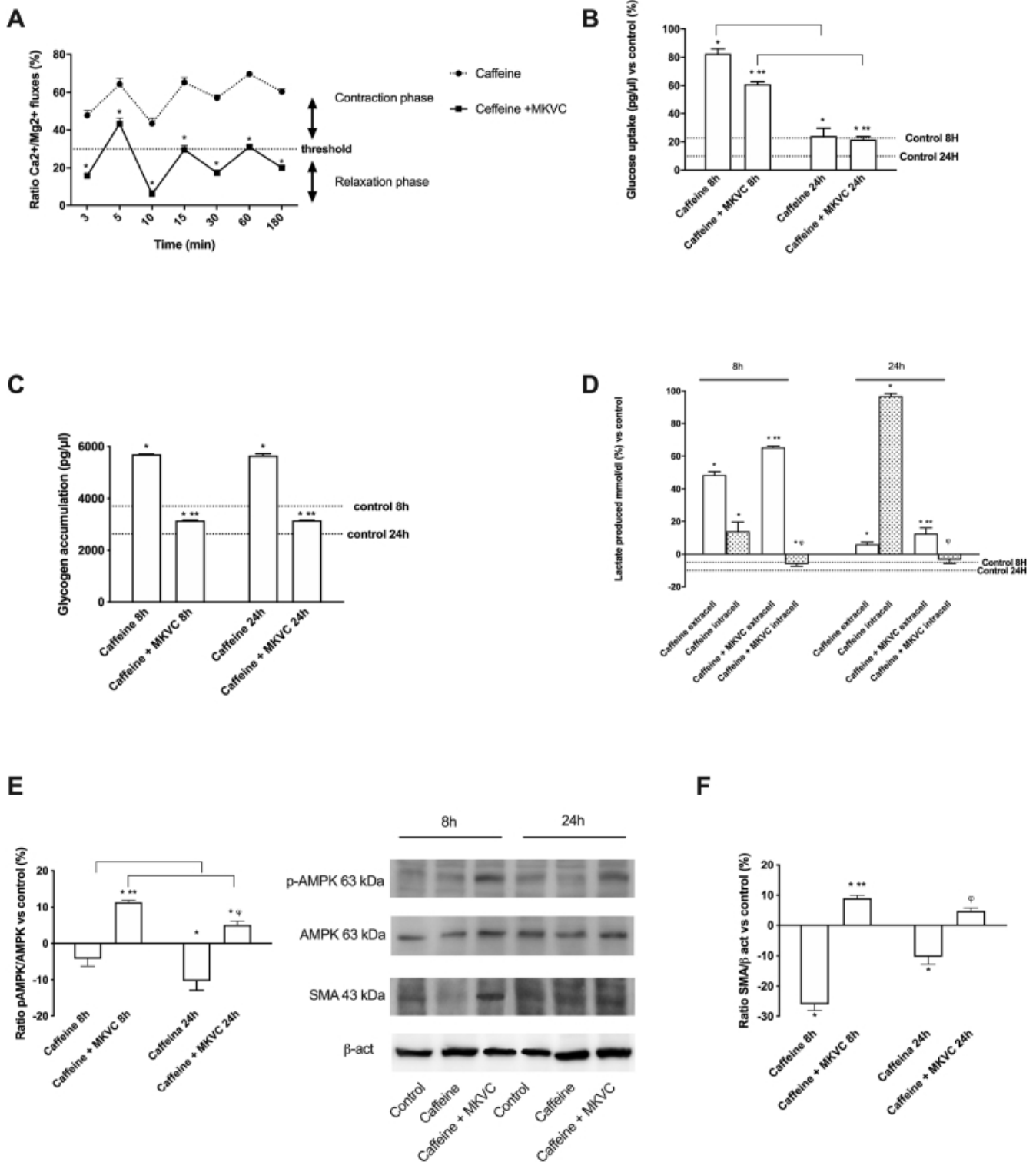
Figure 32. Effects of caffeine on C2C12 cells. In A The graph shows a ratio from calcium movements and magnesium flux normalized to control values ranging from 3min to 180min. After the administration (time 0), a series of oscillations of the Ca2 + /Mg2 + ratio was observed, which correspond to cycles of contraction and relaxation of the cells. Data are reported as means ± SD (%) of five independent experiments. In B glucose uptake, in C glycogen accumulation, and in D lactate analysis with intracellular and extracellular quantification. All these parameters were investigated at two time points (8 h and 24 h). Data are reported as means ± SD of five independent experiments. ∗p < 0.05 vs control; ∗∗p < 0.05 vs caffeine; φ p < 0.05 vs intracellular caffeine; the bars p < 0.05 the same treatment between the different time points. In E AMPK phosphorylation and in F SMA expression was analyzed by Western blot and densitometric analysis. The images reported are an example of each protein from five independent experiments normalized on specific total protein when possible and verified by β-actin detection. Data are reported as means ± SD (%) vs control (0 line). ∗p < 0.05 vs control; ∗∗p < 0.05 vs caffeine 8 h; φ p < 0.05 vs caffeine 24 h.

# 6) ANTI-OSTEOPOROTIC EFFECTS OF EQUISETUM ARVENSE, COMBINED WITH ARTEMISIA ANNUA AND BOSWELLIA SERRATA, ON IN VITRO MODEL FOR BONE REMODELING

Research on age-related osteoporosis is taken from work project number three (WP3), entitled *"Longevity from Tradition"*, which is a section of the Project of Excellence on AGING named *"Molecular determinants of the onset of sarcopenia and osteoporosis and exploration of potential therapeutic strategies (MODESTHE)"*. Osteoporosis, the most common chronic metabolic bone disease, is characterized by low bone mass and increased bone fragility. Nowadays more than 200 million individuals are suffering from osteoporosis and still the number of affected people is dramatically increasing due to an aging population and longer life, representing a major public health problem. Current osteoporosis treatments are mainly designed to decrease bone resorption, presenting serious adverse effects that limit their safety for long-term use; therefore, new therapeutic approaches are required to treat osteoporosis and reduce the side effects related to the use of anti-osteoporotic drugs [212-214]. As regards, traditional medicine is a rich source of bioactive compounds waiting for discovery and investigation, and therefore botanicals have recently received increasing attention. In this context, several studies reported the efficacy of *Equisetum arvense* extract on the reduction of the risk of fracture related to osteoporosis [215]. In particular, *Equisetum arvense* has a high concentration of silica, and it has been demonstrated *in vitro* that the *Equisetum arvense* extract induces bone regeneration and inhibits osteoclastogenesis; moreover, it has been reported that *Equisetum arvense* extract enhances bone mineralization and bone formation in ovariectomized rats. Additionally, recent evidence revealed that a diet containing *Equisetum arvense* extract (120 mg/kg) increases bone mineral density in rats [119]. However, there are scarce studies to support the hypothesis of the beneficial effects of *Equisetum arvense* on bone health, and the European Food Safety Authority concluded that there is not enough evidence of the bone-protecting influence of *Equisetum arvense* extract [216]. To date, the aim of this study was to investigate whether *Equisetum arvense* extract could inhibit bone resorption, combined in an oral treatment with other nutraceuticals with anti-inflammatory and antioxidant properties, both in an *in vitro* model of glucocorticoid-induced osteoporosis and in an *in vivo* model of osteoporotic mice.

## 6.1. MATERIALS AND METHODS

### 6.1.1. Cell Culture

The human epithelial intestinal cells (CaCo-2 cell line) purchased from the American Type Culture Collection (ATCC) were cultured in Dulbecco's Modified Eagle's Medium/Nutrient F-12 Ham (DMEM-F12, Merck Life Science, Rome, Italy) supplemented with 10 % foetal bovine serum (FBS), 2 mM l-glutamine and 1% penicillin–streptomycin and maintained in an incubator at 37 °C and 5% $CO_2$. The experiments were carried out using cells at passage numbers between 26 and 32 to maintain the correct physiology and explore paracellular permeability and transport properties [217]. This *in vitro* model, accepted by EMA and FDA, was widely used to predict absorption, metabolism, and bioavailability of several substances after oral intake in humans [172,173, 218]. During the experiments, $1 \times 10^4$ cells were plated in 96-well plates to study cell viability by MTT and ROS production in a

complete medium. The medium was changed using DMEM without red phenol supplemented with 0.5 % FBS, 2 mM l-glutamine and 1% penicillin–streptomycin at 37 °C for 8h to synchronize the cells. To perform the absorption analyses $2 \times 10^4$ cells were plated on 6.5 mm Transwell® with 0.4 µm pore polycarbonate membrane inserts (Merck Life Science, Italy) in a 24 well plate.

The MC3T3-E1 mouse calvaria-derived preosteoblast cell line, which contributed remarkably to the investigation of the role of osteoblasts in bone formation [219], was obtained from ATCC and cultured in Dulbecco's Modified Eagle's Medium (DMEM, Merck Life Science, Rome, Italy) containing 10% FBS, 2 mM l-glutamine and 1% penicillin–streptomycin and maintained in an incubator at 37°C and 5% $CO_2$. The culture medium was changed every 2–3 days, and cells of a passage number 23 were used for the project [220]. For the experiments, $1 \times 10^4$ cells were plated in 96 well plates to study cell viability by MTT; moreover $5 \times 10^3$ cells/well were seeded on a 96-well plate to analyze Alkaline Phosphatase (ALP) activity by specific kit, calcium deposition by Alizarin Red and to evaluate the main intracellular pathway involved.

Murine macrophage RAW264.7 cells were purchased from ATCC cultured in DMEM supplemented with 10% FBS, 2 mM l-glutamine and 1% penicillin/streptomycin at 37°C in a humidified atmosphere of 5% $CO_2$ [221]. This cell line is appropriate to study osteoclast biology since RAW264.7 cells could respond to stimuli *in vitro* and, subsequently, generate multi-nucleated cells with the hallmark characteristics expected for fully differentiated osteoclasts [222]; in accordance with literature, it is recommended to use RAW264.7 cells above passage 18 [223,224]. After reaching the confluence, cells were trypsinized and $5 \times 10^5$ cells/cm$^2$ were placed in a lower compartment of the plate [225] to determine mature osteoclast; furthermore, differentiation media containing 10 ng/mL RANKL + 10 ng/mL MCSF was replenished every 2–3 days [226]. After being cultured for 5 days, RAW264.7-derived osteoclasts were used to evaluate cell viability, TRAP positive cells and to evaluate the main intracellular pathway involved; additionally, RAW264.7-dervied osteoclast were used in a co-culture model to evaluate bone resorption activity using a specific assay.

### 6.1.2. Reagent Preparation

For both *in vivo* and *in vitro* experiments, *Equisetum arvense* extract, *Artemisia annua* extract and *Boswellia serrata* extract were purchased from market, since they are common readily available nutraceuticals. Firstly, to evaluate the effects on intestinal cells leading to finding the non-toxic concentration, a dose–response study was performed, testing the extracts with a concentrations range reported in the literature. To date, the cells were treated with increasing concentrations of *Equisetum arvense* (range from 10µg/ml to 100 µg/ml [163]), *Artemisia annua* (range from 0.4µM to 10µM [227]) and *Boswellia serrata* (range from 5µM to 50µM [228]). The best concentration of each extract was maintained for all successive experiments. During the project development, all substances were dissolved directly in the stimulation medium consisting of DMEM without red phenol and FBS but supplemented with 1% penicillin/streptomycin and 2 mM L-glutamine. All of these agents were tested alone and in combination (in this work the compound was referred to as ABE) following the hypothesis of a new potential formula to be used in humans.

### 6.1.3. Experimental Protocol

In order to analyze the beneficial effects of *Equisetum arvense* extract, *Artemisia annua* and *Boswellia serrata*, alone and combined, on human bones after oral intake, the project was divided into four steps; firstly, it was verified the ability of *Equisetum arvense* extract, *Artemisia annua* and *Boswellia serrata*, alone and combined, to cross the intestinal barrier in an *in vitro* model of human intestine in order to exclude negative effects and, secondly, their effects on osteoblast cells were analyzed evaluating several parameters and mechanism of actions of their metabolism. In this regards, intestinal CaCo-2 cell line was used in a dose–response study to assess the best concentration able to exert the most beneficial effects on cell viability and ROS production; consequently, the best concentration of *Equisetum arvense*, *Artemisia annua* and *Boswellia serrata* were combined in a new formulation named ABE and tested on an intestinal *in vitro* barrier model to verify intestinal integrity through TEER measurement, tight junction (TJs) analysis by ELISA kit, and permeability assay by Papp measurement. For all these experiments, the treatments were evaluated over a period of 6h (the maximum time of absorption of the molecules) and, after each stimulation, the basolateral medium was collected to be used on osteoblastic cells. MC3T3-E1, one of the most commonly used osteoblast-like cell lines, was treated every 24 h for 14 days and 21 days, changing culture media every 3 days [213, 220] and, at the end of stimulation, the mitochondrial metabolism, ALP activity and mineralized nodules were tested.

Since the study aimed to evaluate the protective role of bioactive compounds during osteoporosis, a condition occurring when osteoblast go to senescence reducing the OPG levels and allowing the activation of osteoclast-based resorption [112], in phase 3 of this project further experiments were conducted using an *in vitro* model of glucocorticoid-induced osteoporosis. Therefore, a coculture system for bone resorption was established in which osteoblasts (MC3T3-E1 cells) and osteoclasts (RAW 264.7 cells) were allowed to interact mimicking bone tissue, in which osteoporotic conditions were induced pre-treating MC3T3-E1 with 1µM of dexamethasone (DEX) for 3 days [229]. Subsequently the coculture were treated with *Equisetum arvense* extract, alone and combined with *Artemisia annua* and *Boswellia serrata*, to evaluate the antiresorptive activity of the new formulation analyzing, on the one hand, osteoblast maturation mechanisms and bone recovery and, on the other hand, osteoclast activation inhibition and the reduction of bone resorption.

### 6.1.4. Cell Viability

The analysis of cell viability was performed using a classical technique based on the MTT-based *In vitro* Toxicology Assay Kit (Merck Life Science, Rome, Italy) [217], following the manufacturer's instructions. Indeed, at the end of stimulation, the cells were incubated with 1% MTT dye for 2 h in an incubator at 37 °C, 5% $CO_2$, and 95% humidity, and then the purple formazan crystals were dissolved in an equal volume of MTT Solubilization Solution. The absorbance was analyzed by spectrophotometer (Infinite 200 Pro MPlex, Tecan, Männedorf, Switzerland) at 570 nm with correction at 690 nm, and results were expressed compared to the control (0% line), which represented untreated cells. The results reported an increase in the percentage of viable cells compared to the control and indicated a higher number of viable cells plus the control. This strategy can lead to a high level of safety of the stimulation and, consequently, to a correct analysis of the results.

### 6.1.5. ROS production

In CaCo-2, the ROS production was measured by analyzing the reduction of cytochrome C using a standard protocol [117], measuring the absorbance at 550 nm through the spectrometer (Infinite 200 Pro MPlex, Tecan). $O_2$ ratio was expressed as the mean ± SD (%) of nanomoles per reduced cytochrome C per microgram of protein compared to the control. The data reported represent means of five independent experiments performed in triplicate.

### 6.1.6. *In vitro* Intestinal Barrier Experimental Model

Cells plated on the Transwell® insert were maintained in complete medium for 21 days before the stimulations, changing the medium at alternative day on the apical or basolateral side [217]. Before stimulation on the apical side, the medium was changed to a medium at pH 6.5, which mimicked the lumen of the small intestine, while on the basolateral side was changed to a pH 7.4 to reproduce the blood condition [217]. During treatments, the cells were maintained in an incubator at 5 % $CO_2$ and, at the end of stimulations, both apical and basolateral medium was collected for subsequent analyses. At the end of the stimulation, in order to evaluate whether *Equisetum arvense* extract, alone and combined with *Artemisia annua* and *Boswellia serrata*, could be able to cross the intestinal barrier and arrive to bone tissue, the TEER values were evaluated by EVOM3, coupled with STX2 chopstick electrodes (World Precision Instruments, Sarasota, FL, USA). On day 21, when TEER value ≥ to 400 $\Omega cm^2$ [174], the medium at the apical and basolateral environments were changed to create different pH conditions [217]. The cells were kept for 15 min at 37 °C and 5% $CO_2$, after which the TEER values were measured again before the start of the experiment to verify a stabilization of the values. The cells were stimulated with *Equisetum arvense* extract, alone and combined with *Artemisia annua* and *Boswellia serrata*, for 1h to 6h before the successive analysis, including the permeability assay measured by Papp (cm/s) analysis, following formula:

$$Papp = dQ/dt *1/m0 *1/A *V \, Donor$$

dQ: amount of substance transported (nmol or μg);

dt: incubation time (sec);

m0: amount of substrate applied to donor compartment (nmol or μg);

A: surface area of Transwell® membrane ($cm^2$);

VDonor: volume of the donor compartment ($cm^3$).

Negative controls without cells were tested to exclude Transwell® membranes influence. The analysis was performed in triplicates and reproduced five times.

### 6.1.7. Occludin quantification assay

The Human Occludin (OCLN) ELISA kit (MyBiosource, San Diego, CA, USA) was used to analyze the occludin presence in CaCo-2 cell lysates, according to the manufacturer's instruction [217]. The enzymatic reaction was analyzed by a spectrometer (Infinite 200 Pro MPlex, Tecan) at 450 nm. The concentration is expressed as pg/mL compared to a standard curve (range from 0 to 1500 pg/ml) and the results are expressed as a percentage (%) versus control (0 line). Data reported are representative of means of five independent experiments performed in triplicate.

### 6.1.8. Claudin quantification assay

The Human Claudin4 was measured in CaCo-2 lysates by ELISA kit (Cusabio Technology LLC, Houston, USA), following the manufacturer's instructions [217]. The reaction was analyzed by a spectrometer (Infinite 200 Pro MPlex, Tecan) at 450 nm. The concentration is expressed as pg/mL comparing data to the standard curve (range from 0 to 1000 pg/ml) and the results are expressed as a percentage (%) versus control (0 line) of five independent experiments performed in triplicate.

### 6.1.9. Human tight junction protein 1 (ZO-1) quantification assay

The Human Tight Junction Protein 1 (TJP1) ELISA kit (MyBiosource, San Diego, CA, USA) was measured in CaCo-2, following the manufacturer's instructions [217]. The plates were read by a spectrometer (Infinite 200 Pro MPlex, Tecan) at 450 nm. The concentration is expressed as pg/mL comparing data to the standard curve (range from 0 to 1000 pg/ml) and the results are expressed as a percentage (%) versus control (0 line) of five independent experiments performed in triplicate.

### 6.1.10. Establishment of a Coculture System for Bone Resorption.

Osteoblast/osteoclast *in vitro* coculture model was established using Transwell® inserts (Merck Life Science, Italy), which were plated on bone resorption assay kit 24 well (PG Research, Tokyo, Japan) in order to evaluate osteoclast bone resorption activity [230]. The establishment of a co-culture system containing both bone-forming cells (osteoblasts) and bone-resorbing cells (osteoclasts) more closely mimicked the *in vivo* environment as a cytocompatibility assessment *in vitro* for bone remodeling [231]. Briefly, the bottom of the inserts was composed of polyester materials with a pore size of 0.4 $\mu$m, which only permits the passage of small, soluble factors. RAW264.7 cells were embedded at a density of 5 × $10^5$ cells/cm$^2$ in the lower compartment (bone resorption assay plate) of each insert and differentiated in osteoclast; after 4 days, MC3T3-E1 cells were incubated at a density of 5 x $10^4$ cells/cm$^2$ in the upper compartment of the inserts and maintained in a 24 well plate. After MC3T3-E1 cells were cultured for 24h, the Transwell® inserts with MC3T3-E1 cells were combined in the bone resorption assay plate with RAW264.7-derived osteoclasts. This coculture system was maintained in complete DMEM supplemented with 10% heat-inactivated fetal calf serum (FCS) in 5% $CO_2$ at 37°C for 5 days before performing the experiments.

### 6.1.11. Alkaline Phosphatase (ALP) Activity Assay

The ALP activity was measured after 14 days of treatment to evaluate osteoblast functions following protocol reported in literature [220]. Briefly, the cells were washed with cold PBS 1x and lysed with lysis buffer containing 50 mM Tris-HCL (pH 7.4) and 1% Triton X-100; the total protein extract obtained was centrifuged at 14000 RPM for 20 min at 4°C and the supernatant was collected for determining ALP activity and protein concentration. ALP activity was quantified with 4 mg/mL of 4-nitrophenyl phosphate (4NPP) dissolved in 0.2 M of 2-amino-2-methyl-1-propanol with 4 mM of MgCl2 as a substrate for 30 min at 37°C. The reaction was stopped by 0.1 M NaOH, and the yellow solution was measured at 405 nm using a spectrometer (Infinite 200 Pro MPlex, Tecan). At the same time, protein concentration was measured using the Pierce BCA Protein Assay Kit (ThermoFisher Scientific, Waltham, MA, USA). The results were obtained normalizing ALP activity data to the concentration of protein and showed as (%) compared to control (0 line).

### 6.1.12. Alizarin Red Staining and Quantitative Analysis of Mineralization

After 21 days of treatment, MC3T3-E1 cells were stained with alizarin red to examine the mineralization nodules, according to protocol reported in literature [232]. The cells were washed with PBS 1x and fixed in 75% ethyl alcohol for 30min at 4°C and, at the end of the time, the plate was washed with distilled water and stained in 1% alizarin red solution (pH 4.2) for 30min at 37°C. Unbound dye was removed by washing several times with distilled water and mineralized nodules were observed using a low magnification microscope and photographed (DMi1, Leica, Germany). To quantify matrix mineralization, 1mL of 100 mM cetylpyridinium chloride was added to each well and incubated for 1h to dissolve and release the calcium- bound alizarin red. The absorbance of released alizarin red was measured at 570 nm using a spectrometer (Infinite 200 Pro MPlex, Tecan) and the results were expressed as (%) compared to control (0 line).

### 6.1.13. TRAP staining and the TRAP activity assay.

In order to analyze osteoclast activity, multinucleated osteoclasts were observed using TRAP kit (Merck Life Science, Rome, Italy) as described in the manufacturer's instructions [233]. Briefly, RAW-264.7-derived osteoclasts were fixed with 1:1 citrate buffer:acetone and then the cells were stained with TRAP kit reagents. The cells containing three or more nuclei were marked as TRAP-positive and the percentage of multinucleated cells in each sample was counted using a microscope (DMi1, Leica, Germany) in order to quantify the influence of the treatments. Subsequently, TRAP activity was determined using para-Nitropheny Phosphate (pNPP) and the absorbance of the resulting, yellow-colored product was measured at 405 nm using a spectrometer (Infinite 200 Pro MPlex, Tecan) and the results were expressed as (%) compared to control (0 line).

### 6.1.14. Biomimetic Calcium Phosphate Assay and Resorption Pit Assay

In order to quantify osteoclastic activity, bone resorption assay plates and fluorescein-labeled CaP-coated 24-well plates (PG Research, Tokyo, Japan) were used according to the manufacture's instruction [230]. Briefly, at the end of the stimulation, $100\mu$L of the cell culture supernatant was transferred into a 96-well plate for fluorescence measurement, adding $50\mu$L of bone resorption assay buffer to each well. The fluorescence intensity was measured using a fluorescence plate reader (Infinite 200 Pro MPlex, Tecan) with excitation and emission wavelengths of 485 and 535 nm. The results were expressed as (%) compared to control (0 line).

### 6.1.15. OPG kit

OPG was analyzed by OPG/TNFRSF11B Duo Set (R&D Systems, Minneapolis, MN, USA) following the manufacturer's instructions [217]. Briefly, 100 µL of samples or standards were added to the well and incubated for 2h at room temperature protected from light, and after washing, 100µL of the Detection Antibody were added to each well and incubated as previously described. After 2h, 100µL of the working dilution of Streptavidin-HRP A were added to each well and incubated for 20 min at room temperature. At the end of the time, 100µL of Substrate Solution were added to each well, incubated for 20 min at room temperature and 50µL of Stop Solution were used to stop the enzymatic reaction. The optical density of each well was measured at 450 nm using a spectrometer (Infinite 200

Pro MPlex, Tecan). The results were interpolated with the standard curve (6.25 to 6.25 pg/ml) and expressed as a percentage (%) compared to the control.

### 6.1.16. RANK kit

RANK was analyzed by Mouse RANKL ELISA Kit (abcam, Cambridge, UK) following the manufacturer's instructions [234]. Briefly, 100 µL of samples or standards were added to the well and incubated for 2.5h at room temperature protected from light, and after washing 4 times, 100µL of Biotinylated RANKL Detection Antibody were added to each well and incubated for 1h at room temperature. After washing, 100µL of the HRP-Streptavidin solution were added to each well and incubated for 45 min at room temperature. At the end of the time, 100µL of TMB One-Step Substrate Reagent were added to each well, incubated for 30 min at room temperature and then 50µL of Stop Solution were used to stop the enzymatic reaction. The optical density of each well was measured at 450 nm using a spectrometer (Infinite 200 Pro MPlex, Tecan). The results were interpolated with the standard curve (2.74 to 2000 pg/ml) and expressed as a percentage (%) compared to the control.

### 6.1.17. Western Blot

At the end of each stimulation, both cell types were washed with ice-cold PBS 1X supplemented with 2 mM sodium orthovanadate and then lysed with ice-cold Complete Tablet Buffer (Roche, Milan, Italy) supplemented with 2 mM sodium orthovanadate, 1 mM phenylmethanesulfonyl fluoride (PMSF; Merck Life Science, Rome, Italy), 1:50 mix Phosphatase Inhibitor Cocktail (Merck Life Science, Rome, Italy) and 1:200 mix Protease Inhibitor Cocktail (Calbiochem, San Diego, CA, USA). Cell lysates were obtained by centrifugation at 14.000 g for 20 min at 4°C. 30µg of each protein extract were resolved on 15% SDS-PAGE gel and transferred to a polyvinylidene difluoride membrane, which was incubated overnight with the specific primary antibodies at 4 °C: BMP2 (1:500, Santa Cruz, CA, United States); ERK1-2 (1:500, Santa Cruz, CA, United States); p38 (1:500, Santa Cruz, CA, United States), RANKL (1:500, Santa Cruz, CA, United States) and GSK3b (1:1000, ThermoFisher Scientific, Waltham, MA, USA). All protein expressions were normalized and verified through β-actin detection (1:5000, Merck Life Science, Rome, Italy), and expressed as mean ± SD (%) of five independent experiments.

### 6.1.18. Statistical Analysis

Data collected were processed using Prism GraphPad statistical software 9.4.1 using one-way analysis of variance (ANOVA), followed by Bonferroni post hoc tests. Comparisons between the groups were performed using a two-tailed Student's t-test. Multiple comparisons among groups were analyzed by two-way ANOVA followed by a two-sided Dunnett post hoc test. All results were expressed as mean ± SD of at least 5 independent experiments produced in triplicates. Differences with a $p < 0.05$ were considered statistically significant.

## 6.2. RESULTS

### 6.2.1. Safety analysis of Equisetum arvense extract, Artemisia annua and Boswellia serrata on intestinal cells

Before analyzing the absorption mechanism of natural extracts, the cellular toxicities of *Equisetum arvense*, *Artemisia annua* and *Boswellia serrata* were evaluated to determine the concentrations that would not interfere with the cellular metabolism in CaCo-2 cells during the time. As reported in Fig. 33 (panels A to C), all samples showed a time-dependent profile on cell viability, with a peak between 3h and 4h, leading to exclude any cytotoxic effect. Indeed, cells treated with *Equisetum arvense* extract 50μg/ml showed high viabilities compared to control ($p < 0.05$) and compared to the other concentration tested during all stimulation time. In the same way, from 2h to 6h, *Artemisia annua* 2μM and *Boswellia serrata* 5μM exhibited a better effect on CaCo-2 cells also compared to other forms evaluated ($p < 0.05$). These molecular mechanisms underlie that the agent didn't induce cytotoxicity, probably improving self-protective response of intestinal cells; for this reason, *Equisetum arvense* extract 50μg/ml, *Artemisia annua* 2μM and *Boswellia serrata* 5μM were chosen to be used in the final formulation.

Moreover, further experiments were carried out to verify if *Equisetum arvense*, combined with *Artemisia annua* and *Boswellia serrata*, could improve mitochondrial metabolism and prevent oxidative stress, since ROS production has been implicated in the alteration of cellular homeostasis. For this reason, cell viability and ROS production were evaluated on CaCo-2 cells from 2h to 6h of simulation; as shown in Fig. 33D, when all the agents were combined, no significant changes in mitochondrial metabolism were observed, rather the combination of *Equisetum arvense* extract 50μg/ml, *Artemisia annua* 2μM and *Boswellia serrata* 5μM was able to increase cell viability compared to the untreated cells and, especially, compared to individual substances ($p<0.05$), indicating maintenance of a self-protection response even by the complete formulation. These data were confirmed also by ROS production analysis (Fig. 33E), in which the positive role of the combination was confirmed ($p < 0.05$); indeed, *Equisetum arvense* extract 50μg/ml, *Artemisia annua* 2μM and *Boswellia serrata* 5μM were able to reduce the ROS production ($p < 0.05$) compared to control during the period analyzed, however the effect was amplified when all agents were combined confirming a better biological profile of the concentration chosen.
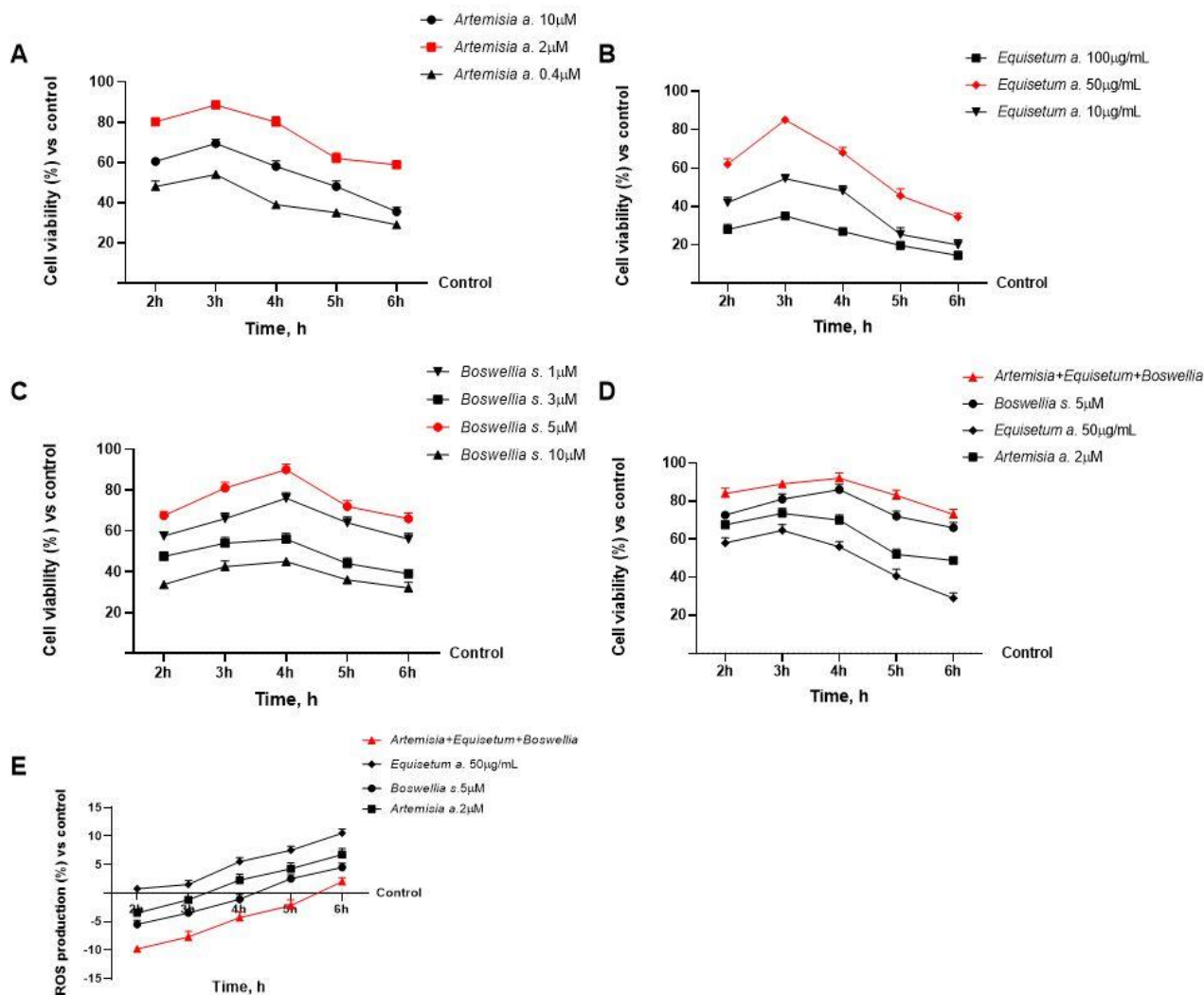
Figure 33. Cell viability and ROS production on CaCo-2 cells. From A to C dose-response and time-dependent study on cell viability measured by MTT test of each single extract from 2h to 6h (A *Artemisia annua*; B *Equisetum arvense* and C *Boswellia serrata*); D and E: Cell viability analysis and ROS production measured by MTT test and reduction of Cytochrome C of each natural extract, alone and combined, from 2h to 6h. Data are mean ± SD of five independent experiments performed in triplicates.

### 6.2.2. Effect of *Equisetum arvense* extract, *Artemisia annua* and *Boswellia serrata* on permeability to cross intestinal barrier

To evaluate absorption mechanism and to obtain additional information regarding natural extract bioavailability across the intestinal barrier, additional experiments were carried *in vitro* mimicking the complexity of human intestine. Therefore, a 3D model was recreated seeding CaCo-2 cells on the apical part of the Transwell® insert, in order to measure the intestinal integrity, and the basolateral part was collected and analyzed to evaluate the permeability rate and the plasmatic bioavailability through the barrier. This model helps to determine the permeability of a substance across the intestinal barrier and is recognized as an excellent pre-clinical model. In this context, *Equisetum arvense* extract 50μg/ml, *Artemisia annua* 2μM and *Boswellia serrata* 5μM, alone and combined, were tested from 1h to 6h to measure TEER values and the Papp rate to predict their plasmatic bioavailability, which is an important parameter related to natural extract absorption. The data (Fig. 34, panels A to C) show that intestinal adsorption has a physiological trend. TEER analysis examined during the 21 days of

101

enterocytes maturation, permit to verify a correct barrier formation increasing TEER values till to a start a plateau phase (21 day), the exact moment in which the experiments start. Subsequently, the TEER analysis reveals that only *Boswellia serrata* (Fig. 34A) is able to maintain epithelial integrity and the ionic conductance of the paracellular pathway in the epithelial monolayer ($p < 0.05$) compared to control, with a main effect at 4h; however, *Equisetum arvense* and *Artemisia annua* had a poor effect during the same time of the simulation ($p < 0.05$), suggesting a slight bioavailability of these two natural extracts. In the same way, permeability rate and analysis of the flux of non-electrolyte tracers (expressed as permeability coefficient) reveled the same results, as reported in figure 34B. Indeed, the data obtained from the extracellular environment suggest that not all the substances had crossed the intestinal barrier leading to plasmatic environments, showing that only *Boswellia serrata* could arrive at systemic level better than *Equisetum arvense* and *Artemisia annua* ($p < 0.05$). In contrast, the combination between *Equisetum arvense* extract 50μg/ml, *Artemisia annua* 2μM and *Boswellia serrata* 5μM was able to maintain the epithelial integrity increasing the ionic flux of the paracellular exchanges across the intestinal epithelial, compared to control and to single agents ($p<0.05$), confirming the correct functioning of the intestinal epithelium in term of permeability rate. This effect was more evident at 4 h at which the combination between *Equisetum arvense* extract 50μg/ml, *Artemisia annua* 2μM and *Boswellia serrata* 5μM exerted the maximum effect compared to control ($p < 0.05$) and to other single agents ($p<0.05$). These data are important to predict human absorption based on the Papp conversion in which the combination between *Equisetum arvense* extract 50μg/ml, *Artemisia annua* 2μM and *Boswellia serrata* 5μM is able to improve the absorption and the plasmatic concentration within 4h of intestinal digestion, supporting the hypothesis of a better bioavailability of the product. The improvement of permeability may be not only dependent on the transcellular transport through the cell membrane, but also paracellular transport of *Boswellia serrata* from the tight junction to the lateral space. Furthermore, to assess the state of epithelial integrity of CaCo-2 cells after the passage of *Equisetum arvense*, *Artemisia annua* and *Boswellia serrata*, alone and combined, further experiments were carried out evaluating TJs, such as claudin 4 and occludin, members of the claudin family considered the principal barrier-forming protein which contribute to TJ stabilization and optimal barrier function, and Zo-1, a member of the junctional adhesion molecule family able to maintain the TJ structure and to modulate barrier integrity (figure 34 D, E, and F, respectively). As expected *Equisetum arvense* and *Artemisia annua* alone maintained TJs activity at the basal level compared to control ($p<0.05$), meanwhile *Boswellia serrata* showed a greatest effects on the same parameters analyzed ($p < 0.05$); also in this case the combination between *Equisetum arvense* extract 50μg/ml, *Artemisia annua* 2μM and *Boswellia serrata* 5μM is able to improve TJs activity compared to control and compared to single agents ($p<0.05$), supporting the hypothesis about the importance of a bioavailable component in the formulation, capable of inducing a greater absorption associated with the increases of intestinal barrier functions mediated by TJ and ionic conductance of the paracellular mechanism.
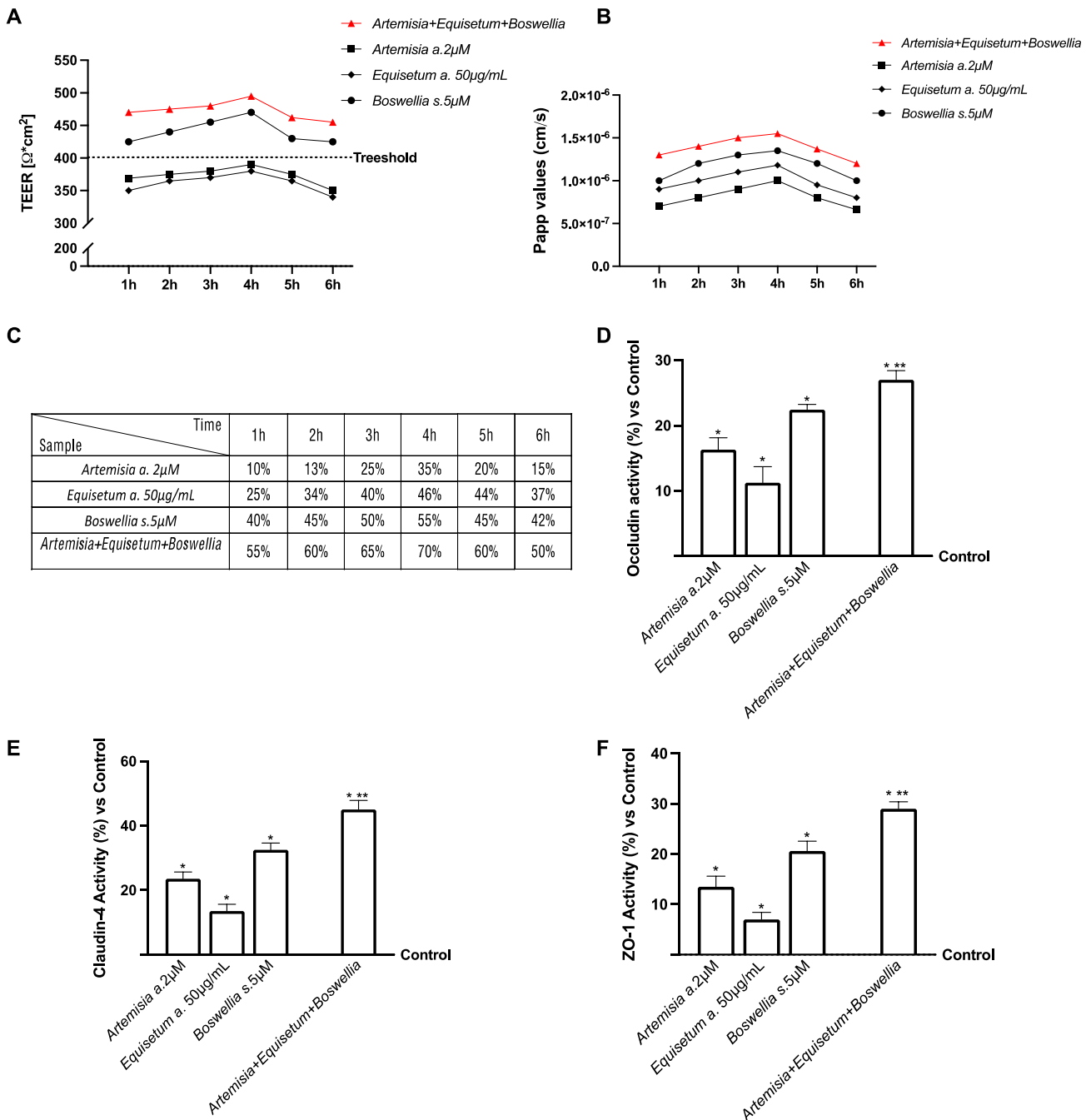
Figure 34. Permeability study on CaCo-2 cells. A: TEER Value using EVOM3; B: the Papp values; C: plasmatic value referred to Papp data in which data < $0.2 \times 10^{-6}$ cm/s means very poor absorption with a bioavailability < 1 %, data between $0.2 \times 10^{-6}$ and $2 \times 10^{-6}$ cm/s with bioavailability between 1 and 90 %, and data > $2 \times 10^{-6}$ cm/s means very good absorption with a bioavailability over 90 %; D: the analysis of Occludin measured by ELISA test; E: the analysis of Claudin 4 by ELISA kit; F: the analysis of Zo-1 by ELISA test. Data are mean ± SD of five independent experiments performed in triplicates. In A control correspond to the breck point (at 300 value). * $p < 0.05$ vs control;  **$p < 0.05$ single agents.

### 6.2.3. *Equisetum arvense* extract, *Artemisia annua* and *Boswellia serrata* Increased Osteoblast Maturation in Preosteoblastic MC3T3-E1 Cells

Decreased bone mass is associated with a physiologic decrease of the osteoblastic activity, leading to a slower rate of bone mineral apposition which follows an increase in the number of adipocytes, osteoclasts, and enhance bone resorption. Therefore, to investigate the impact of *Equisetum arvense*, *Artemisia annua* and *Boswellia serrata* on bone homeostasis, the effects of these natural extract on

103

osteoblast activity were examined after intestinal absorption, analyzing the three characterized stages of osteoblast differentiation and maturation process, such as matrix maturation, cell proliferation and matrix mineralization. To date ALP activity, cell viability, and mineralization assays were performed on MC3T3-E1 cell line treated with intestinal metabolizes for 14 and 21 days, time related to the physiological processes of osteoblast maturation. As reported in figure 35A, ALP activity were increased after 14 days of treatment with *Equisetum arvense* extract 50µg/ml, *Artemisia annua* 2µM and *Boswellia serrata* 5µM compared to untreated cell (p<0.05 vs. control); this effect was amplified when all single agents were combined (about 56% vs. *Equisetum arvense* extract 50µg/ml; about 36% vs. *Artemisia annua* 2µM and about 43% vs. *Boswellia serrata* 5µM; p<0.05), suggesting that the new combination plays a crucial role in the mineralization of newly-formed bone maybe increasing it during osteoblast differentiation. At the same time, treatment with *Equisetum arvense* extract 50µg/ml, *Artemisia annua* 2µM and *Boswellia serrata* 5µM alone greatly improve cell viability of osteoblastic cells (p<0.05 vs. control), confirming the absence of any cytotoxic effect of the new formulation. Also in this case, the combination between *Equisetum arvense* extract, *Artemisia annua* and *Boswellia serrata* was able to amplify the beneficial effects compared to single agents (about 14% vs. *Equisetum arvense* extract 50µg/ml; about 15% vs. *Artemisia annua* 2µM and about 26% vs. *Boswellia serrata* 5µM; p<0.05), increasing cell viability beyond physiological limits and leading to the assumption that cell proliferative activity is due to the combination of natural extracts. All these findings were confirmed by mineralization assay, which examined mineralized nodule formation in MC3T3-E1 cells using Alizarin red S method. Moreover, figure 35C-D showed successful mineralized osteoblast cells *in vitro*, since all single agents were able to produce calcium phosphate and osteoblast mineralization (p<0.05); as expected, the combination between *Equisetum arvense* extract, *Artemisia annua* and *Boswellia serrata* presented higher mineralization rate than single agents (about 44% vs. *Equisetum arvense* extract 50µg/ml; about 75% vs. *Artemisia annua* 2µM and about 53% vs. *Boswellia serrata* 5µM; p<0.05), confirming that the new combination is able to produce bone matrix mineralized by osteoblast differentiation, improving the induction of calcium and phosphate-based minerals.



Figure 35. The effect of the *Equisetum arvense*, *Artemisia annua* and *Boswellia serrata*, alone and combined, on MC3T3-E1 cells. A: Cell viability analysis measured by MTT test; B: ALP activity quantification; C: mineralized nodules quantification. Data are mean ± SD of five independent experiments performed in triplicates. In A the threshold corresponds to starting proliferation cut off (at 90% of cell viability [235]). * p < 0.05 vs control;  **p < 0.05 single agents.

Finally, as reported in figure 36, to support the data obtained, further experiments were conducted analyzing the main intracellular pathways involved in osteoblast differentiation and maturation. To date, the role of bone morphogenetic protein type 2 (BMP-2) was investigated since it activates two MAPKs, (e.g., ERK and p38), which in turn up-regulate bone formation-related gene expression and promote osteoblastic differentiation and mineralization. As reported in figure 36A-C, *Equisetum arvense* extract 50µg/ml, *Artemisia annua* 2µM and *Boswellia serrata* 5µM alone were able to activates both p38 and ERK compared to untreated cells ($p<0.05$); furthermore, better results were observed when all natural extracts were combined, since it improved BMP-2 expression (about 28% vs. *Equisetum arvense* extract 50µg/ml; about 63% vs. *Artemisia annua* 2µM and about 45% vs. *Boswellia serrata* 5µM; $p<0.05$) activating p38 and ERK, showing synergistic effects involving both BMP and MAPK pathways leaded to osteoblastic differentiation in MC3T3-E1 cells. All these findings demonstrated that natural extract enhanced the differentiation and mineralized nodule formation of bone-forming osteoblasts, developing several matrix proteins leading calcium deposition and bone formation; therefore, these data confirm an active role of the *Equisetum arvense*, *Artemisia annua* and *Boswellia serrata*-based formulation in stimulating osteoblastic activity.
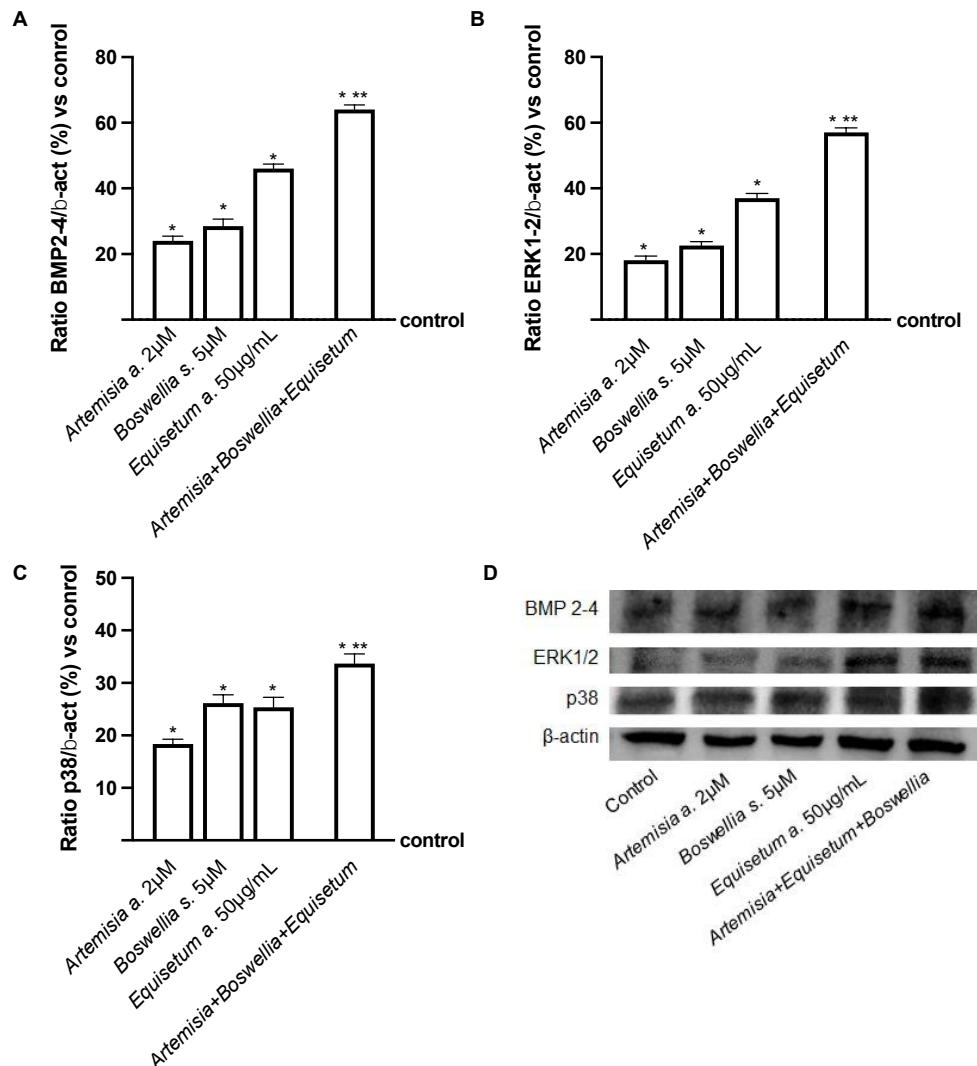


Figure 36. Molecular pathways involved on MC3T3-E1 cells differentiation. A: BMP2-4 densitometric analysis of the specific Western blot; B: ERK1-2 densitometric analysis of the specific Western blot; C: p38 densitometric analysis of the specific Western blot; E: Western blot lane of each parameters reported as an example. Data are mean ± SD of five independent experiments performed in triplicates. * $p < 0.05$ vs control; **$p < 0.05$ single agents.

### 6.2.4. *Equisetum arvense* extract, *Artemisia annua* and *Boswellia serrata* Modulate RAW 264.7-derived Osteoclast Differentiation

Bone remodeling is regulated by the balance between osteoclasts (bone resorption) and osteoblasts (bone formation). Alterations in osteoclast differentiation are one of the major causes of skeletal diseases, such as osteoporosis; therefore, to evaluate the effect of *Equisetum arvense*, *Boswellia serrata* and *Artemisia annua*, alone and combined, on osteoclast differentiation after intestinal metabolism, RAW264.7-derived osteoclast were induced using differentiation media containing M-CSF and RANKL, and co-treatment with natural extract for 5 days. As reported in figure 37A-B, *Equisetum arvense* extract 50μg/ml, *Artemisia annua* 2μM and *Boswellia serrata* 5μM did not affect the viability of cells ($p < 0.05$ compared to control); notwithstanding, natural extract treatment inhibited TRAP activity during osteoclast differentiation compared to untreated cells (about -3.9%), decreasing the number of TRAP-stained multinucleated positive cells ($p < 0.05$). The beneficial effects of *Equisetum arvense*, *Boswellia serrata* and *Artemisia annua* are amplified when the natural extracts are combined since, thanks to their synergistic effect, cell viability is slightly increased ($p < 0.05$) confirming the absence of cell damage; at the same time macrophage differentiation into osteoclasts is inhibited after treatment more efficiently than single agents (about 2 times vs. *Equisetum arvense* extract 50μg/ml; about 2.15 times vs. *Artemisia annua* 2μM and about 2 times vs. *Boswellia serrata* 5μM; $p < 0.05$). These results indicate that the new formulation prevents osteoclast differentiation by inhibiting the activity of TRAP. Subsequently, to define better the role of natural extract on osteoclastogenesis, additional experiments were performed analyzing the role of natural extracts on GSK-3β, a molecule highly expressed on osteoclast precursor which is inactivated by RANKL during osteoclast differentiation. To date, as reported in figure 37C-D, *Equisetum arvense* extract 50μg/ml, *Artemisia annua* 2μM and *Boswellia serrata* 5μM were able to maintain active GSK-3β, reducing the possibility of RANKL binding to its receptor ($p < 0.05$) and to induce RAW264.7 differentiation into osteoclast; in the same way, the combination of all agent tested improve GSK-3β expression (about 27% vs. *Equisetum arvense* extract 50μg/ml; about 36% vs. *Artemisia annua* 2μM and about 44% vs. *Boswellia serrata* 5μM; $p < 0.05$), inhibiting RANKL-mediated osteoclastogenesis. All these findings confirmed the negative regulator activity of *Equisetum arvense*, *Boswellia serrata* and *Artemisia annua* to osteoclast differentiation.
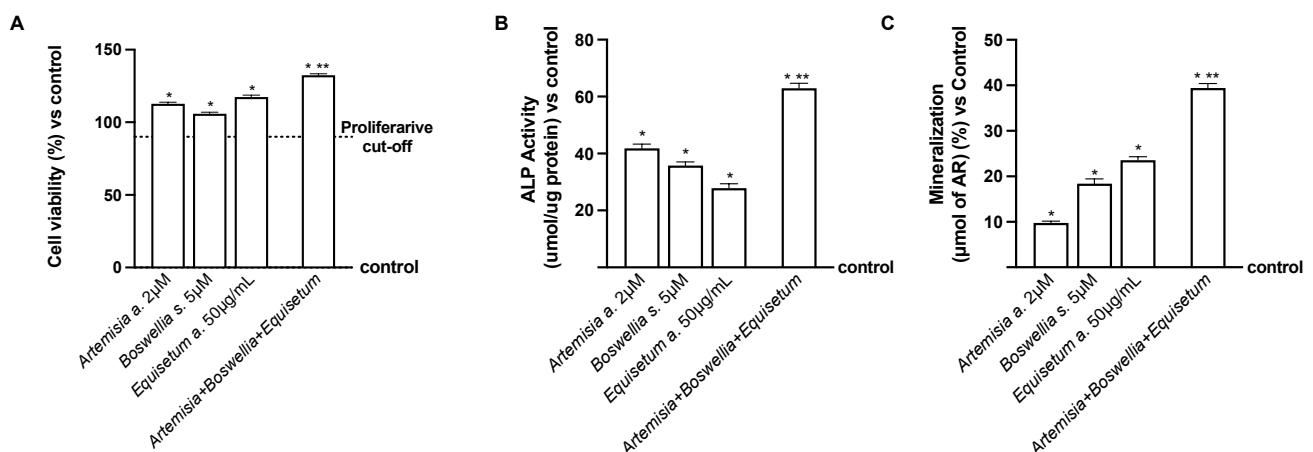
Figure 37. The effect of the *Equisetum arvense*, *Artemisia annua* and *Boswellia serrata*, alone and combined, on RAW264.7-derived osteoclast. A: Cell viability analysis measured by MTT test; B: TRAP activity quantification using quantification kit; C and D: GSK-3β and RANKL densitometric analysis of the specific Western blot, which is reported as an example in E. Data are mean ± SD of five independent experiments performed in triplicates. * $p < 0.05$ vs control; **$p < 0.05$ single agents.

### 6.2.5. Osteoporosis condition co-culture

Bone homeostasis depends on the synergistic activities of osteoclasts and osteoblasts, and any imbalance between bone formation and resorption may lead to a number of diseases, including osteoporosis. Osteoclast and osteoblast cells communicate with each other through RANKL/OPG pathway, since osteoclastogenesis is controlled by RANKL in a dose-dependent manner, while OPG reverses the effects of RANKL by acting as a decoy receptor. Therefore, given these premises, the effects of *Equisetum arvense*, *Boswellia serrata* and *Artemisia annua*, alone and combined, on bone homeostasis under the more closely physiological conditions of osteoporosis, were investigated using a co-culture system of preosteoblast MC3T3-E1 cells and RAW 264.7-derived osteoclast cells. The osteoporotic conditions were induced by pretreating MC3T3-E1 cells with 1μM of DEX for 3 days; consequently, the effects of natural extract treatment after intestinal passage on both osteoblast and osteoclast activity were examined. Firstly, RANKL/OPG ratio was analyzed after osteoporosis induction (figure 38), showing a strong and statistically significant upregulation (about 16%; $p < 0.05$) of RANKL with OPG downregulation in the co-culture compared to control (about 11.5%; $p < 0.05$). Conversely, treatment with *Equisetum arvense* extract 50μg/ml, *Artemisia annua* 2μM and *Boswellia serrata* 5μM alone were able to revert this condition decreasing RANKL and, consequently, improving OPG activity ($p<0.05$). Encouraging results were shown when the natural extracts were combined, bringing RANKL/OPG ratio to levels almost comparable to the control ($p<0.05$), since OPG activity is largely increased (about 31% vs. *Equisetum arvense* extract 50μg/ml; about 67% vs. *Artemisia annua* 2μM and about 50% vs. *Boswellia serrata* 5μM; $p<0.05$) by avoiding the ligand between RANKL and its receptor.

These data allow to hypothesize that the new combination is able to maintain RANKL/OPG balance at the initial stage of osteoporosis.
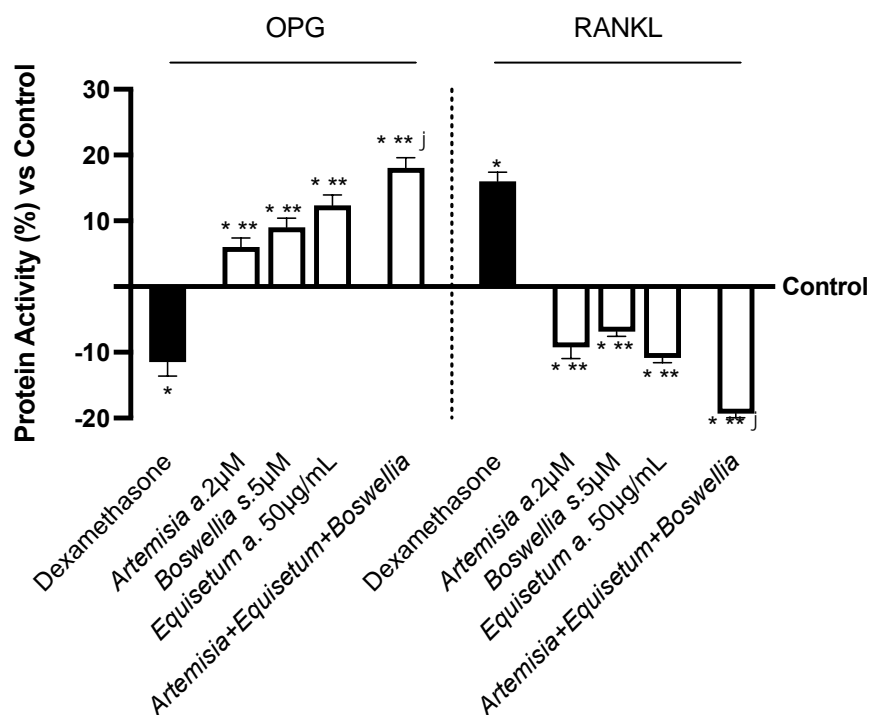


Figure 38. OPG/RANK axis on MC3T3/RAW 264.7-derived osteoclast co-culture. OPG and RANK activity were measured by ELISA test. Data are mean ± SD of five independent experiments performed in triplicates. * $p < 0.05$ vs control; **$p < 0.05$ vs. 1μM of DEX and $\varphi$ $p < 0.05$ vs. single agents.

Based on the results obtained, further experiments were performed in order to evaluate in the co-culture model the beneficial effects of *Equisetum arvense*, *Boswellia serrata* and *Artemisia annua*, alone and combined, on osteoblast and osteoclast differentiations and activity. As reported in figure 39A-B, 1μM DEX decreased ALP activity and mineralization process compared to untreated cells ($p < 0.05$); conversely *Equisetum arvense* extract 50μg/ml, *Artemisia annua* 2μM and *Boswellia serrata* 5μM alone increased MC3T3-E1 differentiation and mineralization compared to control and, more evidently, to 1μM DEX ($p < 0.05$). As expected, higher ALP activity and improved mineralized nodules were observed with natural extract combination compared to 1μM DEX ($p < 0.05$), confirming the previous result obtained about the beneficial effect of the new formulation in increasing osteoblast functions. Similarly, as shown in figure 39C-D, 1μM DEX promoted TRAP activity in the co-cultured system improving osteoclast resorption activity ($p < 0.05$); in contrast, *Equisetum arvense* extract 50μg/ml, *Artemisia annua* 2μM and *Boswellia serrata* 5μM treatment did not affect osteoclast differentiation and activity ($p < 0.05$). Although natural extract alone reduced the osteoclast differentiation in RAW 264.7-derived osteoclast, their synergistic effect treating the co-culture system greatly reduced osteoclast maturation compared to single agents and, particularly, to 1μM DEX (about 61% vs. *Equisetum arvense* extract 50μg/ml; about 67% vs. *Artemisia annua* 2μM and about 55% vs. *Boswellia serrata* 5μM; $p < 0.05$); accordingly, osteoclast resorptive activity was highly reduced compared to the single substances and, especially, compared to 1μM DEX (about 1.4 times vs. *Equisetum arvense* extract 50μg/ml; about 1.4 times vs. *Artemisia annua* 2μM and about 1.5 times vs. *Boswellia serrata* 5μM; $p < 0.05$), confirming a key role of this new combination in preventing the differentiation of osteoclastic progenitors. These results demonstrated that the homeostasis of bone remodeling is maintained by the balance of bone resorption and bone formation after treatment with *Equisetum arvense*, *Boswellia serrata* and *Artemisia annua*., speculating that the new combination could slow the onset of bone diseases such as osteoporosis.
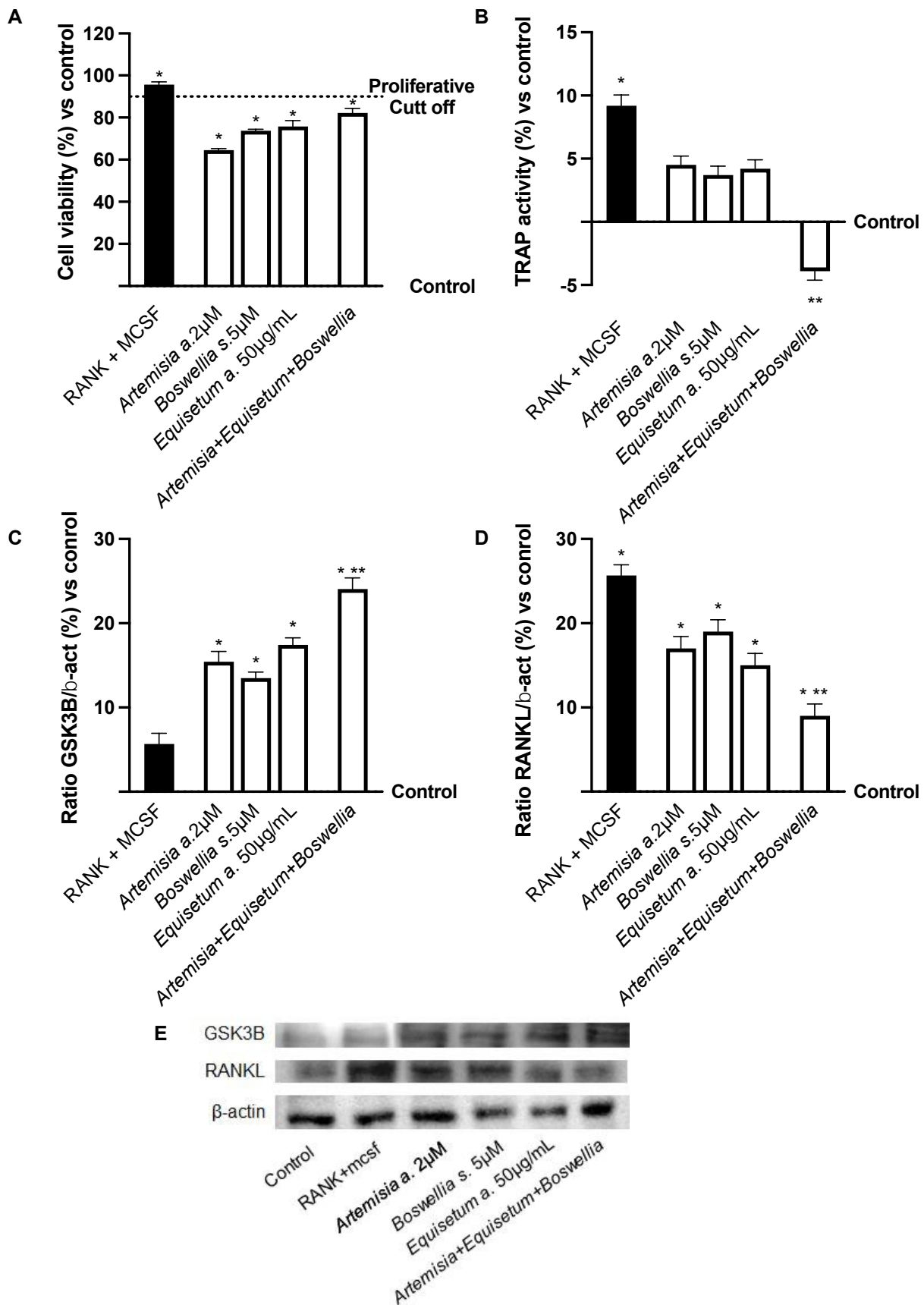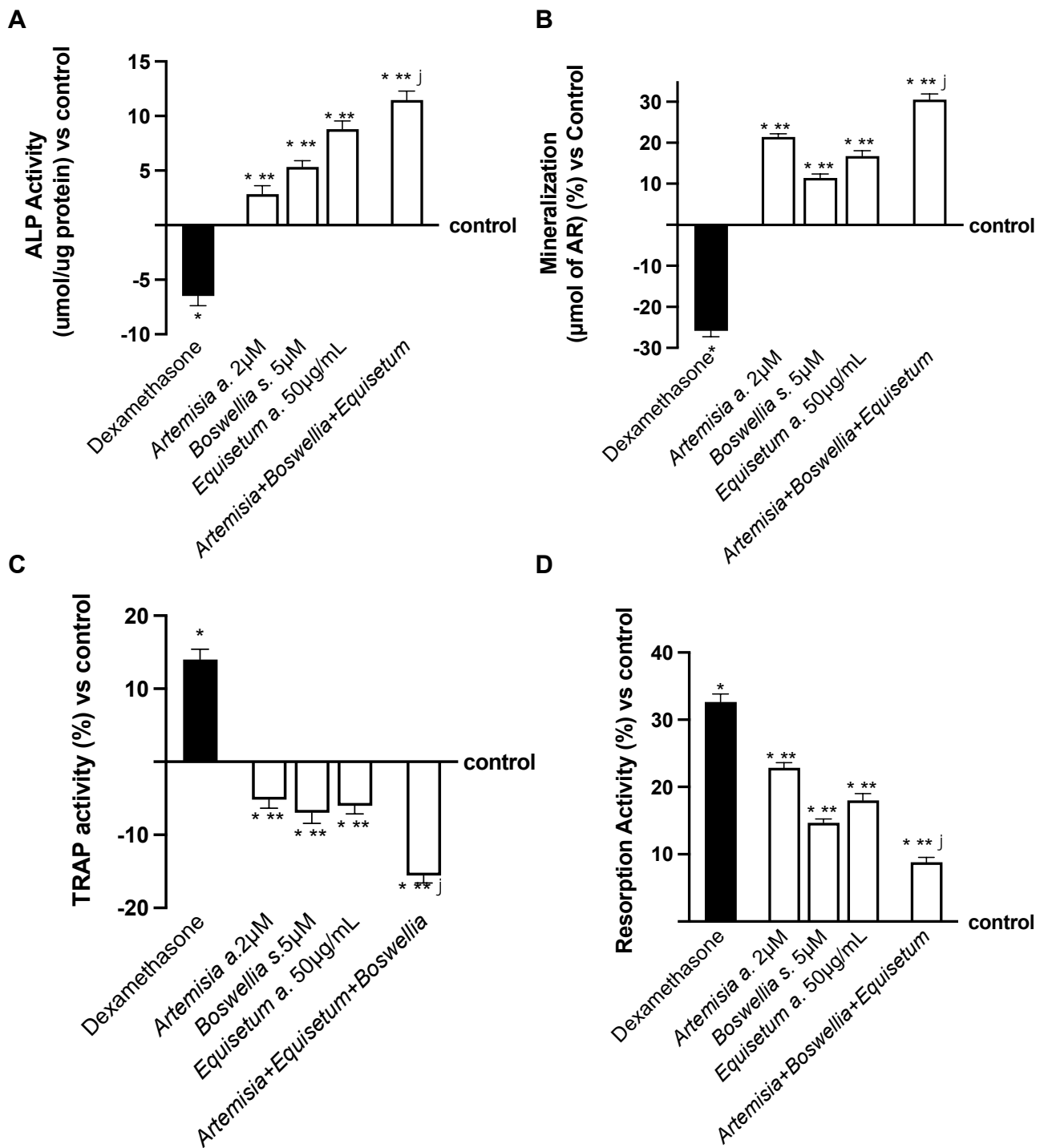
Figure 39. The effects of *Equisetum arvense*, *Artemisia annua* and *Boswellia serrata*, alone and combined, on osteoblast and osteoclast differentiation and activity in the co-culture system. A: ALP activity quantification; B: mineralized nodules quantification; C: TRAP activity quantification using quantification kit; D: bone pit resorption activity measured by bone resorption assay plates. Data are mean ± SD of five independent experiments performed in triplicates. * $p < 0.05$ vs control; **$p < 0.05$ vs. 1μM of DEX and $\varphi$ $p < 0.05$ vs. single agents.

# 7) NEW HYALURONIC ACID FROM PLANT ORIGIN TO IMPROVE JOINT PROTECTION—AN IN VITRO STUDY

Research on prevention of joint protection is taken from the article entitled "*New Hyaluronic Acid from Plant Origin to Improve Joint Protection—An In vitro Study*" [165]. In recent decades, hyaluronic acid (HA) has attracted great attention as a new treatment option for osteoarthritis. Classical therapies are not able to stop the cartilage degeneration process, nor do they favor tissue repair. Nowadays, it is accepted that high molecular weight HA can reduce inflammation by promoting tissue regeneration; therefore, the aim of this study was to verify the efficacy of a new high molecular weight HA of plant origin in maintaining joint homeostasis and preventing the harmful processes of osteoarthritis. The bioavailability of vegetable HA extract was investigated in a 3D intestinal barrier model that mimics human oral intake while excluding damage to the intestinal barrier. Furthermore, the chemical significance and biological properties of HA from plant were investigated in conditions that simulate osteoarthritis. The data demonstrated that HA from plant crosses the intestinal barrier without side effects as it has a chemical–biological profile, which could be responsible for many specific chondrocyte functions. Furthermore, in the osteoarthritis model, HA from plant can modulate the molecular mechanism responsible for preventing and restoring the degradation of cartilage. According to the results, this new form of HA appears to be well absorbed and distributed to chondrocytes, preserving their biological activities. Therefore, the oral administration of GreenIuronic® in humans can be considered a valid strategy to obtain beneficial therapeutic effects during osteoarthritis.

## 7.1 MATERIALS AND METHODS

### 7.1.1. Agents Preparation
GreenIuronic® was obtained from White Tremella (Silver Ear), which is a traditional foodstuff with medicinal applications in China [236]. The production process involves several steps necessary to obtain a final extract and includes a new technology based on patent N°WO2021/250566 from Vivatis Pharma GBHE, Grüner Deich 1–3, 20,097 Hamburg, Germany. Briefly, the process involves steps of extraction, purification, and refining by alcohol solution, sieving, and crushing. The resulting powder is then packed and tested for metals and stored [237]. In addition, sodium hyaluronate (Merck Life Science, Rome, Italy) was tested to verify the mechanism of action of GreenIuronic®. All these substances are prepared directly in water for HA determination or directly in Dulbecco's Modified Eagle's Medium (DMEM, Merck Life Science, Rome, Italy) without phenol red and supplemented with 0.5% fetal bovine serum (FBS, Merck Life Science, Rome, Italy), 2 mM L-glutamine (Merck Life Science, Rome, Italy), and 1% penicillin–streptomycin (Merck Life Science, Rome, Italy) for biological analysis.

### 7.1.2. HPLC Analysis
The determination of the HA was also confirmed by HPLC (Shimadzu, Kyoto, Japan) analysis according to the method reported in the literature [238]. Briefly, 20 μL of TRIS buffer (3.0 g TRIZMA base, 4.0 g sodium acetate trihydrate, 1.46 g sodium chloride, and 50 mg crystalline bovine serum albumin dissolved in 100 mL of 0.12 M HCl, pH 7.3 with 6 M HCl. All chemicals are purchased from Merck Life

Science, Rome, Italy), 30 μL of chondroitinase AC solution (Merck Life Science, Rome, Italy) (diluted to 10 U/mL with water), and 20 μL of GreenIuronic® test solution (200 mg dissolved in 100 mL of water) were pipetted into a conical 1.5 mL vial. The vial was placed in a warm water bath at 37 °C for 3 h. After cooling at room temperature, the sample was diluted to 1 mL by adding 930 μL of mobile phase A (reagent purchased from Merck Life Science, Rome, Italy, and column from Phenomenex Srl, Bologna, Italy) and the mixture was analyzed by HPLC-UV and HPLC-HRMS systems. A control solution was prepared by replacing the enzyme aliquot with TRIS buffer.

### 7.1.3. Colorimetric Determination of Hyaluronic Acid

The assay performed to quantify the concentration of HA on material samples was the same reported in the literature [239.]. Briefly, 1 mg of raw sample was dissolved in 1 mL of deionized water, and 200 μL of resuspended samples were displaced in new Eppendorf, diluted with 1.2 mL of sulfuric acid (Merck Life Science, Rome, Italy) with 0.0125 M tetraborate (Merck Life Science, Rome, Italy), shaken for 20 s and then boiled at 100 °C for 5 min. Once the samples were allowed to cool on ice, 20 μL of 0.15% hydroxydiphenyl (Merck Life Science, Rome, Italy) (dissolved in 0.5% NaOH, Merck Life Science, Rome, Italy) was added and stirred; 100 μL of each sample was placed in a 96 multi-well plate and the absorbance was measured at 340 nm by a spectrophotometer (Infinite 200 Pro MPlex, Tecan, Männedorf, Switzerland). The data obtained were compared to a calibration curve generated using glucuronic acid (0, 0.25, 0.5, 1, 1.5, 2 mg/mL Merck Life Science, Rome, Italy) [240] and the results were expressed as mean (%w/w) ± SD compared to control (0 line).

### 7.1.4. Molecular Weight Determination

The determination of the molecular weight of HA before exploring its biological effects was carried out using 1% agarose gel, following the method reported in the literature [241]. Briefly, 0.3 g agarose (Merck Life Science, Rome, Italy) was dissolved in 30 mL of Tris-acetate-EDTA (TAE) buffer (48.5 g tris base, 11.4 mL acetic acid, and 0.5 M EDTA pH 8, all substances were purchased from Merck Life Science, Rome, Italy) and the solution was heated for 30 s in a microwave at high power. The gel was poured into the holder and allowed to solidify before performing a pre-run at 100 V for 45 min, using the Mini-Sub Cell GT System (Bio-Rad, Hercules, CA, USA). In the meantime, samples were prepared by dissolving 200 μg of raw samples in 16 μL of TAE buffer 1×. Before running the gel, 4 μL of loading buffer (0.2% Bromophenol Blue, 1 mL of TAE 1×, and 8.5 mL of glycerol, which were purchased from Merck Life Science, Rome, Italy) was added to each sample and to the molecular weights (mixture of 5 μL of Select-HA HiLadder and 5 μL Select-HA Mega Ladder, Echelon Biosciences, Tebu-Bio Srl, Magenta, Italy). The samples were run at 100 V until the samples reached 1 cm from the end of the gel. Then, the gel was hydrated in $H_2O$ for 24 h at room temperature in agitation and then the gel was placed in 30% ethanol with 0.015% Stains All dye (Merck Life Science, Rome, Italy) for 24 h in the dark. The gel was decolored for 30 min in $H_2O$ in the dark before proceeding with image acquisition using ChemiDoc™ Touch Imaging System (Bio-Rad, Hercules, CA, USA). The image obtained was analyzed by Image Lab 3.0 software (Bio-Rad Hercules, CA, USA).

### 7.1.5. Cell Culture

The human epithelial intestinal cells, CaCo-2, purchased from the American Type Culture Collection (ATCC), were cultured in Dulbecco's Modified Eagle's Medium/Nutrient F-12 Ham (DMEM-F12, Merck Life Science, Rome, Italy) containing 10% FBS (Merck Life Science, Rome, Italy), 2 mM L-glutamine and 1% penicillin–streptomycin (Merck Life Science, Rome, Italy) maintaining in an incubator at 37 °C and 5% $CO_2$ [170]. The cells used for the experiments were at passage numbers between 26 and 32 in order to preserve the integrative paracellular permeability and transport properties [175] maintaining the similarity to the intestinal absorption mechanism following oral intake in humans. The cells were plated in a different manner to perform several experiments including 1 × $10^4$ cells in 96 well plates to study cell viability by MTT-based *In vitro* Toxicology Assay Kit (Merck Life Science, Rome, Italy) and ROS production using cytochrome C (Merck Life Science, Rome, Italy) in a complete medium. Eight hours before the stimulation the cells were incubated with DMEM without red phenol and supplemented with 0.5% FBS (Merck Life Science, Rome, Italy), 2 mM L-glutamine, and 1% penicillin–streptomycin (both from Merck Life Science, Rome, Italy) at 37 °C to synchronize them. In addition, 2 × $10^4$ cells were plated on 6.5 mm Transwell® (Corning® Costar®, Merck Life Science, Rome, Italy) with a 0.4 µm pore polycarbonate membrane insert (Corning® Costar®, Merck Life Science, Rome, Italy) in a 24 well plate to perform the absorption analyses [166]. Cells plated on the Transwell® insert were maintained in a complete medium, which was changed every other day on the basolateral and apical sides for 21 days before the simulations [149]. Before the stimulation, on the apical side, the medium was brought to pH 6.5 as the pH in the lumen of the small intestine, while the pH 7.4 on the basolateral side represented blood [242]. This *in vitro* model is widely used [166, 171] and accepted by European Medicines Agency (EMA) and FDA to predict the absorption, metabolism, and bioavailability of several substances after oral intake in humans [172,173].

The immortalized human juvenile costal chondrocyte cell line T/C-28a2 (purchased from Merck Life Science, Rome, Italy) was cultured in DMEM-F12 medium supplemented with 10% FBS (Merck Life Science, Rome, Italy), 2 mM L-glutamine (Merck Life Science, Rome, Italy), and antibiotics (50 UI/mL penicillin and 50 µg/mL streptomycin, Merck Life Science, Rome, Italy)) and maintained in an incubator at 5% $CO_2$ and 95% humidity [243]. This cell line is representative and the most commonly used cells for mimicking joints [244] and they were used between passages 3 and 10 245]. For the experiments 1 × $10^4$ cells were seeded in 96 well plates to study cell viability by MTT-based *In vitro* Toxicology Assay Kit (Merck Life Science, Rome, Italy), ROS production using cytochrome C (Merck Life Science, Rome, Italy), and Crystal Violet (Merck Life Science, Rome, Italy) in a complete medium; additionally, 1 × $10^6$ cells were plated on a 6-well to determine HA concentration, using quantification kit, and to analyze molecular pathways by Western-blot analysis or ELISA kit.

### 7.1.6. Experimental Protocol

In order to analyze the beneficial effects of hyaluronic acid on articular joints in humans after oral intake, the experiments were divided into two steps; the aim of the first one was to verify the ability of HA to cross the intestinal barrier *in vitro* model excluding negative effects, and of the second one was to check the direct effects on chondrocytes analyzing several parameters and mechanism of actions. For this

reason, in intestinal CaCo-2 cells, a dose–response study ranging from 0.125 to 1 $\mu g/\mu L$ [246] was performed to assess the concentration able to exert beneficial effects on cell viability and ROS production. Subsequently, the best concentration of GreenIuronic® and hyaluronic acid salt were tested on an intestinal *in vitro* barrier model to verify intestinal integrity through TEER measurement, tight junction analysis by ELISA kit, and permeability assay by Papp measurement, also analyzing the total amount of hyaluronic acid that had crossed the intestinal barrier. For all these experiments, cells were treated in a time-dependent manner from 2 to 6 h, as reported in the literature [170]. In addition, after each stimulation, the basolateral medium was collected to be used on chondrocytes cells. T/C-28a2, a chondrocyte cell line widely used to study articular joints, was treated for 3 days [247] and, at the end of stimulation, the mitochondrial metabolism, cell proliferation, ROS production, and hyaluronic acid quantification were tested. Finally, in order to mimic OA conditions, further experiments were performed pre-treating T/C-28a2 with 10 $\mu g/mL$ of LPS (Merck Life Science, Rome, Italy) for 24 h [248], and then stimulating with GreenIuronic® and sodium hyaluronate for 3 days to evaluate if they are able to restore the damage. In these conditions, the survival mechanisms and articular recovery were investigated.

### 7.1.7. Cell Viability

The analysis of cell viability was performed using a classical technique based on the MTT-based *In vitro* Toxicology Assay Kit (Merck Life Science, Rome, Italy) [196], following the manufacturer's instructions. Indeed, at the end of stimulation, the cells were incubated with 1% MTT dye for 2 h in an incubator at 37 °C, 5% $CO_2$, and 95% humidity, and then the purple formazan crystals were dissolved in an equal volume of MTT Solubilization Solution. The absorbance was analyzed by spectrophotometer (Infinite 200 Pro MPlex, Tecan, Männedorf, Switzerland) at 570 nm with correction at 690 nm, and results were expressed compared to the control (0% line), which represented untreated cells. The results reported an increase in the percentage of viable cells compared to the control and indicated a higher number of viable cells plus the control. This strategy can lead to a high level of safety of the stimulation and, consequently, to a correct analysis of the results.

### 7.1.8. *In vitro* Intestinal Barrier Model

An intestinal barrier model, using CaCo-2 cells, was performed to analyze the passage through the intestinal barrier of GreenIuronic® and sodium hyaluronate, having, as a final destination, the chondrocyte where they could exert their beneficial effects. For this reason, the TEER values were determined with EVOM3, coupled with STX2 chopstick electrodes (World Precision Instruments, Sarasota, FL, USA); this assay was carried out every 2 days for 21 days until reaching a TEER value ≥ 400 $\Omega cm2$ before the stimulation [170], the time required for the cell monolayer formation, for cell differentiation, and for the exposition of the intestinal villi. On day 21, the medium at the apical and basolateral environments was changed to create different pH conditions: pH around 6.5 at the apical level (acidic pH mimicking lumen of small intestine) and pH around 7.4 at the basolateral level (neutral pH mimicking human blood) [149]. The cells were kept for 15 min at 37 °C and 5% $CO_2$, after that, the TEER values were measured again before the start of the experiment to verify the stabilization of the values. The cells were stimulated with GreenIuronic® and sodium hyaluronate for 2 h to 6 h before the successive analysis, including the permeability assay measured by Papp analysis [170].

Briefly, the Papp (cm/s) was calculated with the following formula [170,149]:

$$Papp = dQ/dt \twoheadrightarrow 1/m0 \twoheadrightarrow 1/A \twoheadrightarrow V\ Donor$$

dQ: amount of substance transported (nmol or μg);

dt: incubation time (sec);

m0: amount of substrate applied to donor compartment (nmol or μg);

A: surface area of Transwell membrane (cm$^2$);

VDonor: volume of the donor compartment (cm$^3$).

Negative controls without cells were tested to exclude Transwell membrane influence.

### 7.1.9. Occludin Quantification Assay

The Human Occludin ELISA kit (OCLN kit, MyBiosource, San Diego, CA, USA) analyzed the occludin presence in CaCo-2 cell lysates, according to the manufacturer's instruction [170]. Briefly, CaCo-2 cells were lysed with cold Phosphate-Buffered Saline (PBS, Merck Life Science, Rome, Italy) 1×, centrifuged at 1500× g for 10 min at 4 °C, and 100 μL of each sample was transferred to the strip well before the incubation at 37 °C for 90 min. The supernatants were removed, and the strips were incubated with 100 μL of Detection Solution A for 45 min at 37 °C; then, the strips were washed with Wash Solution and incubated with 100 μL of Detection Solution B for an additional 45 min. At the end of this time, 90 μL of Substrate Solution was added followed by an incubation for 20 min at 37 °C in the dark, and then 50 μL of Stop Solution was used to block the enzymatic reaction. The plate was analyzed by a spectrophotometer (Infinite 200 Pro MPlex, Tecan, Männedorf, Switzerland) at 450 nm. The concentration is expressed as pg/mL compared to a standard curve (range from 0 to 1500 pg/mL) and the results are expressed as percentage (%) versus control (0 line).

### 7.1.10. Claudin 1 Detection

The Human Claudin1 was measured in CaCo-2 lysates by ELISA kit (Cusabio Technology LLC, Huston, TX, USA), following the manufacturer's instructions [170]. Briefly, the cells were lysed with cold PBS 1× (Merck Life Science, Rome, Italy) and centrifuged at 1500× g for 10 min at 4 °C. Then, 100 μL of each sample was added to the ELISA plate and incubated at 37 °C for 2 h; after which, the plate was washed and 100 μL of Biotin-antibody was added to the wells and incubated for 1 h at 37 °C. After this time, the wells were washed and 100 μL of HRP-avidin were added in each well, and the samples were incubated for 1 h at 37 °C. Then, 90 μL of TMB Substrate was also added to the samples and the plate was incubated for 20 min at 37 °C protected from light. At the end, 50 μL of Stop Solution was used to stop the reaction and the plate was analyzed by a spectrophotometer (Infinite 200 Pro MPlex, Tecan, Männedorf, Switzerland) at 450 nm. The concentration was expressed as pg/mL, comparing data to the standard curve (range from 0 to 1000 pg/mL), and the results were expressed as percentage (%) versus control (0 line).

### 7.1.11. ZO-1 Detection

The Human Tight Junction Protein 1 ELISA kit (MyBiosource, San Diego, CA, USA) was measured in CaCo-2, following the manufacturer's instructions [170]. Briefly, the cells were rinsed with ice-cold PBS

1× (Merck Life Science, Rome, Italy) and processed with two freeze-thaw cycles; then, cell lysates were centrifuged for 5 min at 5000× g at 4 °C. After which, 100 μL of each sample were collected and incubated on the ELISA plate at 37 °C for 90 min; after washing, 100 μL of Detection Solution A was added to each well and incubated for 45 min at 37 °C. The wells were washed and 100 μL Detection Solution B was added to the samples. After an incubation of 45 min, the wells were washed again and 90 μL of Substrate Solution was added to each well, and then the samples were incubated for 20 min at 37 °C in the dark. Finally, 50 μL of Stop Solution was added and then the plates were read by a spectrophotometer (Infinite 200 Pro MPlex, Tecan, Männedorf, Switzerland) at 450 nm. The concentration was expressed as pg/mL, comparing data to standard curve (range from 0 to 1000 pg/mL), and the results were expressed as percentage (%) versus control (0 line).

### 7.1.12. Crystal Violet Staining

At the end of stimulation time, the cells were fixed with 1% glutaraldehyde (Merck Life Science, Rome, Italy) for 15 min at room temperature, washed, and stained with 100 μL 0.1% aqueous crystal violet (Merck Life Science, Rome, Italy) for 20 min at room temperature and solubilized with 100 μL 10% acetic acid before reading the absorbance at 595 nm using a spectrophotometer (Infinite 200 Pro MPlex, Tecan, Männedorf, Switzerland). The estimated number was determined by comparing data to the control cells normalized to T0 (measurement at the beginning of the stimulation) [203]. The results were expressed as percentage (%) versus control (0 line).

### 7.1.13. ROS Production

The quantification of superoxide anion release was obtained following a standard protocol based on the reduction in cytochrome C [203], and the absorbance in culture supernatants was measured at 550 nm using the spectrophotometer (Infinite 200 Pro MPlex, Tecan, Männedorf, Switzerland). The O2 rate was expressed as the mean ± SD (%) of nanomoles per reduced cytochrome C per microgram of protein compared to the control (0 line) [203].

### 7.1.14. Quantification of Hyaluronic Acid in Cell Culture

At the end of stimulations, both cell types were lysed with 100 μL of cold PBS1× to measure the total HA following the instructions of the Hyaluronic Acid ELISA Kit (ClueClone). Briefly, 50 μL of sample and reagent A were added to each well and after gently shaking the plate was incubated for 1 h at 37 °C. At the end, the wells were washed three times and 100 μL of reagent B was added before incubating the plate for 30 min at 37 °C, then 90 μL of substrate solution was added before incubating the plate for 20 min at 37 °C. At the end, 50 μL of stop solution was added immediately before reading at 450 nm by a spectrophotometer (Infinite 200 Pro MPlex, Tecan, Männedorf, Switzerland) [249,250]. The results were expressed as means ± SD (%) versus control (0 line).

### 7.1.15. ERK/MAPK Activity

The analysis of ERK/MAPK activity was performed using the InstantOneTM ELISA (Thermo Fisher, Milan, Italy) on chondrocytes lysates [141]. Briefly, 50 μL of lysate samples prepared in Lysis Buffer were tested in ELISA microplate strips after the incubation for 1 h at room temperature in a microplate shaker pre-coated with the antibody cocktail. After that, the strips were incubated with the detection

reagent for 20 min before stopping the reaction with a stop solution. The absorbance was measured by a spectrophotometer at 450 nm (Infinite 200 Pro MPlex, Tecan, Männedorf, Switzerland) and the results were expressed as means ± SD (%) versus control (0 line).

### 7.1.16. OPG Activity

The OPG/TNFRSF11B Duo Set (R&D Systems, Minneapolis, MN, USA) was applied according to the manufacturer's instructions to verify the OPG involvement [251]. Briefly, 100 µL of samples or standards were added to the well and incubated for 2 h at room temperature protected from light and, after washing, 100 µL of the Detection Antibody was added to each well and incubated as previously described. After 2 h, 100 µL of the working dilution of Streptavidin-HRP A was added to each well and incubated for 20 min at room temperature. At the end of the time, 100 µL of Substrate Solution was added to each well, incubated for 20 min at room temperature, and then 50 µL of Stop Solution was used to stop the enzymatic reaction. The absorbance of each well was measured at 450 nm by a spectrophotometer (Infinite 200 Pro MPlex, Tecan, Männedorf, Switzerland) and the results were interpolated with the standard curve (6.25 to 625 pg/mL) and the results were expressed as means ± SD (%) compared to control (0 line).

### 7.1.17. NFKB Analysis

The NF-kB (p65) Transcriptional factor Assay kit was carried out to analyze the NF-κB DNA binding activity, following the manufacturer's instruction (Cayman Chemical Company, Ann Arbor, MI, USA) [162]. The concentration was calculated by comparing results to the standard curve (generated by NF-kB (p65) Transcriptional factor positive control (ranging from 0 to 10 µL/well according to differently scaled dilutions) and reported as means ± SD (%) compared to control (0 line).

### 7.1.18. BAX Assay

BAX activity was determined in chondrocyte lysates using an ELISA kit (Human Bax ELISA Kit, MyBiosource, San Diego, CA, USA) according to the manufacturer's instructions [252]. The absorbance of the samples was measured at 450 nm by a spectrophotometer (Infinite 200 Pro MPlex, Tecan, Männedorf, Switzerland) and the results were compared to the standard curve (range from 0 to 2000 pg/mL) and expressed as means ± SD (%) normalized to control value (0 line).

### 7.1.19. Caspase 9 Assay

The Caspase 9 activity was investigated in chondrocytes lysates by ELISA kit (Caspase 9 Human ELISA Kit, Thermoscientific, Waltham, MA, USA), according to the manufacturer's instructions, reading the sample's absorbance at 450 nm with a spectrometer (Infinite 200 Pro MPlex, Tecan, Männedorf, Switzerland). The data were obtained by comparison to a standard curve (ranging from 1.6 to 100 ng/mL), and the results were expressed as means ± SD (%) compared to control value (0 line) [253].

### 7.1.20. Western-Blot Analysis

At the end of each stimulation, chondrocytes were washed with ice-cold PBS 1× (Merck Life Science, Rome, Italy), and lysed using Complete Tablet Buffer (Roche, Basel, Switzerland) supplemented with 2 mM sodium orthovanadate (Na3VO4), 1 mM phenylmethanesulfonyl fluoride (PMSF) (Merck Life

Science, Rome, Italy), 1:50 mix Phosphatase Inhibitor Cocktail (Merck Life Science, Rome, Italy), and 1:200 mix Protease Inhibitor Cocktail (Merck Life Science, Rome, Italy) to obtain a total protein extract that was centrifuged at 14,000× g for 20 min at 4 °C. Then, 35 µg of proteins for each extract was resolved on 8% and 10% SDS-PAGE gel and transferred to a polyvinylidene difluoride (PVDF) membrane, which was incubated overnight with the specific primary antibodies such as Cyclin D1 (1:500, Santa Cruz, CA, USA) and CD44 (1:500, Santa Cruz, CA, USA). All protein expressions were normalized and verified through β-actin detection (1:5000, Merck Life Science, Rome, Italy), and expressed as mean ± SD (%) compared to control value (0 line).

### 7.1.21. Statistical Analysis

Data obtained from each experimental protocol and assay were collected and analyzed using GraphPad Prism 7 statistical software through mixed variance analysis. In particular, for all growth curves, bar graphs, and line graphs, five independent experiments were performed in triplicates and included in the statistical analysis. All time points in growth curves were presented as the mean of the three biological replicates with mean errors < 5%. The two-tailed Student's t-test was followed by Welch's t test to analyze two groups. Multiple comparisons between groups were analyzed by two-way ANOVA followed by a two-tailed Dunnett post hoc test. Error bars in the bar charts and line charts represent the standard deviation. For TEER analyses, one-way ANOVA followed by Bonferroni post hoc tests was performed to see if the means were significantly different between groups. All results were expressed as mean ± SD of at least 5 independent experiments performed in triplicates. Differences with a p value < 0.05 were considered statistically significant. Data normality was assessed with the Kolmogorov–Smirnov test.

### 7.2 RESULTS

### 7.2.1. Characterization of GreenIuronic®

High-Performance Liquid Chromatography analysis of GreenIuronic® (Figure 40) revealed the presence of HA, which was detected as the corresponding disaccharide ΔDi-HA generated by chondroitinase AC enzymatic hydrolysis of the Tremella extract. The identity of this disaccharide was established by comparison with the ΔDi-HA reference standard and by the protonated and sodiate positive ions detected in its mass spectrum. Moreover, the same analysis also revealed the absence of chondroitin 4 and 6 mono-sulfates, which eluted at 6.25 and 5.35 min, respectively. However, because of the absence of sulfate group in the disaccharide chondroitin 0 sulfate (ΔD-0S), arising from chondroitine hydrolysis, the HPLC method, based on ion-pair retention, did not allow the separation between the disaccharides ΔDi-HA and ΔD-0S: indeed, they eluted at 2.25 min.
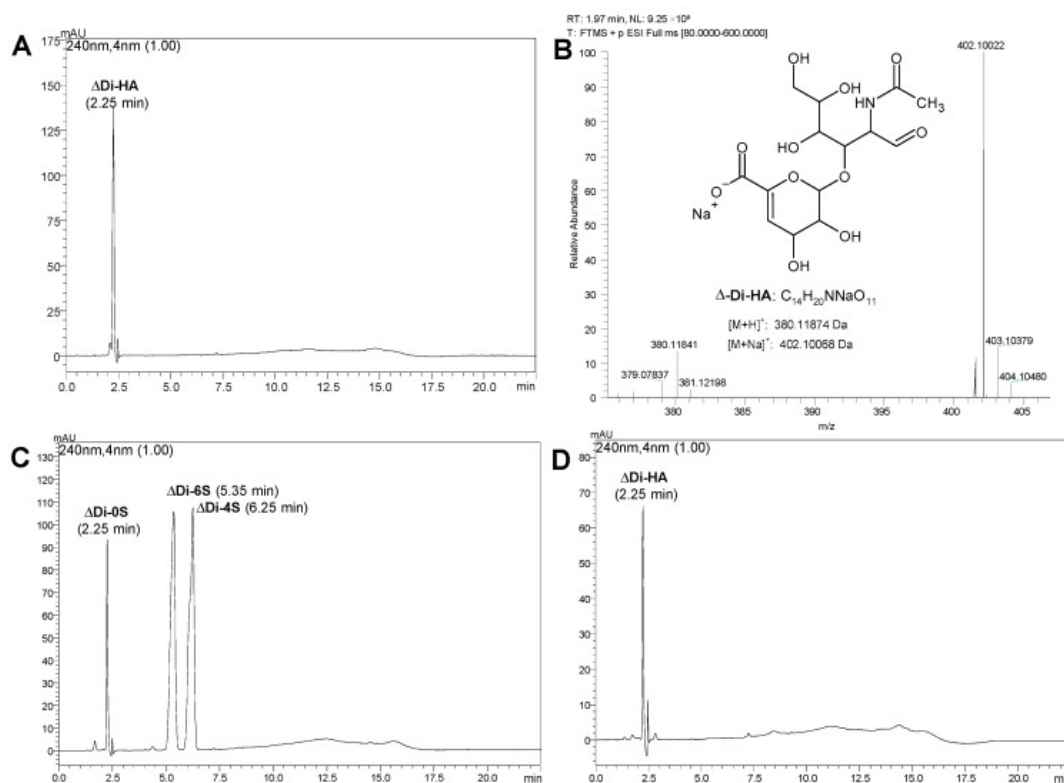
Figure 40. HPLC-UV and high-resolution mass spectrometry (HRMS) analysis of GreenIuronic® after enzymatic hydrolysis with chondroitinase AC. In (A,B) HPLC-UV chromatogram of GreenIuronic® sample and its positive HRMS spectrum. In (C,D) HPLC-UV chromatograms of a mixture of chondroitin disaccharides standard ΔDi-0S, ΔDi-4S, and ΔDi-6S and a solution of the disaccharide standard ΔDi-HA of HA.

Moreover, since HPLC-UV analysis revealed a possible high concentration of HA in GreenIuronic® samples, additional experiments were carried out to quantify the content of glucuronic acid in GreenIuronic® and in sodium hyaluronate samples. As reported in Table 4, the content of glucuronic acid in GreenIuronic® is about 90%, which is higher than that of sodium hyaluronate (about 62%). These data support what was observed in previous experiments in HPLC (reported above) about the purity of the GreenIuronic® material.

| Raw Material | Mean (%*w/w*) ± SD |
|---|---|
| Sodium Hyaluronate | 62.5 ± 2.121 |
| GreenIuronic® | 90.5 ± 6.364 |

Table 4. Quantification of HA. The % w/w of all HA forms normalized on standard curves generated using glucuronic acid standard (ranging from 0 to 2 mg/mL) analyzed at 340 nm by spectrophotometry (Infinite 200 Pro MPlex, Tecan). Data are expressed as means ± standard deviation (SD) (%) of five independent experiments performed in triplicates.

Finally, for the analysis of GreenIuronic® size distribution, agarose gel electrophoresis was used to define a range of the molecular weight. Agarose gel retards the electrophoretic mobility of HA molecules in a molecular weight-dependent manner indicating that GreenIuronic® may be considered the HMWHA (>1650 kDa), as can be seen in Figure 41. On the contrary, sodium hyaluronate was confirmed to have the lower molecular weight HA (LMWHA) (between 300 and 500 kDa). These results indicate that GreenIuronic® molecular weight is higher than that of sodium hyaluronate and further

experiments were performed in order to confirm the hypothesis that HMWHA exerts more beneficial effects compared to those of LMWHA.
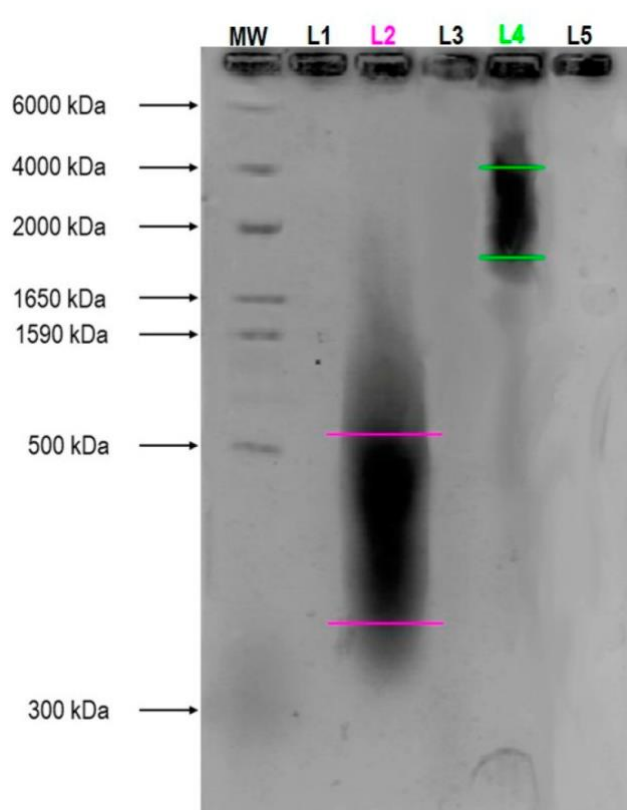


Figure 41. In the figure an example of HA molecular weight determination on 1% Agarose gel. The sample loads are described as follows by the abbreviations: MW = standard molecular weight Mega + HiLadder specific for HA detection; L1 = lane empty loaded with 10 μL TAE buffer; L2 = lane loaded with 100 μg/10 μL Sodium Hyaluronate; L3 = lane empty loaded with 10 μL TAE buffer; L4 = lane loaded with 100 μg/10 μL GreenIuronic®; L5 = lane empty loaded with 10 μL TAE buffer.

### 7.2.2. Dose–Response and Time-Course Study of GreenIuronic® on CaCo-2 Cells

Before studying the permeability and transport of GreenIuronic®, the human immortalized colorectal adenocarcinoma (CaCo-2) cell line was used to perform a dose–response study to exclude any cytotoxic effects. The analysis was performed comparing the effects of GreenIuronic® to sodium hyaluronate, testing them at the same concentration (ranging from 0.125 to 1 μg/μL) on cell viability and ROS production in CaCo-2 cells in a time-course study (from 2 to 6 h). The cell viability of the CaCo-2 cells, measured by 3-(4,5-Dimethylthiazol-2-yl)-2,5-diphenyltetrazolium bromide (MTT) assay, showed time and concentration-dependent effects of both substances (Figure 42A), and the beneficial effects compared to control ($p < 0.05$) were maintained during all periods of stimulation excluding any cytotoxic effect at all dosage tested. In particular, the cells treated with GreenIuronic® 1 μg/μL showed high variability compared to control ($p < 0.05$) and compared to other concentrations tested ($p < 0.05$) suggesting that GreenIuronic® 1 μg/μL is non-toxic to intestinal epithelial cells exhibiting the best profile also compared to sodium hyaluronate at the same concentration and time ($p < 0.05$). Additional experiments were carried out in order to confirm the safety of GreenIuronic® on intestinal epithelium analyzing if the substances tested could induce oxidative stress. For this reason, ROS production was evaluated on CaCo-2 cells from 2 to 6 h of stimulations with both GreenIuronic® and sodium hyaluronate. As shown in Figure 42B, none of the concentrations tested was able to increase the ROS production maintaining them at normal physiological conditions. GreenIuronic® 1 μg/μL maintains a

low ROS level during all periods analyzed better than the other concentrations tested and all sodium hyaluronate concentrations, and it was maintained for all further experiments.
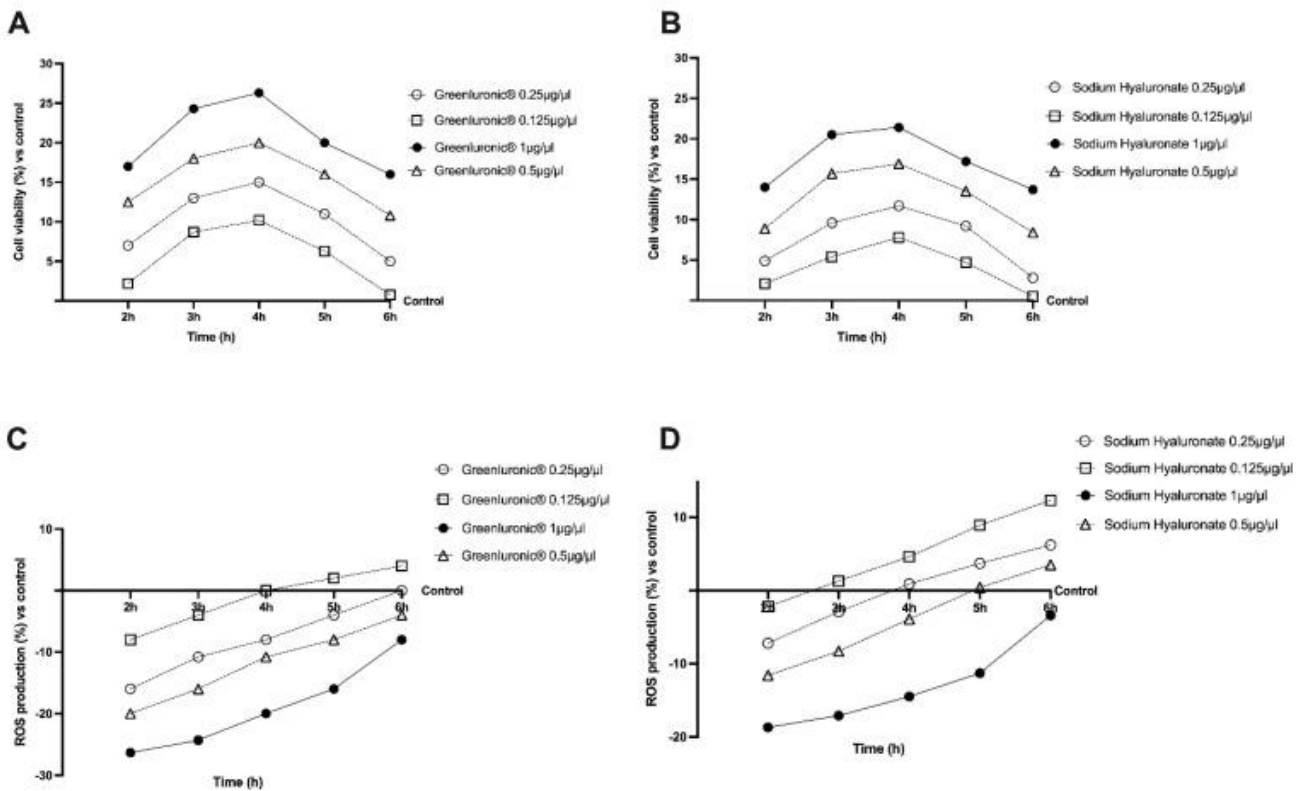


Figure 42. Cell viability and ROS production on CaCo-2 cells. In panel (A,B) dose–response study on cell viability measured by MTT test of both GreenIuronic® and Sodium Hyaluronate from 2 to 6 h. In panel (C,D) ROS production of both GreenIuronic® and Sodium Hyaluronate measured by reduction in cytochrome C from 2 to 6 h. Data are mean ± SD of five independent experiments performed in triplicates vs. control values (0% line).

### 7.2.3. Permeability Analysis of GreenIuronic® Using an *In vitro* Model of Intestinal Barrier

To assess permeability, and to obtain additional information about the GreenIuronic® intestinal absorption, further experiments were carried out performing a 3D *in vitro* model in order to mimic the *in vivo* complexity of the intestinal barrier. In this context, 1 µg/µL GreenIuronic® and 1 µg/µL sodium hyaluronate were tested from 2 to 6 h in order to measure transepithelial electrical resistance (TEER) values, the apparent permeability coefficient (Papp) values, and the HA concentration to predict their bioavailability. The data obtained show that intestinal adsorption has a physiological trend as can be observed from the analysis of TEER and tight junction (TJ). In particular, the passage through the intestinal epithelium demonstrates that both sodium hyaluronate and GreenIuronic® were able to maintain the epithelial integrity increasing the ionic flux of the paracellular exchanges across the intestinal epithelial compared to control ($p < 0.0001$). Indeed, GreenIuronic® demonstrates a better effect compared to sodium hyaluronate during all times of the stimulation ($p < 0.0001$), as reported in Figure 43A. Afterwards, also the evaluation of TJ confirmed these results; indeed, GreenIuronic® exerted the greatest effects on occludin ($p = 0.0286$, about 31%, Figure 43B), claudin-1 ($p = 0.0299$, about 37%, Figure 43C), and zonula occludens-1 (ZO-1) ($p = 0.0299$, about 50%, Figure 43D) compared to sodium hyaluronate and compared to control value (reported as 0 line, $p < 0.05$). From these encouraging results, which confirmed the correct functioning of the intestinal epithelium, further experiments were carried out measuring the permeability rate, analyzing the flux of non-electrolyte

tracers (expressed as permeability coefficient as reported) and how much HA has crossed the intestinal barrier to reach the target site. Data obtained from the analysis of the basolateral environment (Figure 43E) confirmed our previous findings since the amount of GreenIuronic® was higher compared to sodium hyaluronate ($p < 0.05$) with a maximum effect at 4 h compared to sodium hyaluronate (about 20%, $p < 0.013$). In addition, the data obtained from the quantification of the basolateral level (Figure 43F) supported the hypothesis about the importance of predicting human absorption; GreenIuronic® has a higher amount of HA that crosses the barrier and reaches the plasma level compared to control ($p < 0.0001$) and compared to sodium hyaluronate (about 30%, $p < 0.0001$) with the greatest effects between 4 and 5 h.
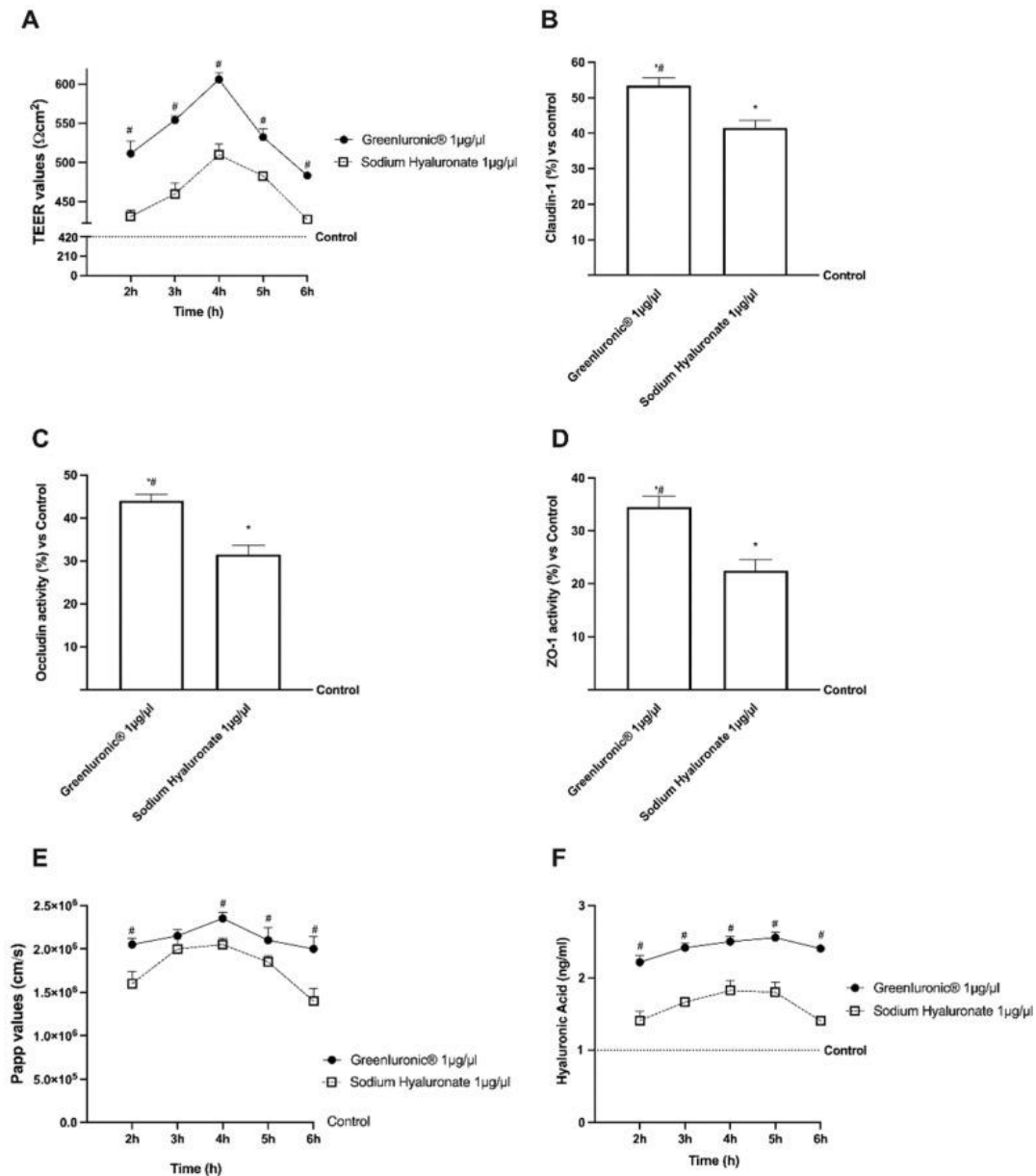


Figure 43. Permeability study on CaCo-2 cells. In (A) TEER Value using EVOM3; from (B–D) the analysis of TJ measured by Enzyme-Linked Immunosorbent Assay (ELISA) test (Occludin, Claudin1, and ZO-1, respectively); in (E) the Papp values in which data $< 0.2 \times 10^{-6}$ cm/s mean very poor absorption with a bioavailability $< 1\%$, data between $0.2 \times 10^{-6}$ and $2 \times 10^{-6}$ cm/s with bioavailability between 1 and 90%, and data $> 2 \times 10^{-6}$ cm/s mean very good absorption with a bioavailability over 90%. In (F) HA quantification measured by ELISA kit. Data are mean ± SD of five independent experiments performed in triplicates. From (B–D) means± SD are expressed comparing data to control value (0% line) and * $p < 0.05$ vs. control; # $p < 0.05$ vs. Sodium Hyaluronate 1 µg/µL. On the contrary, in (A,E,F) the control samples are specifically reported and both GreenIuronic® and sodium hyaluronate are $p < 0.0001$ vs. control; # $p < 0.05$ vs. Sodium Hyaluronate 1 µg/µL.

### 7.2.4. Effects of GreenIuronic® Crossed Intestinal Barrier on Chondrocytes

Since the exogenous hyaluronic acid administered into articular cartilage has a direct biological effect on chondrocytes, several experiments were carried out to explore the effect of GreenIuronic®, compared to sodium hyaluronate, on chondrocytes after intestinal absorption in terms of mitochondrial metabolism and cell proliferation. As expected (Figure 44A), both 1 µg/µL GreenIuronic® and sodium hyaluronate were able to improve cell viability compared to control ($p < 0.05$); in particular, GreenIuronic® induces the main effect on cell viability (about 50%, $p < 0.05$) compared to sodium hyaluronate reducing ROS production (about 38% $p < 0.05$), as reported in Figure 44B. Furthermore, as reported in Figure 44C, GreenIuronic® induces an improvement in cell proliferation compared to control ($p < 0.05$), and compared to sodium hyaluronate, by about 60%, indicating that GreenIuronic® is able to stimulate the proliferative activity of chondrocytes. Since the importance of the activity on cell proliferation includes the ability to modulate joint production of HA in cells, the HA quantification in chondrocytes (Figure 44D) revealed that a large amount of HA present in GreenIuronic® and sodium hyaluronate was captured by chondrocytes after intestinal passage compared to the control ($p < 0.05$). In particular, approximately 75% of HA was induced by GreenIuronic® compared to sodium hyaluronate ($p < 0.05$) in chondrocytes, confirming that HMWHA is better utilized by chondrocytes.
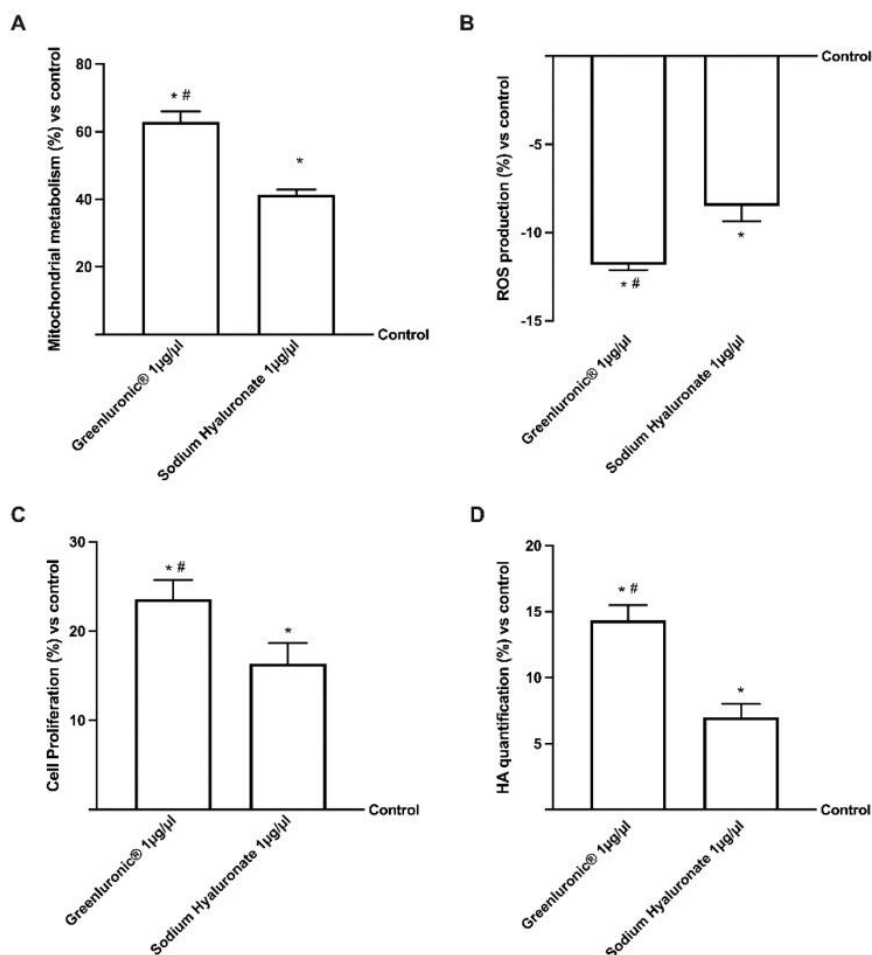


Figure 44. Analysis of GreenIuronic® and Sodium Hyaluronate on human chondrocyte (T/C-28a2) cells functions. In (A) the mitochondrial metabolism tested by MTT test; in (B) the ROS production; in (C) the proliferation analysis by crystal violet assay; and in (D) the HA quantification by ELISA kit. Data are expressed as mean ± SD compared to control (0% line) of five independent experiments performed in triplicates. * $p < 0.05$ vs. control; # $p < 0.05$ vs. Sodium Hyaluronate 1 µg/µL.

**7.2.5. Effects of HA Crossed Intestinal Barrier on Chondrocytes under OA Condition**

From the data obtained under physiological conditions, it can be assumed that GreenIuronic® is also effective after oral administration and is an important starting point for determining the success of therapy in joint damage, such as OA. Oxidative stress and inflammation are known to be involved in cartilage degeneration of OA and it is similarly approved that the degree of anti-inflammatory, immunomodulatory, analgesic, and anti-OA effects of HA is determined by MW and route of administration. Based on these results, in the last phase, the *in vitro* study was conducted by analyzing the effects of both 1 µg/µL of GreenIuronic® and sodium hyaluronate on T/C-28a2 cells pretreated with 10 µg/mL of lipopolysaccharide (LPS) for 24 h in order to simulate the condition of OA. The effects of chondrocyte metabolism were shown in Figure 45 where the beneficial effects of GreenIuronic® can be observed. Specifically, chondrocytes treated only with 10 µg/mL of LPS significantly reduced cell viability (panel 45A, about 10%) and improved ROS production (panel 6B about 23%) compared to control ($p < 0.05$) but this effect was significantly reduced by the presence of both agents. In particular, GreenIuronic® was able to counteract these negative effects caused by LPS alone ($p < 0.05$) better than sodium hyaluronate (about 47% on cell viability and two times on ROS production, respectively, $p < 0.05$). These data were also confirmed by nuclear factor kappa B (NFkB) analysis (Figure 45C) in which the beneficial potential of GreenIuronic® against inflammation, a key point in the mechanisms involved during OA processes, was observed. Indeed, the cells treated with only 10 µg/mL of LPS increased inflammatory processes compared to control (about 18%, $p < 0.05$) assuming the beginning of chronic processes leading to cell death, and this situation was reversed following stimulation with both HA agents. In particular, 1 µg/µL GreenIuronic® was able to reduce the negative effect produced by LPS (about 1.25 times more) better than sodium hyaluronate (about 50%, $p < 0.05$). This recovery mechanism was confirmed also by proliferation assay (panel 45D) in which T/C-28a2 cells lost their proliferative properties when treated only with 10 µg/mL of LPS ($p < 0.05$ compared to control). On the contrary, both 1 µg/µL GreenIuronic® and sodium hyaluronate counteract this negative effect compared to control ($p < 0.05$), but GreenIuronic® was able to restore the damage by about 62% compared to sodium hyaluronate ($p < 0.05$), supporting its use during OA injuries. Finally, this recovery mechanism was also confirmed by the analysis of HA, which showed that under OA conditions, GreenIuronic® is able to improve a much higher amount of HA released in stressed chondrocytes than sodium hyaluronate at the same concentration, approximately by about 21% ($p < 0.05$).
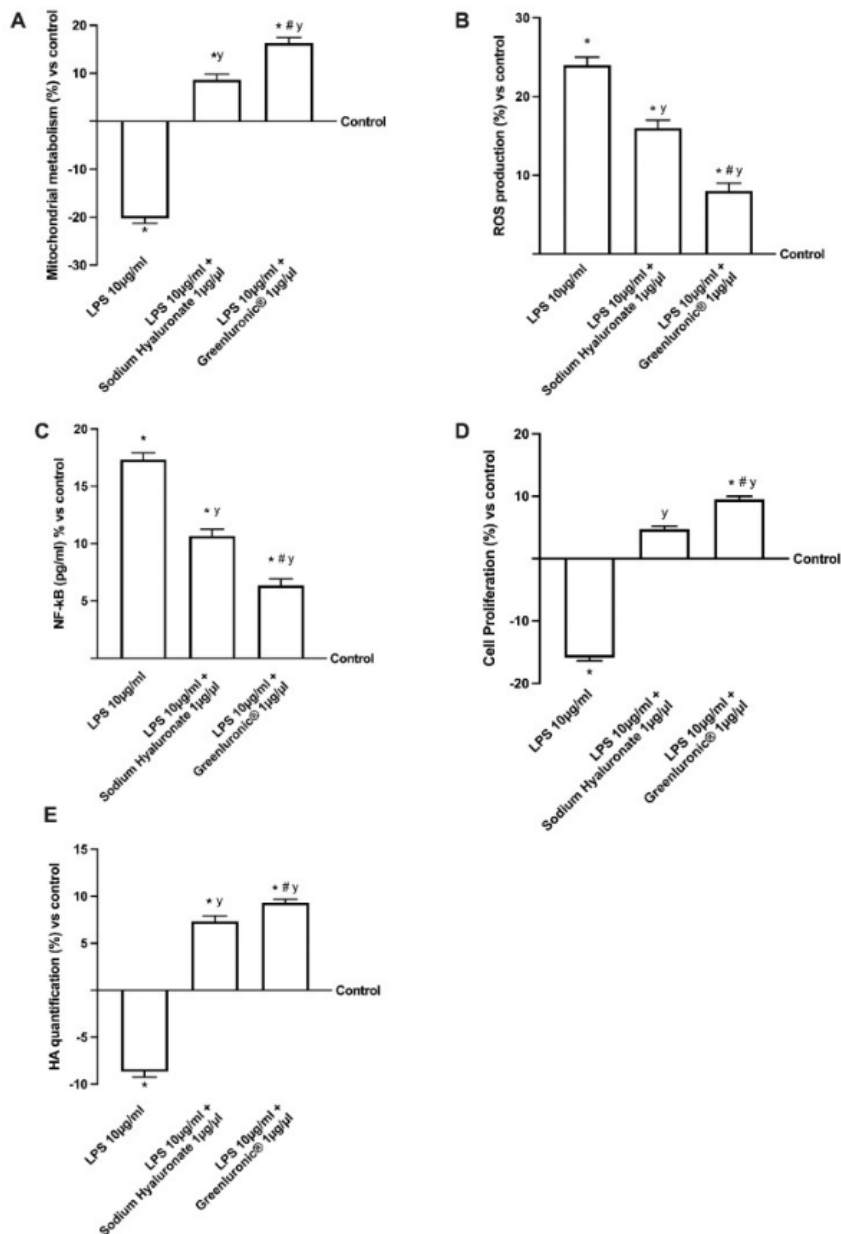
Figure 45. GreenIuronic® and Sodium Hyaluronate effects on T/C-28a2 cells during OA conditions. In (A) mitochondrial metabolism tested by MTT test; in (B) ROS production; in (C) NFkB analysis by ELISA test; in (D) proliferation analysis by crystal violet; and in (E) HA quantification by ELISA kit. Data are mean ± SD of five independent experiments performed in triplicates expressed as a percentage compared to control (0% line). * $p < 0.05$ vs. control; y $p < 0.05$ vs. 10 µg/mL of LPS; # $p < 0.05$ vs. Sodium Hyaluronate 1 µg/µL.

In order to demonstrate that LPS is able to reproduce the OA condition *in vitro* leading to chondrocyte death, additional experiments were carried out to explore the involvement of the apoptosis process. As reported in Figure 46, several markers related to apoptotic processes were evaluated in response to 10 µg/mL of LPS and to both 1 µg/mL GreenIuronic® and sodium hyaluronate. In particular, the stimulation with 10 µg/mL of LPS treatment on T/C-28a2 cells enhanced BAX and Caspase 9 activities (Figure 46A,B), about 22% and 18% compared to control (p < 0.05), indicating a dramatic improvement of the apoptosis process supporting the chondrocyte death during OA. Contemporary, the stimulation with both 1 µg/µL GreenIuronic® and sodium hyaluronate added after 10 µg/mL of LPS caused a

125

statistically significant reduction in both these markers. In particular, GreenIuronic® exerted the main effects compared to sodium hyaluronate on Bax (about 2 times less, $p < 0.05$) and Caspase-9 activities (about 1.5 times less, $p < 0.05$), suggesting that GreenIuronic® contributes to cell protection. These data were also confirmed by the activation of risk pathways such as mitogen-activated protein kinases/extracellular signal-regulated kinase (ERK/MAPK) activity (Figure 46C), which demonstrated that GreenIuronic® reverts the 10 µg/mL LPS damage, activating the survival pathways and restoring the chondrocyte to normal conditions (about 25% compared to sodium hyaluronate, $p < 0.05$).
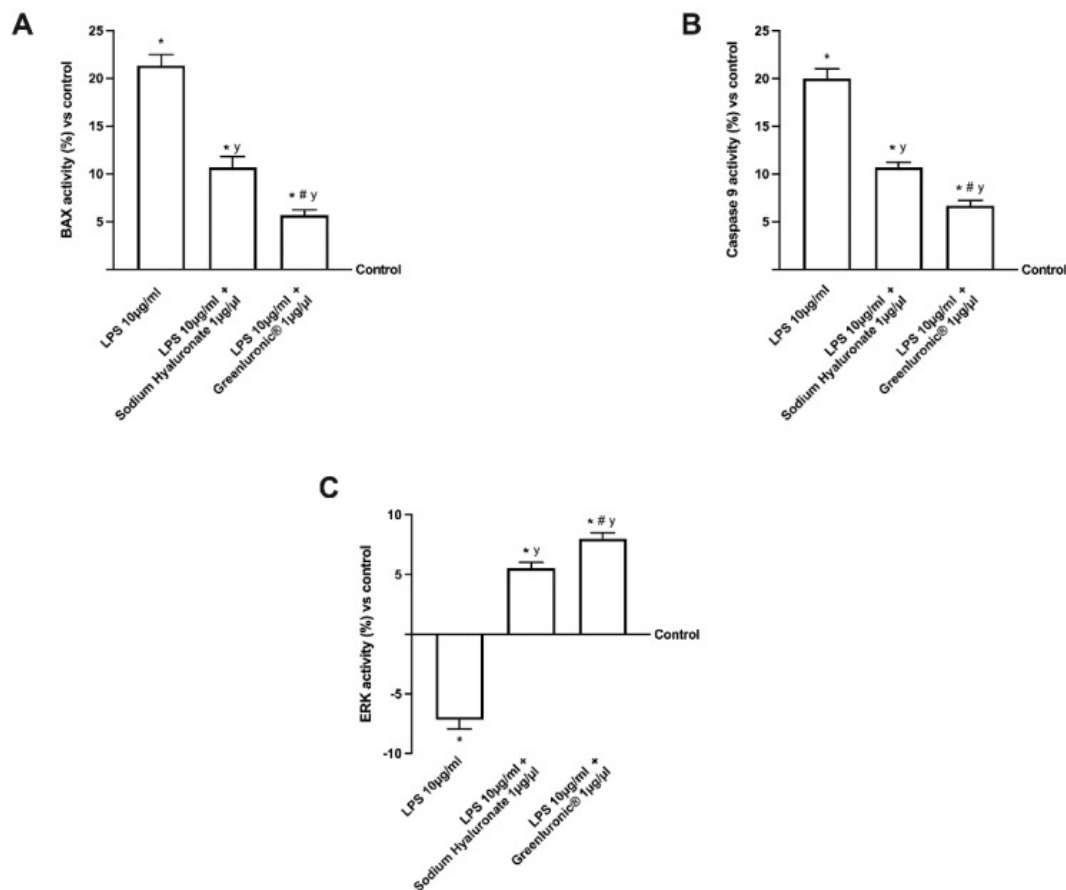


Figure 46. Analysis of the main intracellular pathways activated in T/C-28a2 cells during AO conditions. The results demonstrated a reduction in apoptotic pathways and an improvement of the survival pathways supporting the ability of HA to restore the OA damage. In (A) BAX activity; in (B) Caspase 9 activity; in (C) ERK/MAPK activity; all these results are obtained from specifically ELISA kit. Data are mean ± SD of five independent experiments performed in triplicates compared to the control value (0% line). * $p < 0.05$ vs. control; y $p < 0.05$ vs. 10 µg/mL of LPS; # $p < 0.05$ vs. Sodium Hyaluronate 1 µg/µL.

Finally, to explore the possible effector molecules responsible for the maintenance of chondrocyte wellbeing, the activity of cyclin D1, osteoprotegerin (OPG), and CD44 were investigated. As reported in Figure 47A–D, 10 µg/mL of LPS confirmed its negative effect on T/C-28a2 cells compared to control ($p < 0.05$) downregulating OPG activity, CD44 and cyclin D1 expressions (about 18%, 8%, and 12% compared to control, respectively) modifying negatively chondrocytes activity. Conversely, both 1 µg/µL GreenIuronic® and sodium hyaluronate were able to reduce the damage induced by 10 µg/mL of LPS ($p < 0.05$), confirming the positive role of HA contained in two agents in stimulating chondrocyte metabolism. In particular, 1 µg/mL GreenIuronic® appears to be able to induce main effects compared to sodium hyaluronate ($p < 0.05$) to counteract the negative effects of OA induction. Indeed, 1 µg/mL

GreenIuronic® is able to restore the damage induced by 10 µg/mL of LPS in all parameters tested (about 60% for OPG, one time more for CD44, and 57% for cyclin D1 expression, $p < 0.05$), suggesting that it could ameliorate chondrocyte pathological conditions by activating them through the markers responsible for articular joint homeostasis.
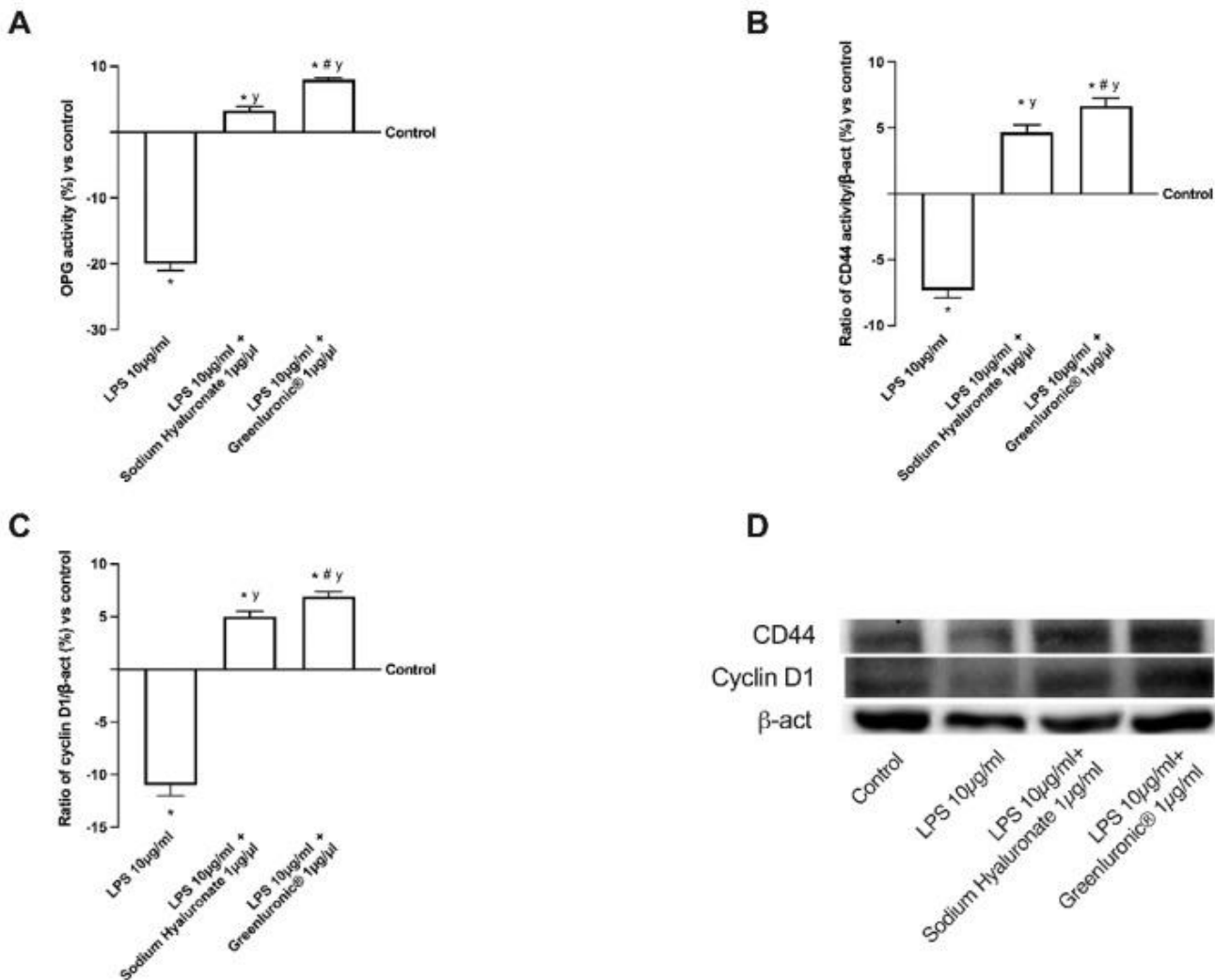


Figure 47. Western-blot and densitometric analysis of the main intracellular pathways activated in T/C-28a2 cells during AO conditions. In (A) OPG activity measured by ELISA test, in (B) the CD44, and in (C) cyclin D1 densitometric analysis of the specific Western blot, which is reported as an example in (D). Data are mean ± SD of five independent experiments performed in triplicates compared to control value (0% line). * $p < 0.05$ vs. control; y $p < 0.05$ vs. 10 µg/mL of LPS; # $p < 0.05$ vs. Sodium Hyaluronate 1 µg/µL.

# 8) CONCLUSIONS AND FUTURE PROSPECTIVES

Every person – in every country in the world – should have the opportunity to live a long and healthy life. However, as is well known, environments and lifestyles can promote health or be detrimental to it [254]. The environments in which we live can greatly influence behavior, exposure to health risks during life, access to services (for example, health and social care) and all changes related to aging [254]. Hence, the concept of an aging population is a relatively new problem from the historical point of view [255]. Since ancient times, aging has been described in many different ways by philosophers and scientists. The age-old question whether old age is itself a disease has been tackled, starting from the Roman playwright Terence, who argued "*senectus ipsa est morbus*" (old age itself is a disease) and from Cicero who some decades later will argue in De Senectute : "*pugnandum, tamquam contra morbum sic contra senecutem*" (one must fight against aging, as one does against a disease).These quotations summarize a long-held view of aging and old age addressed by several scholars [31]. Due to this popular belief, in the past decades, aging has emerged as the strongest and most well-established risk factor for human disease development and major causes of death and disability [256]. Notwithstanding, with the birth of modern medicine in the nineteenth century, this old tenet has been somehow overcome by understanding what causes aging and finding remedies, solutions, and challenges for age-related diseases. Indeed, for many years the explanation was that aging *per se* is a physiological condition which favors the onset of many diseases. However, their relationship is likely much more complex. A major reason is that they share the basic mechanisms [257], identified as "seven pillars" which include adaptation to stress, loss of proteostasis, stem cell exhaustion, metabolism derangement, macromolecular damage, epigenetic modifications, and inflammation [258]. All these factors lead to consider as the primary feature of aging the accumulation of cellular senescence induced by harmful stimuli from inside and outside the cell [259]. Cellular senescence affects the body in two ways: firstly, excessive accumulation of senescent cells inevitably affects tissue regeneration; secondly, senescent cells secrete a large number of inflammatory factors and present with the senescence-associated secretory phenotype (SASP), which has negative effects on the surrounding environment [260]. The cellular impaired microenvironment contributes to age-related conditions [261]. Following this idea, the difference between aging and diseases would rely on the rate/speed and intensity of aging cellular and molecular processes, combined with specific organ/ systems genetic and lifestyle/habit predisposition. Thus, in the long run, all the functional domains undergo a physiological decline that eventually can lead to overt clinical diseases favored by organ/system-specific genetic and environmental factors [262]. Furthermore, this progressive path generates a continuum between the healthy juvenile status and the impaired, unhealthy elderly one; therefore, since the desire for healthy aging without suffering is a desire shared by all modern civilization, modern medicine has been highly concentrated on finding many strategies for ameliorating age-related diseases, undergoing a gradual shift in its underlying concept, from "sick care" to "health care" [263]. Indeed, only recently have scientists extensively expounded the biology of aging, bringing into focus the evolutionarily conserved mechanisms of aging available to control the functional declines and onset of diseases linked to aging processes.
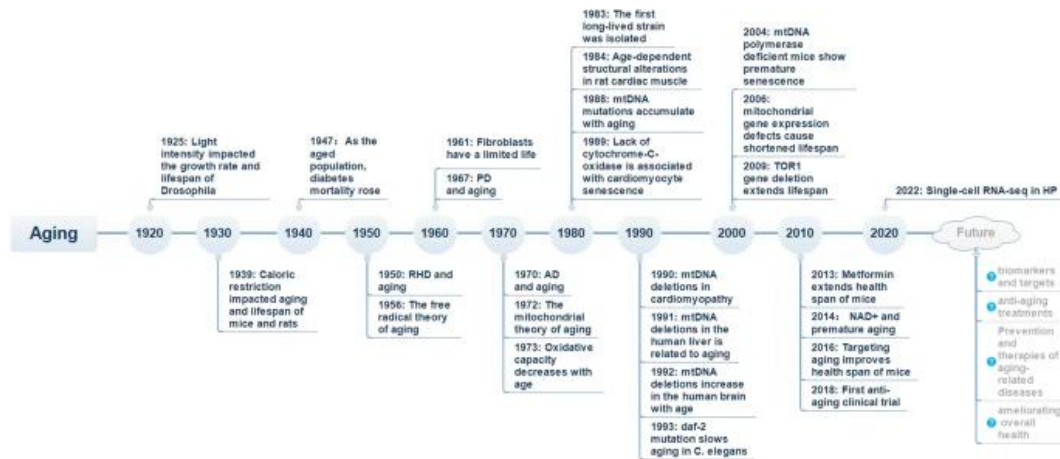
Figure 48. Timeline of research on aging and aging-related diseases. From "*Aging and aging-related diseases: from molecular mechanisms to interventions and treatments*" [264]

Although aging is not a disease *per se*, it is a significant shared risk driver for every major cause of death, disease, and disability compared to sedentary lifestyle activities and obesity [265]. Because as an individual gets old, the physiological functions decline, contributing to when and how one gets sick and passes on, causes a significant burden on social and economic stability [266]. Based on the study of the Global Burden of Disease in 2017(GBD 2017), 92 of 293 (31.4%) diseases were determined to be age-related, and the most common aging-related diseases included neurodegenerative diseases, cancer, cardiovascular diseases, and metabolic diseases [262]. Despite this apparent connection, in earlier years, aging was thought to be unmodifiable, but subsequent discoveries point to a change in thinking and suggest that there is a chance to promote longevity and reduce the occurrence of age-related health conditions. Indeed, today scientists have recognized the impact of slowing aging processes, causing aging biology and age-related health conditions to receive the needed attention across all bio and medical research fields [264; 262]. Furthermore, current research focused on understanding the aging process which facilitates the identification of therapeutic targets for age-related diseases and the development of pharmacological agents suitable for approved clinical use in the future [267]. Interestingly, evidence indicates that pharmacological interventions can affect the aging process and its hallmarks, raising the possibility of slowing aging and promoting healthy aging [268]. For example, strategies for counteracting mechanisms of ageing to prevent disease, known as 'geroprotection', are far reaching, and currently include recommendations for exercise, diet, and other aspects of lifestyle. Some of them are reported in the table below.

Figure table:

| | DNA damage | Eroded telomeres | Epigenetic changes | Impaired proteostasis* | Mitochondrial dysfunction | Altered nutrient sensing | Stem cell dysfunction | Cellular senescence | Impaired intercellular communication |
|---|---|---|---|---|---|---|---|---|---|
| Rapamycin | | | | ●● | ● | ●● | ● | ● | ● |
| Senolytics | | | | | | | | ● | ● |
| Metformin | | | | | | ● | | ● | ● |
| Acarbose | | | ● | | | ● | | | |
| Spermidine | | | ● | ●● | ●● | | ● | | ●● |
| NAD⁺ enhancers | | | | | | | | ● | |
| NSAIDs | | | | | | ● | | | ● |
| Lithium | | ● | | ● | ● | | | | |
| Reverse transcriptase inhibitors | ● | | | | | | | | |
| Systemic circulating factors | | | ●● | | | | ●● | | ●● |
| Glucosamine | | | | ● | ● | ● | | | |
| Glycine | | | | | | ● | | ● | |
| 17α-oestradiol | | | | | | ● | | ● | |

● Compound inhibits the hallmark   ● Role in ageing phenotype or lifespan shown experimentally

Figure 49. Drugs and their influence on different hallmarks of ageing. From *"The quest to slow ageing through drug discovery"* [268]

However, these alone are not sufficient to prevent the ills of old age, and increasing efforts are directed to tackling the underlying processes of ageing [269]. Today, scientists have recognized the impact of alternative remedies in slowing aging processes, in order to modulat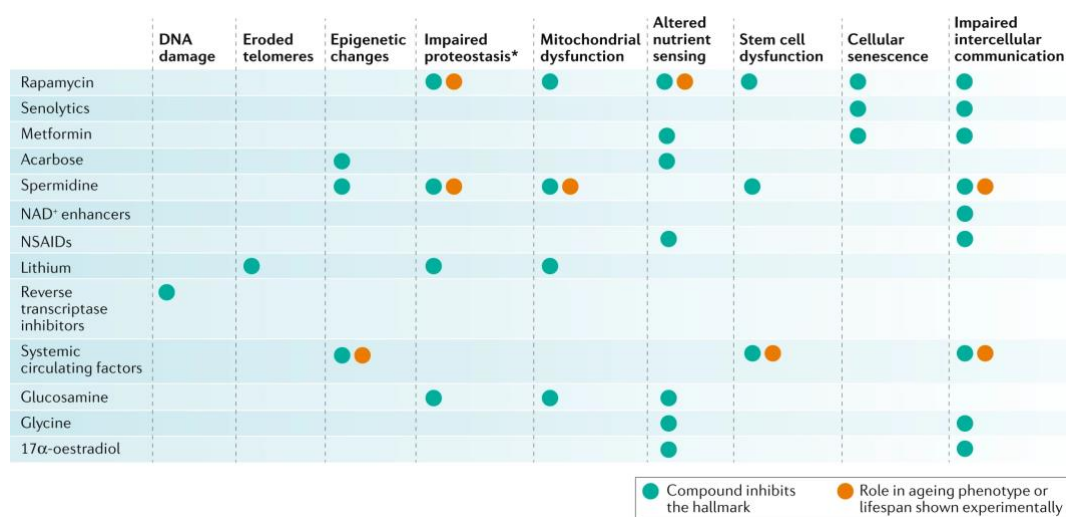e aging biology and age-related health conditions. One of the major challenges explored for health improvement during aging is the nutritional interventions, which may be viewed as a viable approach [270]. Since ancient times, the medicinal properties of plants are always believed for its therapeutic effect and treating many diseases, until a time where a shift was observed towards commercial drugs. However, a change has begun where phytomedicine is gaining its popularity once again [271]. This change is due to its effectiveness, both in terms of treatment and cost. Phytomedicines, which are also called herbal drugs/medicine, basically consist of the use of plant or its part which are found to have medicinal properties and can be used in the treatment of various diseases as well as improvement in overall health [270]. The role of phytomedicine in aging is very crucial as it possesses important bioactive compounds and constituents (such as polyphenols, flavonoids, phenolic acids, and others) which are considered to provide anti-aging properties as well as helps in reducing age-associated problems. The phytomedicines provide a wide range of health benefits such as antioxidant and anti-inflammatory activity, anticolesterolemic properties, antimicrobial, hepatoprotective activity, analgesic etc. Moreover, some natural leaves are used as phytotherapeutics and have proven to help in minimizing the complications of the elderly [272]. Indeed, the scientific community extensively uses small-molecule, natural products, and dietary interventions to discover evolutionarily conserved mechanisms of aging. Moreover, they are known to modulate mitochondrial function, senescence, and nutrient-sensing metabolic signals to improve cellular aging and age-related diseases, notably metabolic diseases, cardiovascular diseases, neurodegenerative diseases, and degenerative joint disorders [31]. Furthermore, this scientific evidence defined the possible use of the naturally derived active ingredients in pharmaceutical formulations, named dietary supplements, with the aim of improving the processes of aging. Indeed, dietary supplements and natural products, consisting of various products and ingredients from herbal, marine, and botanical sources, continue to receive remarkable patronage from consumers worldwide [273]. Dietary supplements and natural products have a fascinating history concerning their health benefits in human life and diseases before the birth of western drugs. To ensure health safety in the

population, several countries' Food and Drugs Administrations (FDA) and international health institutions have issued numerous guidelines on dietary supplements and natural product medical applications [274]. Although most regulatory authorities prohibit dietary supplements and natural products from diagnosing, mitigating, treating, curing, or preventing human diseases, a greater pool of FDA-approved drugs is optimized from natural products [275]. Therefore, in the context of aging research, several natural products and dietary supplements continue to be studied extensively for their anti-aging properties or are used as research tools to explore and discover molecular mechanisms underpinning biological aging [17].

With these premises this research, in its various phases, demonstrates the important role of some nutraceuticals during aging, showing promising results in various fields of diseases related to aging. Actually, during the development of this project, the possibility of using a plant-derived compound or growth factor therapy, with therapeutic value to bind multiple molecular targets with a beneficial pharmacological effect on healthy aging, was demonstrated. Indeed, as regards of aging-neurodegenerative disease, this thesis demonstrated that BDNF treatment could modulate neurons neuroplasticity, promoting the health of nervous tissue, and also the ability to counteract the effects of pro-inflammatory cytokines and oxidative damage, which are the mechanisms underlying age-related neurodegeneration. Moreover, both in *in vitro* and in *in vivo* models, the study of the intracellular pathways demonstrated a significant increase in the expression of ApoE, which is a member of the low-density lipoprotein receptor gene family, mainly produced by the astrocytes in the brain. ApoE has been identified as the receptor that mediates amyloid β (Aβ) uptake and clearance by astrocytes, thus increasing glial LDLR levels, which may promote Aβ degradation within the brain; these data indicate a positive effect on brain trophism exerted by BDNF SKA and an increase in SIRT1 phosphorylation, confirming a potential role in counteracting the known mechanisms that lead to brain aging. Indeed, SIRT1 has recently been shown to play a role in normal cognitive function and synaptic plasticity, counteracting not only cognitive decline and neurodegenerative disease but also mediating chronic pain, associated with peripheral nerve injury, in aging. However, because of the difficulties associated with the administration of exogenous proteins into the central nervous system, it is important to consider the possibility of stimulating endogenous sources of BDNF. In this context, recent research has emphasized the role of PEA as it has a neuroprotective effect, acting on several BDNF targets in the central and peripheral nervous system; it is able to improve its effects by cooperating with antioxidant molecules such as *Equisetum arvense L.*, which has attracted particular attention since it is a rich source of phenolic compounds, flavonoids, and phenolic acids. All these molecules play an important role not only in central nervous system but also in the peripheral nervous system, thanks to the oxidative stress response mechanism and the activation of SIRT1. Indeed, recent scientific evidence revealed that SIRT1 agonists can relieve chronic pain through regulating inflammation, oxidative stress, synaptic plasticity, and mitochondrial dysfunction; thus, another novelty of this research path is the observation about cooperative mechanism of a combination of nutraceuticals with anti-inflammatory and antioxidant properties able to modulate SIRT1 activity. Therefore, the second research field of this thesis aimed to contribute, in an experimental *in vitro* model, to identify a powerful food supplement for patients suffering from peripheral nerve injury and sensitization. For this purpose, 0.2µM PEA 80 mesh and 50µg/ml *Equisetum Arvense* (titrated 10% silica), alone and combined in a new food supplement called EquiPEA™, were used to evaluate the

ability to modulate the main mechanisms underlying nerve fiber damage and, consequently, pain involving the endocannabinoid system. Indeed, CB receptors act on GABAergic neurons by entering the physiological mechanism of pain regulation. According to that, results revealed that EquiPEA™ acts on the GABAergic system through the CB1 receptor. Furthermore, several studies affirmed that CB receptors on GABAergic neurons might also be needed for modulation of the nervous recovery mechanism located on Schwann cells, which detect nerve injury and provide the first response, playing a critical role in the development and maintenance of neuropathic pain. Furthermore, mimicking *in vitro* the neuropathy condition, in particular about inflammation and oxidative stress leading to the imbalance of ion transport, data revealed that the combination of PEA withEquisetum arvense L.seems to be able to repair the damage on myelin sheath that protects the axon and simultaneously able to act on NGF release and on bind p75 neurotrophin receptor reproducing the mechanism of analgesic effect observed in human. Indeed, as reported above an increase on NGF level in various inflammatory conditions may be considered an important hallmark of the human chronic pain condition. It should be emphasized that the results obtained in the first two field demonstrated that treating both acute and persistent pain during aging represents a complex task due to high prevalence of chronic co-morbidities, organ failures and age-related declining conditions; therefore, the therapeutic potential of natural remedies may be applied to other aging diseases, such as metabolic disorders and musculoskeletal diseases, which are also related to neuropathic pain. Based on this, the nutraceuticals treatment should begin before any chronic diseases appear, and it should delay the onset of the first age-related chronic disease. Therefore, because the goal of a nutraceuticals is to increase health span, as part three of this thesis, the possibility of controlling the changes in cholesterol metabolism, which are at the basis of metabolic syndrome and cardiovascular diseases, was investigated using plant-extracted active ingredients. Indeed, the anti-cholesterol activity of Esterol10® revealed that it proved to be more effective than conventional therapies in promoting the lowering of cholesterol in hepatocytes, through a reduction in the synthesis of cholesterol and its conversion into bile acids through the choleretic process which is a complex biochemical process that leads to the production of bile, an iso-osmotic electrolyte solution that forms in the liver as a product of its secretory function. Taken together, these results demonstrated that Esterol10® significantly improves hepatic metabolism by regulating the synthesis of cholesterol through the improvement of HMGCoA reductase and the reduction of its receptor expression. In this context, liver function is determined by the synthesis of total cholesterol while improving the production of bile acid and free cholesterol, as determined by tests for total cholesterol, free cholesterol, and bile acids. In fact, experimental results confirmed better anti-cholesterol efficacy when combined in a single blend, compared to RYR alone or Atorvastatin, suggesting the potential use of this formulation to supplement or replace statins. Anti-cholesterol therapies based on new and safer plant extracts and their mixtures are necessary to assist or replace statins. Although our results from *in vitro* experiments cannot be directly extrapolated to the antilipidemic and anti-cholesterolemic clinical effects, they must be confirmed in a more complex system, such as an *in vivo* model. At the same time, this study confirmed the molecular mechanism activated by Esterol10® including AMPK, which has a direct impact on glucose and lipid metabolism. Furthermore, the analysis showed that the formulation modulates SREBP, HMGCR, LDLr, and all other enzymes involved in cholesterol biosynthesis. Although it well known the positive effects on cardiovascular events mediated by statin therapy, adverse effects that include statin associated muscle

symptoms are commonly reported. This frequent condition in humans revealed a range from mild-to-moderate muscle pain, weakness, or fatigue to potentially life-threatening rhabdomyolysis, which is reported by 10% to 25% of patients receiving statin therapy. Therefore, multiple lines of research explored topics directly related to nutrients that further refined information on evidence-based nutrition recommendations to support skeletal muscle health. The supplements commonly used for the maintenance of skeletal muscle health are usually made up of proteins and amino acids (e.g., leucine, creatinine, and carnitine), associated with vitamins (e.g., vitamin D or vitamin C) or minerals (e.g., magnesium. or potassium), essential for many metabolic processes. Therefore, results obtained from field four of this thesis show that the combination of specific nutrients exerts a positive effect on myoblasts through the activation of intracellular mechanisms capable of stabilizing the beneficial effects of the individual agents on mitochondrial health. In particular, this effect was observed by the cell viability analysis which can rule out any cytotoxic effect or mitochondrial imbalance in the absence of limited respiration, which otherwise leads to a concomitant high rate of cell apoptosis. In addition, the results support the hypothesis that MKVC can promote physiological differentiation on C2C12 cells as demonstrated by the analysis of cyclin D1, which is abundant in proliferating myoblasts, and confirmed by the analysis of desmin. Furthermore, MKVC shows a significant impact on mitochondrial activity and on its membrane potential because it is capable of increasing ATP production and oxygen consumption. One of the main areas of interest driving research towards the development of new supplements for the muscle is their possible role in controlling muscle cramps, typical sudden, involuntary, painful, and palpable muscle contractions that last from seconds to minutes. For this reason, muscle contraction-relaxation cycle was further investigated, confirming the importance of this mechanism in the genesis of cramps, indicating that MKVC better modulates a state of hypercontraction, restoring ion fluxes to more physiological values and remodeling the contractile phase with less cell fatigue in an *in vitro* model. Another important element in the balance between contraction and relaxation is the maintenance of a physiological value of inflammatory cytokines. MKVC can maintain the level of TNF-$\alpha$ indicating that it could have a great effect in hypercontractility conditions. Furthermore, the results of this work showed that MKVC induces less intracellular accumulation of lactate, resulting in increased glucose consumption to support aerobic activity in C2C12 cells. These data suggest that glucose concentration and glycogen accumulation are consumed under physiological conditions after MKVC stimulation.

Furthermore, for the purposes of this thesis, it was deemed necessary considering that decrease in muscle mass and strength negatively affects bone mass leading to osteoporosis, which is linked and commonly associated with aging. Indeed, the changes in bone aging that lead to osteoporosis depend on several causes, including hormonal alterations, skeletal unloading, and accumulation of senescent cells. Typically, the maintenance of bone homeostasis requires a balance of activity from osteoblasts and osteoclasts. Moreover, osteoporosis results from decreased bone formation and increased bone resorption due to osteoblasts and osteoclasts. Currently, several treatments for bone mass loss are approved by the FDA, but most of them are associated with serious adverse effects. For that, alternative options are most required, and recent studies have proposed improving osteoblast differentiation for osteoporosis prevention and treatment. On the other hand, several natural extracts that are safe and inexpensive have demonstrated some positive effects on bone-related diseases. In this context, a new food supplement based on *Artemisa annua*, *Boswellia serrata* and *Equisetum arvense* has been investigated

to improve osteoblast activities by modulating alkaline phosphatase (ALP) and mineralized nodules in an *in vitro* co-culture of osteoblast/osteoclast. The main results revealed for the first time that the protein levels of osteoclastic markers were significantly decreased. At the same time, the balance between osteoprotegerin (OPG)/RANKL was maintained by osteoblast OPG production, which inhibits osteoclast formation by inducing osteoblast functions. Moreover, since these extracts will be used as human food supplements, an *in vitro* 3D intestinal model analysis was carried out to mimic the oral human intake. Additionally, *in vivo* experiments demonstrated that the combination of *Artemisa annua*, *Boswellia serrata* and *Equisetum arvense* significantly promoted bone formation in aged-induced osteoporotic mouse model. Particularly significant was the increase in the osteoblast-related parameters and bone histomorphometry parameters. Collectively, these results demonstrated for the first time that this new formulation can promote osteoblastic differentiation via the activation of the conventional pathways and promote bone formation. Finally, another decline condition related to the musculoskeletal aging process that greatly impacts older people's quality of life is osteoarthritis (OA). This common and debilitating joint disorder contributes to joint pain and functional impairment. For this reason, the application of nutraceuticals in the field 5, osteoarticular disorders and osteoarthritis, has also been investigated. Therefore, the possibility of using plant-derived HA in a dietary supplement to be taken orally sparked interest in designing a new nutraceutical (called GreenIuronic®) able to counteract the harmful consequences of OA. Based on the results obtained, the presence of a high molecular weight ingredient related to HA supports its use to counteract the adverse effects of OA, since high molecular weight HA is nowadays the best treatment option for knee OA by intra-articular injection. Consequently, the effects of GreenIuronic® obtained from 3D model that mimics intestinal absorption clearly demonstrated that HA is effectively absorbed and biodistributed to the chondrocytes and exerts its biological functions in those tissues. In addition, GreenIuronic® treatment indicated that a substantial part of HA is absorbed without damaging the intestinal epithelium; this is a crucial point since HA has a role in decreasing the permeability by enhancing tight junction proteins. In epithelial cells, the formation of tight junctions plays an important role in the intestinal barrier, and this is mediated by proteins such as claudins, occludin, and ZO-1 that are necessary for epithelial barrier activity. Furthermore, the second important purpose of this work was to test the ability of GreenIuronic® to stimulate chondrocyte biological activity under physiological and pathological conditions. As expected, GreenIuronic® was able to stimulate cell viability and induce chondrocyte proliferation without causing adverse effects, also compared to conventional HA supplementation Indeed, thanks to the presence of HMWHA, the beneficial effects of GreenIuronic® on the activity of chondrocytes support the hypothesis of its use in inflammatory joint conditions. Since OA is a disease of the whole joint and a multifactorial entity, there are various therapeutic strategies that involve numerous fields of medicine: rheumatology, orthopedics, geriatrics, psychiatry, general practitioners, and physiotherapists. The goal of OA therapy is to reduce pain and increase patients' quality of life. In this context, HA has shown not only beneficial effects on articular cartilage trophism, but also antinociceptive effects with a significant reduction in pain in particular and the beneficial effects of GreenIuronic® have also been confirmed by the quantity of HA, contained in this new formulation, which reached the target site and was absorbed into the joint without damaging it. All these findings were confirmed also during OA condition in which GreenIuronic® binds CD44 on chondrocytes to exert its biological activities, demonstrating that the association of HA with CD44 increased the HA

absorption/production suppressing proinflammatory processes, suppressing the expression of the apoptosis process regulating cartilage production, improving OPG activity, and proliferation process, modulating cyclin D1 expression.

The complex scenario emerged thanks to results obtained during the PhD program confirmed the relationship between dietary supplement and chronic age-related diseases, which deserve and stimulate two different, even if complementary, types of conclusions: the former refers to the fact that major age-related diseases have a common molecular pathways, while the latter faces the possibility of implementing new therapeutic approaches using naturally derived active ingredients to solve and/or improve the implications and problems encountered during age-related diseases here presented. Based on the results obtained, evidently, regulatory hallmark strategies that explain the connection between aging and physiological events and lifestyle have offered a gateway for potential drug development. Herbs/botanicals, phytotherapy elements and active principle-derived natural compounds, minerals, and other dietary supplements, which have been demonstrated to have anti-aging properties and are used as a start-off for discovering potent anti-aging drugs [17]. However, we cannot be sure in which way these natural products and dietary supplements modulate the mechanisms of aging to reflect the treatment effectiveness of healthy aging in outbred populations of heterogeneous environments. Moreover, insufficient knowledge and understanding of clinical research and lack of funding on the side of dietary and natural product scientists also hinder the proper implementation of alternative approach. Also, institutional ethical and review boards mostly have regulatory systems that favor researchers on synthetic drugs rather than natural supplements, whose constituents are not well-defined and characterized. Indeed, more in-depth studies are needed to confirm the role of naturally derived active ingredients in modulating the mechanisms of ageing. To date, human clinical trials centered on uncovering the medical potential of natural products and dietary supplements on the health of the elderly population present both challenges and opportunities to increase demand for primary health care and long-term care ageing. Nevertheless, the main problem which may be countered is the delivery of the molecule to the affected cells; although numerous studies have explored the possibility of administering natural products attempting to orally administration, data obtained have so far yielded poor results due to the fact that nutraceuticals couldn't cross through the intestinal barrier or BBB through due to their poor bioavailability. Therefore, as found in the projects, the use of engineered solvents, capable of caging the active ingredient and transporting it across biological membranes, could be a viable alternative to the problem of low bioavailability that would be found if the supplement were made available on the market. Thus, it is time for ethical and institutional review boards to consider enacting well-designed interventional studies regulatory requirements that support natural supplement characteristics on human aging and aging-related diseases. In conclusion, the series of research presented in this thesis add new experimental evidence on the possibility of acting on the human aging process and on the degeneration of some tissues that lead to aging-related diseases using natural dietary products. Modern scientific research allows today to reveal the precise cellular and molecular mechanisms of active ingredients used for centuries, in an empirical way, in traditional medicine. This will allow, in the near future, to guide the body, together with the principles of Lifestyle Medicine, on the path of healthy aging allowing individuals to obtain health benefits and live a longer and healthier life, integrated into society.

# 9) REFERENCES

1. De Magalhães JP, Stevens M, Thornton D. The Business of Anti-Aging Science. Trends Biotechnol. 2017;35(11):1062-1073. doi:10.1016/j.tibtech.2017.07.004.

2. Jayantha WM, Qian QK, Yi CO. Applicability of 'Aging in Place'in redeveloped public rental housing estates in Hong Kong. Cities 2018;. 83, 140-151.

3. https://www.istat.it/it/files/2021/11/REPORT-PREVISIONI-DEMOGRAFICHE.pdf

4. Atella V, Piano Mortari A, Kopinska J, et al. Trends in age-related disease burden and healthcare utilization. Aging Cell. 2019;18(1):e12861. doi:10.1111/acel.12861

5. van Beek JH, Kirkwood TB, Bassingthwaighte JB. Understanding the physiology of the ageing individual: computational modelling of changes in metabolism and endurance. Interface Focus. 2016;6(2):20150079. doi:10.1098/rsfs.2015.0079

6. Diwan B, Sharma R. Nutritional components as mitigators of cellular senescence in organismal aging: a comprehensive review. Food Sci Biotechnol. 2022;31(9):1089-1109. Published 2022 Jun 18. doi:10.1007/s10068-022-01114-y

7. Borghesan M, Hoogaars WMH, Varela-Eirin M, Talma N, Demaria M. A Senescence-Centric View of Aging: Implications for Longevity and Disease. Trends Cell Biol. 2020;30(10):777-791. doi:10.1016/j.tcb.2020.07.002

8. Verburgh K. Nutrigerontology: why we need a new scientific discipline to develop diets and guidelines to reduce the risk of aging-related diseases. Aging Cell. 2015;14(1):17-24. doi:10.1111/acel.12284

9. Gholami A, Emadi F, Amini A, Shokripour M, Chashmpoosh M, Omidifar N. Functionalization of Graphene Oxide Nanosheets Can Reduce Their Cytotoxicity to Dental Pulp Stem Cells. Journal of Nanomaterials. 2020; https://doi.org/10.1155/2020/6942707

10. Sohrabi Z, Eftekhari MH, Eskandari MH, Rezaianzadeh A, Sagheb MM. Intradialytic Oral Protein Supplementation and Nutritional and Inflammation Outcomes in Hemodialysis: A Randomized Controlled Trial. Am J Kidney Dis. 2016;68(1):122-130. doi:10.1053/j.ajkd.2016.02.050

11. van der Rijt S, Molenaars M, McIntyre RL, Janssens GE, Houtkooper RH. Integrating the Hallmarks of Aging Throughout the Tree of Life: A Focus on Mitochondrial Dysfunction. Front Cell Dev Biol. 2020;8:594416. Published 2020 Nov 26. doi:10.3389/fcell.2020.594416.

12. Guerville F, De Souto Barreto P, Ader I, et al. Revisiting the Hallmarks of Aging to Identify Markers of Biological Age. J Prev Alzheimers Dis. 2020;7(1):56-64. doi:10.14283/jpad.2019.50

13. Dodig S, Čepelak I, Pavić I. Hallmarks of senescence and aging. Biochem Med (Zagreb). 2019;29(3):030501. doi:10.11613/BM.2019.030501

14. Arnoult N, Karlseder J. Complex interactions between the DNA-damage response and mammalian telomeres. Nat Struct Mol Biol. 2015;22(11):859-866. doi:10.1038/nsmb.3092

15. Zhu Y, Liu X, Ding X, Wang F, Geng X. Telomere and its role in the aging pathways: telomere shortening, cell senescence and mitochondria dysfunction. Biogerontology. 2019;20(1):1-16. doi:10.1007/s10522-018-9769-1

16. Fang EF, Scheibye-Knudsen M, Brace LE, et al. Defective mitophagy in XPA via PARP-1 hyperactivation and NAD(+)/SIRT1 reduction. Cell. 2014;157(4):882-896. doi:10.1016/j.cell.2014.03.026

17. Chen Y, Hamidu S, Yang X, et al. Dietary Supplements and Natural Products: An Update on Their Clinical Effectiveness and Molecular Mechanisms of Action During Accelerated Biological Aging. Front Genet. 2022;13:880421. Published 2022 Apr 28. doi:10.3389/fgene.2022.880421

18. Kane AE, Sinclair DA. Epigenetic changes during aging and their reprogramming potential. Crit Rev Biochem Mol Biol. 2019;54(1):61-83. doi:10.1080/10409238.2019.1570075

19. Yu G, Hyun S. Proteostasis-associated aging: lessons from a Drosophila model. Genes Genomics. 2021;43(1):1-9. doi:10.1007/s13258-020-01012-9

20. Josefson R, Andersson R, Nyström T. How and why do toxic conformers of aberrant proteins accumulate during ageing?. Essays Biochem. 2017;61(3):317-324. Published 2017 Jul 11. doi:10.1042/EBC20160085

21. Gottschling DE, Nyström T. The Upsides and Downsides of Organelle Interconnectivity. Cell. 2017;169(1):24-34. doi:10.1016/j.cell.2017.02.030

22. Andréasson C, Ott M, Büttner S. Mitochondria orchestrate proteostatic and metabolic stress responses. EMBO Rep. 2019;20(10):e47865. doi:10.15252/embr.201947865

23. McHugh D, Gil J. Senescence and aging: Causes, consequences, and therapeutic avenues. J Cell Biol. 2018;217(1):65-77. doi:10.1083/jcb.201708092

24. Hudgins AD, Tazearslan C, Tare A, Zhu Y, Huffman D, Suh Y. Age- and Tissue-Specific Expression of Senescence Biomarkers in Mice. Front Genet. 2018;9:59. Published 2018 Feb 23. doi:10.3389/fgene.2018.00059

25. Ermolaeva M, Neri F, Ori A, Rudolph KL. Cellular and epigenetic drivers of stem cell ageing. Nat Rev Mol Cell Biol. 2018;19(9):594-610. doi:10.1038/s41580-018-0020-3

26. Ferrucci L, Fabbri E. Inflammageing: chronic inflammation in ageing, cardiovascular disease, and frailty. Nat Rev Cardiol. 2018;15(9):505-522. doi:10.1038/s41569-018-0064-2

27. McGuire PJ. Mitochondrial Dysfunction and the Aging Immune System. Biology (Basel). 2019;8(2):26. Published 2019 May 11. doi:10.3390/biology8020026

28. Pinti M, Cevenini E, Nasi M, et al. Circulating mitochondrial DNA increases with age and is a familiar trait: Implications for "inflamm-aging". Eur J Immunol. 2014;44(5):1552-1562. doi:10.1002/eji.201343921

29. Pieren DKJ, Smits NAM, van de Garde MDB, Guichelaar T. Response kinetics reveal novel features of ageing in murine T cells. Sci Rep. 2019;9(1):5587. Published 2019 Apr 3. doi:10.1038/s41598-019-42120-1

30. Desdín-Micó G, Soto-Heredero G, Aranda JF, et al. T cells with dysfunctional mitochondria induce multimorbidity and premature senescence. Science. 2020;368(6497):1371-1376. doi:10.1126/science.aax0860

31. Franceschi C, Garagnani P, Morsiani C, et al. The Continuum of Aging and Age-Related Diseases: Common Mechanisms but Different Rates. Front Med (Lausanne). 2018;5:61. Published 2018 Mar 12. doi:10.3389/fmed.2018.00061

32. Sahiner M, Yilmaz AS, Gungor B, Ayoubi Y, Sahiner N. Therapeutic and Nutraceutical Effects of Polyphenolics from Natural Sources. Molecules. 2022;27(19):6225. Published 2022 Sep 22. doi:10.3390/molecules27196225

33. Gururaja GM, Mundkinajeddu D, Kumar AS, Dethe SM, Allan JJ, Agarwal A. Evaluation of Cholesterol-lowering Activity of Standardized Extract of Mangifera indica in Albino Wistar Rats. Pharmacognosy Res. 2017;9(1):21-26. doi:10.4103/0974-8490.199770

34. Chauhan B, Kumar G, Kalam N, Ansari SH. Current concepts and prospects of herbal nutraceutical: A review. J Adv Pharm Technol Res. 2013;4(1):4-8. doi:10.4103/2231-4040.107494

35. Zeisel SH. Regulation of "nutraceuticals". Science. 1999;285(5435):1853-1855. doi:10.1126/science.285.5435.1853

36. McKee AE, Farrell AT, Pazdur R, Woodcock J. The role of the U.S. Food and Drug Administration review process: clinical trial endpoints in oncology. Oncologist. 2010;15 Suppl 1:13-18. doi:10.1634/theoncologist.2010-S1-13

37. Gilsenan MB. Nutrition & health claims in the European Union: A regulatory overview. Trends in Food Science & Technology, 2011; 22(10), 536-542.

38. Tarumi T, Zhang R. Cerebral blood flow in normal aging adults: cardiovascular determinants, clinical implications, and aerobic fitness. J Neurochem. 2018;144(5):595-608. doi:10.1111/jnc.14234

39. Aarsland D, Creese B, Politis M, et al. Cognitive decline in Parkinson disease. Nat Rev Neurol. 2017;13(4):217-231. doi:10.1038/nrneurol.2017.27

40. Soria Lopez JA, González HM, Léger GC. Alzheimer's disease. Handb Clin Neurol. 2019;167:231-255. doi:10.1016/B978-0-12-804766-8.00013-3

41. Lane CA, Hardy J, Schott JM. Alzheimer's disease. Eur J Neurol. 2018;25(1):59-70. doi:10.1111/ene.13439

42. Blesa J, Trigo-Damas I, Quiroga-Varela A, Jackson-Lewis VR. Oxidative stress and Parkinson's disease. Front Neuroanat. 2015;9:91. Published 2015 Jul 8. doi:10.3389/fnana.2015.00091

43. Hayes MT. Parkinson's Disease and Parkinsonism. Am J Med. 2019;132(7):802-807. doi:10.1016/j.amjmed.2019.03.001

44. Kalia LV, Lang AE. Parkinson's disease. Lancet. 2015;386(9996):896-912. doi:10.1016/S0140-6736(14)61393-3

45. Shelat PB, Chalimoniuk M, Wang JH, et al. Amyloid beta peptide and NMDA induce ROS from NADPH oxidase and AA release from cytosolic phospholipase A2 in cortical neurons. J Neurochem. 2008;106(1):45-55. doi:10.1111/j.1471-4159.2008.05347.

46. Xiang W, Schlachetzki JC, Helling S, et al. Oxidative stress-induced posttranslational modifications of alpha-synuclein: specific modification of alpha-synuclein by 4-hydroxy-2-nonenal increases dopaminergic toxicity. Mol Cell Neurosci. 2013;54:71-83. doi:10.1016/j.mcn.2013.01.004

47. Suárez-Rivero JM, Villanueva-Paz M, de la Cruz-Ojeda P, et al. Mitochondrial Dynamics in Mitochondrial Diseases. Diseases. 2016;5(1):1. Published 2016 Dec 23. doi:10.3390/diseases5010001

48.  Massano J, Bhatia KP. Clinical approach to Parkinson's disease: features, diagnosis, and principles of management. Cold Spring Harb Perspect Med. 2012;2(6):a008870. doi:10.1101/cshperspect.a008870

49.  Kausar S, Wang F, Cui H. The Role of Mitochondria in Reactive Oxygen Species Generation and Its Implications for Neurodegenerative Diseases. Cells. 2018;7(12):274. Published 2018 Dec 17. doi:10.3390/cells7120274

50.  Mattson MP, Arumugam TV. Hallmarks of Brain Aging: Adaptive and Pathological Modification by Metabolic States. Cell Metab. 2018;27(6):1176-1199. doi:10.1016/j.cmet.2018.05.011

51.  Baker DJ, Petersen RC. Cellular senescence in brain aging and neurodegenerative diseases: evidence and perspectives. J Clin Invest. 2018;128(4):1208-1216. doi:10.1172/JCI95145

52.  Brawek B, Skok M, Garaschuk O. Changing Functional Signatures of Microglia along the Axis of Brain Aging. Int J Mol Sci. 2021;22(3):1091. Published 2021 Jan 22. doi:10.3390/ijms22031091

53.  Ativie F, Albayram O, Bach K, Pradier B, Zimmer A, Bilkei-Gorzo A. Enhanced microglial activity in FAAH(-/-) animals. Life Sci. 2015;138:52-56. doi:10.1016/j.lfs.2014.12.016

54.  Uberti F, Morsanuto V, Ruga S, Stoppa I, Galla R, Notte F, Molinari C. Effect of mixed lipoic acid, vitamin D, phosphatidylserine and homotaurine to obtain a new formulation for brain ageing prevention. EC Neurol, 2019; 11, 302-312.

55.  Colucci-D'Amato L, Speranza L, Volpicelli F. Neurotrophic Factor BDNF, Physiological Functions and Therapeutic Potential in Depression, Neurodegeneration and Brain Cancer. Int J Mol Sci. 2020;21(20):7777. Published 2020 Oct 21. doi:10.3390/ijms21207777

56.  Palasz E, Wysocka A, Gasiorowska A, Chalimoniuk M, Niewiadomski W, Niewiadomska G. BDNF as a Promising Therapeutic Agent in Parkinson's Disease. Int J Mol Sci. 2020;21(3):1170. Published 2020 Feb 10. doi:10.3390/ijms21031170

57.  Wang ZH, Xiang J, Liu X, et al. Deficiency in BDNF/TrkB Neurotrophic Activity Stimulates δ-Secretase by Upregulating C/EBPβ in Alzheimer's Disease. Cell Rep. 2019;28(3):655-669.e5. doi:10.1016/j.celrep.2019.06.054

58.  PERIPHERAL NERVOUS SYSTEM AGING: IMPLICATIONS FOR GERIATRIC OUTCOMES, The Gerontologist, Volume 55, Issue Suppl_2, November 2015, Pages 769–770, https://doi.org/10.1093/geront/gnv406.01

59.  Verdú E, Ceballos D, Vilches JJ, Navarro X. Influence of aging on peripheral nerve function and regeneration. J Peripher Nerv Syst. 2000;5(4):191-208. doi:10.1046/j.1529-8027.2000.00026.x

60.  Goto K, Naito K, Nakamura S, et al. Protective mechanism against age-associated changes in the peripheral nerves. Life Sci. 2020;253:117744. doi:10.1016/j.lfs.2020.117744

61.  Menorca RM, Fussell TS, Elfar JC. Nerve physiology: mechanisms of injury and recovery. Hand Clin. 2013;29(3):317-330. doi:10.1016/j.hcl.2013.04.002

62.  Jortner BS. Common Structural Lesions of the Peripheral Nervous System. Toxicol Pathol. 2020;48(1):96-104. doi:10.1177/0192623319826068

63.  Kamil K, Yazid MD, Idrus RBH, Das S, Kumar J. Peripheral Demyelinating Diseases: From Biology to Translational Medicine. Front Neurol. 2019;10:87. Published 2019 Mar 19. doi:10.3389/fneur.2019.00087

64.  Salzer JL. Schwann cell myelination. Cold Spring Harb Perspect Biol. 2015;7(8):a020529. Published 2015 Jun 8. doi:10.1101/cshperspect.a020529

65.  Stangel M, Hartung HP. Remyelinating strategies for the treatment of multiple sclerosis. Prog Neurobiol. 2002;68(5):361-376. doi:10.1016/s0301-0082(02)00105-3

66.  Szewczyk AK, Jamroz-Wiśniewska A, Haratym N, Rejdak K. Neuropathic pain and chronic pain as an underestimated interdisciplinary problem. Int J Occup Med Environ Health. 2022;35(3):249-264. doi:10.13075/ijomeh.1896.01676

67.  Modrak M, Talukder MAH, Gurgenashvili K, Noble M, Elfar JC. Peripheral nerve injury and myelination: Potential therapeutic strategies. J Neurosci Res. 2020;98(5):780-795. doi:10.1002/jnr.24538

68.  El Soury M, Fornasari BE, Carta G, Zen F, Haastert-Talini K, Ronchi G. The Role of Dietary Nutrients in Peripheral Nerve Regeneration. Int J Mol Sci. 2021;22(14):7417. Published 2021 Jul 10. doi:10.3390/ijms22147417

69.  Artukoglu BB, Beyer C, Zuloff-Shani A, Brener E, Bloch MH. Efficacy of Palmitoylethanolamide for Pain: A Meta-Analysis. Pain Physician. 2017;20(5):353-362.

70.  Ghonghadze M, Pachkoria K, Okujava M, Antelava N, Gongadze N. ENDOCANNABINOIDS RECEPTORS MEDIATED CENTRAL AND PERIPHERAL EFFECTS (REVIEW). Georgian Med News. 2020;(298):137-143.

71. Pallag A, Filip GA, Olteanu D, et al. Equisetum arvense L. Extract Induces Antibacterial Activity and Modulates Oxidative Stress, Inflammation, and Apoptosis in Endothelial Vascular Cells Exposed to Hyperosmotic Stress. Oxid Med Cell Longev. 2018;2018:3060525. Published 2018 Feb 14. doi:10.1155/2018/3060525

72. Song FH, Liu DQ, Zhou YQ, Mei W. SIRT1: A promising therapeutic target for chronic pain. CNS Neurosci Ther. 2022;28(6):818-828. doi:10.1111/cns.13838

73. Cicero AFG, Fogacci F, Banach M. Red Yeast Rice for Hypercholesterolemia. Methodist Debakey Cardiovasc J. 2019;15(3):192-199. doi:10.14797/mdcj-15-3-192

74. Writing Group Members, Mozaffarian D, Benjamin EJ, et al. Heart Disease and Stroke Statistics-2016 Update: A Report From the American Heart Association [published correction appears in Circulation. 2016 Apr 12;133(15):e599]. Circulation. 2016;133(4):e38-e360. doi:10.1161/CIR.0000000000000350

75. Booth JN 3rd, Colantonio LD, Howard G, et al. Healthy lifestyle factors and incident heart disease and mortality in candidates for primary prevention with statin therapy. Int J Cardiol. 2016;207:196-202. doi:10.1016/j.ijcard.2016.01.001

76. Arnett DK, Blumenthal RS, Albert MA, et al. 2019 ACC/AHA Guideline on the Primary Prevention of Cardiovascular Disease: A Report of the American College of Cardiology/American Heart Association Task Force on Clinical Practice Guidelines [published correction appears in Circulation. 2019 Sep 10;140(11):e649-e650] [published correction appears in Circulation. 2020 Jan 28;141(4):e60] [published correction appears in Circulation. 2020 Apr 21;141(16):e774]. Circulation. 2019;140(11):e596-e646. doi:10.1161/CIR.0000000000000678

77. Authors/Task Force Members, Piepoli MF, Hoes AW, et al. 2016 European Guidelines on cardiovascular disease prevention in clinical practice: The Sixth Joint Task Force of the European Society of Cardiology and Other Societies on Cardiovascular Disease Prevention in Clinical Practice (constituted by representatives of 10 societies and by invited experts): Developed with the special contribution of the European Association for Cardiovascular Prevention & Rehabilitation (EACPR). Eur J Prev Cardiol. 2016;23(11):NP1-NP96. doi:10.1177/2047487316653709

78. Poli A, Barbagallo CM, Cicero AFG, et al. Nutraceuticals and functional foods for the control of plasma cholesterol levels. An intersociety position paper. Pharmacol Res. 2018;134:51-60. doi:10.1016/j.phrs.2018.05.015

79. Patti AM, Toth PP, Giglio RV, et al. Nutraceuticals as an Important Part of Combination Therapy in Dyslipidaemia. Curr Pharm Des. 2017;23(17):2496-2503. doi:10.2174/1381612823666170317145851

80. Stone NJ, Robinson JG, Lichtenstein AH, et al. 2013 ACC/AHA guideline on the treatment of blood cholesterol to reduce atherosclerotic cardiovascular risk in adults: a report of the American College of Cardiology/American Heart Association Task Force on Practice Guidelines [published correction appears in J Am Coll Cardiol. 2014 Jul 1;63(25 Pt B):3024-3025] [published correction appears in J Am Coll Cardiol. 2015 Dec 22;66(24):2812]. J Am Coll Cardiol. 2014;63(25 Pt B):2889-2934. doi:10.1016/j.jacc.2013.11.002

81. Howard BV, Van Horn L, Hsia J, et al. Low-fat dietary pattern and risk of cardiovascular disease: the Women's Health Initiative Randomized Controlled Dietary Modification Trial. JAMA. 2006;295(6):655-666. doi:10.1001/jama.295.6.655

82. Mannarino MR, Ministrini S, Pirro M. Nutraceuticals for the treatment of hypercholesterolemia. Eur J Intern Med. 2014;25(7):592-599. doi:10.1016/j.ejim.2014.06.008

83. Kłosiewicz-Latoszek L, Cybulska B, Stoś K, Tyszko P. Hypolipaemic nutraceutics: red yeast rice and Armolipid, berberine and bergamot. Ann Agric Environ Med. 2021;28(1):81-88. doi:10.26444/aaem/130629

84. Houston M. The role of nutraceutical supplements in the treatment of dyslipidemia. J Clin Hypertens (Greenwich). 2012;14(2):121-132. doi:10.1111/j.1751-7176.2011.00576.x

85. Houston MC, Fazio S, Chilton FH, et al. Nonpharmacologic treatment of dyslipidemia. Prog Cardiovasc Dis. 2009;52(2):61-94. doi:10.1016/j.pcad.2009.02.002

86. Banach M, Bruckert E, Descamps OS, et al. The role of red yeast rice (RYR) supplementation in plasma cholesterol control: A review and expert opinion. Atheroscler Suppl. 2019;39:e1-e8. doi:10.1016/j.atherosclerosissup.2019.08.023

87. Banach M, Patti AM, Giglio RV, et al. The Role of Nutraceuticals in Statin Intolerant Patients. J Am Coll Cardiol. 2018;72(1):96-118. doi:10.1016/j.jacc.2018.04.040

88. Ghasi S, Nwobodo E, Ofili JO. Hypocholesterolemic effects of crude extract of leaf of Moringa oleifera Lam in high-fat diet fed wistar rats. J Ethnopharmacol. 2000;69(1):21-25. doi:10.1016/s0378-8741(99)00106-3

89. Pinto JT, Oliveira TTD, Alvarenga LF, Barbosa AS, Pizziolo VR, Costa, MRD. Pharmacological activity of the hydroalcoholic extract from Hovenia dulcis thunberg fruit and the flavonoid dihydromyricetin during

hypercholesterolemia induced in rats. Brazilian Journal of Pharmaceutical Sciences, 2014 50, 727-735. doi: 10.1590/S1984-82502014000400007

90. Forbes-Hernández TY, Giampieri F, Gasparrini M, et al. Lipid Accumulation in HepG2 Cells Is Attenuated by Strawberry Extract through AMPK Activation. Nutrients. 2017;9(6):621. Published 2017 Jun 16. doi:10.3390/nu9060621

91. Lupo MG, Macchi C, Marchianò S, et al. Differential effects of red yeast rice, Berberis aristata and Morus alba extracts on PCSK9 and LDL uptake. Nutr Metab Cardiovasc Dis. 2019;29(11):1245-1253. doi:10.1016/j.numecd.2019.06.001

92. Bauer J, Morley JE, Schols AMWJ, et al. Sarcopenia: A Time for Action. An SCWD Position Paper. J Cachexia Sarcopenia Muscle. 2019;10(5):956-961. doi:10.1002/jcsm.12483

93. Tournadre A, Vial G, Capel F, Soubrier M, Boirie Y. Sarcopenia. Joint Bone Spine. 2019;86(3):309-314. doi:10.1016/j.jbspin.2018.08.001

94. Budui SL, Rossi AP, Zamboni M. The pathogenetic bases of sarcopenia. Clin Cases Miner Bone Metab. 2015;12(1):22-26. doi:10.11138/ccmbm/2015.12.1.022

95. Livshits G, Kalinkovich A. Inflammaging as a common ground for the development and maintenance of sarcopenia, obesity, cardiomyopathy and dysbiosis. Ageing Res Rev. 2019;56:100980. doi:10.1016/j.arr.2019.100980

96. Scicchitano BM, Pelosi L, Sica G, Musarò A. The physiopathologic role of oxidative stress in skeletal muscle. Mech Ageing Dev. 2018;170:37-44. doi:10.1016/j.mad.2017.08.009

97. Wilson D, Jackson T, Sapey E, Lord JM. Frailty and sarcopenia: The potential role of an aged immune system. Ageing Res Rev. 2017;36:1-10. doi:10.1016/j.arr.2017.01.006

98. Dort J, Fabre P, Molina T, Dumont NA. Macrophages Are Key Regulators of Stem Cells during Skeletal Muscle Regeneration and Diseases. Stem Cells Int. 2019;2019:4761427. Published 2019 Jul 14. doi:10.1155/2019/4761427

99. Howard EE, Pasiakos SM, Blesso CN, Fussell MA, Rodriguez NR. Divergent Roles of Inflammation in Skeletal Muscle Recovery From Injury. Front Physiol. 2020;11:87. Published 2020 Feb 13. doi:10.3389/fphys.2020.00087

100. Mercken EM, Capri M, Carboneau BA, et al. Conserved and species-specific molecular denominators in mammalian skeletal muscle aging. NPJ Aging Mech Dis. 2017;3:8. Published 2017 May 5. doi:10.1038/s41514-017-0009-8

101. Wang T. Searching for the link between inflammaging and sarcopenia. Ageing Res Rev. 2022;77:101611. doi:10.1016/j.arr.2022.101611

102. Sciorati C, Gamberale R, Monno A, et al. Pharmacological blockade of TNFα prevents sarcopenia and prolongs survival in aging mice. Aging (Albany NY). 2020;12(23):23497-23508. doi:10.18632/aging.202200

103. Li CW, Yu K, Shyh-Chang N, et al. Circulating factors associated with sarcopenia during ageing and after intensive lifestyle intervention. J Cachexia Sarcopenia Muscle. 2019;10(3):586-600. doi:10.1002/jcsm.12417

104. Rong YD, Bian AL, Hu HY, Ma Y, Zhou XZ. Study on relationship between elderly sarcopenia and inflammatory cytokine IL-6, anti-inflammatory cytokine IL-10. BMC Geriatr. 2018;18(1):308. Published 2018 Dec 12. doi:10.1186/s12877-018-1007-9

105. Pan L, Xie W, Fu X, et al. Inflammation and sarcopenia: A focus on circulating inflammatory cytokines. Exp Gerontol. 2021;154:111544. doi:10.1016/j.exger.2021.111544

106. Vitale G, Salvioli S, Franceschi C. Oxidative stress and the ageing endocrine system. Nat Rev Endocrinol. 2013;9(4):228-240. doi:10.1038/nrendo.2013.29

107. Ilich JZ, Kelly OJ, Inglis JE. Osteosarcopenic Obesity Syndrome: What Is It and How Can It Be Identified and Diagnosed?. Curr Gerontol Geriatr Res. 2016;2016:7325973. doi:10.1155/2016/7325973

108. Confortin SC, Ono LM, Marques LP, Ceolin G, d'Orsi E, Barbosa AR. Osteopenia/osteoporosis and its association with sarcopenia: EpiFloripa aging study 2013/2014. Portuguese Journal of Public Health, 2020 38(1), 15-22. doi: 10.1159/000508924

109. Carina V, Della Bella E, Costa V, et al. Bone's Response to Mechanical Loading in Aging and Osteoporosis: Molecular Mechanisms. Calcif Tissue Int. 2020;107(4):301-318. doi:10.1007/s00223-020-00724-0

110. Jardí F, Laurent MR, Kim N, et al. Testosterone boosts physical activity in male mice via dopaminergic pathways. Sci Rep. 2018;8(1):957. Published 2018 Jan 17. doi:10.1038/s41598-017-19104-0

111. Galea GL, Meakin LB, Harris MA, et al. Old age and the associated impairment of bones' adaptation to loading are associated with transcriptomic changes in cellular metabolism, cell-matrix interactions and the cell cycle. Gene. 2017;599:36-52. doi:10.1016/j.gene.2016.11.006

112. Pignolo RJ, Law SF, Chandra A. Bone Aging, Cellular Senescence, and Osteoporosis. JBMR Plus. 2021;5(4):e10488. Published 2021 Apr 2. doi:10.1002/jbm4.10488

113. Chandra A, Rajawat J. Skeletal Aging and Osteoporosis: Mechanisms and Therapeutics. Int J Mol Sci. 2021;22(7):3553. Published 2021 Mar 29. doi:10.3390/ijms22073553

114. Duncan EL. Gene Testing in Everyday Clinical Use: Lessons from the Bone Clinic. J Endocr Soc. 2020;5(4):bvaa200. Published 2020 Dec 30. doi:10.1210/jendso/bvaa200

115. Luther J, Yorgan TA, Rolvien T, et al. Wnt1 is an Lrp5-independent bone-anabolic Wnt ligand. Sci Transl Med. 2018;10(466):eaau7137. doi:10.1126/scitranslmed.aau7137

116. Chu L, Liu X, He Z, et al. Articular Cartilage Degradation and Aberrant Subchondral Bone Remodeling in Patients with Osteoarthritis and Osteoporosis. J Bone Miner Res. 2020;35(3):505-515. doi:10.1002/jbmr.3909

117. Martiniakova M, Babikova M, Omelka R. Pharmacological agents and natural compounds: available treatments for osteoporosis. J Physiol Pharmacol. 2020;71(3):10.26402/jpp.2020.3.01. doi:10.26402/jpp.2020.3.01

118. Park KR, Kim B, Lee JY, Moon HJ, Kwon IK, Yun HM. Effects of Scoparone on differentiation, adhesion, migration, autophagy and mineralization through the osteogenic signalling pathways. J Cell Mol Med. 2022;26(16):4520-4529. doi:10.1111/jcmm.17476

119. Słupski W, Jawień P, Nowak B. Botanicals in Postmenopausal Osteoporosis. Nutrients. 2021;13(5):1609. Published 2021 May 11. doi:10.3390/nu13051609

120. Mariani E, Frasca D. Editorial: Immunobiology of Osteoarticular Diseases. Front Immunol. 2021;12:698992. Published 2021 May 13. doi:10.3389/fimmu.2021.698992

121. He Y, Li Z, Alexander PG, et al. Pathogenesis of Osteoarthritis: Risk Factors, Regulatory Pathways in Chondrocytes, and Experimental Models. Biology (Basel). 2020;9(8):194. Published 2020 Jul 29. doi:10.3390/biology9080194

122. Greene MA, Loeser RF. Aging-related inflammation in osteoarthritis. Osteoarthritis Cartilage. 2015;23(11):1966-1971. doi:10.1016/j.joca.2015.01.008

123. HAYFLICK L. THE LIMITED IN VITRO LIFETIME OF HUMAN DIPLOID CELL STRAINS. Exp Cell Res. 1965;37:614-636. doi:10.1016/0014-4827(65)90211-9

124. Campisi J. Cellular senescence: putting the paradoxes in perspective. Curr Opin Genet Dev. 2011;21(1):107-112. doi:10.1016/j.gde.2010.10.005

125. Loeser RF, Collins JA, Diekman BO. Ageing and the pathogenesis of osteoarthritis. Nat Rev Rheumatol. 2016;12(7):412-420. doi:10.1038/nrrheum.2016.65

126. Abramoff B, Caldera FE. Osteoarthritis: Pathology, Diagnosis, and Treatment Options. Med Clin North Am. 2020;104(2):293-311. doi:10.1016/j.mcna.2019.10.007

127. Goldring MB, Goldring SR. Articular cartilage and subchondral bone in the pathogenesis of osteoarthritis. Ann N Y Acad Sci. 2010;1192:230-237. doi:10.1111/j.1749-6632.2009.05240.x

128. Zheng L, Zhang Z, Sheng P, Mobasheri A. The role of metabolism in chondrocyte dysfunction and the progression of osteoarthritis. Ageing Res Rev. 2021;66:101249. doi:10.1016/j.arr.2020.101249

129. Liu S, Deng Z, Chen K, et al. Cartilage tissue engineering: From proinflammatory and anti-inflammatory cytokines to osteoarthritis treatments (Review). Mol Med Rep. 2022;25(3):99. doi:10.3892/mmr.2022.12615

130. Coppé JP, Patil CK, Rodier F, et al. Senescence-associated secretory phenotypes reveal cell-nonautonomous functions of oncogenic RAS and the p53 tumor suppressor. PLoS Biol. 2008;6(12):2853-2868. doi:10.1371/journal.pbio.0060301

131. Freund A, Orjalo AV, Desprez PY, Campisi J. Inflammatory networks during cellular senescence: causes and consequences. Trends Mol Med. 2010;16(5):238-246. doi:10.1016/j.molmed.2010.03.003

132. De Ceuninck F, Dassencourt L, Anract P. The inflammatory side of human chondrocytes unveiled by antibody microarrays. Biochem Biophys Res Commun. 2004;323(3):960-969. doi:10.1016/j.bbrc.2004.08.184

133. Sohn DH, Sokolove J, Sharpe O, et al. Plasma proteins present in osteoarthritic synovial fluid can stimulate cytokine production via Toll-like receptor 4. Arthritis Res Ther. 2012;14(1):R7. Published 2012 Jan 8. doi:10.1186/ar3555

134. Alaaeddine N, Olee T, Hashimoto S, Creighton-Achermann L, Lotz M. Production of the chemokine RANTES by articular chondrocytes and role in cartilage degradation. Arthritis Rheum. 2001;44(7):1633-1643. doi:10.1002/1529-0131(200107)44:7<1633::AID-ART286>3.0.CO;2-Z

135. Freund A, Patil CK, Campisi J. p38MAPK is a novel DNA damage response-independent regulator of the senescence-associated secretory phenotype. EMBO J. 2011;30(8):1536-1548. doi:10.1038/emboj.2011.69

136. Rodier F, Campisi J. Four faces of cellular senescence. J Cell Biol. 2011;192(4):547-556. doi:10.1083/jcb.201009094

137. Baker DJ, Wijshake T, Tchkonia T, et al. Clearance of p16Ink4a-positive senescent cells delays ageing-associated disorders. Nature. 2011;479(7372):232-236. Published 2011 Nov 2. doi:10.1038/nature10600

138. Rose J, Söder S, Skhirtladze C, et al. DNA damage, discoordinated gene expression and cellular senescence in osteoarthritic chondrocytes. Osteoarthritis Cartilage. 2012;20(9):1020-1028. doi:10.1016/j.joca.2012.05.009

139. Zhou HW, Lou SQ, Zhang K. Recovery of function in osteoarthritic chondrocytes induced by p16INK4a-specific siRNA in vitro. Rheumatology (Oxford). 2004;43(5):555-568. doi:10.1093/rheumatology/keh127

140. de Hooge AS, van de Loo FA, Bennink MB, Arntz OJ, de Hooge P, van den Berg WB. Male IL-6 gene knock out mice developed more advanced osteoarthritis upon aging. Osteoarthritis Cartilage. 2005;13(1):66-73. doi:10.1016/j.joca.2004.09.011

141. Molinari C, Morsanuto V, Ruga S, et al. The Role of BDNF on Aging-Modulation Markers. Brain Sci. 2020;10(5):285. Published 2020 May 9. doi:10.3390/brainsci10050285

142. Uberti F, Morsanuto V, Ghirlanda S, et al. Highly Diluted Acetylcholine Promotes Wound Repair in an In vivo Model. Adv Wound Care (New Rochelle). 2018;7(4):121-133. doi:10.1089/wound.2017.0766

143. Saba J, Turati J, Ramírez D, et al. Astrocyte truncated tropomyosin receptor kinase B mediates brain-derived neurotrophic factor anti-apoptotic effect leading to neuroprotection. J Neurochem. 2018;146(6):686-702. doi:10.1111/jnc.14476

144. Yuan J, Zhang Y, Wang X, Ma H. Exogenous Brain-Derived Neurotrophic Factor at a 50 ng/mL Concentration has a Significant Protective Effect on Bilirubin-Induced Cerebral Cortex Neuronal Injury. Clin Lab. 2017;63(9):1421-1429. doi:10.7754/Clin.Lab.2017.170303

145. Schildge S, Bohrer C, Beck K, Schachtrup C. Isolation and culture of mouse cortical astrocytes. J Vis Exp. 2013;(71):50079. Published 2013 Jan 19. doi:10.3791/50079

146. Kim HJ, Magrané J. Isolation and culture of neurons and astrocytes from the mouse brain cortex. Methods Mol Biol. 2011;793:63-75. doi:10.1007/978-1-61779-328-8_4

147. Thomaz A, Jaeger M, Buendia M, et al. BDNF/TrkB Signaling as a Potential Novel Target in Pediatric Brain Tumors: Anticancer Activity of Selective TrkB Inhibition in Medulloblastoma Cells. J Mol Neurosci. 2016;59(3):326-333. doi:10.1007/s12031-015-0689-0

148. Lü L, Li J, Zhu Y, Mak YT, Yew DT. H2O2-induced changes in astrocytic cultures from control and rapidly aging strains of mouse. Int J Neurosci. 2008;118(9):1239-1250. doi:10.1080/00207450601059429

149. Uberti F, Morsanuto V, Ghirlanda S, Molinari C. Iron Absorption from Three Commercially Available Supplements in Gastrointestinal Cell Lines. Nutrients. 2017;9(9):1008. Published 2017 Sep 13. doi:10.3390/nu9091008

150. DiMarco RL, Hunt DR, Dewi RE, Heilshorn SC. Improvement of paracellular transport in the Caco-2 drug screening model using protein-engineered substrates. Biomaterials. 2017;129:152-162. doi:10.1016/j.biomaterials.2017.03.023

151. Obringer C, Manwaring J, Goebel C, Hewitt NJ, Rothe H. Suitability of the in vitro Caco-2 assay to predict the oral absorption of aromatic amine hair dyes. Toxicol In vitro. 2016;32:1-7. doi:10.1016/j.tiv.2015.11.007

152. Zorkina YA, Volgina NE, Gorlachev GE, et al. Effect of γ-irradiation on expression of tight and adherens junction protein mRNA on in vitro blood-brain barrier model. Bull Exp Biol Med. 2014;158(1):127-136. doi:10.1007/s10517-014-2708-5

153. Kulczar C, Lubin KE, Lefebvre S, Miller DW, Knipp GT. Development of a direct contact astrocyte-human cerebral microvessel endothelial cells blood-brain barrier coculture model. J Pharm Pharmacol. 2017;69(12):1684-1696. doi:10.1111/jphp.12803

154. Uberti F, Lattuada D, Morsanuto V, et al. Vitamin D protects human endothelial cells from oxidative stress through the autophagic and survival pathways. J Clin Endocrinol Metab. 2014;99(4):1367-1374. doi:10.1210/jc.2013-2103

155. Uberti F, Morsanuto V, Aprile S, et al. Biological effects of combined resveratrol and vitamin D3 on ovarian tissue. J Ovarian Res. 2017;10(1):61. Published 2017 Sep 15. doi:10.1186/s13048-017-0357-9

156. Cappellano G, Uberti F, Caimmi PP, et al. Different expression and function of the endocannabinoid system in human epicardial adipose tissue in relation to heart disease. Can J Cardiol. 2013;29(4):499-509. doi:10.1016/j.cjca.2012.06.003

157. Dutta S, Sengupta P. Men and mice: Relating their ages. Life Sci. 2016;152:244-248. doi:10.1016/j.lfs.2015.10.025

158. Walker MK, Boberg JR, Walsh MT, et al. A less stressful alternative to oral gavage for pharmacological and toxicological studies in mice. Toxicol Appl Pharmacol. 2012;260(1):65-69. doi:10.1016/j.taap.2012.01.025

159. Bachmanov AA, Reed DR, Beauchamp GK, Tordoff MG. Food intake, water intake, and drinking spout side preference of 28 mouse strains. Behav Genet. 2002;32(6):435-443. doi:10.1023/a:1020884312053

160. Kaushal N, Nair D, Gozal D, Ramesh V. Socially isolated mice exhibit a blunted homeostatic sleep response to acute sleep deprivation compared to socially paired mice. Brain Res. 2012;1454:65-79. doi:10.1016/j.brainres.2012.03.019

161. Ruga S, Galla R, Ferrari S, et al. New approach to the treatment of neuropathic pain. In vitro study on the cellular effects of a combination with palmitoylethanolamide (under review)

162. Morsanuto V, Galla R, Molinari C, Uberti F. A New Palmitoylethanolamide Form Combined with Antioxidant Molecules to Improve Its Effectivess on Neuronal Aging. Brain Sci. 2020;10(7):457. Published 2020 Jul 17. doi:10.3390/brainsci10070457

163. Bessa Pereira C, Gomes PS, Costa-Rodrigues J, et al. Equisetum arvense hydromethanolic extracts in bone tissue regeneration: in vitro osteoblastic modulation and antibacterial activity. Cell Prolif. 2012;45(4):386-396. doi:10.1111/j.1365-2184.2012.00826.x

164. DiMarco RL, Hunt DR, Dewi RE, Heilshorn SC. Improvement of paracellular transport in the Caco-2 drug screening model using protein-engineered substrates. Biomaterials. 2017;129:152-162. doi:10.1016/j.biomaterials.2017.03.023.

165. Galla R, Ruga S, Aprile S, et al. New Hyaluronic Acid from Plant Origin to Improve Joint Protection-An In vitro Study. Int J Mol Sci. 2022;23(15):8114. Published 2022 Jul 23. doi:10.3390/ijms23158114

166. Ceriotti L, Meloni M. La valutazione dell'assorbimento intestinale in vitro. L'integratore Nutr 2014;17:62-65

167. Rayner MLD, Laranjeira S, Evans RE, Shipley RJ, Healy J, Phillips JB. Developing an In vitro Model to Screen Drugs for Nerve Regeneration. Anat Rec (Hoboken). 2018;301(10):1628-1637. doi:10.1002/ar.23918

168. Muscella A, Vetrugno C, Cossa LG, Marsigliante S. TGF-β1 activates RSC96 Schwann cells migration and invasion through MMP-2 and MMP-9 activities. J Neurochem. 2020;153(4):525-538. doi:10.1111/jnc.14913

169. Chua P, Lim WK. Optimisation of a PC12 cell-based in vitro stroke model for screening neuroprotective agents. Sci Rep. 2021;11(1):8096. Published 2021 Apr 14. doi:10.1038/s41598-021-87431-4

170. Galla R, Grisenti P, Farghali M, Saccuman L, Ferraboschi P, Uberti F. Ovotransferrin Supplementation Improves the Iron Absorption: An In vitro Gastro-Intestinal Model. Biomedicines. 2021;9(11):1543. Published 2021 Oct 26. doi:10.3390/biomedicines9111543

171. Christides T, Wray D, McBride R, Fairweather R, Sharp P. Iron bioavailability from commercially available iron supplements. Eur J Nutr. 2015;54(8):1345-1352. doi:10.1007/s00394-014-0815-8

172. Fda.Gov. Available online: https://www.fda.gov/media/117974/download (accessed on 12 May 2021)

173. Ema.Eu. Available online: https://www.ema.europa.eu/en/documents/scientific-guideline/ich-m9-biopharmaceutics-classification-system-based-biowaivers-step-2b-first-version_en.pdf (accessed on 6 August 2018)

174. Guha S, Alvarez S, Majumder K. Transport of Dietary Anti-Inflammatory Peptide, γ-Glutamyl Valine (γ-EV), across the Intestinal Caco-2 Monolayer. Nutrients. 2021;13(5):1448. Published 2021 Apr 24. doi:10.3390/nu13051448

175. Uberti F, Morsanuto V, Ruga S, et al. Study of Magnesium Formulations on Intestinal Cells to Influence Myometrium Cell Relaxation. Nutrients. 2020;12(2):573. Published 2020 Feb 22. doi:10.3390/nu12020573

176. Muangsanit P, Day A, Dimiou S, et al. Rapidly formed stable and aligned dense collagen gels seeded with Schwann cells support peripheral nerve regeneration. J Neural Eng. 2020;17(4):046036. Published 2020 Aug 25. doi:10.1088/1741-2552/abaa9c

177. Uberti F, Ruga S, Farghali M, Galla R, Molinari C. A Combination of $\alpha$-Lipoic Acid (ALA) and Palmitoylethanolamide (PEA) Blocks Endotoxin-Induced Oxidative Stress and Cytokine Storm: A Possible Intervention for COVID-19 [published online ahead of print, 2021 Aug 18]. J Diet Suppl. 2021;1-23. doi:10.1080/19390211.2021.1966152

178. Du Y, Luan J, Jiang RP, Liu J, Ma Y. Myrcene exerts anti-asthmatic activity in neonatal rats via modulating the matrix remodeling. Int J Immunopathol Pharmacol. 2020;34:2058738420954948. doi:10.1177/2058738420954948

179. Endo T, Kadoya K, Kawamura D, Iwasaki N. Evidence for cell-contact factor involvement in neurite outgrowth of dorsal root ganglion neurons stimulated by Schwann cells. Exp Physiol. 2019;104(10):1447-1454. doi:10.1113/EP087634

180. Rzemieniec J, Litwa E, Wnuk A, et al. Neuroprotective action of raloxifene against hypoxia-induced damage in mouse hippocampal cells depends on ERα but not ERβ or GPR30 signalling. J Steroid Biochem Mol Biol. 2015;146:26-37. doi:10.1016/j.jsbmb.2014.05.005

181. Al Suhaibani A, Ben Bacha A, Alonazi M, Bhat RS, El-Ansary A. Testing the combined effects of probiotics and prebiotics against neurotoxic effects of propionic acid orally administered to rat pups. Food Sci Nutr. 2021;9(8):4440-4451. Published 2021 Jun 23. doi:10.1002/fsn3.2418

182. Ruga S, Galla R, Penna C, Molinari C, Uberti F. The Activity of Ten Natural Extracts Combined in a Unique Blend to Maintain Cholesterol Homeostasis-In vitro Model. Int J Mol Sci. 2022;23(7):3805. Published 2022 Mar 30. doi:10.3390/ijms23073805

183. Huang CH, Shiu SM, Wu MT, Chen WL, Wang SG, Lee HM. Monacolin K affects lipid metabolism through SIRT1/AMPK pathway in HepG2 cells. Arch Pharm Res. 2013;36(12):1541-1551. doi:10.1007/s12272-013-0150-2

184. Frigerio J, Tedesco E, Benetti F, et al. Anticholesterolemic Activity of Three Vegetal Extracts (Artichoke, Caigua, and Fenugreek) and Their Unique Blend. Front Pharmacol. 2021;12:726199. Published 2021 Nov 23. doi:10.3389/fphar.2021.726199

185. Huang J, Yang G, Huang Y, Zhang S. Inhibitory effects of 1,25(OH)2D3 on the proliferation of hepatocellular carcinoma cells through the downregulation of HDAC2. Oncol Rep. 2017;38(3):1845-1850. doi:10.3892/or.2017.5848

186. Takashina M, Inoue S, Tomihara K, et al. Different effect of resveratrol to induction of apoptosis depending on the type of human cancer cells. Int J Oncol. 2017;50(3):787-797. doi:10.3892/ijo.2017.3859

187. Boesch-Saadatmandi C, Rimbach G, Jungblut A, Frank J. Comparison of tetrahydrofuran, fetal calf serum, and Tween 40 for the delivery of astaxanthin and canthaxanthin to HepG2 cells. Cytotechnology. 2011;63(1):89-97. doi:10.1007/s10616-010-9324-7

188. Zhang Y, Zhang B, Zhang A, et al. Synergistic growth inhibition by sorafenib and vitamin K2 in human hepatocellular carcinoma cells. Clinics (Sao Paulo). 2012;67(9):1093-1099. doi:10.6061/clinics/2012(09)18

189. Zou Y, Niu P, Gong Z, et al. Relationship between reactive oxygen species and sodium-selenite-induced DNA damage in HepG2 cells. Front Med China. 2007;1(3):327-332. doi:10.1007/s11684-007-0063-x

190. Bagherieh M, Kheirollahi A, Zamani-Garmsiri F, Emamgholipour S, Meshkani R. Folic acid ameliorates palmitate-induced inflammation through decreasing homocysteine and inhibiting NF-κB pathway in HepG2 cells [published online ahead of print, 2021 Feb 17]. Arch Physiol Biochem. 2021;1-8. doi:10.1080/13813455.2021.1878539

191. Lim DW, Jeon H, Kim M, et al. Standardized rice bran extract improves hepatic steatosis in HepG2 cells and ovariectomized rats. Nutr Res Pract. 2020;14(6):568-579. doi:10.4162/nrp.2020.14.6.568

192. Molinari C, Ruga S, Farghali M, Galla R, Bassiouny A, Uberti F. Preventing c2c12 muscular cells damage combining magnesium and potassium with vitamin D3 and curcumin. J Tradit Complement Med. 2021;11(6):532-544. Published 2021 Jun 2. doi:10.1016/j.jtcme.2021.05.003

193. Wang F, Chen H, Chen Y, et al. Diet-induced obesity is associated with altered expression of sperm motility-related genes and testicular post-translational modifications in a mouse model. Theriogenology. 2020;158:233-238. doi:10.1016/j.theriogenology.2020.09.023

194. Shao D, Wang Y, Huang Q, et al. Cholesterol-Lowering Effects and Mechanisms in View of Bile Acid Pathway of Resveratrol and Resveratrol Glucuronides. J Food Sci. 2016;81(11):H2841-H2848. doi:10.1111/1750-3841.13528

195. Mullen PJ, Lüscher B, Scharnagl H, Krähenbühl S, Brecht K. Effect of simvastatin on cholesterol metabolism in C2C12 myotubes and HepG2 cells, and consequences for statin-induced myopathy. Biochem Pharmacol. 2010;79(8):1200-1209. doi:10.1016/j.bcp.2009.12.007

196. Molinari C, Morsanuto V, Ghirlanda S, et al. Role of Combined Lipoic Acid and Vitamin D3 on Astrocytes as a Way to Prevent Brain Ageing by Induced Oxidative Stress and Iron Accumulation. Oxid Med Cell Longev. 2019;2019:2843121. Published 2019 Feb 28. doi:10.1155/2019/2843121

197. Chae HS, You BH, Kim DY, et al. Sauchinone controls hepatic cholesterol homeostasis by the negative regulation of PCSK9 transcriptional network. Sci Rep. 2018;8(1):6737. Published 2018 Apr 30. doi:10.1038/s41598-018-24935-6

198. Chean J, Chen CJ, Gugiu G, et al. Human CEACAM1-LF regulates lipid storage in HepG2 cells via fatty acid transporter CD36. J Biol Chem. 2021;297(5):101311. doi:10.1016/j.jbc.2021.101311

199. Cao S, Xu P, Yan J, et al. Berberrubine and its analog, hydroxypropyl-berberrubine, regulate LDLR and PCSK9 expression via the ERK signal pathway to exert cholesterol-lowering effects in human hepatoma HepG2 cells. J Cell Biochem. 2019;120(2):1340-1349. doi:10.1002/jcb.27102

200. Park S, Scheffler TL, Gunawan AM, et al. Chronic elevated calcium blocks AMPK-induced GLUT-4 expression in skeletal muscle. Am J Physiol Cell Physiol. 2009;296(1):C106-C115. doi:10.1152/ajpcell.00114.2008

201. Chen HW, Huang HC. Effect of curcumin on cell cycle progression and apoptosis in vascular smooth muscle cells. Br J Pharmacol. 1998;124(6):1029-1040. doi:10.1038/sj.bjp.0701914

202. Ojuka EO, Jones TE, Han DH, et al. Intermittent increases in cytosolic Ca2+ stimulate mitochondrial biogenesis in muscle cells. Am J Physiol Endocrinol Metab. 2002;283(5):E1040-E1045. doi:10.1152/ajpendo.00242.2002

203. Uberti F, Bardelli C, Morsanuto V, Ghirlanda S, Cochis A, Molinari C. Stimulation of the Nonneuronal Cholinergic System by Highly Diluted Acetylcholine in Keratinocytes. Cells Tissues Organs. 2017;203(4):215-230. doi:10.1159/000451023

204. Molinari C, Morsanuto V, Ruga S, Stoppa I, Notte F, Farghali M. Role of vitamin D3 and alginates in prevention of NSAID-dependent cellular injury. EC Gastroenterology and Digestive System, 2019; 6(3), 211-223.

205. Gouadon E, Lecerf F, German-Fattal M. Differential effects of cyclosporin A and tacrolimus on magnesium influx in Caco2 cells. J Pharm Pharm Sci. 2012;15(3):389-398. doi:10.18433/j3qk57

206. Chen SE, Jin B, Li YP. TNF-alpha regulates myogenesis and muscle regeneration by activating p38 MAPK. Am J Physiol Cell Physiol. 2007;292(5):C1660-C1671. doi:10.1152/ajpcell.00486.2006

207. Uberti F, Ruga S, Morsanuto V, Galla R, Farghali M, Molinari C. Role of ribonucleotides in improving muscle cell function. Journal of Food Science and Nutrition Research, 2020 3(4), 231-251.

208. Myers SA, Nield A, Chew GS, Myers MA. The zinc transporter, Slc39a7 (Zip7) is implicated in glycaemic control in skeletal muscle cells. PLoS One. 2013;8(11):e79316. Published 2013 Nov 12. doi:10.1371/journal.pone.0079316

209. Hong J, Kim BW, Choo HJ, et al. Mitochondrial complex I deficiency enhances skeletal myogenesis but impairs insulin signaling through SIRT1 inactivation. J Biol Chem. 2014;289(29):20012-20025. doi:10.1074/jbc.M114.560078

210. Gartz M, Darlington A, Afzal MZ, Strande JL. Exosomes exert cardioprotection in dystrophin-deficient cardiomyocytes via ERK1/2-p38/MAPK signaling. Sci Rep. 2018;8(1):16519. Published 2018 Nov 8. doi:10.1038/s41598-018-34879-6

211. Carter S, Solomon TPJ. In vitro experimental models for examining the skeletal muscle cell biology of exercise: the possibilities, challenges and future developments. Pflugers Arch. 2019;471(3):413-429. doi:10.1007/s00424-018-2210-4

212. Mannino F, D'Angelo T, Pallio G, et al. The Nutraceutical Genistein-Lycopene Combination Improves Bone Damage Induced by Glucocorticoids by Stimulating the Osteoblast Formation Process. Nutrients. 2022;14(20):4296. Published 2022 Oct 14. doi:10.3390/nu14204296

213. Liu L, Wang D, Qin Y, et al. Astragalin Promotes Osteoblastic Differentiation in MC3T3-E1 Cells and Bone Formation in vivo. Front Endocrinol (Lausanne). 2019;10:228. Published 2019 Apr 16. doi:10.3389/fendo.2019.00228

214. Macías I, Alcorta-Sevillano N, Rodríguez CI, Infante A. Osteoporosis and the Potential of Cell-Based Therapeutic Strategies. Int J Mol Sci. 2020;21(5):1653. Published 2020 Feb 28. doi:10.3390/ijms21051653

215. Fumie S, Hisako F, Takashi T, et al. Equisetum arvense Inhibits Alveolar Bone Destruction in a Rat Model with Lipopolysaccharide (LPS)-Induced Periodontitis. International Journal of Dentistry. 2022 International Journal of Dentistry, vol. 2022;15 https://doi.org/10.1155/2022/7398924

216. European Food Safety Authority, 2013; Outcome of the consultation with Member States and EFSA on the basic substance application for Equisetum arvense L. and the conclusions drawn by EFSA on the specific points raised. EFSA Supporting Publication 2013; 10( 6):EN-427. 33 pp. doi:10.2903/sp.efsa.2013.EN-427

217. Galla R, Ruga S, Ferrari S, et. al. In vitro analysis of the effects of plant-derived chondroitin sulfate from intestinal barrier to chondrocytes. Journal of Functional Foods. 2022;105285, https://doi.org/10.1016/j.jff.2022.105285.

218. Fedi A, Vitale C, Ponschin G, Ayehunie S, Fato M, Scaglione S. In vitro models replicating the human intestinal epithelium for absorption and metabolism studies: A systematic review. J Control Release. 2021;335:247-268. doi:10.1016/j.jconrel.2021.05.028

219. Izumiya M, Haniu M, Ueda K, et al. Evaluation of MC3T3-E1 Cell Osteogenesis in Different Cell Culture Media. Int J Mol Sci. 2021;22(14):7752. Published 2021 Jul 20. doi:10.3390/ijms22147752

220. Yodthong T, Kedjarune-Leggat U, Smythe C, et al. Enhancing Activity of Pleurotus sajor-caju (Fr.) Sing β-1,3-Glucanoligosaccharide (Ps-GOS) on Proliferation, Differentiation, and Mineralization of MC3T3-E1 Cells through the Involvement of BMP-2/Runx2/MAPK/Wnt/β-Catenin Signaling Pathway. Biomolecules. 2020;10(2):190. Published 2020 Jan 27. doi:10.3390/biom10020190

221. Liang Q, Lv M, Zhang X, et al. Effect of Black Tea Extract and Thearubigins on Osteoporosis in Rats and Osteoclast Formation in vitro [published correction appears in Front Physiol. 2020 Feb 25;11:136]. Front Physiol. 2018;9:1225. Published 2018 Sep 3. doi:10.3389/fphys.2018.01225

222. Kong L, Smith W, Hao D. Overview of RAW264.7 for osteoclastogensis study: Phenotype and stimuli. J Cell Mol Med. 2019;23(5):3077-3087. doi:10.1111/jcmm.14277

223. Collin-Osdoby P, Osdoby P. RANKL-mediated osteoclast formation from murine RAW 264.7 cells. Methods Mol Biol. 2012;816:187-202.

224. Taciak B, Białasek M, Braniewska A, et al. Evaluation of phenotypic and functional stability of RAW 264.7 cell line through serial passages. PLoS One. 2018;13(6):e0198943. Published 2018 Jun 11. doi:10.1371/journal.pone.0198943

225. Chen ST, Kang L, Wang CZ, et al. (-)-Epigallocatechin-3-Gallate Decreases Osteoclastogenesis via Modulation of RANKL and Osteoprotegrin. Molecules. 2019;24(1):156. Published 2019 Jan 3. doi:10.3390/molecules24010156

226. Jarrar H, ÇetІn Altindal D, GÜmÜŞderelİoĞlu M. The inhibitory effect of melatonin on osteoclastogenesis of RAW 264.7 cells in low concentrations of RANKL and MCSF. Turk J Biol. 2020;44(6):427-436. Published 2020 Dec 14. doi:10.3906/biy-2007-85

227. Ding Y, Liang C, Yang SY, et al. Phenolic compounds from Artemisia iwayomogi and their effects on osteoblastic MC3T3-E1 cells. Biol Pharm Bull. 2010;33(8):1448-1453. doi:10.1248/bpb.33.1448

228. Rajabian A, Farzanehfar M, Hosseini H, Arab FL, Nikkhah A. Boswellic acids as promising agents for the management of brain diseases. Life Sci. 2023;312:121196. doi:10.1016/j.lfs.2022.121196

229. Xie B, Zeng Z, Liao S, Zhou C, Wu L, Xu D. Kaempferol Ameliorates the Inhibitory Activity of Dexamethasone in the Osteogenesis of MC3T3-E1 Cells by JNK and p38-MAPK Pathways. Front Pharmacol. 2021;12:739326. Published 2021 Oct 5. doi:10.3389/fphar.2021.739326

230. Ishikawa S, Tamaki M, Ogawa Y, et al. Inductive Effect of Palmatine on Apoptosis in RAW 264.7 Cells. Evid Based Complement Alternat Med. 2016;2016:7262054. doi:10.1155/2016/7262054

231. Park E, Kim J, Kim MC, et al. Anti-Osteoporotic Effects of Kukoamine B Isolated from Lycii Radicis Cortex Extract on Osteoblast and Osteoclast Cells and Ovariectomized Osteoporosis Model Mice. Int J Mol Sci. 2019;20(11):2784. Published 2019 Jun 6. doi:10.3390/ijms20112784

232. Feng Y, Su L, Zhong X, et al. Exendin-4 promotes proliferation and differentiation of MC3T3-E1 osteoblasts by MAPKs activation. J Mol Endocrinol. 2016;56(3):189-199. doi:10.1530/JME-15-0264

233. Yeh CC, Su YH, Lin YJ, et al. Evaluation of the protective effects of curcuminoid (curcumin and bisdemethoxycurcumin)-loaded liposomes against bone turnover in a cell-based model of osteoarthritis. Drug Des Devel Ther. 2015;9:2285-2300. Published 2015 Apr 20. doi:10.2147/DDDT.S78277

234. Wang W, Zhang LM, Guo C, Han JF. Resveratrol promotes osteoblastic differentiation in a rat model of postmenopausal osteoporosis by regulating autophagy. Nutr Metab (Lond). 2020;17:29. Published 2020 Apr 16. doi:10.1186/s12986-020-00449-9

235. Schmidt C, Schneble-Löhnert N, Lajqi T, Wetzker R, Müller JP, Bauer R. PI3Kγ Mediates Microglial Proliferation and Cell Viability via ROS. Cells. 2021;10(10):2534. Published 2021 Sep 24. doi:10.3390/cells10102534

236. Yang D, Liu Y, Zhang L. Tremella polysaccharide: The molecular mechanisms of its drug action. Prog Mol Biol Transl Sci. 2019;163:383-421. doi:10.1016/bs.pmbts.2019.03.002

237. Vivatis Pharma GMBH, 8 June 2020. Plant Producing Hyaluronic Acid. PCT/IB2021/055031. [(accessed on 1 June 2022)]. Available online: https://patents.google.com/patent/WO2021250566A1/en?oq=WO2021250566+(A1)++-++PRO-CESS+FOR+EXTRACTING+A+HYALURONIC+ACID+FROM+A+FUNGUS%2c+A+HYALURONIC+ACID+OF+PLANT+ORIGIN+AND+USE+THEREOF, Italian Patent Identification and Selection of a Plant Starting Material of a Plant Chondroitin Sulfate and Hyaluronic Acid, and Transformation of such Plant Starting Material to Obtain Ingredients for Use in Foods, Supple-Ments, Medical Devices or Drugs. 102019000008409. 8 June 2021. [(accessed on 1 June 2022)]. Available online: https://patentscope.wipo.int/search/en/detail.jsf?docId=WO202024580

238. Ji D, Roman M, Zhou J, Hildreth J. Determination of chondroitin sulfate content in raw materials and dietary supplements by high-performance liquid chromatography with ultraviolet detection after enzymatic hydrolysis: single-laboratory validation. J AOAC Int. 2007;90(3):659-669.

239. Blumenkrantz N, Asboe-Hansen G. New method for quantitative determination of uronic acids. Anal Biochem. 1973;54(2):484-489. doi:10.1016/0003-2697(73)90377-1

240. Vojvodić Cebin A, Komes D, Ralet MC. Development and Validation of HPLC-DAD Method with Pre-Column PMP Derivatization for Monomeric Profile Analysis of Polysaccharides from Agro-Industrial Wastes. Polymers (Basel). 2022;14(3):544. Published 2022 Jan 28. doi:10.3390/polym14030544

241. Lee HG, Cowman MK. An agarose gel electrophoretic method for analysis of hyaluronan molecular weight distribution. Anal Biochem. 1994;219(2):278-287. doi:10.1006/abio.1994.1267

242. Yee S. In vitro permeability across Caco-2 cells (colonic) can predict in vivo (small intestinal) absorption in man--fact or myth. Pharm Res. 1997;14(6):763-766. doi:10.1023/a:1012102522787

243. Santoro A, Conde J, Scotece M, et al. Choosing the right chondrocyte cell line: Focus on nitric oxide. J Orthop Res. 2015;33(12):1784-1788. doi:10.1002/jor.22954

244. Pang KL, Chow YY, Leong LM, et al. Establishing SW1353 Chondrocytes as a Cellular Model of Chondrolysis. Life (Basel). 2021;11(4):272. Published 2021 Mar 25. doi:10.3390/life11040272

245. Claassen H, Schicht M, Brandt J, et al. C-28/I2 and T/C-28a2 chondrocytes as well as human primary articular chondrocytes express sex hormone and insulin receptors--Useful cells in study of cartilage metabolism. Ann Anat. 2011;193(1):23-29. doi:10.1016/j.aanat.2010.09.005

246. Aslan M, Simsek G, Dayi E. The effect of hyaluronic acid-supplemented bone graft in bone healing: experimental study in rabbits. J Biomater Appl. 2006;20(3):209-220. doi:10.1177/0885328206051047

247. López-Senra E, Casal-Beiroa P, López-Álvarez M, et al. Impact of Prevalence Ratios of Chondroitin Sulfate (CS)- 4 and -6 Isomers Derived from Marine Sources in Cell Proliferation and Chondrogenic Differentiation Processes. Mar Drugs. 2020;18(2):94. Published 2020 Jan 31. doi:10.3390/md18020094

248. Sui C, Zhang L, Hu Y. MicroRNA-let-7a inhibition inhibits LPS-induced inflammatory injury of chondrocytes by targeting IL6R. Mol Med Rep. 2019;20(3):2633-2640. doi:10.3892/mmr.2019.10493

249. Aborehab NM, El Bishbishy MH, Refaiy A, Waly NE. A putative Chondroprotective role for IL-1β and MPO in herbal treatment of experimental osteoarthritis. BMC Complement Altern Med. 2017;17(1):495. Published 2017 Nov 22. doi:10.1186/s12906-017-2002-y

250. Roberts HM, Moore JP, Thom JM. The effect of aerobic walking and lower body resistance exercise on serum COMP and hyaluronan, in both males and females. Eur J Appl Physiol. 2018;118(6):1095-1105. doi:10.1007/s00421-018-3837-8

251. Vorkapic E, Kunath A, Wågsäter D. Effects of osteoprotegerin/TNFRSF11B in two models of abdominal aortic aneurysms. Mol Med Rep. 2018;18(1):41-48. doi:10.3892/mmr.2018.8936

252. Chaaban I, Hafez H, AlZaim I, et al. Transforming iodoquinol into broad spectrum anti-tumor leads: Repurposing to modulate redox homeostasis. Bioorg Chem. 2021;113:105035. doi:10.1016/j.bioorg.2021.105035

253. Jieensinue S, Zhu H, Li G, Dong K, Liang M, Li Y. Tanshinone IIA reduces SW837 colorectal cancer cell viability via the promotion of mitochondrial fission by activating JNK-Mff signaling pathways. BMC Cell Biol. 2018;19(1):21. Published 2018 Sep 25. doi:10.1186/s12860-018-0174-z

254. https://www.who.int/health-topics/ageing#tab=tab_1

255. Rudnicka E, Napierała P, Podfigurna A, Męczekalski B, Smolarczyk R, Grymowicz M. The World Health Organization (WHO) approach to healthy ageing. Maturitas. 2020;139:6-11. doi:10.1016/j.maturitas.2020.05.018

256. Fabbri E, Zoli M, Gonzalez-Freire M, Salive ME, Studenski SA, Ferrucci L. Aging and Multimorbidity: New Tasks, Priorities, and Frontiers for Integrated Gerontological and Clinical Research. J Am Med Dir Assoc. 2015;16(8):640-647. doi:10.1016/j.jamda.2015.03.013

257. Kennedy BK, Berger SL, Brunet A, et al. Geroscience: linking aging to chronic disease. Cell. 2014;159(4):709-713. doi:10.1016/j.cell.2014.10.039

258. Goh J, Wong E, Soh J, Maier AB, Kennedy BK. Targeting the molecular & cellular pillars of human aging with exercise [published online ahead of print, 2021 Dec 30]. FEBS J. 2021;10.1111/febs.16337. doi:10.1111/febs.16337

259. Hernandez-Segura A, Nehme J, Demaria M. Hallmarks of Cellular Senescence. Trends Cell Biol. 2018;28(6):436-453. doi:10.1016/j.tcb.2018.02.001

260. Birch J, Gil J. Senescence and the SASP: many therapeutic avenues. Genes Dev. 2020;34(23-24):1565-1576. doi:10.1101/gad.343129.120

261. Cuollo L, Antonangeli F, Santoni A, Soriani A. The Senescence-Associated Secretory Phenotype (SASP) in the Challenging Future of Cancer Therapy and Age-Related Diseases. Biology (Basel). 2020;9(12):485. Published 2020 Dec 21. doi:10.3390/biology9120485

262. Li Z, Zhang Z, Ren Y, et al. Aging and age-related diseases: from mechanisms to therapeutic strategies. Biogerontology. 2021;22(2):165-187. doi:10.1007/s10522-021-09910-5

263. Fries CJ. Healing Health Care: From Sick Care Towards Salutogenic Healing Systems. Soc Theory Health. 2020;18(1):16-32. doi:10.1057/s41285-019-00103-2

264. Guo J, Huang X, Dou L, et al. Aging and aging-related diseases: from molecular mechanisms to interventions and treatments. Signal Transduct Target Ther. 2022;7(1):391. Published 2022 Dec 16. doi:10.1038/s41392-022-01251-0

265. Qian M, Liu B. Pharmaceutical Intervention of Aging. Adv Exp Med Biol. 2018;1086:235-254. doi:10.1007/978-981-13-1117-8_15

266. Lublóy Á. Medical crowdfunding in a healthcare system with universal coverage: an exploratory study. BMC Public Health. 2020;20(1):1672. Published 2020 Nov 9. doi:10.1186/s12889-020-09693-3

267. Zhao Y, Seluanov A, Gorbunova V. Revelations About Aging and Disease from Unconventional Vertebrate Model Organisms. Annu Rev Genet. 2021;55:135-159. doi:10.1146/annurev-genet-071719-021009

268. Bartke A. New Directions in Research on Aging. Stem Cell Rev Rep. 2022;18(4):1227-1233. doi:10.1007/s12015-021-10305-9

269. Partridge L, Fuentealba M, Kennedy BK. The quest to slow ageing through drug discovery. Nat Rev Drug Discov. 2020;19(8):513-532. doi:10.1038/s41573-020-0067-7

270. Bhattacharya T, Dey PS, Akter R, Kabir MT, Rahman MH, Rauf A. Effect of natural leaf extracts as phytomedicine in curing geriatrics. Exp Gerontol. 2021;150:111352. doi:10.1016/j.exger.2021.111352

271. Bjørklund G, Dadar M, Martins N, et al. Brief Challenges on Medicinal Plants: An Eye-Opening Look at Ageing-Related Disorders. Basic Clin Pharmacol Toxicol. 2018;122(6):539-558. doi:10.1111/bcpt.12972

272. Scapinello J, Aguiar GPS, Dal Magro C, Capelezzo AP, Niero R, Dal Magro J, de Oliveira D, Oliveira JV. Extraction of bioactive compounds from Philodendron bipinnatifidum Schott ex Endl and encapsulation in PHBV by SEDS technique. Industrial Crops and Products, 2018 125, 65-71. doi:10.1016/j.indcrop.2018.08.079

273. Chaiyana W, Charoensup W, Sriyab S, Punyoyai C, Neimkhum W. Herbal Extracts as Potential Antioxidant, Anti-Aging, Anti-Inflammatory, and Whitening Cosmeceutical Ingredients. Chem Biodivers. 2021;18(7):e2100245. doi:10.1002/cbdv.202100245

274. https://www.fda.gov/food/dietary-supplements

275. Newman DJ, Cragg GM. Natural Products as Sources of New Drugs over the Nearly Four Decades from 01/1981 to 09/2019. J Nat Prod. 2020;83(3):770-803. doi:10.1021/acs.jnatprod.9b01285